Ditopic molecular architectures for the recognition of anionic species

Pedro Miguel Veríssimo Mateus

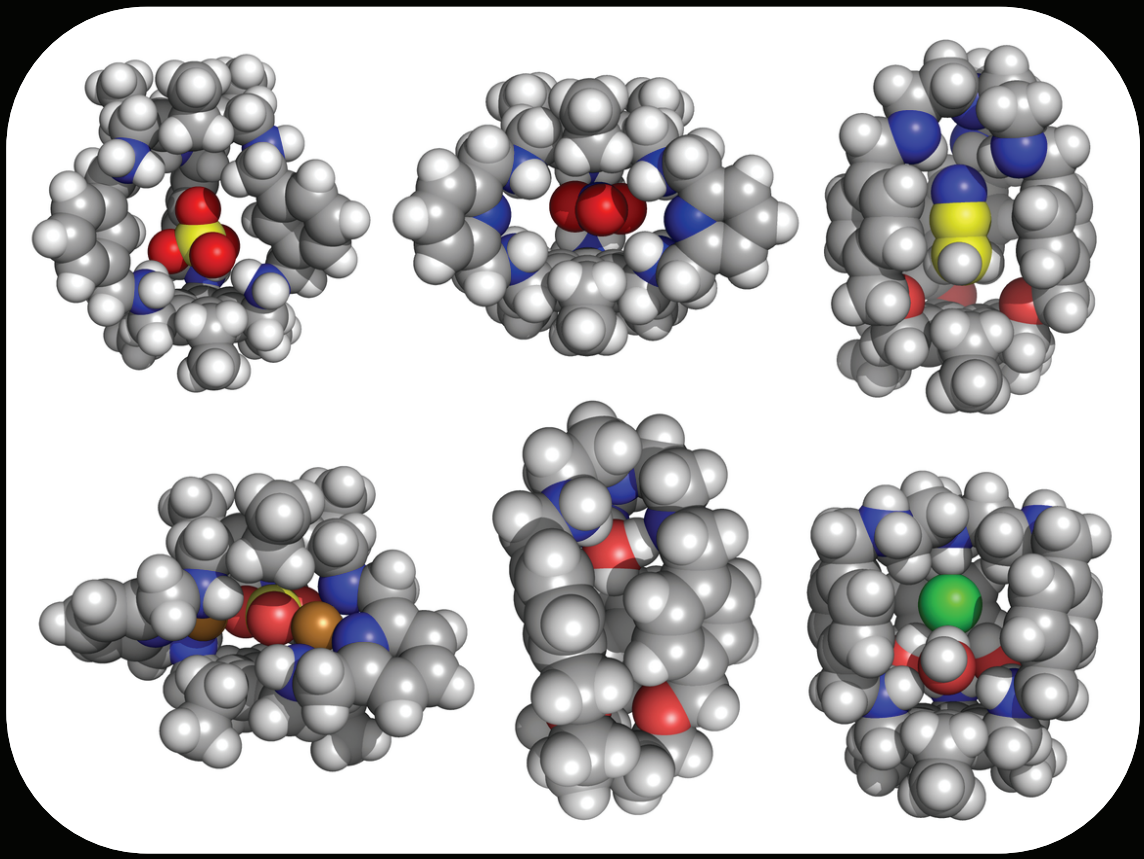

Dissertation presented to obtain the Ph.D degree in Chemistry

Instituto de Tecnologia Química e Biológica | Universidade Nova de Lisboa

Oeiras,
August, 2011

INSTITUTO DE TECNOLOGIA QUÍMICA E BIOLÓGICA /UNL

Knowledge Creation

Ditopic molecular architectures for the recognition of anionic species

Pedro Miguel Veríssimo Mateus

Dissertation presented to obtain the Ph.D degree in Chemistry

Instituto de Tecnologia Química e Biológica | Universidade Nova de Lisboa

Oeiras, August, 2011

INSTITUTO
DE TECNOLOGIA
QUÍMICA E BIOLÓGICA
/UNL

Knowledge Creation

The work described in this thesis was entirely carried out in Instituto de Tecnologia Química e Biológica, Oeiras, Portugal. Pedro Mateus has received financial support from Fundação para a Ciência e Tecnologia, ref. SFRH/BD/36159/2007.

FCT Fundação para a Ciência e a Tecnologia
MINISTÉRIO DA CIÊNCIA, TECNOLOGIA E ENSINO SUPERIOR

”*Un savant dans son laboratoire n'est pas un technicien; c'est aussi un enfant placé en face des phénomènes naturels qui l'impressionnent comme un conte de fées.*”

Marie Curie

Para a minha família.

Table of Contents

Foreword

This thesis represents the culmination of four years of work in the Coordination and Supramolecular Chemistry group at Instituto de Tecnologia Química e Biológica – UNL, under the supervision of Professor Rita Delgado.

All the work contained in this thesis was directly planned and carried out by the candidate, with the following exceptions:

- Elemental analysis and ESI-MS data were carried out by M. Conceição Almeida from the Elemental Analysis and Mass Spectrometry Service at the ITQB.

- The X-ray diffraction of all crystals obtained in this work was performed by Dr. Paula Brandão from the Universidade de Aveiro, Portugal, as well as the preliminary solving of the crystal structures presented in Chapter 7.

- Structure solving of the crystal structures present in Chapters 2-5 was done by Prof. Vítor Félix, from the Universidade de Aveiro, Portugal, as well as the description and discussion of the crystal structures in Chapters 2-5.

- The molecular mechanics and molecular dynamics calculations and respective discussion in Chapter 2 were performed by Dr. Sílvia Carvalho and Prof. Vítor Félix, from the Universidade de Aveiro, Portugal.

- The magnetic properties, the DFT calculations and the magneto-structural correlations of the trinuclear copper(II) cryptate and respective discussion in Chapter 4 were performed by Dr. Joan Cano and Prof. Francesc Lloret, from the Universitat de València, Spain.

Acknowledgements

It is my pleasure to take this opportunity to acknowledge the people that have contributed directly or indirectly to the successful outcome of this work.

First and foremost I owe my deepest gratitude to my supervisor, Prof. Rita Delgado, for receiving me in her group and for providing invaluable support and guidance, whilst granting me freedom in the planning and conduction of the work. I'm truly thankful not only for all the knowledge and important values of honesty and rigor I've acquired from Prof. Rita Delgado but also for the friendship and advice, which meant a great deal to me.

Very special thanks to my lab colleagues Luís Lima, Feng Li, Catarina Esteves and Nicolas Bernier for all the help and friendship. A warm thanks also to Prof. Judite Costa for introducing me to the acquisition of potentiometric data and her friendship.

A big thanks to all my friends, too numerous to mention here but they know who they are.

I wish to acknowledge Dr. Paula Brandão and Prof. Vítor Félix for the X-ray crystallographic data acquisition and analysis and also Dr. Sílvia Carvalho for the molecular mechanics and molecular dynamics calculations.

I am grateful to Dr. Joan Cano and Prof. Francesc Lloret from the Universitat de València for the study of the magnetic properties, DFT calculations and magneto-structural correlations of the trinuclear copper(II) cryptate.

A note of appreciation to Dr. Helena Matias and Dr. Pedro Lamosa from CERMAX for support with the NMR, to Dr. Manuela Pereira for support with the EPR machine, to Dr. Filipe de Oliveira for help with the EPR spectra simulations, to Conceição Almeida from the Elemental Analysis and Mass Spectrometry Service at the ITQB for providing elemental analysis and ESI-MS data and to Prof. Christopher Maycock for taking the time to correct the English of the Title and Summary of this thesis.

I would like to thank ITQB and its staff for the great research conditions offered, namely the NMR spectrometers which are part of the National NMR Network and were purchased in the framework of the National Program for

Scientific Re-equipment, contract REDE/1517/RMN/2005, with funds from POCI 2010 (FEDER) and Fundação para a Ciência e a Tecnologia (FCT). FCT is also acknowledged for the B.I. grant under project POCI/QUI/56569/2004 and for the PhD grant, SFRH/BD/36159/2007.

Last but not least, I am overwhelmingly grateful to my family for their endless support and encouragement, especially to my dearest mother to whom I owe more than I can ever repay. Very special thanks to my wife and son for their love, support and understanding.

List of publications and communications

Thesis publications:

1) "Selective recognition of tetrahedral dianions by a hexaaza cryptand receptor", P. Mateus, R. Delgado, P. Brandão, S. Carvalho, V. Félix, *Org. Biomol. Chem.* **2009**, *7*, 4661–4637.
2) "Polyaza cryptand receptor selective for dihydrogen phosphate", P. Mateus, R. Delgado, P. Brandão, V. Félix, *J. Org. Chem.* **2009**, *74*, 8638–8646.
3) "Recognition of oxalate by a copper(II) polyaza macrobicyclic complex", P. Mateus, R. Delgado, P. Brandão, V. Félix, *Chem. Eur. J.* **2011**, *17*, 7020–7031.
4) "A trinuclear copper(II) cryptate and its μ_3-CO_3 cascade complex: thermodynamics, structural and magnetic properties", P. Mateus, R. Delgado, F. Lloret, J. Cano, P. Brandão, V. Félix, *Chem. Eur. J.* **2011**, 17, 11193–11203.
5) "Thermodynamics and structural aspects of dicarboxylate binding by two polyaza macrobicyclic receptors", P. Mateus, R. Delgado, P. Brandão, V. Félix, *preliminary manuscript*.
6) "Two new polyoxapolyaza macrobicyclic receptors for recognition of zwitterionic amino acids", P. Mateus, R. Delgado, P. Brandão, V. Félix, *preliminary manuscript.*

Other publications:

1) "Recognition of anions by polyammonium macrocyclic and cryptand receptors. Influence of the dimensionality on the binding behavior", P. Mateus, N. Bernier, R. Delgado, *Coord. Chem. Rev.*, **2010**, *254*, 1726–1747.
2) "Properties of metal complexes of a new dioxadiaza macrocycle containing a dibenzofuran unit and acetate pendant arms", P. Mateus, F. Li, R. Delgado, C. V. Esteves, P. Brandão, V. Félix, *Eur. J. Inorg. Chem.*, **2011**, 4700–4708.

Communications at international scientific meetings:

Oral

1) "New hexaaza macrobicyclic cyclophane for recognition of tetrahedral dianions" (FC14), *1st Portuguese Young Chemists Meeting* (PYCheM), 15-17 de October 2008, Lisbon, Portugal. Awarded with "1st Prize for Best Flash Communication".
2) "Recognition of oxalate by a new copper(II) polyaza macrobicyclic complex" (OC20), International Symposium on Metal Complexes, ISMEC2010, 7-11 June 2010, Bilbao, Spain.

Poster

1) "Properties of metal complexes of a new dioxadiaza macrocycle containing a dibenzofuran unit and acetate pendant arms" (PSB 7), *II International Symposium on Macrocyclic & Supramolecular Chemistry*, 24-28 June 2007, Salice Terme, Italy.
2) "A polyaza cryptand host for the recognition of tetrahedral dianions" (P161), *IV International Symposium on Macrocyclic & Supramolecular Chemistry*, 21-25 June 2009, Maastricht, The Netherlands.
3) "Trinuclear copper(II) complex of a macrobicyclic ligand" (P76), *8th Inorganic Chemistry Conference*, 16 and 17 October 2009, Curia, Portugal.
4) "A new copper(II) polyaza macrobicyclic complex as a receptor for the recognition of carboxylates" (P103), *2nd Portuguese Young Chemists Meeting*, 21-24 April 2010, Aveiro, Portugal.
5) "Anion recognition by polyamine macrobicyclic receptors. Selectivity tuning through small structural changes" (IIIa.039), *3rd EuCheMS Chemistry Congress*, 29 August-02 September 2010, Nurnberg, Germany.

Keywords

Supramolecular Chemistry
Molecular recognition
Cryptand receptors
Anionic substrates
Cascade complexes
Triangular copper(II) complexes
Indicator displacement assays
Sensors

Summary

Anions are ubiquitous and very important species in biological, medicinal, industrial and environmental processes. In biology, anions are essential for normal metabolic functions, where their specific recognition, transport and detection play a very important role. On the other hand, the uncontrolled release of anions into the environment poses a significant threat.

The development of synthetic receptors capable of sequestering anions should, therefore, provide solutions to a number of problems of current interest. To be suitable for real-life applications, as for instance the detection and quantification of biologically active anions in clinical laboratories or the environmental monitoring and/or removal of pollutants, synthetic receptors need to be able to function in aqueous solution. However, due to the high dielectric constant and good hydrogen bond donor and acceptor capabilities, water is the most challenging medium for anion recognition.

Polyamine macrobicycles are one of the most successful groups of compounds used in the recognition of anions in aqueous solutions, due to the binding properties of the ammonium group and the encapsulating abilities of the macrobicyclic architecture. However, although polyamine macrobicycles have proved to be extremely versatile compounds and possess very interesting anion binding properties, the reported cases of true selectivity, where one analyte is bound without any interference from all possible competitors, are scarce. This fact is possibly related, at least in part, to the inability of existing receptors to have the necessary rigidity and complementarity for the recognition of the partner. Thus there is still much to be done for the improvement of the design of polyamine macrobicycles.

The objective of this work was to take advantage of the ease of modification of the macrobicyclic architecture and, by small structural changes, try to increase its preorganization and to add building blocks that would allow selectivity for a particular anion.

Bearing this in mind, the initial work aimed at obtaining a more rigid macrobicyclic architecture by using the 2,4,6-triethylbenzene scaffold instead of the tren [tris(2-aminoethyl)amine] subunit commonly used as building block in the design of polyammonium cryptands. Therefore, a receptor with *m*-xylyl groups as spacers (xyl) was synthezised and its ability to encapsulate anions of different shape, size and charge was evaluated. These studies, described in detail in Chapter 2, revealed a remarkable selectivity for dianionic tetrahedral species by the protonated receptor. Association constants determined by potentiometric measurements fell within the range 5.03–5.30 log units for the dianionic species and 1.49–2.97 log units for monoanionic ones. Single crystal X-ray determination of $[(H_6xyl)(SO_4)(H_2O)_6](SO_4)_2.9.5H_2O$ showed that one sulfate anion was encapsulated into the receptor cage.

The work described in Chapter 3 shows how the selectivity pattern can be modified by slight structural changes in the receptor framework. Using the same macrobicyclic scaffold as xyl and changing from *m*-xylyl spacers to pyridyl ones, a cavity containing hydrogen bond acceptors was produced (pyr). This had a very significant impact in the selectivity pattern. Apparently, as in naturally occurring phosphate-binding protein (PBP), the presence of hydrogen bond acceptors in the H_npyr^{n+} receptor enhanced the affinity for hydrogen phosphate. Therefore, at low pH dihydrogen phosphate had an affinity of the order of sulfate, in spite of the higher charge of the latter anion and it was capable of effectively competing with sulfate at the receptor at higher pH. At a pH of about 7.0 the H_npyr^{n+} receptor was selective for hydrogen phosphate.

The structural motifs of the pyr compound, the C_3 symmetry and the three pyridyl spacers, suggested that it would be interesting to study its copper(II) complexes in solution and in the solid state (Chapter 4). Unexpectedly, crystals of the trinuclear copper complex grown at pH ≈ 6, revealed the presence of carbonate (formed by spontaneous CO_2 uptake from the air) bridging the three copper centres. The CO_2 fixation was likely derived from the nucleofilic attack of the hydroxo group of the $[Cu_3pyrOH]^{5+}$ complex on the electrophilic carbon of CO_2. Apparently, the ability of pyr to bring into close proximity three metal ions

played a crucial role in lowering the pK_a of coordinated water molecules. This allowed hydroxo complexes to be formed in slightly acidic media that in turn permitted CO_2 fixation to occur without the need for a high pH. This resembled the reactivity of the carbonic anhydrase enzyme. The production of $[Cu_3pyr(\mu_3\text{-}CO_3)]^{4+}$ in the presence of large amounts of NO_3^-, indicated that carbonate bridging was preferred to nitrate in spite of the same geometry of both anions and the higher concentration of nitrate in solution. It was also found that the architecture of pyr was responsible for the interesting magnetic properties of $[Cu_3pyr(\mu_3\text{-}CO_3)]^{4+}$ observed.

Chapter 5 describes the synthesis of a new heteroditopic polyamine macrobicyclic compound ($btpN_7$), in which one of the head units was appropriate for the coordination of copper(II) while the other head was available for additional hydrogen bonding and electrostatic interactions with substrates. These studies revealed a clear preference for oxalate by the receptor $[CuH_hbtpN_7H_2O]^{(2+h)+}$ over other dicarboxylate substrates of varied chain length, arising from cooperativity between metal-anion coordination, electrostatic and hydrogen bonding interactions. Indeed, this is in accordance with the ideal size of this dicarboxylate, which allowed it to take full advantage of the potential binding sites of the receptor. A qualitative indicator-displacement study, which was in agreement with the potentiometric studies, demonstrated that the copper(II) cryptate receptor could be used as a selective visual sensor for oxalate.

The dicarboxylate binding abilities of $btpN_7$ were further investigated, this time using the compound only in its protonated forms (Chapter 6). Its selectivity pattern was compared with that of its bis-tren analogue, in order to shed light on the influence of the introduction of the 2,4,6-triethylbenzene head unit on the binding properties and selectivity pattern. The results revealed that both compounds were able to form stable associations with the dianionic substrates in competitive aqueous solution and that although the selectivity pattern was unaffected by the introduction of 2,4,6-triethylbenzene head unit, the affinity towards dicarboxylates was significantly reduced.

Finally, in Chapter 7 two new mixed polyoxapolyaza heteroditopic macrobicyclic compounds are described which were designed to have cavities containing both cationic (ether groups) and anionic binding sites (ammonium groups) with the intention of using them for the recognition of zwitterionic amino acids in aqueous solution. The results showed that $H_nbtpN_4O_3^{n+}$ could bind the amino acids in mixed methanol/water solution, although the determined association constants showed only very moderate affinity by the receptor for the zwitterionic substrates.

Throughout this research different types of binding sites have been introduced into the macrobicyclic architecture in conjunction with slight structural changes. The change of building blocks allowed selectivity to be shifted from sulfate to phosphate and yielded a receptor appropriate for dicarboxylate recognition and a receptor suitable for zwitterionic amino acids. Thus a total of five different previously unreported polyamine macrobicyclic compounds were obtained with varied and interesting anion binding behaviour and selectivities in highly competitive aqueous solution.

Resumo

Os aniões são espécies muito importantes em áreas como a biologia, a medicina, a indústria e o ambiente. Na biologia os aniões são essenciais para o normal funcionamento do metabolismo onde o seu reconhecimento, transporte e detecção desempenham um papel muito importante. Por outro lado, a libertação descontrolada de aniões no meio ambiente representa uma ameaça significativa.

O desenvolvimento de receptores sintéticos capazes de encapsular aniões pode, portanto, fornecer soluções para alguns dos problemas actuais. Em aplicações concretas, como por exemplo a detecção e doseamento de aniões biologicamente activos em laboratórios clínicos ou a monitorização e/ou remoção de poluentes do meio ambiente, os receptores sintéticos têm de ser capazes de funcionar em solução aquosa. No entanto, a água é o meio mais competitivo no reconhecimento de aniões, devido à sua elevada constante dieléctrica e às suas capacidades de doação e aceitação de ligações de hidrogénio.

As poliaminas macrobicíclicas estão entre os compostos com maior sucesso no reconhecimento de aniões em solução aquosa, devido às propriedades de ligação do grupo amónio e às capacidades de encapsulamento da arquitectura macrobicíclica. No entanto, apesar de as poliaminas macrobicíclicas se terem mostrado extremamente versáteis e possuidoras de propriedades muito interessantes no que diz respeito ao reconhecimento de aniões, os casos de verdadeira selectividade descritos na literatura, em que um analito é reconhecido sem interferência de todos os possíveis competidores, são escassos. Este facto está possivelmente relacionado, pelo menos em parte, com a incapacidade dos receptores existentes possuírem a rigidez e a complementaridade necessárias para o reconhecimento de um único substrato. Há assim ainda muito por fazer no sentido de melhorar a concepção de poliaminas macrobicíclicas.

Neste trabalho pretendeu-se tirar partido da facilidade de modificação da arquitectura macrobicíclica e com pequenas alterações estruturais tentar aumentar a sua preorganização, nomeadamente incorporando unidades

estruturais que permitam aumentar a selectividade para um anião em particular na presença dos seus competidores.

Com este objectivo, o trabalho inicial visou a obtenção de uma estrutura macrobicíclica mais rígida por utilização de 2,4,6-trietilbenzeno como plataforma estrutural em vez da tren [tris(2-aminoetil)amina], esta última muito utilizada na construção de criptandos do tipo poliamónio. Deste modo, foi sintetizado um receptor com espaçadores do tipo *m*-xililo (xyl) e avaliada a sua capacidade de agarrar aniões de diferentes formas, tamanhos e cargas. Estes estudos, descritos em detalhe no Capítulo 2, revelaram que o receptor na sua forma protonada possui uma selectividade notável para espécies dianiónicas tetraédricas. As constantes de associação, determinadas por método potenciométrico, são da ordem de 5,02–5,30 unidades logarítmicas para as espécies dianiónicas e de 1,49–2,97 unidades logarítmicas para as monoaniónicas. Uma estrutura determinada por difracção de raios-X de cristal único mostrou um anião sulfato encapsulado pelo receptor.

O trabalho descrito no Capítulo 3 mostra como a selectividade pode ser modificada através de pequenas alterações no receptor. Utilizando a mesma estrutura macrobicíclica que no caso do composto xyl mas substituindo os espaçadores *m*-xililo por piridilo, construiu-se uma cavidade contendo aceitadores de ligações de hidrogénio (pyr). Este procedimento teve um impacto muito significativo na selectividade. A presença de aceitadores de ligações de hidrogénio no receptor H_npyr^{n+} faz aumentar a afinidade para o ião hidrogenofosfato, tal como acontece na proteína específica para fosfato (PBP). Deste modo, o anião dihidrogenofosfato apresenta uma afinidade para o receptor da mesma ordem de grandeza da do ião sulfato a baixo pH, apesar da maior carga deste último ião, e é capaz de competir com o ião sulfato para valores de pH mais elevados. A pH aproximadamente 7,0 o receptor H_npyr^{n+} é selectivo para o ião hidrogenofosfato.

Os motivos estruturais do composto pyr, a simetria C_3 e os três espaçadores piridilo, sugeriram o estudo dos seus complexos de cobre(II) em solução aquosa e no estado sólido (Capítulo 4). Inesperadamente, os cristais formados a pH ≈ 6,

revelaram a presença de carbonato (produzido por absorção espontânea de CO_2 do ar) coordenado simultaneamente pelos três iões cobre(II). A fixação de CO_2 advém possivelmente de um ataque nucleofílico do grupo hidróxido do complexo $[Cu_3pyrOH]^{5+}$ ao carbono electrofílico do CO_2. A capacidade do composto pyr de coordenar os três iões metálicos e de os colocar a curta distância uns dos outros parece desempenhar um papel crucial na diminuição do pK_a de uma molécula de água coordenada ao metal. Isto permite que a fixação de CO_2 ocorra a um pH relativamente baixo, o que se assemelha ao funcionamento do enzima anidrase carbónica. A formação de $[Cu_3pyr(\mu_3\text{-}CO_3)]^{4+}$ na presença de grande quantidade de NO_3^-, indicou que a coordenação de ião carbonato é preferida à do nitrato, apesar de ambos os aniões possuírem a mesma geometria e de o ião nitrato se encontrar em concentração mais elevada em solução. Também se verificou que a arquitectura do composto pyr é responsável pelas propriedades magnéticas interessantes do ião complexo $[Cu_3pyr(\mu_3\text{-}CO_3)]^{4+}$.

No Capítulo 5 descreve-se a síntese de um novo composto macrobicíclico heteroditópico do tipo poliamina ($btpN_7$), no qual uma das unidades estruturais é apropriada para a coordenação de cobre(II) enquanto a outra pode servir para estabelecimento de ligações de hidrogénio e interacções electrostáticas adicionais. Estes estudos revelaram uma preferência do receptor $[CuH_hbtpN_7H_2O]^{(2+h)+}$ para o oxalato em relação a outros substratos do tipo dicarboxilato com cadeias alifáticas de comprimento variado, resultante da cooperatividade entre a coordenação ao metal, interacções electrostáticas e ligações de hidrogénio. A preferência do anião oxalato para o $[CuH_hbtpN_7H_2O]^{(2+h)+}$ advém do tamanho ideal do substrato que tira partido de todos os potenciais locais de ligação do receptor. Um estudo baseado no método de deslocamento de indicador, concordante com os estudos potenciométricos, demostrou que o criptato de cobre(II) pode ser utilizado como sensor visual selectivo para iões oxalato.

Investigou-se, também, a capacidade do receptor $H_nbtpN_7^{n+}$ para captar iões dicarboxilato (Capítulo 6). A sua selectividade foi comparada com a do seu análogo derivado bis-tren, de forma a esclarecer a influência da plataforma 2,4,6-

trietilbenzeno nas capacidades de associação do composto. Os resultados revelaram que ambos os compostos são capazes de formar associações estáveis com os substratos dianiónicos em meio aquoso muito competitivo e que, apesar da selectividade não ser afectada pela introdução de 2,4,6-trietilbenzeno, a afinidade para com os dicarboxilatos é significativamente menor.

Finalmente, no Capítulo 7 são descritos dois novos compostos macrobicíclicos heteroditópicos do tipo polioxapoliaza que foram concebidos para possuírem cavidades contendo sítios de ligação para catiões (grupos éter) e também para aniões (grupos amónio), com a intenção de os utilizar como receptores para aminoácidos zwiteriónicos em solução aquosa. Os resultados mostraram que o receptor $H_nbtpN_4O_3^{n+}$ pode associar-se a aminoácidos no solvente metanol/água, apesar das constantes de associação determinadas corresponderem apenas a uma afinidade moderada do receptor para com os substratos zwiteriónicos.

Ao longo deste trabalho foram introduzidos numa arquitectura macrobicíclica diferentes tipos de sítios de ligação assim como pequenas alterações estruturais. A alteração de elementos estruturais permitiu que a selectividade se deslocasse do ião sulfato para o ião fosfato, originou um receptor apropriado para o reconhecimento de dicarboxilatos e um receptor adequado para aminoácidos zwiteriónicos. Assim, sintetizaram-se cinco compostos macrobicíclicos diferentes do tipo poliamina inteiramente novos, com comportamento variado e interessante no que diz respeito à sua interacção com aniões e à sua selectividade, em meio aquoso muito competitivo.

Index of Figures

Index of Schemes

Index of Tables

List of compounds and complexes discussed in this work

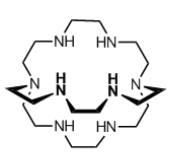

1

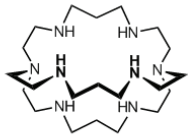

2

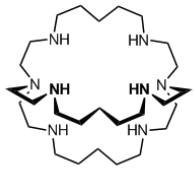

3

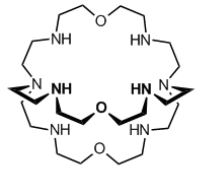

4

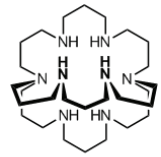

5

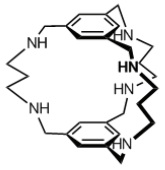

6

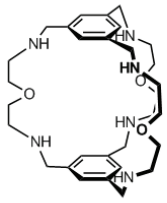

7

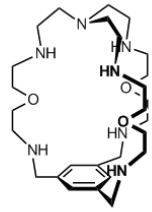

8

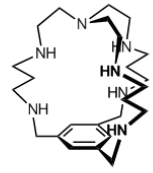

9

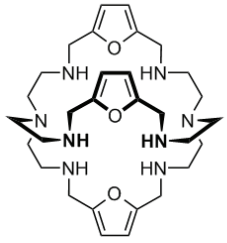

10

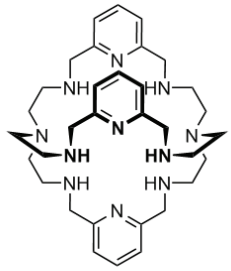

11

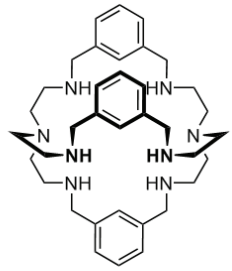

12

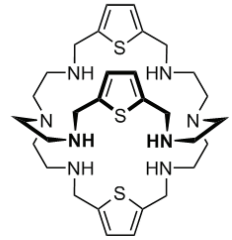

13

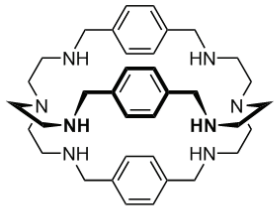

14

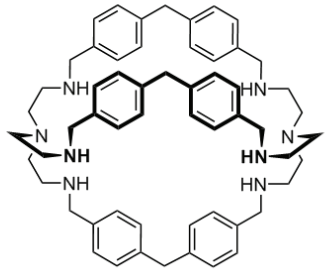

15

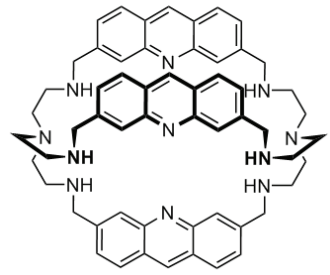

16

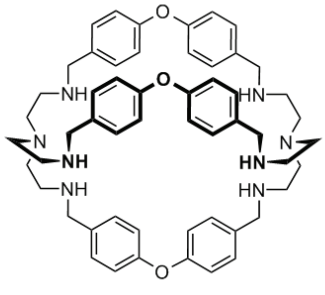

17

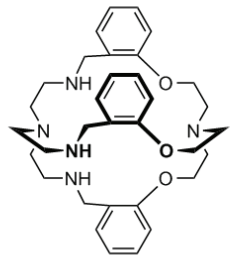

18

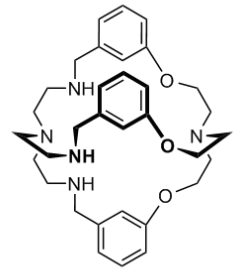

19

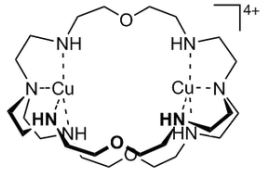

20

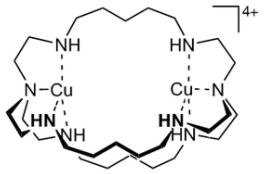

21

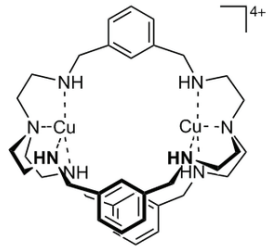

22

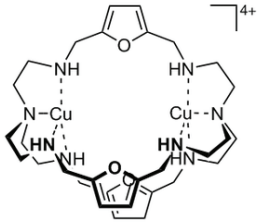

23

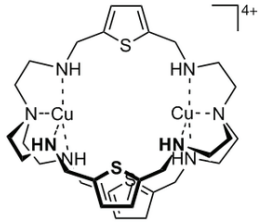

24

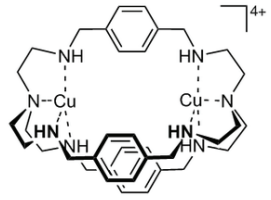

25

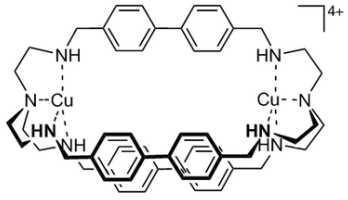

26

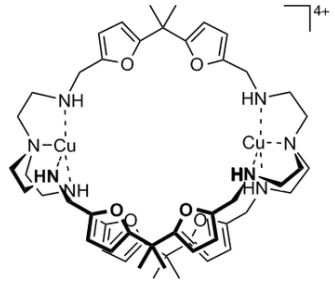

27

List of compounds synthesized and studied in this work

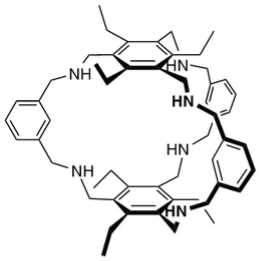

xyl

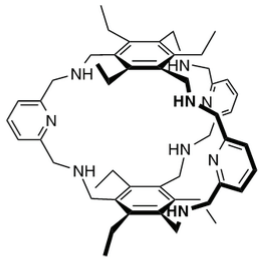

pyr

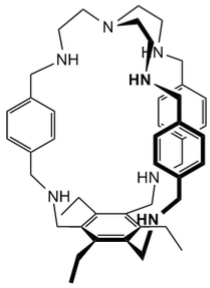

$btpN_7$

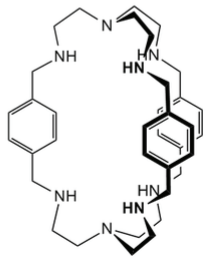

t_2pN_8

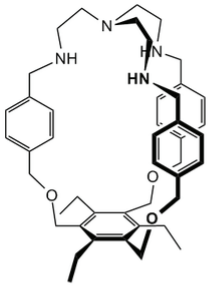

$btpN_4O_3$

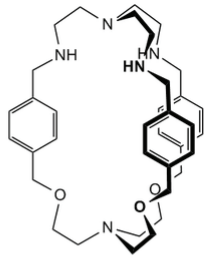

$t_2pN_5O_3$

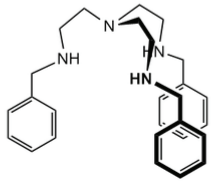

tbN_4

List of abbreviations and symbols

1D	one dimension
2D	two dimensions
^3J (H,H)	vicinal proton-proton coupling constant
AcOH	acetic acid
adi^{2-}	Adipate
ADP	adenosine diphosphate
AMP	adenosine monophosphate
ATP	adenosine triphosphate
BM	Bohr magneton
btc^{3-}	benzenetricarboxylate
ch^{3-}	cyclohexanetricarboxylate
c_i	concentration of species i
$c_i^{\ominus}$	concentration of species i in the standard state
CmpA	bicarbonate binding protein
COSY	correlation spectroscopy
D	zero-field splitting parameter
Dct	C_4-dicarboxylate transport system
DctB	periplasmic sensor domain
DFT	density functional theory
DHP	3,4-dihydro-2*H*-pyran
DMF	dimethylformamide
DMSO	dimethylsulfoxide
DNA	deoxyribonucleic acid
E	electromotive force
E_j	liquid junction potential
$E^{o\prime}$	formal electrode potential
EPR	electron paramagnetic resonance
ESI	electrospray ionization
Et_3N	triethylamine

EtOH	ethanol
FAD	flavin adenine dinucleotide
fum^{2-}	fumarate
g	g factor
glu^{2-}	glutarate
h	Planck constant
H	magnetic field
H_2aep	2-aminoethylphosphonate
H_2amp	aminomethylphosphonate
Hgly	glycine
Hbala	*β*-alanine
Hgaba	*γ*-aminobutyrate
Htau	taurine
HMQC	heteronuclear multiple quantum coherence
I	ionic strength
iph^{2-}	isophthalate
IR	infrared
J	coupling constant
k	Boltzmann constant
K_{ass}	association (or binding) constant
K_{eff}	effective association (or binding) constant
$K_{H_hL_lA_a}$	stepwise protonation constant
K_i^H	stepwise protonation constant
$K_{M_mH_hL_l}$	stepwise stability constants
$K_{M_mH_hL_lA_a}$	stepwise stability constants of cascade associations
K_w	ionic product of water
M	magnetization
mal^{2-}	malonate
$male^{2-}$	maleate
MD	molecular dynamics
MeCN	acetonitrile

MeOH	methanol
MM	molecular mechanics
MsCl	mesylenesulphonyl chloride
NMR	nuclear magnetic resonance
NOESY	nuclear Overhauser effect spectroscopy
NrtA	nitrate binding protein
oxa^{2-}	oxalate
PBP	phosphate binding protein
pD	$-\log [D^+]$
ph^{2-}	phthalate
PhOH	phenol
pim^{2-}	pimelate
QFR	menaquinol:fumarate oxidoreductase
R	receptor
r.t.	room temperature
RNA	ribonucleic acid
S	substrate
SBP	sulfate binding protein
suc^{2-}	succinate
T	temperature
THF	tetrahydrofuran
THP	tetrahydro-2*H*-pyran-2-yl
TMS	tetramethylsilane
tph^{2-}	terephthalate
tren	tris-(aminoethyl)amine
trpn	tris-(aminopropyl)amine
Ts	toluenesulphonyl
TsCl	toluenesulphonyl chloride
TsOH	toluenesulphonic acid
UV	ultraviolet
v/v	volume/volume

vis	visible
X	molar fraction
$\beta_{H_hL_lA_a}$	overall association constant
β_i^H	overall protonation constant
$\beta_{M_mH_hL_l}$	overall stability constants
$\beta_{M_mH_hL_lA_a}$	overall stability constants of cascade associations
δ	chemical shift
ΔΔG	difference in binding free energies
θ	Weiss parameter
ν	frequency
χ_M	magnetic susceptibility

Colour code for the crystal structure diagrams

The colour labelling scheme adopted in the molecular diagrams representing the crystal structures, except otherwise stated in the respective figure caption, is the following:

Hydrogen	White
Carbon	Grey
Nitrogen	Blue
Oxygen	Red
Sulfur	Yellow
Copper	Golden yellow
Fluorine	Pink
Chlorine	Green
Bromine	Brown
Iodine	Purple
Phosphorus	Orange
Hydrogen bonds	Green dashed lines

Molecular diagrams depicted in Chapter 1 were drawn with PyMOL (W. L. DeLano, The PyMOL Molecular Graphics System DeLano Scientific, San Carlos, CA, USA, 2002. http://www.pymol.org.)

Chapter 1

Introduction

1.1 Supramolecular Chemistry

Throughout the years chemists have strived to attain control over the formation and breaking of the covalent bond and by doing so, numerous methods for constructing new molecules of increasing complexity were developed.[1] About 40 years ago a new paradigm emerged that sought to achieve increasing complexity by taking advantage of the non-covalent intermolecular forces (electrostatic interactions, hydrogen bonding, van der Waals interactions, etc), giving rise to a new field called *Supramolecular Chemistry*. The term was introduced by one of its pioneers, Jean-Marie Lehn, Nobel prize laureate in 1987, whom defined it as the *"...chemistry of molecular assemblies and of the intermolecular bond"* or *"the chemistry beyond the molecule"*,[1] as it deals with the complex entities formed by the association of two or more chemical species held together by non-covalent intermolecular forces.

Many of supramolecular chemistry's concepts, terminology and definitions were already known for quite some time: in 1894 Fischer introduced the notion of complementarity with the famous lock and key principle, twelve years later Ehrlich created the concept of receptor by observing that molecules only act when bound, and the term supermolecule was introduced in 1937 by Wolf. However, it was only with the work of Nobel Prize winners, Pedersen, Lehn and, Cram in the late 1960´s and early 1970´s that Supramolecular Chemistry was conceptualized as new field of chemistry.[2]

In the beginning, the field dealt mainly with the so called host-guest chemistry, but the area rapidly evolved to include self-assembly, self-replication, catalysis by artificial enzymes and enzyme models, molecular devices and other processes that involve non-covalent interactions. Nowadays Supramolecular Chemistry is a highly interdisciplinary field interfacing chemistry, biology, and physics and materials science.[2,3]

1.2 Molecular recognition

Molecular recognition is defined by the selection of a substrate (or substrates) by a given receptor (or host) molecule through the establishment of non-covalent interactions between them, and it is at the basis of every aspect of supramolecular chemistry.[1]

The receptor is the molecular entity possessing convergent binding sites located in strategic points of its architecture of a well defined size and shape. The binding sites are characterized by their electronic properties such as charge, polarity, polarisability, size, shape, number and location in the receptor framework. The substrate (or guest) in turn can be viewed as a species (cationic, anionic or neutral) with diverging binding sites, complementary to those of the receptor. Together they form a third entity called supermolecule, with its own thermodynamic and structural properties.[1]

It should be stressed, however, that binding alone cannot be called recognition. Recognition requires a high degree of geometrical and interactional complementarity between the receptor with respect to a given substrate, which allows the latter to be selected in the presence of any other competitor, including the solvent. In order to achieve selective binding several aspects must be taken into account:

a) steric complementarity – receptor and substrate must present matching size and shape;
b) interactional complementarity – presence of complementary binding sites in the correct disposition on the receptor and on the substrate, such as positive/negative charge, charge/dipole, dipole/dipole, hydrogen bond donor/acceptor, etc;
c) multiple interaction sites – the weak nature of non-covalent interactions requires that the binding sites are numerous, well located and acting cooperatively.

d) the medium – the solvent in which the recognition takes place play a very important role due to its interaction with both binding partners, as well as with the supermolecule itself.

1.2.1 Molecular interactions in molecular recognition

The formation of a supermolecule requires the establishment of non-covalent interactions between the receptor and the substrate(s). There are several types of non covalent interactions fundamental in Supramolecular Chemistry:[4]

- Electrostatic interactions
- van der Waals interactions
- Hydrogen bonds
- Solvophobic/hydrophobic interactions
- π–π interactions
- Cation–π interactions
- Anion–π interactions

As non-covalent interactions are considerably weaker than covalent ones, several and varied interactions need to be used in a cooperative way to form a stable supramolecular association. Finding an appropriate combination of molecular interactions is essential to the design of efficient molecular recognition systems.

1.2.2 Complementarity and preorganization

As already mentioned, *complementarity* requires a receptor with binding sites that are of the correct electronic character (polarity, hydrogen bond donor/acceptor ability, hardness or softness, etc) to complement those of the substrate. In addition, the binding sites in the receptor have to be spatially arranged in its framework in such a way as to make it possible to attract the binding sites of the substrate(s), without giving rise to unfavourable interactions. If the strategic spatial disposition of the binding sites is such that the receptor does

not need to undergo a significant conformational change upon binding of the substrate, and, thus, binding energy is not expended in the process, the receptor is *preorganized*.[5]

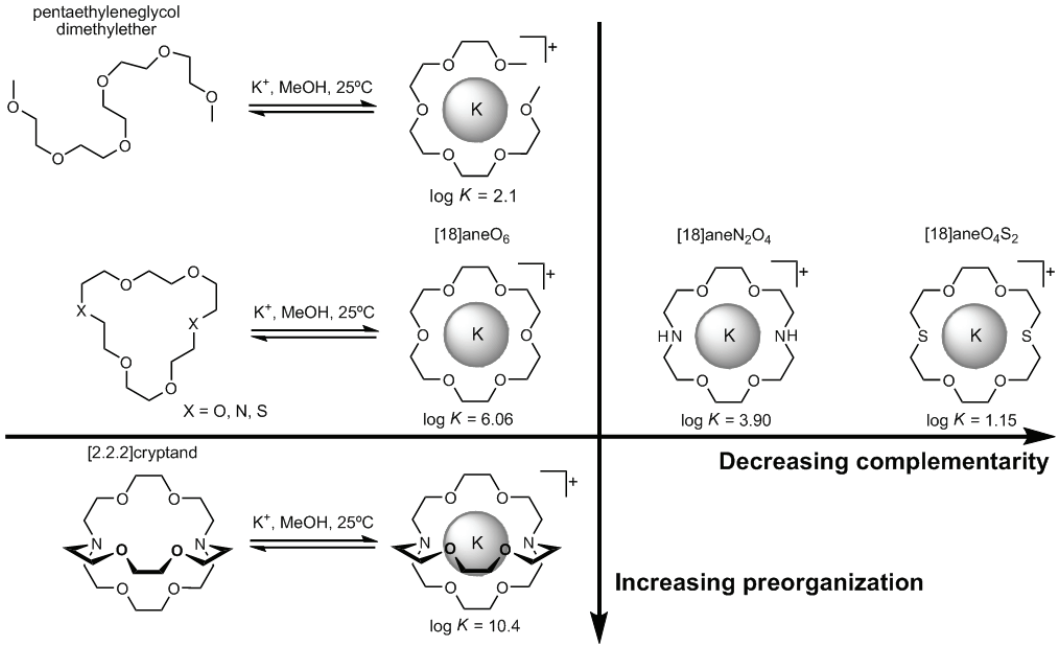

Scheme 1.1 Preorganization and complementarity effects in the coordination of K^+ by polyether receptors.

If solvation effects are not considered, the binding process starts with the conformational readjustment of the receptor in order to arrange its binding sites in the most complementary way to bind the guest and concomitantly minimising unfavourable interactions between binding sites. Of course this has an energetic cost, which for preorganized receptors is paid in advance during the synthesis.

In Scheme 1.1 the effects of preorganization and complementarity on the coordination of potassium ion towards polyether receptors are illustrated. It is clear that increasing preorganization from pentaethyleneglycol dimethylether to the [2.2.2]cryptand yields a large increase in affinity.[6,7] It is also noticeable that if two oxygen donors in [18]aneO$_6$ are replaced by two nitrogen donors, as in [18]aneN$_2$O$_4$, the affinity drops 2.16 log units,[8] because nitrogen is a softer base than oxygen and thus not complementary to hard alkali metal cations such as K^+,

according to the Pearson theory of hard and soft acids and bases (HSAB).[9] On the other hand, substitution by two sulphur donors in [18]aneO_4S_2 results in an even larger affinity drop due to the soft nature of the sulphur donors.[10]

1.2.3 The solvent

Considering complementarity and preorganization factors alone is insufficient to describe the complexity of host-guest processes. Indeed the lock and key principle is an oversimplification that describes the interaction of two partners based on exclusively enthalpic binding, omitting the all important role of the solvent.[11]

Both receptor and substrate can have a large variety of non-covalent interactions with the solvent itself. Furthermore in dilute conditions, where binding processes usually take place, the solvent is in a much larger quantity than both receptor and substrate. The amount and location of the solvent molecules, or in other words the extent of solvation, as well as the strength of the receptor-solvent and substrate-solvent interactions, critically affects the dynamics and energetics of the association process and depends strongly on the nature of the solvent employed.

Polar solvents are able to interact with receptor and substrate molecules *via* strong interactions (ion-dipole, dipole-dipole and hydrogen bonding), which hampers the binding of charged species by increasing the amount of energy necessary to break receptor-solvent and substrate-solvent interactions. Scheme 1.2 represents the association process taking solvation into account.

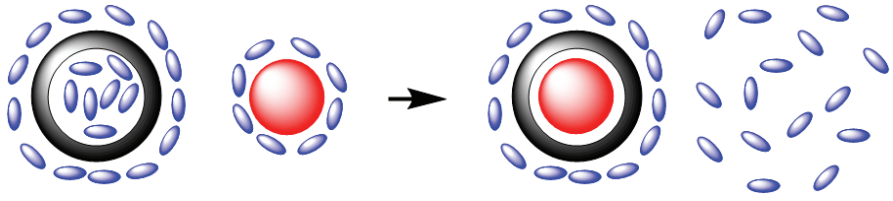

Scheme 1.2 The association process in solution. The black circle represents the receptor, the red circle depicts the substrate and the blue ellipsoids represent the solvent molecules.

In solution, receptor and substrate are surrounded by solvent molecules which interact with them. When the association process takes place, several of these interactions must be broken and new ones must be established between the receptor and the substrate. Breaking the receptor-solvent and substrate-solvent interactions requires enthalpic energy to be expended while enthalpic gain will result from the newly formed receptor-substrate interactions. Complementarity and preorganization play a very important role in maximizing the enthalpic term. On the other hand, the removal of solvent molecules from the receptor and substrate releases solvent molecules to the bulk were they have more freedom, increasing entropy and at the same time increasing the enthalpic term due to increasing solvent-solvent interactions. However receptor-substrate association is also accompanied by conformational restriction of the binding partners which contributes to a loss of entropy.

It is the final balance of all these possible enthalpic and entropic losses, gains and compensations that will determine the affinity of a receptor for a substrate in a given solvent.

1.2.4 Binding constant

The binding of a substrate by a receptor, is an equilibrium process. The equilibrium constant for a binding process is designated binding or association constant. The determination of the association constant is crucial for the assessment of the affinity and selectivity of a substrate towards a given receptor. The equilibrium that is established between a receptor and a substrate, in a simple 1:1 stoichiometry is represented by the following equilibrium:

$$R + S \rightleftharpoons RS$$

The respective binding constant is calculated by Equation 1.1:

$$K_{ass} = a_{RS}/a_R\, a_S \qquad (1.1)$$

Because the activity (a_i) of a chemical species, i, is dimensionless, so is the binding constant. It is common practice to determine binding constants in a

certain medium of constant ionic strength or to work in very low concentrations in order to define the binding constant as a concentration quotient:

$$K_{ass} = [RS]/[R]\,[S] \qquad (1.2)$$

where $[i] = c_i/c_i^{\ominus}$, c_i and $c_i^{\ominus}$ being the concentration of species i and the concentration in the standard state (1 mol dm^{-3}), respectively.

Binding constants are calculated from experimental data obtained by any method that measures a physical property whose magnitude significantly changes in the association event (for instance by potentiometry, NMR, UV-vis or fluorescence methods).[12,13]

In systems where receptors and substrates can have multiple protonation equilibria and thus binding depends on environmental conditions such as the pH or where competitive reactions can occur, the effective binding constant (K_{eff}) is usually more appropriate to describe the system. The K_{eff} value is defined as the quotient between the total amount of supramolecular species formed and the total amounts of the free receptor and free substrate:[14]

$$K_{eff} = \Sigma[(H_{i+j}S)R]/\Sigma[H_iS]\times\Sigma[H_jR] \qquad (1.3)$$

This value takes into consideration the different basicities of receptors and substrates, thus provides a suitable way to derive selectivity trends. It should be noted that the K_{eff} value is a concentration quotient which is not a true equilibrium constant, however it is calculated using the association constant.

1.2.5 Selectivity

As mentioned in 1.2, binding does not mean recognition. The recognition process requires the selective binding of one substrate by a receptor in the presence of other competing substrates. Thus, selectivity is a key concept in molecular recognition; however, to achieve it is also the most challenging task.

Thermodynamic selectivity[15] is expressed as a difference in binding free energies $\Delta\Delta G$ or a ratio of binding constants. In a system where a receptor R can

bind the substrate S^1 and the competitor S^2, the following equilibria are to be considered:

$$R + S^1 \rightleftharpoons RS^1 \qquad K_1 = [RS^1]/[R][S^1] \qquad (1.4)$$

$$R + S^2 \rightleftharpoons RS^2 \qquad K_2 = [RS^2]/[R][S^2] \qquad (1.5)$$

$$RS^2 + S^1 \rightleftharpoons RS^1 + S^2 \qquad K_3 = K_1/K_2 = [RS^1][S^2]/[RS^2][S^1] \qquad (1.6)$$

The K_1/K_2 ratio accounts for the ability of S^1 to displace S^2 from the receptor, and thus reflects the selectivity for S^1 over S^2. If $K_1 > K_2$, the ratio $K_1/K_2 > 1$ and the equilibrium (Equation 1.6) is displaced toward the right side, that is, R preferably binds S^1. The larger the K_1/K_2 value the greater the selectivity.

This is, however, an oversimplification and does not reflect the true situation, because the binding events were considered in the absence of the competitor and, then, the results are related to one another. In real cases, thermodynamic selectivity is the outcome of binding the target guest in the presence of all possible competitors.[16] In addition, the K_1/K_2 ratio approach does not take into consideration factors such as pH and basicity of the components of the system and, thus, has often been the source of misleading interpretations. This is especially important when the receptor and substrates are involved in multiple and overlapping equilibria, and present very different basicity properties, as is the case of the receptors and most of the substrates studied in this work.

A more appropriate method to establish thermodynamic selectivity in the previously mentioned cases is based on the knowledge of the equilibrium constants of all equilibria involved in the system. Once the equilibrium constants are known the concentrations of each species in the system can be calculated at any pH value and, thus, the distribution of the associated species as a function of pH for the mixed $R/S^1/S^2/\ldots/S^n$ systems and to represent their overall percentages of formation, see Figure 1.1.[17]

This method allows attribution of selectivities over the entire pH range and has the advantage of not requiring any assumption of the location of the protons in the interacting species, taking into account the differences in basicity of the

partners, and being able to assess the selectivity towards a substrate of interest in the presence of multiple competitors.

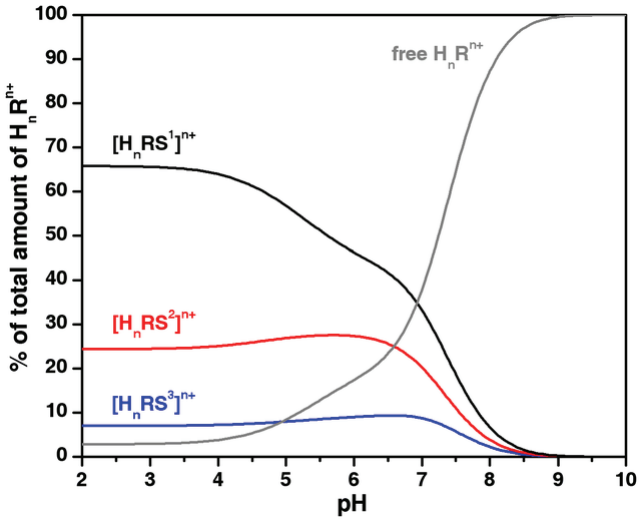

Figure 1.1 Distribution diagram of the overall amount of supramolecular species formed between a receptor of general formula H_nR^{n+} and substrates 1 (S^1), 2 (S^2) and 3 (S^3), with H_nR^{n+}, S^1, S^2 and S^3 in equimolar amounts at a given solvent, ionic strength and temperature.

1.2.6 Receptor molecules

Receptors are organic structures held by covalent bonds that are able to bind ionic or neutral substrates by means of several intermolecular interactions, giving rise to an assembly of two or more species, a supermolecule.[1]

In order to achieve high affinity and recognition, the factors mentioned in 1.2 must be taken into account in the design of the receptor. Complementarity requires a well-defined three dimensional architecture with the correct arrangement of binding sites that will be able to involve its guest in order to establish numerous non-covalent binding interactions. Thus it is convenient to use molecules that contain cavities, clefts or pockets into which the substrate may fit. These cavities, clefts or pockets should be “decorated” with numerous binding sites converging to its interior.

Macrocyclic and macropolycyclic structures are particularly suitable in this regard. The cavities defined by these types of compounds can be tailored to the appropriate size and shape, and provide means for the strategic spatial

arrangement of the binding sites. The balance between rigidity and flexibility can also be tuned by judicious choice of the building blocks that make up the receptor framework and is of particular importance for the binding and the dynamic properties of the ensemble.

The ingenuity of supramolecular chemists has conceived molecular receptors of extremely varied structural types, ranging from acyclic to macropolycyclic compounds. Their overall shape and appearance has led to the coining of several trivial names: podands, [18] crown ethers,[19] cryptands,[20] spherands,[21] cavitands,[22] carcerands,[23] calixarenes,[24] cryptophanes,[25] to name only a few (see Scheme 1.3). Despite obvious differences among their design, size, and molecular architecture, they all have cavities or clefts and can entrap guests.

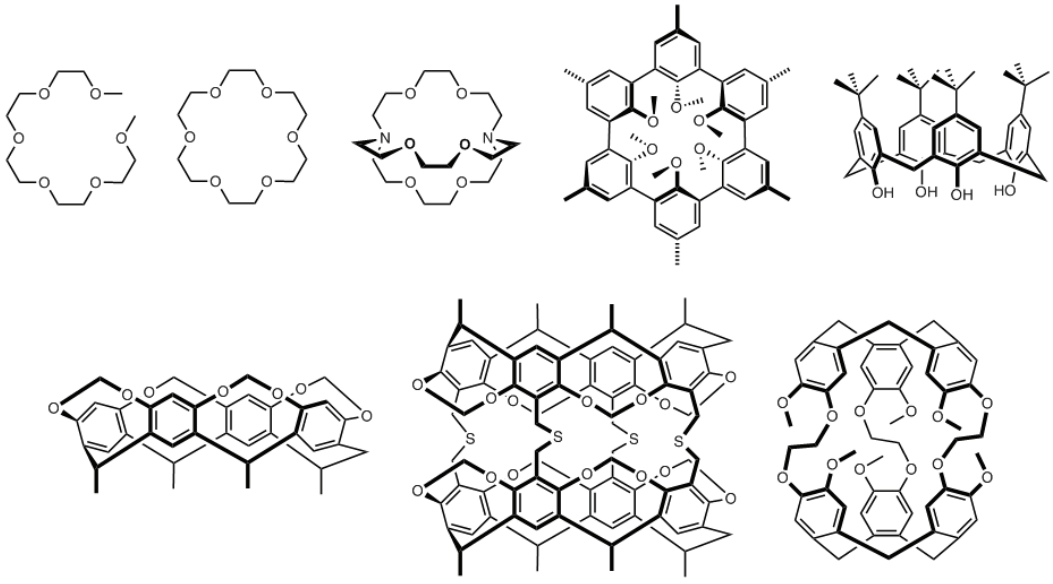

Scheme 1.3 Different types of receptors. Upper row, from left to right: podand, crown ether, cryptand, spherand and calixarene. Lower row from left to right: cavitand, carcerand and cryptophane.

Receptors can also be classified as monotopic, when possessing a single receptor unit and binding a single substrate and polytopic if containing two or more discrete binding subunits. The latter can still be divided into homotopic and heterotopic receptors depending on whether they contain identical or different binding subunits, respectively (Scheme 1.4).

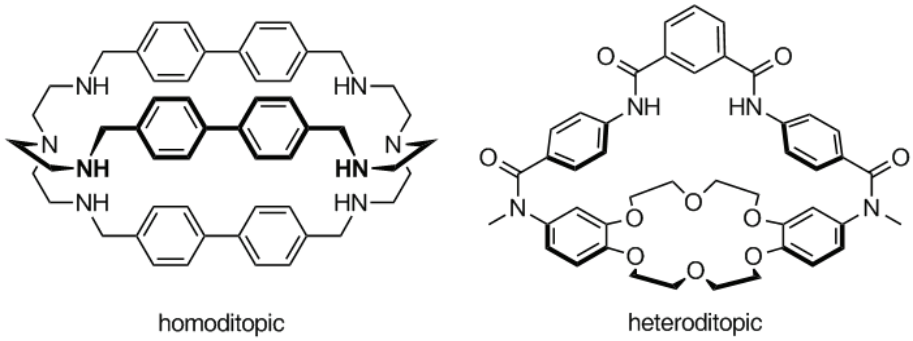

Scheme 1.4 Homoditopic and heteroditopic compounds.

1.2.6.1 The macrobicyclic architecture

A few years after Pedersen's discovery of crown ethers, Jean-Marie Lehn designed three-dimensional analogues, aiming to completely encapsulate metal ions and, therefore, to enhance cation selectivity.[26,27] Indeed the key for the success of macrobicyclic receptors is the preorganized, three-dimensional nature of their cavity, which can be able to encapsulate its substrate, completely replacing its solvation shell and isolating it from the surrounding medium. Macrobicyclic compounds are also known as cryptands for their ability to engulf or 'entomb' its substrate, as in a crypt.

In fact the main motivation to explore the macrobicyclic architecture in the present work was its ability to encapsulate substrates. In addition this architecture offers several different possibilities of design, associated with the relative ease of modification of its structural motifs, as will be shown in the next paragraphs.

Macrobicyclic receptors are constituted by three essential parts: the caps, the spacers and the binding sites (Scheme 1.5).

Caps and spacers are the building blocks that define the cavities in terms of size and shape, which is to be complementary to the substrates. Besides their structural function they can also interact with the substrates by π-π interactions or have hydrogen bond donors or acceptors themselves. In addition they can act as a reporter unit to signal the presence of the substrate by spectroscopic or electrochemical means. The binding sites can be of several types depending on

the substrate of interest, and can be for instance positively charged groups, hydrogen bond donors or acceptors, etc.

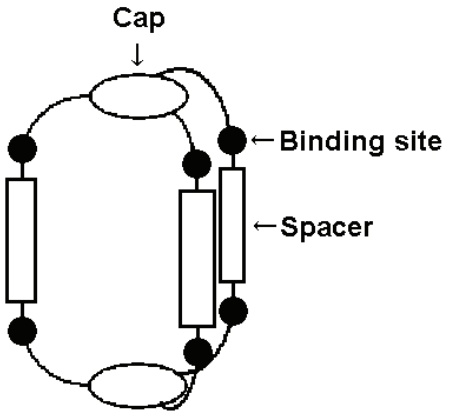

Scheme 1.5 General structure of macrobicyclic compounds.

Several different compounds can be designed by varying the constituent parts. Homoditopic cryptands are obtained if both caps are identical and are suitable receptors for symmetrical substrates, whereas if the caps are different the compounds are heteroditopic and may be useful for the recognition of asymmetric substrates and can also allow the simultaneous binding of cations and anions. The spacers may also be different from one another if the target substrate has several different binding groups.

1.2.6.2 Strategies of synthesis of macrobicycles

Among several strategies for the construction of the macrobicyclic arquitecture,[28] three of them are the most commonly used and are represented in Scheme 1.6.

Generally speaking, it is preferable to use procedures with the smallest number of steps for yield reasons. However, it should be noted that although more laborious, stepwise syntheses may provide intermediate compounds also with interesting binding properties. Steps creating several simultaneous connections are to be avoided due to the probability of polymer formation, which increases with the number of connections to be made, especially if these are

intermolecular. Thus routes containing the smallest number of cyclization steps are preferable.

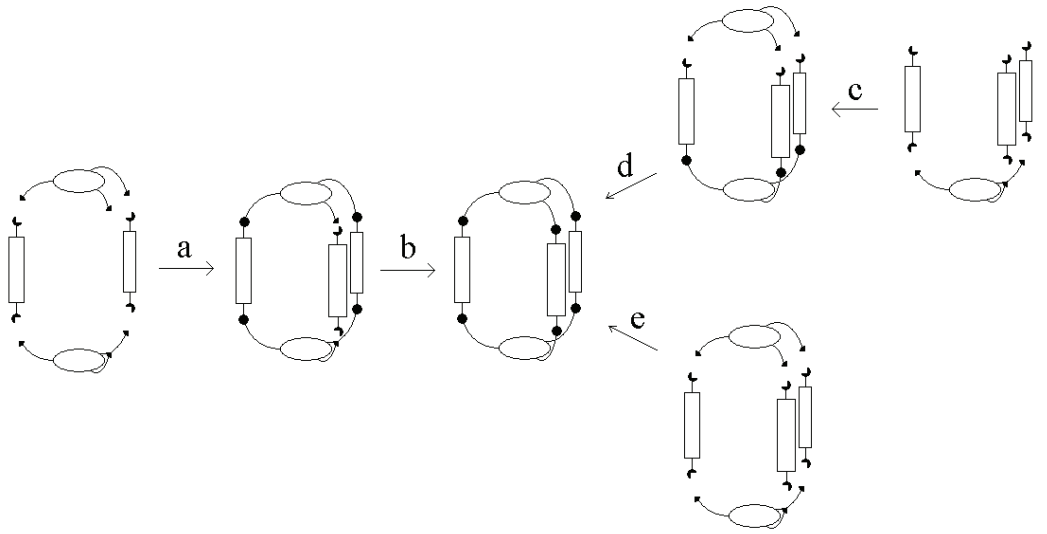

Scheme 1.6 Synthetic strategies (**a-b**, **c-d** and **e**) for the construction of the macrobicyclic architecture.

Route **a-b** consists in a stepwise process requiring first the formation of a macrocycle followed by a second cyclization to yield the macrobicycle. This route has the advantage of allowing the preparation of macrobicycles in which one of the spacers (represented as rectangles in Schemes 1.5 and 1.6) is different from the other two yielding heteroditopic compounds. In addition the macrocyclic intermediate may also be interesting as a receptor itself. The disadvantage is the requirement of two cyclization steps, although, in the second one, only two simultaneous connections are made. Route **c-d** is usually referred to as "tripod-tripod coupling" and consists in preparing first a tripodal intermediate followed by cyclization with another tripod. This path has the advantage over the previous one of requiring only one cyclization step and, of course, the tripodal intermediate may also be an interesting receptor. Following this procedure laterally non-symmetric heteroditopic compounds can be prepared if the two tripods are different. Path **e** is called "tripod capping" and is a "one pot" procedure. It is the most direct way to prepare a macrobicycle, however it consists in a cyclization where six bonds are formed simultaneously, thus the probability of polymer

formation is much higher than in the previous cases. Controlling the chemical nature, geometry and rigidity of the building blocks it is possible to minimize polymer formation and to achieve moderate to high yields. This path gives access to homoditopic compounds only.

1.3 Supramolecular chemistry of anions

1.3.1 Anions as targets for molecular recognition

Anions are ubiquitous species that play very important roles in biological, medicinal, industrial and environmental areas. Biochemically, anions are essential to normal metabolic function, as for instance both ATP and DNA are anionic, the specific recognition and transport of dicarboxylates across biological membranes is crucial in the metabolism of cells[29,30] and the sensing and signalling of amino acids play important roles in regulating cell functions.[31] In biomedical areas it is known that the disease cystic fibrosis is related to a dysfunction of chloride channels,[32] phosphate and sulfate homeostasis is necessary to be maintained in chronic renal disease patients[33,34] and the mechanism of action of the vancomycin antibiotic is highly dependent on carboxylate binding.[35] On the other hand, once released into the environment, anions pose significant threats. Anionic species such as nitrate, sulfate and phosphate coming form intensive use of fertilizers are pollutants of waterways, promoting eutrophication of rivers and lakes.[36] Other anions are extremely toxic such as arsenate, selenate and chromate and are present in wastewaters of industrial plants and radioactive pertechnetate, a product of the nuclear fuel cycle is also a matter of concern.[36] These are just a few examples of the importance of anions as the list could go on.

It is thus clear that the development of synthetic receptors capable to uptake anions can provide solutions to a number of problems of current interest, which is the reason why an increasing number of supramolecular chemists have been interested in this subject.[37-40]

1.3.2 The development of supramolecular chemistry of anions

In 1967/8 two papers were published in the Journal of the American Chemical Society which marked the beginning of Supramolecular Chemistry as a new field of research: Pedersen's article describing the first crown ethers and their cation binding abilities,[41] and Park and Simmons paper reporting the binding of chloride by a diammonium macrobicycle.[42] Pedersen's report immediately boosted the interest in alkali metal ion chemistry. Indeed just seven years later a Chemical Reviews article[19] already reflected the growth in the coordination of alkali metal ions and ammonium cations field, with a total of 221 different macrocyclic receptors included in the review. The same impact did not happen with the Park and Simmons paper, and the supramolecular chemistry of anions was and has been much slower to develop. It was only in the late 1970´s that the interest in this subject was reawaken by a series of papers by Jean-Marie Lehn and co-workers.[43-47] Indeed the first review only appeared in 1983[48] and included only 63 references. This lag stemmed not from failure to recognise the importance of anion recognition but is instead related with the intrinsic difficulties associated with anion binding, as will be discussed in 1.3.3.

1.3.3 Properties of anions

The slow start of the field of anion recognition is related with some intrinsic properties of anions that make them more difficult to encapsulate than cations.[40] Anions are significantly larger than the corresponding isoelectronic alkali metal ions and therefore require a larger receptor cavity for encapsulation which is more challenging from the synthetic point of view. Furthermore, the smaller charge/size ratio of anions also contributes to weaker electrostatic interactions with a receptor when compared with an isoelectronic cation. Anions usually have higher free energies of solvation than cations with the same absolute charge and comparable size, thus stronger interactions are required in water for a receptor to efficiently compete with the water molecules. Many anions are involved in protonation equilibria in aqueous solution and therefore receptors should be active in a pH window in which the anion is not protonated to take advantage of

the electrostatic interactions. Finally, anions exist in several different geometries such as spherical, linear, trigonal planar, tetrahedral, octahedral, or even more complicated as in the case of organic polyanions, which also has consequences in receptor design. It should be noted however that although usually taken as disadvantages the two latter characteristics of anions can also be used to achieve selectivity.

Although these properties have initially hampered faster development of anion recognition, in the last two decades there has been an explosion in this field, which means that ways of overcoming part of the difficulties have been developed.[37-40]

1.3.4 Natural anion receptors

Anion binding plays very important roles in natural systems, since it concerns essential aspects such as the activity of enzymes, the transport of hormones, protein synthesis and DNA regulation.[40] Biological molecular recognition provides study cases and inspiration for the understanding of basic principles of molecular recognition and for the design of model systems and new synthetic receptors. In the next points a few selected examples of anion recognition by biomolecules are described.

1.3.4.1 Chloride channels

The chloride channels catalyse the selective flow of Cl^- ions across cell membranes, thereby regulating electrical excitation in skeletal muscle and the flow of salt and water across epithelial barriers. Genetic defects in chloride channels are responsible for several muscle and kidney diseases. Chloride channels contain an ion-conducting pore in which its narrowest part functions as the selectivity filter of the anion channel. The structures of two chloride channels from *E. coli* and *S. typhimurium* have been determined.[49] As shown in Figure 1.2, Cl^- is bound solely by hydrogen bonding with backbone amide groups and side chain hydroxyl groups. It has been pointed out that the absence of positive charges directly interacting with the anion, that would cause stronger binding,

contributes for the fast association/dissociation rates required for anion transport through membranes.

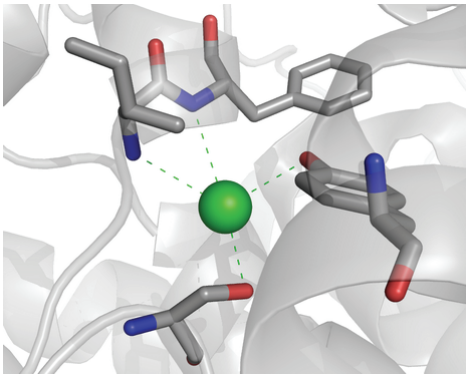

Figure 1.2 Binding site of the chloride channel from *S. Typhimurium*.

1.3.4.2 Sulfate and phosphate binding proteins

The sulfate and phosphate binding proteins (SBP and PBP, respectively) are members of a family of periplasmic proteins that act as receptors for their respective anionic substrates and are involved in the high affinity active transport system to uptake these nutrients into bacteria cells. The structures of SBP from *S. typhimurium* and of PBP from *E. coli* have been determined using X-ray crystallography.[50,51]

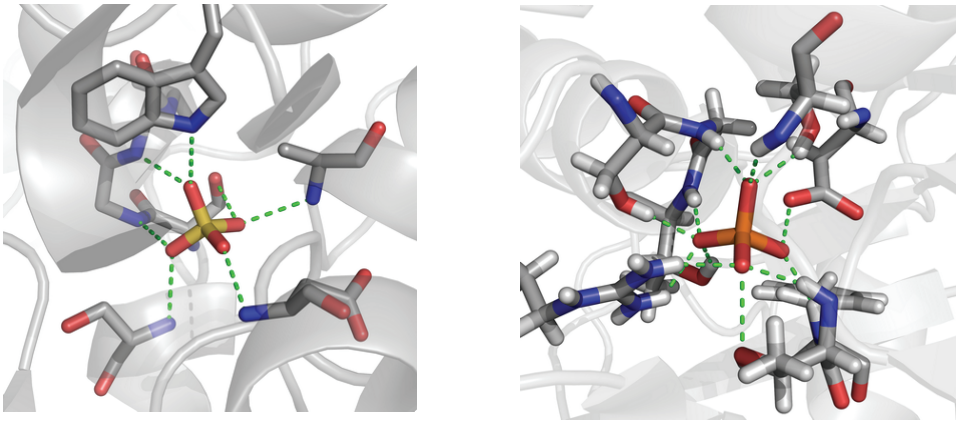

(a) (b)

Figure 1.3 Binding site of SBP from *S. typhimurium* (a) and PBP from *E. coli* (b).

SBP and PBP tightly bind their substrates with a network of 7 and 12 hydrogen bonds, respectively, in the interior of deep clefts completely

inaccessible to the solvent (Figure 1.3). The presence of the carboxylate group of an aspartate residue that functions as a hydrogen bond acceptor for the phosphate OH in PBP is perhaps the most important difference between these proteins. Indeed it allows PBP to discriminate phosphate from other similar tetrahedral oxyanions such as sulfate, which in normal pH lacks OH groups and additionally is repelled by the carboxylate negative charge. Conversely SBP has no hydrogen bond acceptors making it unsuitable for protonated oxyanions.[52]

1.3.4.3 Nitrate and bicarbonate binding proteins

Nitrate and bicarbonate binding proteins (NrtA and CmpA, respectively) are two highly homologous proteins that are members of the same family of periplasmic proteins as SBP and PBP. The crystal structures of NrtA and CmpA from *Synechocystis* 6803, associated to their respective substrates have been reported.[53,54] Both proteins bind the corresponding anions in nearly an identical location.

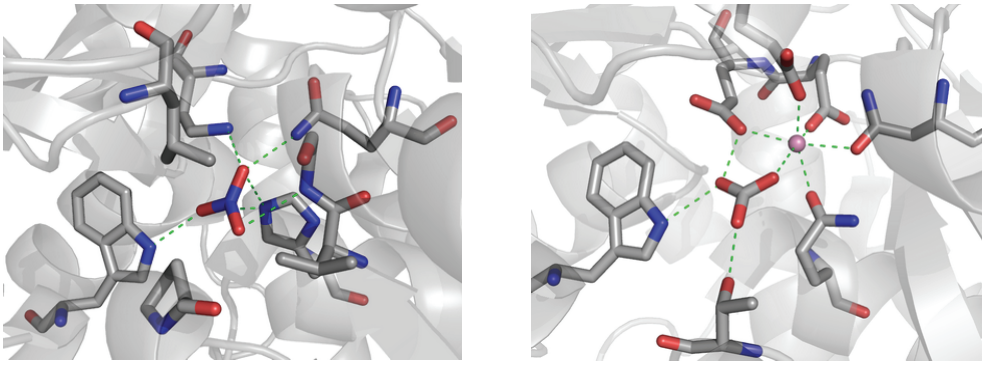

(a) (b)

Figure 1.4 Binding site of NrtA (a) and CmpA (b) from *Synechocystis* 6803.

As shown in Figure 1.4a nitrate is surrounded by hydrophobic residues leucine, proline and valine which shield it from interactions with the solvent. The anion is bound through electrostatic and hydrogen bonding interactions provided by NH of the proteins backbone amides, glycine, histidine and tryptophan.

The most striking difference between NrtA and CmpA is the substitution of a lysine residue of NrtA by a glutamate in CmpA. In NrtA, lysine complements the

negative charge from nitrate while the substitution to glutamate in CmpA inhibits nitrate binding due to charge repulsion. In addition, glutamate in CmpA provides a hydrogen bonding acceptor for the hydroxyl group of bicarbonate and also contributing to the binding of Ca^{2+}, which in turn replaces the positive charge of lysine in NrtA. Thus it seems that the anion selectivity for these two proteins is mostly based on a single amino acid substitution.

1.3.4.4 Periplasmic sensor domain of *Sinorhizobium meliloti*

The periplasmic sensor domain of *Sinorhizobium meliloti* (DctB) is part of the C_4-dicarboxylate transport (Dct) system which is able to monitor the external concentration of C_4-dicarboxylic molecules (succinate, L-malate, fumarate, etc) which are utilized as energy sources during the symbiotic growth of rhizobia. Crystal structures of DctB in the unbound form and in association with succinate and malonate have been determined recently.[55]

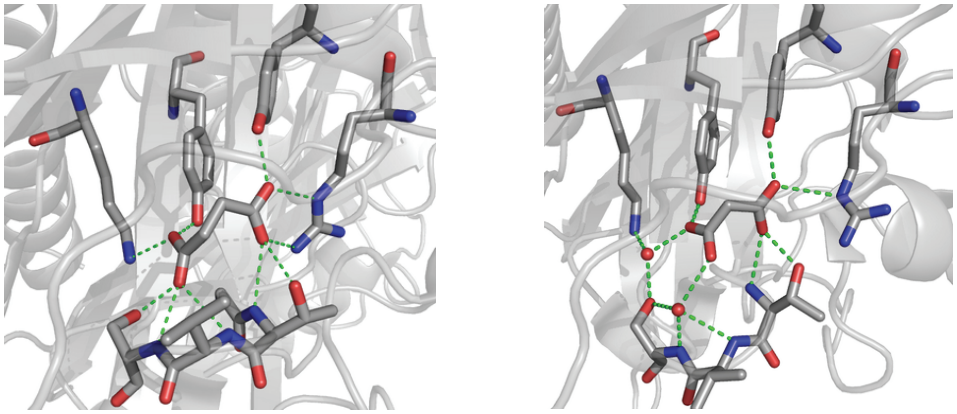

(a) (b)

Figure 1.5 Binding site of DctB from *Sinorhizobium meliloti* occupied by succinate (a) and malonate (b).

Succinate is tightly bound by a network of hydrogen bonds involving the side chains of arginine, lysine, tyrosine, threonine and serine residues and each of the carboxylate groups is bound by a positively charged residue through electrostatic interactions (Figure 1.5a). When succinate is bound, the binding pocket is tightly closed to exclude water access. On the other hand, when the smaller dicarboxylate malonate is bound (Figure 1.5b), the binding pocket becomes more

relaxed, adopting a conformation very similar to that of the *apo* structure. In addition, only one of the carboxylate groups is directly interacting with a positively charged arginine, while the other carboxylate is loosely bound to two water molecules that mediate the hydrogen bonding networks between malonate and the protein. It was concluded that C_3-dicarboxylates, such as malonate, do not bind as tight as the C_4-dicarboxylates, and do not induce conformation changes large enough to trigger subsequent signal transduction events.

1.3.4.5 Menaquinol:fumarate oxidoreductase

Menaquinol:fumarate oxidoreductase (QFR) is an enzyme that catalyzes the oxidation of menaquinol and transfers the electrons to fumarate in bacterial anaerobic respiration. Crystal structures of *E. coli* QFR bound to the substrate, fumarate, and to the inhibitors oxaloacetate and glutarate were reported very recently (Figure 1.6).[56]

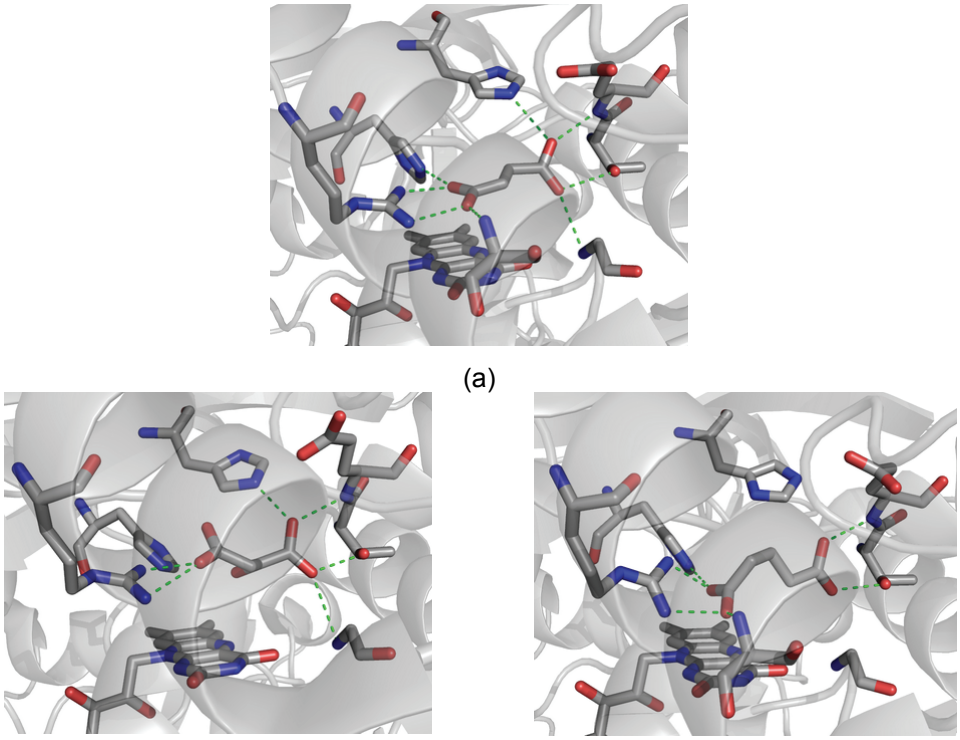

(a) (b) (c)

Figure 1.6 Binding site of QFR from *E. coli* occupied by fumarate (a), oxaloacetate (b) and glutarate (c).

Fumarate is stabilized in a tortioned conformation by seven hydrogen bonds in addition to electrostatic interactions with the side chains of two histidines and one arginine (Figure 1.6a). The structure of QFR associated with the inhibitor oxaloacetate shows that this dicarboxylate binds in a position similar to that of fumarate (Figue 1.6b). In addition, the oxaloacetate carbonyl is positioned laterally, such that the C2 carbonyl is nearly parallel with an adjacent bond of the flavin adenine dinucleotide cofactor (FAD), allowing a charge transfer interaction which presumably accounts for a higher affinity for oxaloacetate than for fumarate. Glutarate, due to its bigger size and higher flexibility is bound in a tortioned conformation stabilized only by five hydrogen bonds, two less than fumarate and oxaloacetate (Figure 1.6c). In addition it was predicted that glutarate has less favourable steric interactions, making it bound less tightly than other QFR substrates.

1.3.5 Synthetic anion receptors

Although inspiration is taken from examples of highly specific anion binding by biomolecules it should be noted, however, that chemistry is not limited to the mimicry of biological systems. The creation of new compounds and processes depends only on the imagination and ingenuity of chemists. Indeed a plethora of different receptors for anions has been devised over the years, with a variety of topologies that range from acyclic to mono and polycyclic structures.[37-40]

Similarly to natural anion receptors, synthetic ones take advantage of positively charged residues,[57-61] Lewis acids[62-66] and hydrogen bond donors[67-73] to bind anionic substrates (Scheme 1.7).

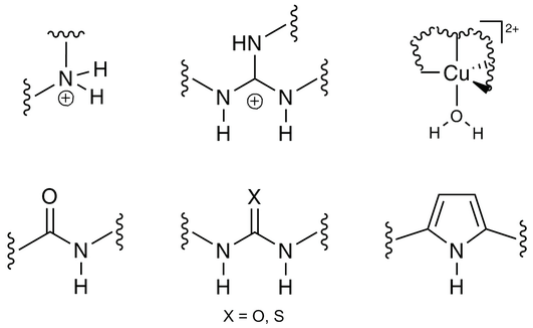

Scheme 1.7 Examples of the most common anion binding sites.

1.3.5.1 Neutral receptors

Neutral anion receptors rely on hydrogen bond donors such as amide, urea, thiourea and pyrrole, used alone or in combination (Scheme 1.8).[67-73]

Although these compounds have the advantage over charged ones of not suffering competition from counterions and being pH independent, they have the disadvantage of hydrogen bonding interactions in polar media being very weak. However, by combining several hydrogen bond donors arranged in a convergent way it is possible to achieve good affinity for anions. Biomolecules, such as the sulfate-binding protein, binds its substrate exclusively by hydrogen bond donation, however it uses a total of seven convergent hydrogen bonds, and additionally the substrate is buried in a deep cavity of low polarity, which is well shielded from the surrounding solvent (see 1.3.4.2). Most neutral receptors can only act in non polar or non protic media,[74] however they may be able to transport anions across membranes and eventually possess biological activity.

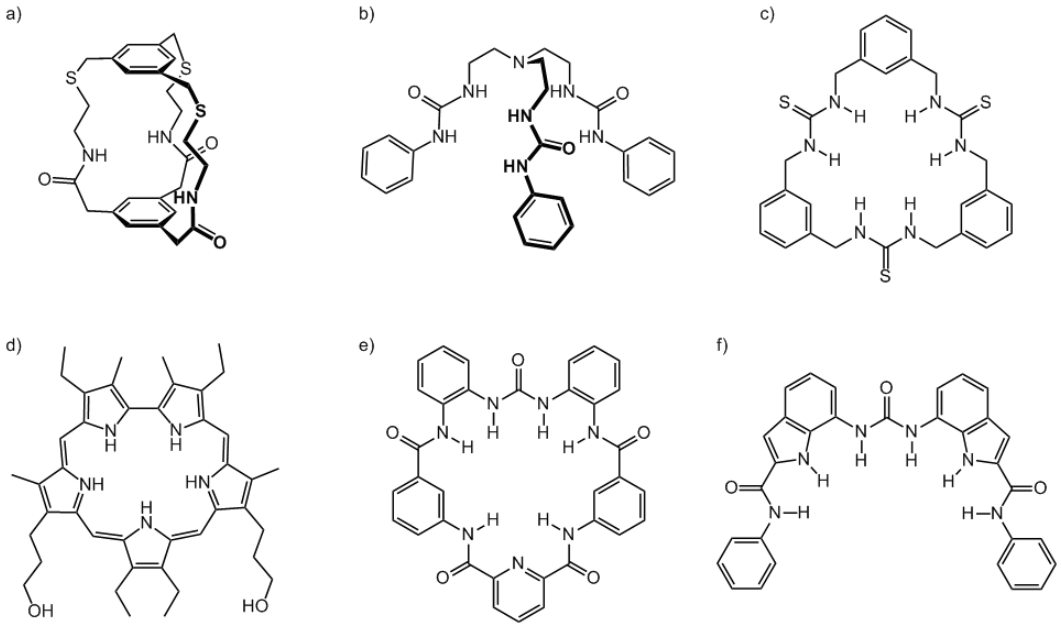

Scheme 1.8 Examples of neutral anion receptors: a) amide based macrobicycle;[75] b) urea based tripodal compound;[76] c) thiourea based macrocycle;[77] d) pyrrole based receptor;[78] e) urea/amide based macrocycle;[79] f) amide/urea/pyrrole based podand.[80]

1.3.5.2 Charged receptors

Using oppositely charged groups in a receptor is clearly the most obvious strategy to bind anions. Positively charged and hydrogen bond donor residues, such as ammonium and guanidinium groups, are common in both natural and synthetic receptors.[57-61] In Scheme 1.9 some examples of charged receptors are illustrated.

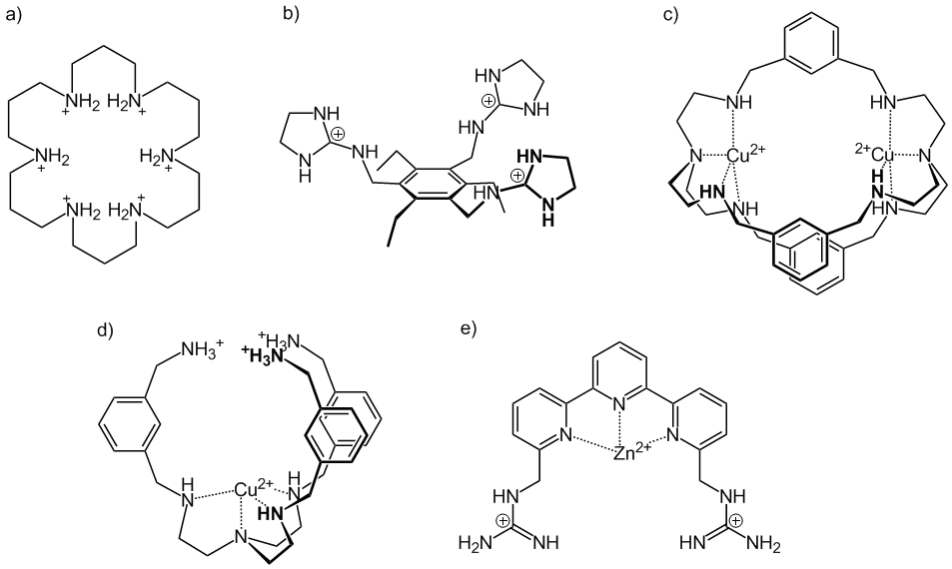

Scheme 1.9 Examples of charged anion receptors: a) macrocyclic polyammonium compound;[81] b) polyguanidinium tripodal compound;[82] c) dinuclear copper macrobicyclic complex;[83] d) tripodal copper complex combined with ammonium binding sites;[84] e) podand copper complex combined with guanidinium binding sites.[85] The charges are localized to better indicate the positively charged moieties of the molecules.

Receptors containing these groups have the advantage of being able to function in aqueous solutions by combining strong electrostatic interactions with the directionality of hydrogen bonds. Lewis acids have also been frequently incorporated in the receptors framework and have the advantage of providing even stronger interaction than electrostatic attraction besides being highly directional.[62-66] In addition there are also receptors that combine several of these binding sites.

Because charged receptors are usually able to form anion associations in aqueous solution, they may be useful in medical diagnostics, in the analysis of biological systems or in environmental monitoring.

1.3.5.2.1 Amine based receptors

The negative charge of anions is of course the primary feature to be considered in their recognition, thus, receptors have been conceived that take advantage of oppositely charged groups placed in appropriate dispositions within the receptor framework. As seen in 1.3.4, biological systems use the side chains of basic amino acids like lysine and arginine for this purpose. Lysine's side chain contains a protonable amino group which provides the necessary positive charge to interact with the anion and can also donate hydrogen bonds. Also, biogenic putrescine, spermidine and spermine are aliphatic polyamines that when protonated can interact with negatively charged groups of DNA, RNA and nucleotides.[86]

Polyamines are in fact one of the most successful groups of compounds used as receptors for the binding of anions in aqueous media. This is due to the versatile nature of the amino group that can be protonated to provide the necessary positive charge to interact with anions and to impart water solubility.[57-59] The amino group can also act as hydrogen bond acceptor and as hydrogen bond donor when protonated. Polyamines can coordinate transition metal ions and thus provide the opportunity to incorporate metal ions in a receptor framework.[62] Not surprisingly the first anion receptors belong to this class of compounds (Scheme 1.10).[42-44]

Scheme 1.10 First reported anion receptors, "katapinand",[42] "soccer ball cryptand[43] and O-bistren[44]

Despite all the already mentioned advantages of ammonium groups in anion receptors, they also suffer from some drawbacks, one of them being the pH dependence.[87] Polyammonium anion receptors usually contain several amine groups in relatively close distance to one another. As amines become protonated

the build up of positive charge in the receptors cavities causes repulsion between ammonium groups which lowers their basicity. Due to this effect sometimes a receptor is not fully protonated until the pH is acidic, which may be disadvantageous for the binding of weakly acidic carboxylates that may not be completely deprotonated. Another problem related with the mutual repulsion of ammonium groups is the effect on the receptor conformation. In fact protonated amine groups tend to move away from each other causing the molecular framework to expand and to adopt conformations where the ammonium groups are turned to the outside of the cavity, thus, losing the convergence of binding sites necessary for anion encapsulation. Finally, every charged species requires a counterion, which in the case of ammonium groups is an anion that can potentially compete with the desired substrate. Usually it is necessary to choose a counterion that interferes the least possible with the association of the substrate of interest. Despite the above mentioned drawbacks, over the years amino groups have been incorporated in a variety of different topologies, from acyclic structures to mono and polycyclic architectures (Scheme 1.11) and studied as receptors of anions.[57-59]

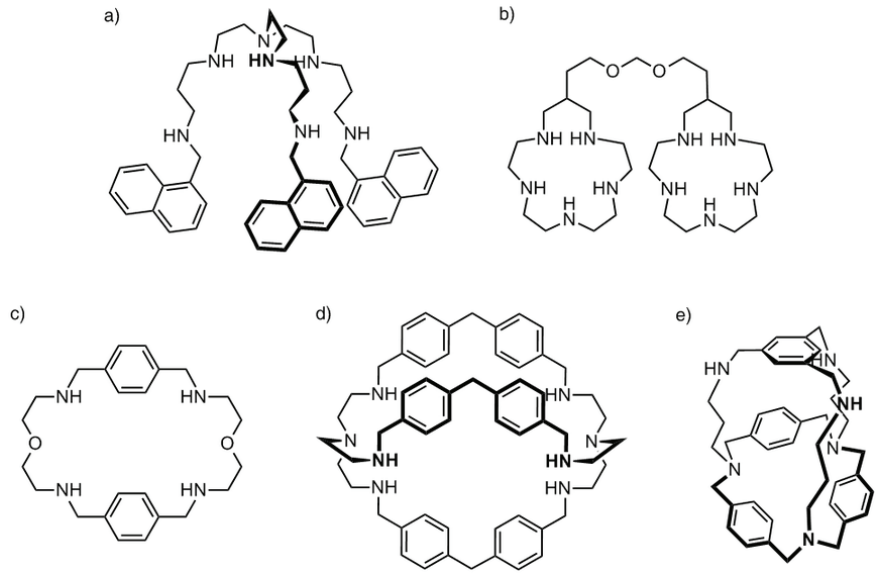

Scheme 1.11 Examples of polyamine compounds of different topologies used as anion receptors in their protonated forms: a) tripodal;[88] b) bis-macrocyclic;[89] c) macrocyclic;[90] d) macrobicyclic[91] and e) macrotricyclic.[92]

1.3.5.2.2 Polyamine macrobicycles

Polyamine macrobicycles were the first type of compounds to be used in anion recognition and have been much used since then.[93-95] The reason for this stems from both the binding properties of the ammonium group and the encapsulating abilities of the macrobicyclic architecture (see 1.2.6.1 and 1.3.5.2.1). Moreover many synthetic strategies were devised for the construction of the macrobicyclic architecture (see 1.2.6.2)[28] and several techniques are available for the formation of C–N bonds,[96] which makes this type of compounds relatively easily accessible.

1.3.5.2.2.1 Synthesis of polyamine macrobicycles

The synthesis of macrobicyclic polyamines has been largely based on the formation of the C–N bond by reaction of amines or sulfonamides with strong electrophiles such as halogeno compounds, aldehydes, acid chlorides and tosylates (*p*-toluenesulphonates). The cyclization step is usually followed by a reduction or a deprotection step.[96]

The first reported amine based macrobicyclic compound was prepared as outlined in Scheme 1.12.[42]

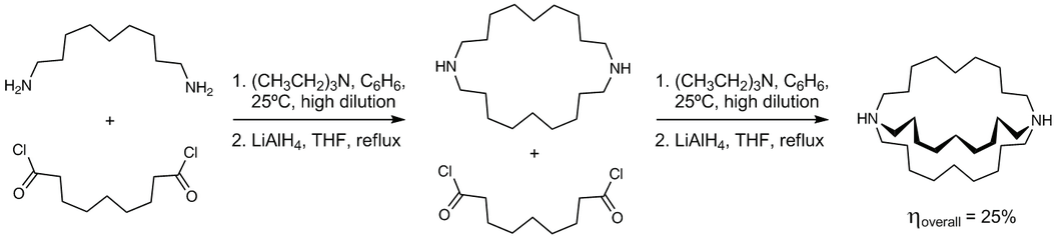

Scheme 1.12 First synthesis of a diaza macrobicyclic compound.

This synthesis follows route **a-b** represented in Scheme 1.6. First, a cyclization step was performed by reaction of a diamine with a diacid chloride in high dilution conditions, followed by reduction of the resulting amide carbonyl with lithium aluminium hydride, in a procedure first described by Stetter.[97] Next a second cyclization is performed by reaction of the diaza macrocycle with a diacid chloride, also under high dilution conditions and followed again by reduction.

A few years later Richman and Atkins published a procedure to prepare macrocyclic amines without requiring high dilution conditions that employed the reaction of a tosylated amine with a mesylated or tosylated alcool,[98] which after deprotection afforded the free amines. The toluenesulfonamide enhances the acidity of the secondary N–H making the amine a better nucleofile and it also acts as a nitrogen protecting group, allowing monoalkylation at the nitrogen atom.

The O-bistren macrobicycle, one of the most used in anion recognition, was initially prepared by the Stetter method in ten steps and overall 7% yield.[99] Adaptation of the Richman-Atkins procedure to the synthesis of O-bistren (Scheme 1.13) followed route **c-d** depicted in Scheme 1.6 and allowed the compound to be obtained in seven steps with an increase of the overall yield to 12%.[100]

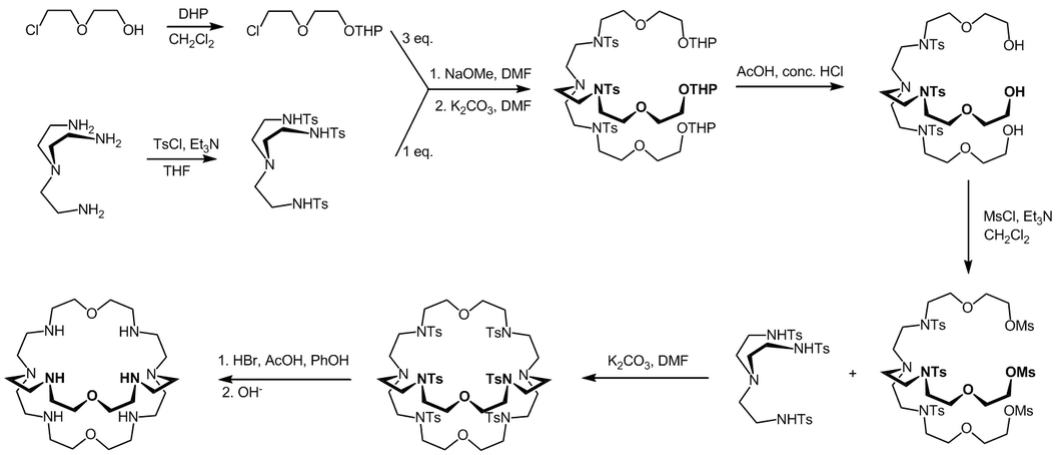

Scheme 1.13 Synthesis of O-bistren by a modified Richman-Atkins procedure.

In 1987 Lehn *et al.* took advantage of the Schiff base condensation reaction between a triamine and an aromatic aldehyde and following the path **e** represented in Scheme 1.6 prepared the cyclophane type hexaimine macrobicyclic compound shown in Scheme 1.14. After reduction with $LiAlH_4$ in THF the hexamine compound was obtained in 70% overall yield, an extraordinary result taking into account the simultaneous formation of six bonds.[91]

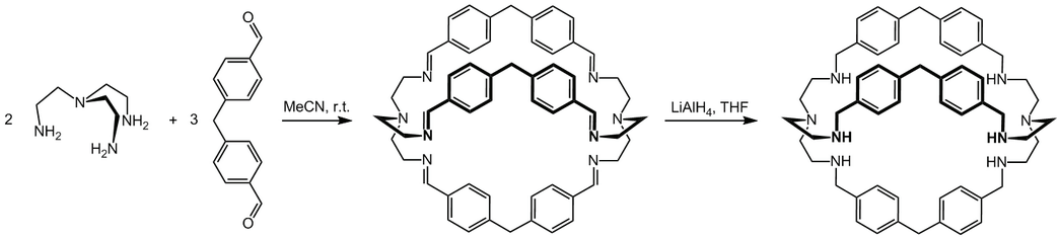

Scheme 1.14 Synthesis of a macrobicyclic polyamine by Schiff base condensation followed by reduction.

Shortly after Nelson *et al.* published the synthesis of four other hexaimine compounds following a similar procedure.[101] In 1991 Chen and Martell reported the reduction of the previous hexaimines using a mild reducing agent $NaBH_4$.[102]

The easy accessibility and high yields of these compounds in comparison with the aliphatic counterparts gave a large contribution to growth of the area of anion recognition.[94,95]

1.3.5.2.2.2 Polyamine macrobicycles as anion receptors

As anion receptors, polyamine macrobicycles have been shown to have some advantages over their macrocyclic counterparts.[103] When comparing macrocycles and cryptands with the same number of amine groups that differ from each other only in the added dimensionality, and have been studied for the same anionic substrates, it is possible to conclude that, in general, the macrocycle of each pair of receptors can bind a large variety of anions, although without any particular selectivity for series of substrates having the same number of identical functional groups. By contrast, the corresponding cryptand, which has a three-dimensional cavity, can be extremely selective when the match between shape and size of the partners is reached and complementarity of interactions also exists. In these cases the substrate is encapsulated into the cavity of the receptor. Because solvent release by both receptor and anion is an important driving force in the association process, the cryptands, having a tri-dimensional cavity are likely to enclose more water molecules than the corresponding macrocycles and thus may benefit from more favorable entropic contributions upon solvent release. Of course that on the other side of the coin the enthalpic

cost of desolvation should be higher than in the case of macrocycles. This may account for the fact that in general the binding constants of the cryptands are not much higher than those of the macrocycles. In fact, the added dimensionality of the cryptands results more in an increase of selectivity than in higher association constants. The selectivity may result from the complete displacement of the water molecules from the inside of the cryptand cavity by the anion that in turn requires the match of shape and size of the cryptand in order that the anion takes advantage of all the receptor binding sites.[103]

Another interesting advantage of polyammonium cryptands over macrocycles is that in the first, the positive charges are better distributed around the cavity and the repulsion between ammonium positive charges is attenuated, being almost completely protonated at pH about 6. At this pH value most of the anions are completely deprotonated allowing a strong interaction. By contrast, the macrocycles are only completely protonated at pH about 4, allowing in most cases only stronger interactions with protonated forms of the anions, which are less charged thus decreasing the binding constant.

Polyammonium cryptands with aliphatic spacers were the first to be developed and the more extensively studied as anion receptors (Scheme 1.15).[94,95]

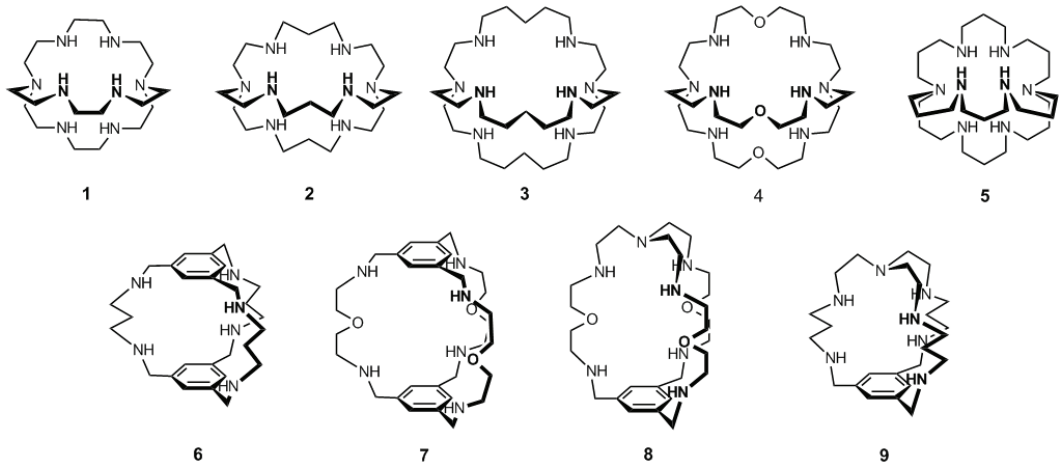

Scheme 1.15 Polyamine cryptands with aliphatic spacers used as anion receptors in their protonated forms.

The cryptand **1** exhibits an extraordinary selectivity for F^- over Cl^- (about 7 orders of magnitude) in aqueous solution.[104] The crystal structure of the fluoride cryptate (Figure 1.7a)[104,105] and the magnitude of the fluoride binding constant with $H_6\mathbf{1}^{6+}$ strongly suggest that this anion binds inside the cryptand cavity in aqueous solution. ^1H NMR titration with, Cl^-, Br^- and I^- at 4.0 pD value indicated little changes from that observed for the receptor, $H_6\mathbf{1}(TsO)_6$, suggesting that only fluoride is encapsulated [106] However, single crystal X-ray diffraction showed that $H_6\mathbf{1}^{6+}$ can also encapsulate the Cl^- anion (Figure 1.7b)[107] but the crystals where prepared in very acid pH and with large excess of anions and thus is not comparable to what happens in solution. Crystal structures of the association of $H_6\mathbf{1}^{6+}$ with Br^- and I^- (Figure 1.7b and c) revealed the anions outside of the cavity.[106-108]

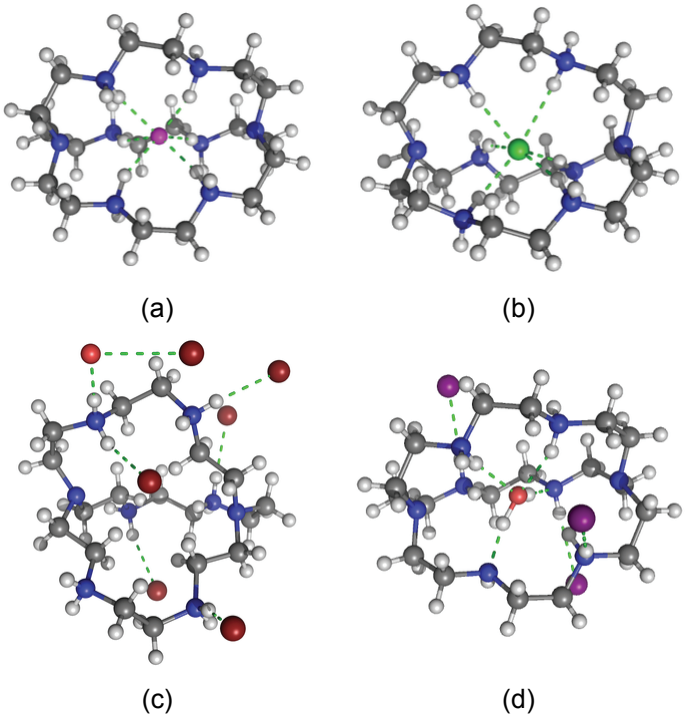

Figure 1.7 Crystal structures of the supermolecules formed by F^- (a) and Cl^- (b) anions with $H_6\mathbf{1}^{6+}$ receptor, in (c) of $H_6\mathbf{1}^{6+}$ in presence of Br^- with the Br^- anions outside the cavity, and in (d) the structure of the included H_2O into the cavity of $H_4\mathbf{1}^{4+}$ receptor with several iodide anions outside the cavity.

Interestingly with cryptand **2**, a slightly extended version of cryptand **1**, the selectivity for F^- over Cl^- drops dramatically to a K_{F^-}/K_{Cl^-} of only 2.24 in aqueous solution.[104]

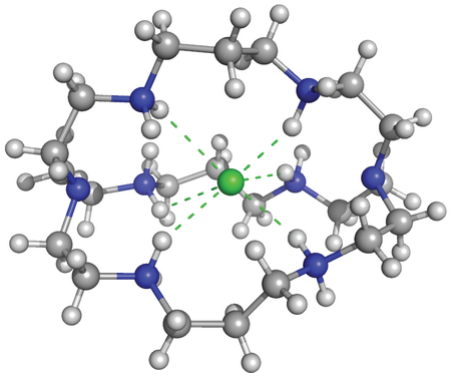

Figure 1.8 Crystal structure of the supermolecule formed by Cl^- anion with $H_6\mathbf{2}^{6+}$ receptor.

This means that the cavity is now too large to provide selectivity for the smaller F^- anion, while better accommodating the Cl^- (Figure 1.8) which is much stronger bound by $H_6\mathbf{2}^{6+}$ than by $H_6\mathbf{1}^{6+}$ (log $K_{H_6\mathbf{2}\,(Cl^-)}$ = 5.75; log $K_{H_6\mathbf{1}\,(Cl^-)}$ < 2).

Further increasing the aliphatic chain of the spacer yields cryptand **3**. The expansion of the cavity afforded enough room for the binding of two fluoride anions instead of only one (Scheme 1.16).[109] Although there is no crystal structure of this supermolecule, potentiometric data support the representation depicted in Scheme 1.16, where each fluoride anion is bound to a tren cap and a proton bridges the two anions.

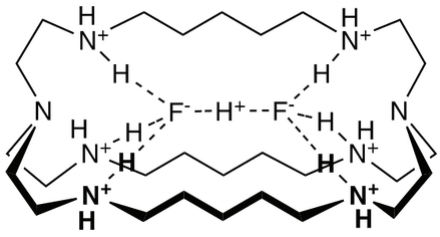

Scheme 1.16 Representation of bifluoride binding by $H_6\mathbf{3}^{6+}$.

The cryptand with diethylylether spacers **4** is also able to bind several monovalent anions in water, with F^- and N_3^- displaying the highest binding constants with $H_6\mathbf{4}^{6+}$, the selectivity trend being ClO_4^- < I^- < HCO_2^- < Br^- < NO_3^- <

Cl^-, < F^- < N_3^- [110] The highest constants found for F^-, in comparison with the other halide anions, is due to its high charge density. Very interesting X-ray structures of $H_6\mathbf{4}^{6+}$ with F^-, Cl^-, Br^- and N_3^- (Figure 1.9) revealed the topological discrimination of the receptor.[110] It is interesting to notice that although cryptand **4** has about the same size and shape as cryptand **3,** the crystal structure of its fluoride association (Figure 1.9a), as well as the potentiometric data, revealed a 1:1 binding mode.

$H_n\mathbf{4}^{n+}$ is also able to bind oxa^{2-} and mal^{2-} in aqueous solution, showing a marked preference for oxalate.[110] Studies have also been performed regarding the binding ability of $H_n\mathbf{4}^{n+}$ towards mono and polyphosphates, as well as towards phosphate nucleotides AMP, ADP and ATP.[110] In these cases the anion binding is strongly dependent on electrostatic interactions between the negative oxygen atoms of the anions and the positive ammonium groups of the receptor, to which are also associated an extensive hydrogen bonding formation N^+–H···$^-$O. The most stable associations were formed between the most charged species, the strongest binding interaction being with $HP_2O_7^{3-}$ suggesting a better accommodation into the cryptand cavity.

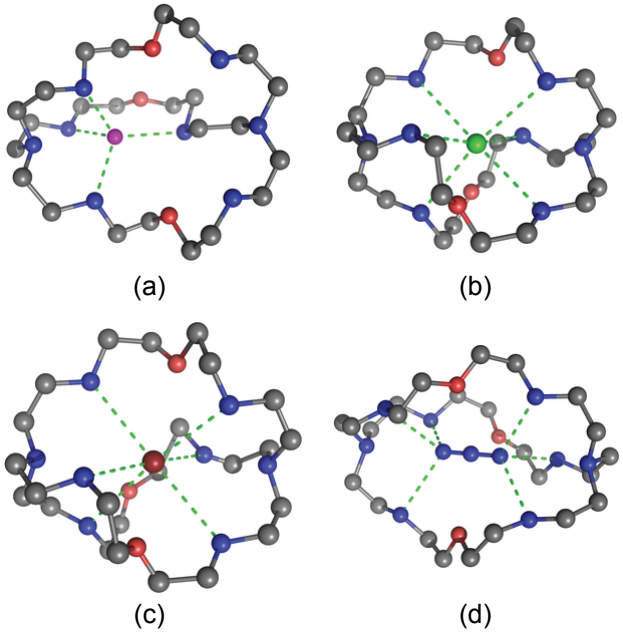

Figure 1.9 X-ray structures of the association of $H_6\mathbf{4}^{6+}$ with F^- (a), Cl^-(b), Br^- (c) and N_3^- (d).

The cryptand **5** is different from the previous compounds because the caps are tris-(aminopropyl)amine (trpn) derived. This feature allows the protonation of all eight amine groups since these are sufficiently distanced to avoid or minimize the electrostatic repulsion between positive charges. As a consequence, the cryptand is able to be completely protonated at a higher pH.[111] The protonated forms of **5** are capable to bind the halides following the trend $I^- > Br^- > Cl^-$, indicating that the binding is not governed only by electrostatic interactions but the match of sizes of the cavity and the substrate should also play an important role.[111] In fact, the large and spherical cavity with an almost symmetrical distribution of charged sites of $H_8\mathbf{5}^{8+}$ may accommodate well the spherical and smaller charge density I^- anion. However $H_8\mathbf{5}^{8+}$ is unable to discriminate I^- from a mixture of the three halides as shown in Figure 1.10a, even though it exhibits a clear preference for the larger anion. On the other hand, if SO_4^{2-} is added to the mixture of halides this cryptand selectively uptakes the sulfate from the aqueous solution, as shown in Figure 1.10b.[111]

A better fit of oxa^{2-} into the cavity of $H_8\mathbf{5}^{8+}$ and an incomplete encapsulation of mal^{2-} anion allows the receptor to discriminate oxa^{2-} from mal^{2-} in water.[111]

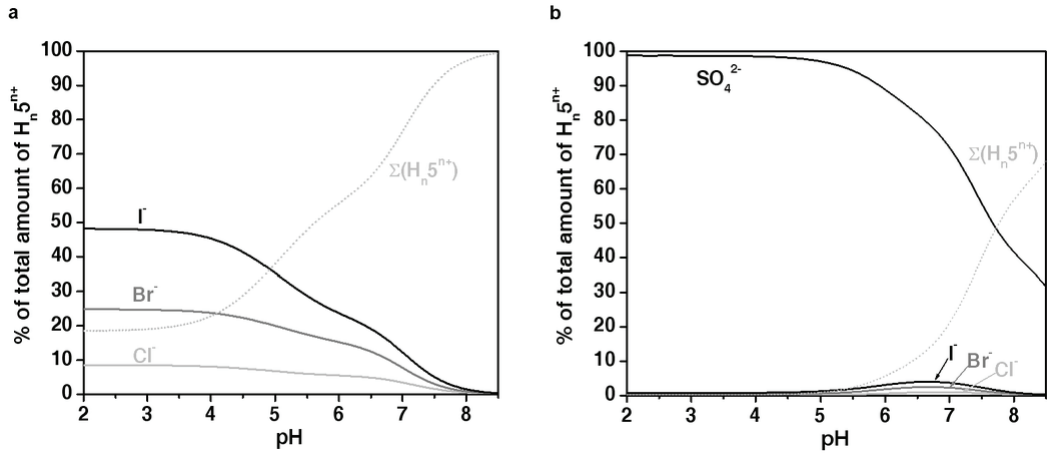

Figure 1.10 Distribution diagrams of the overall amount of supramolecular species formed between $H_n\mathbf{5}^{n+}$ and the mixture of halide anions, Cl^-, Br^- and I^- in the 1:1:1:1 ratio (a) and a mixture of the halides and sulfate (b). $C_{cryp} = C_{A^-} = 2\times10^{-3}$ mol dm^{-3}.

Two benzene capped analogs of cryptands **2** and **4** have been prepared by Heyer and Lehn, as well as a “hybrid” cryptand having a tren cap and a benzene

cap (cryptands **6**, **7** and **8** in Scheme 1.15).[112] These where found to form 1:1 associations with Cl^-, NO_3^-, N_3^-, SO_4^{2-}, $S_2O_6^{2-}$ and oxa^{2-} in aqueous solution, as determined by potentiometry and ^{1}H-NMR. The association constants lie in the range of 2.5–4.0 log units for the monoanions and 5.0–6.5 log units for the dianions. Unfortunately the authors did not specify the association constants for each compound with each anion, thus it is not possible to compare the binding behaviour of cryptands **2** and **4** with cryptands **6** and **7** which would allow evaluating the influence of the introduction of the substitution of the tren caps by the benzene ones.

More recently Steed *et al.* reported the synthesis and binding ability towards halides of cryptand **8**, a mixed tren/benzene capped compound.[113] The study revealed and extraordinary increase of five orders of magnitude in F^-/Cl^- selectivity for $H_6\mathbf{8}^{6+}$ in relation to the similar receptor $H_6\mathbf{2}^{6+}$, in aqueous solution.

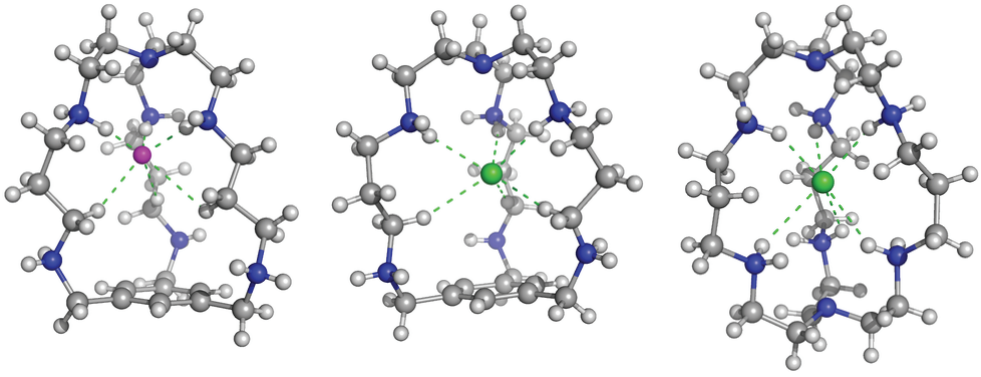

(a) (b) (c)

Figure 1.11 Crystal structure of the supermolecules formed by association of F^- (a) and Cl^- (b) anions with receptor $H_6\mathbf{8}^{6+}$. Crystal structure of and $[H_6\mathbf{2}(Cl)]^{5+}$ (c) is also presented for comparison.

This increase in selectivity takes place despite the fact that crystallographic data revealed that the anions are bound *via* only three ammonium groups coupled with three C–H hydrogen bond donors (Figure 1.11). Apparently the benzene cap places the adjacent amines out of the range for H–bonding, and the halide anions have short contacts with C–H hydrogen atoms. The authors claimed that the higher preorganization of cryptand **8** conferred by the benzene cap compensates the lower intrinsic hydrogen bonding ability of C–H groups. The

associations of $H_6\mathbf{8}^{6+}$ with Br^- and NO_3^- were too low to be detected by potentiometry.

Aromatic units were also used as spacers in the construction of macrobicyclic polyamines (Scheme 1.17). These spacers confer rigidity to the cryptand which may allow better preorganization besides the possibility of interaction with the substrates. Independent work of Lehn,[91] Nelson[101] and Martell[114] have shown that polyamine cryptands with aromatic spacers are more easily prepared than their aliphatic analogs by using simple Schiff's base condensation. This gave further impetus to the anion recognition field with several of this type of compounds being prepared and studied as anion receptors in their protonated forms.[94,95]

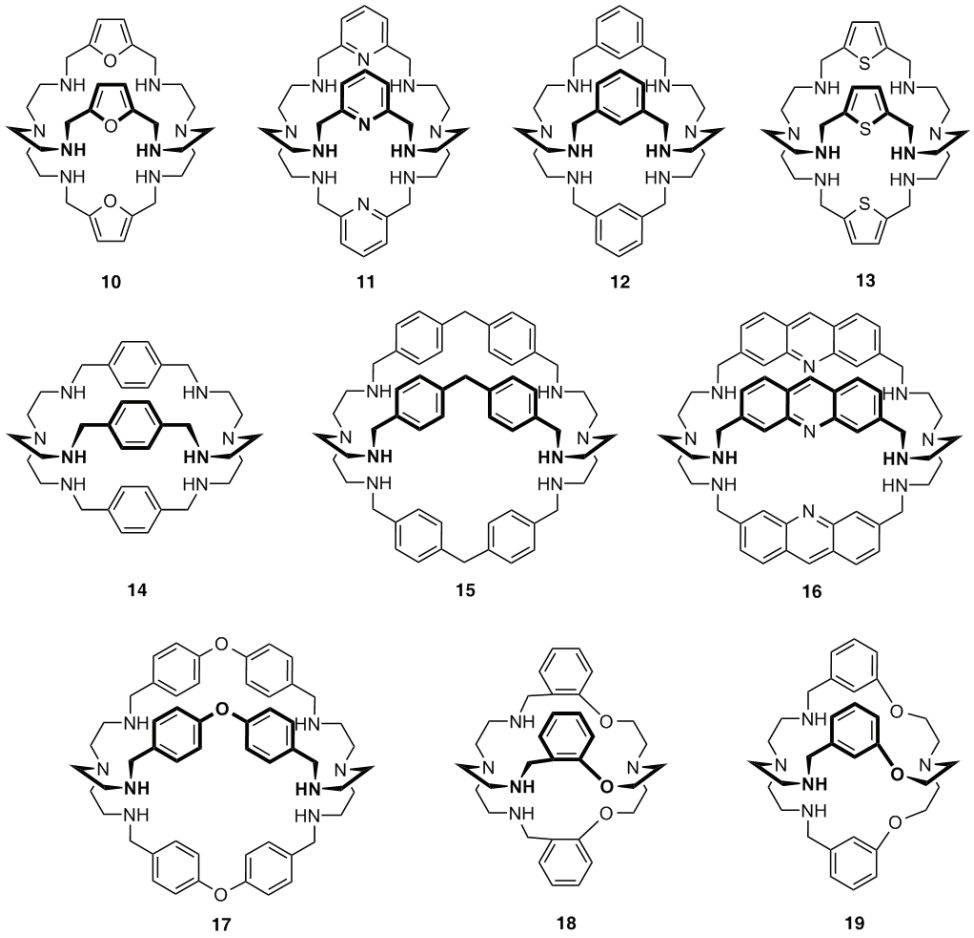

Scheme 1.17 Polyamine cryptands with aromatic spacers used as anion receptors in their protonated forms.

Nelson *et al.* investigated the binding interactions of the H_n**10**$^{n+}$, H_n**11**$^{n+}$ and H_n**12**$^{n+}$ cryptands with different oxoanions in water[115-117] For all these three compounds the binding constants of carboxylates, such as ac^-, lac^-, oxa^{2-} and mal^{2-} are markedly higher for dinegative anions, testifying the dominance of electrostatic interactions. Exceptionally high log *K* values of 8.30, 8.23 and 10.70 were found for the association of H_6**10**$^{6+}$, H_6**11**$^{6+}$ and H_6**12**$^{n+}$, respectively, with oxa^{2-}.[116] It should be noted however that only H_6**12**$^{6+}$ is selective for oxalate in the presence of malonate.

The crystal structures of the oxalate associations with H_6**10**$^{6+}$ and H_6**12**$^{6+}$ [115], illustrated in Figure 1.12a and 1.12b, shows the oxa^{2-} anion completely encapsulated into the receptors cavity forming six hydrogen bonds *via* only one oxygen atom of each carboxylate group. The crystal structure of [H_6**11**(oxa)]$^{4+}$ (Figure 1.12c) shows a different binding mode where the dicarboxylate is not completely encapsulated and the receptor interacts with only one of the carboxylate groups *via* five hydrogen bonds.[116]

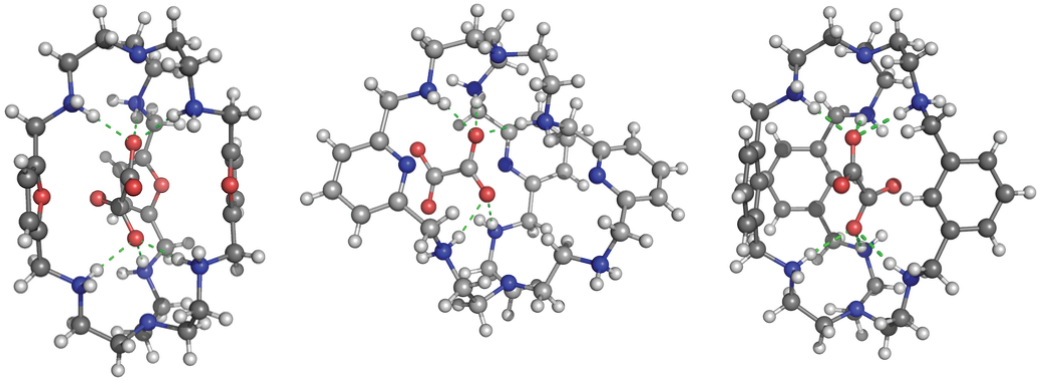

(a) (b) (c)

Figure 1.12 Crystal structures of supermolecules formed between H_6**10**$^{6+}$ (a), H_6**11**$^{6+}$ (b) and H_6**12**$^{n+}$ (c) and the oxalate anion.

The authors suggest that the exceptionally large association constants of the oxalate anion by these receptors can be partly explained by multiple π-stacking interactions. Additionally, this especial interaction comes also from the capability of the macrobicycle to encapsulate specific anions, depending of shape, size, number and position of the binding sites. These results indicate that the

dicarboxylate binding is not governed only by electrostatic interactions but also the geometrical fit of the anion into the receptor play a crucial role.

Nelson *et al.* also found very high association constants for the binding of SO_4^{2-}, SeO_4^{2-} and $S_2O_3^{2-}$ by H_6**10**$^{6+}$, H_6**11**$^{6+}$ and H_6**12**$^{6+}$, ranging from 5.38 to 8.51 log units in aqueous solution.[117] Crystal structures of $[H_6$**10**$(SO_4)]^{4+}$, $[H_6$**10**$(S_2O_3)]^{4+}$, $[H_6$**10**$(CrO_4)]^{4+}$[117] and $[H_6$**12**$(SO_4)]^{4+}$ [118] invariably showed the dianions encapsulated within the receptor cavity. The same authors have found that the receptors H_6**10**$^{6+}$ and H_6**12**$^{n+}$ bind monoanions, such as perchlorate and nitrate, with association constants ranging from 2.29 to 3.73 log units, which means that these two receptors are selective for dianions over monoanions.[119] The crystal structure of the association of nitrate with H_6**12**$^{6+}$ revealed two nitrate anions inside the cavity of the cryptand (Figure 1.13), although there is no evidence that this is also found in solution, as the best model for fitting the potentiometric data indicated only the 1:1 receptor/substrate stoichiometry.[120]

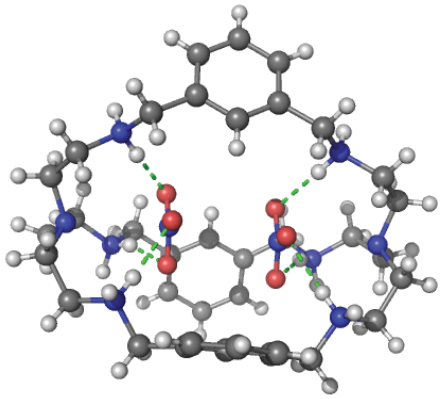

Figure 1.13 Crystal structure of the supermolecule formed by H_6**12**$^{6+}$ with nitrate.

Crystal structures of the H_n**12**$^{n+}$ cryptand with several halide anions were also reported. The crystal structure of the association of H_6**12**$^{6+}$ with F^- revealed the anion encapsulated along with a water molecule, each interacting with one of the tren subunits of the cryptand.[121] The association of H_8**12**$^{8+}$ with Br^- revealed no encapsulation of the anion in the solid state but instead three Br^- where found binding in a cleft mode.[122] Iodide was also found to be encapsulated by H_6**12**$^{6+}$ in the crystal structure but even this large halide cannot fully occupy the cavity of

the receptor.[123] Based in these data it is possible to conclude that the receptor cavity of H_n**12**$^{n+}$ is too large to accommodate halide anions. Unfortunately, besides F^- there are no reported association constants of H_n**12**$^{n+}$ and other halide anions, making it impossible to establish a selectivity trend for the series of anions.

The cryptand **13** with thiophene spacers is relatively unstudied. Only recently Hossain *et al.* reported the first anion association of **13** with an encapsulated chloride bridging the two tertiary amine protons (Figure 1.14a).[124] The ^{1}H NMR titration of the receptor in aqueous solution at pH 2 with Cl^- showed downfield shifts of 0.10 ppm only in the methylene protons adjacent to the tertiary amines in the presence of one equivalent of anion. A 1:1 binding stoichiometry was confirmed by Job's plot and the determined association constant was of 3.60 log units. At higher pH where the tertiary amines are assumed not to be protonated no significant shifts in the ^{1}H NMR signals where found. These results are apparently in agreement with the crystal structure and suggest that the binding occurs only when the tertiary amines are protonated.

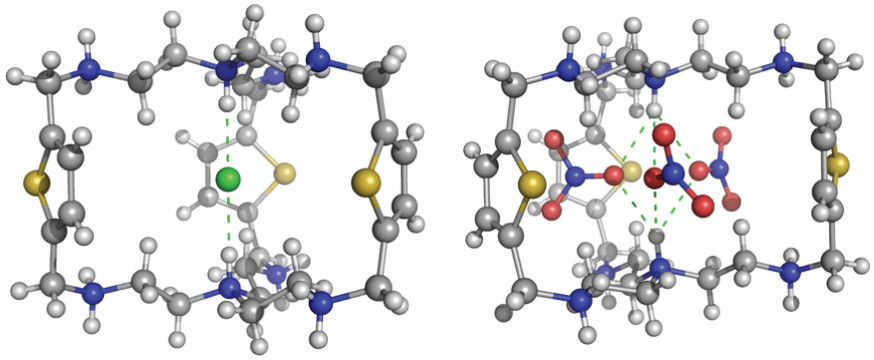

(a) (b)

Figure 1.14 X-ray structures of the association of H_8**13**$^{8+}$ with Cl^- (a) and NO_3^- (b).

Hossain *et al.* also reported a crystal structure of the association of H_8**13**$^{8+}$ with NO_3^-, where three NO_3^- anions are symmetrically oriented in the clefts of the thiophene rings hydrogen bonded to the two tertiary amine protons (Figure 1.14b). Binding studies by ^{1}H NMR titration indicated a 1:1 association with a log *K* of 4.30 in D_2O at pD 2.5, thus failing to correlate the structural data in solid state.[125]

Bowman-James *et al*. investigated the binding of H_n**14**$^{n+}$ with F^-,[126] Cl^- and Br^- anions, [127] and the association constants, determined by ^1H NMR titrations in D_2O at pD 5, were 3.15, 3.37, and 3.34 (in log units) for F^-, Cl^-, and Br^-, respectively. The binding constants of F^- anion with H_n**14**$^{n+}$ were also determined by potentiometric methods, indicating that at pH 5 a mixture of penta- and hexaprotonated species are present in solution. The association constants increase as the pH decrease and the formation of the $[H_6$**14**$(F)_2]^{4+}$ species was also found.[126] Crystal structures of the supramolecular entities formed by H_6**14**$^{6+}$ with F^-, Cl^-, Br^- and I^- were reported (Figure 1.15).[126-128]

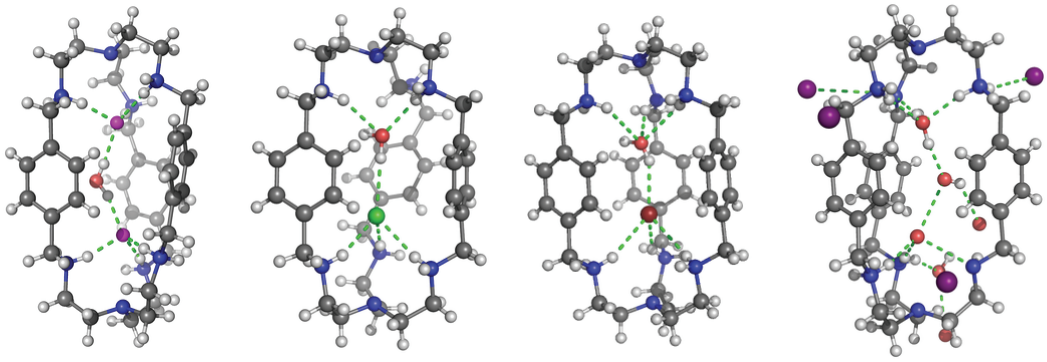

(a) (b) (c) (d)

Figure 1.15 Crystal structures of $[H_6$**14**$(F)_2(H_2O)]^{4+}$ (a), $[H_6$**14**$(Cl)(H_2O)]^{5+}$ (b), $[H_6$**14**$(Br)(H_2O)]^{5+}$ (c) and $[H_4$**14**$(H_2O)_4][I]_4$ (d).

By a slight enlarge of the cavity size relative to H_6**12**$^{6+}$, the H_6**14**$^{6+}$ receptor uptakes two F^- anions and a bridged water molecule into its cavity, through $F^-\cdots H–O–H\cdots F^-$ hydrogen bonds, Figure 1.15a. The other two structures $[H_6$**14**$(Cl)(H_2O)][Cl]_5\cdot 4H_2O.CH_3OH$ and $[H_6$**14**$(Br)(H_2O)][Br]_5\cdot 6.25H_2O$, show a ditopic water/anion motif, and are quite similar to the structure of the fluoride binding by the related cryptand with *m*-xylyl spacers.[127] The halide anions are in a distorted tetrahedron geometry forming hydrogen bonds to three protonated secondary amines of one tren subunit and another one to the internal water molecule (Figure 1.15b and c). The formation of Cl^-/water and Br^-/water entities rather than anion/water/anion entity, as happens for F^-, is probably a reflection of the larger anionic radii for these anions, which makes the fit more favorable for

just one halide in the cavity. Iodide appears to be too large and is found outside the cavity which in turn is occupied by three water molecules [128] (Figure 1.15d).

The cryptands with longer spacers **15**, **16** and **17** are able to bind anions larger than those discussed so far, such as glutarate (glu^{2-}), adipate (adi^{2-}), pimelate (pim^{2-}), phthalate (ph^{2-}), isophthalate (iph^{2-}), terephthalate (tph^{2-}) and nucleotides. [91,129,130] Since their molecular cavities have approximately the same size and shape, they all show a preference for tph^{2-} over other dicarboxylate substrates, with binding constants ranging 4.20 to 4.87 log units for tph^{2-}. Lehn *et al.* reported the crystal structure of the association of H_6**15**$^{6+}$ with tph^{2-} that shows the substrate held inside the cavity by 6 strong hydrogen bonds (Figure 1.16a) in an almost ideal match of the dicarboxylate within the cryptand cavity.[91]

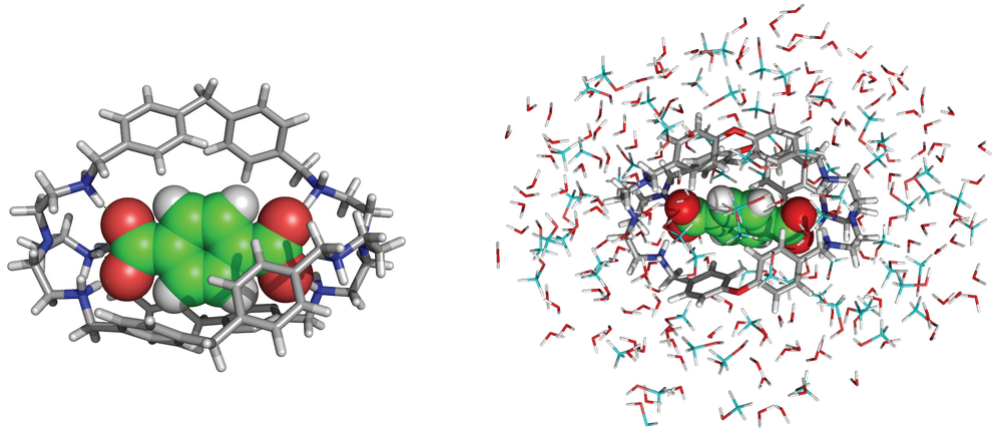

(a) (b)

Figure 1.16 Crystal structure of the cryptate formed by association of H_6**15**$^{6+}$ with the tph^{2-} dianion (a) and snapshot of $[H_6$**17**$(tph)]^{4+}$ taken at 10.5 ns of MD simulation (b). The carbon atoms of the tph^{2-} dianion and of MeOH molecules are represented in green and cyan, respectively.

More recently Delgado *et al.* studied the cryptand H_n**17**$^{n+}$ as a receptor for di- and tricarboxylate anions, ph^{2-}, iph^{2-}, tph^{2-}, benezenetricarboxylate (btc^{3-}), and cyclohexanetricarboxylate (ch^{3-}) in mixed H_2O/MeOH (1:1 v/v) solutions.[130] The effective binding constants at pH 5.5 follow the order: $btc^{3-} > tph^{2-} > ph^{2-} \approx iph^{2-} > ch^{3-}$. Although the charge of the anion clearly plays a significant role in the binding process it is interesting to notice that the difference in log K_{eff} value between btc^{3-} and tph^{2-} is only of ≈ 0.75 at pH 5.5 despite the first having one

more negative charge, probably the result of a better fit in the cavity by tph^{2-}, as molecular modeling studies have shown (Figure 1.16b).

Recently the anion binding ability of cryptands **18** and **19** has also been evaluated.[131-134] Crystal structures of the association of H_n**18**$^{n+}$ with the halides[132,134] have shown that only F^- and Cl^- are encapsulated while Br^- and I^- stay outside the cavity (Figure 1.17). Unfortunately, association constants where not determined for this system, consequently there is no knowledge on the binding behavior in solution.

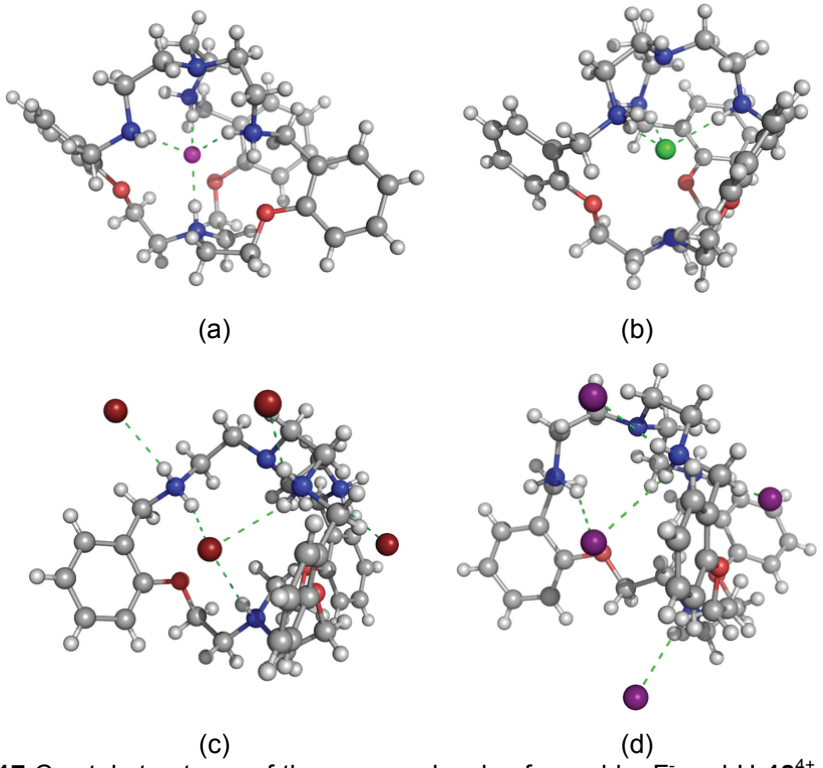

Figure 1.17 Crystal structures of the supermolecules formed by F^- and H_4**18**$^{4+}$ (a); by Cl^- with the H_3**18**$^{3+}$ receptor (b); by H_3**18**$^{3+}$ in presence of Br^- (c) and I^- (d) with the anions outside the cavity.

By a small increase in the cavity size, by changing *o*-xylyl spaces for *m*-xylyl ones, the H_n**19**$^{n+}$ receptor is also able to encapsulate Br^- (Figure 1.18).[131] Crystallization of H_n**19**$^{n+}$ in the presence of binary mixtures of anions were performed in order to evaluate its selectivity. From these studies it was possible to observe that Cl^- is encapsulated in the presence of NO_3^- and SO_4^{2-}.[134] Nitrate

on the other hand is found inside the cavity in the presence of SO_4^{2-}[133] and Br^-.[134] The crystal structure of the sulfate association reveals the dianion outside the cavity of the receptor.[133] Thus, apparently the selectivity follows the order Cl^- > NO_3^- > Br^- > SO_4^{2-}. However ^{1}H-NMR titration of H_3**19**$^{3+}$ in DMSO-d_6 revealed a preference for SO_4^{2-} over NO_3^- with log *K* values of 4.27 and 3.03, respectively.[133]

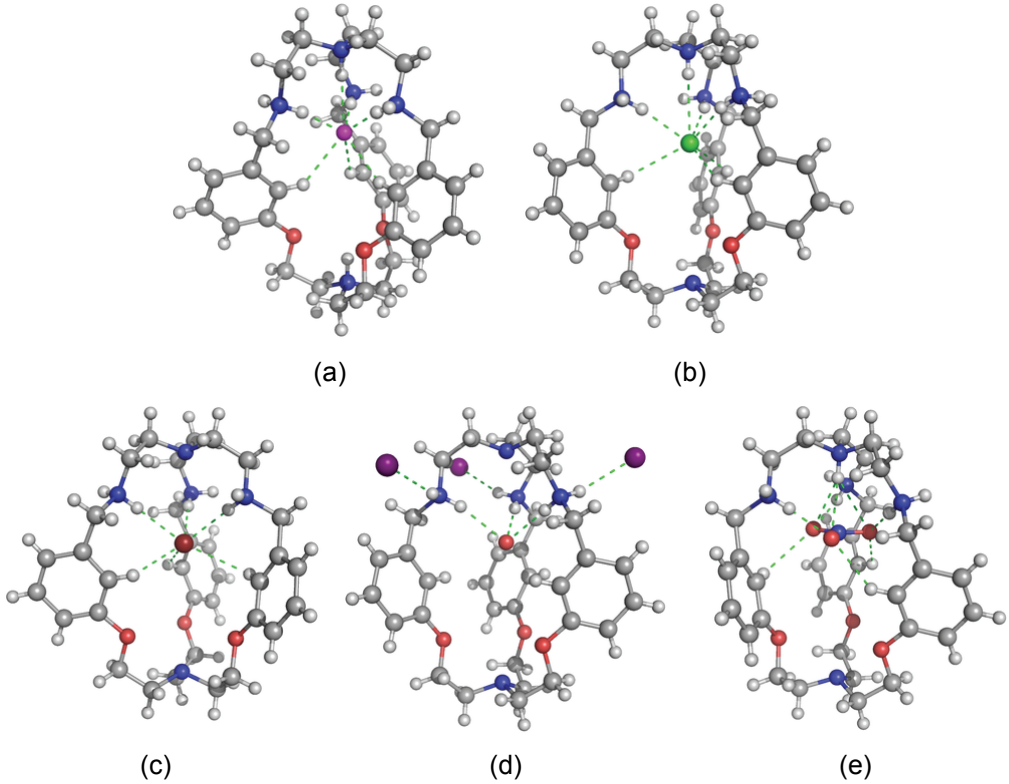

Figure 1.18 Crystal structures of the supermolecules formed by: F^- (a) and Cl^- (b) with H_4**19**$^{4+}$ receptor; by Br^- (c) with H_3**19**$^{3+}$ receptor; in (d) the structure of the included H_2O into the cavity of H_3**19**$^{3+}$ receptor with several I^- anions outside the cavity and in (d) encapsulation of NO_3^- by H_4**19**$^{4+}$.

Tren derived cryptands can also incorporate two metal ions in their cavities (Scheme 1.18), after which an anion can be coordinated to both metal centres, according to a so called cascade mechanism.[135] The tren subunit favours a trigonal bipyramidal stereochemistry around the Cu^{2+} leaving one axial position available to coordination of either a solvent molecule or an anion. Thus dicopper(II) cryptates are able to bind anions in such way that selectivity arises

for the anion with the correct “bite length”, that is, the distance between the two metal centres. The “bite length” can be modulated by varying the length and rigidity of the spacers. Anion encapsulation by these cryptates often induces changes in the UV-vis spectrum that can allow the recognition process to be signalled.[62]

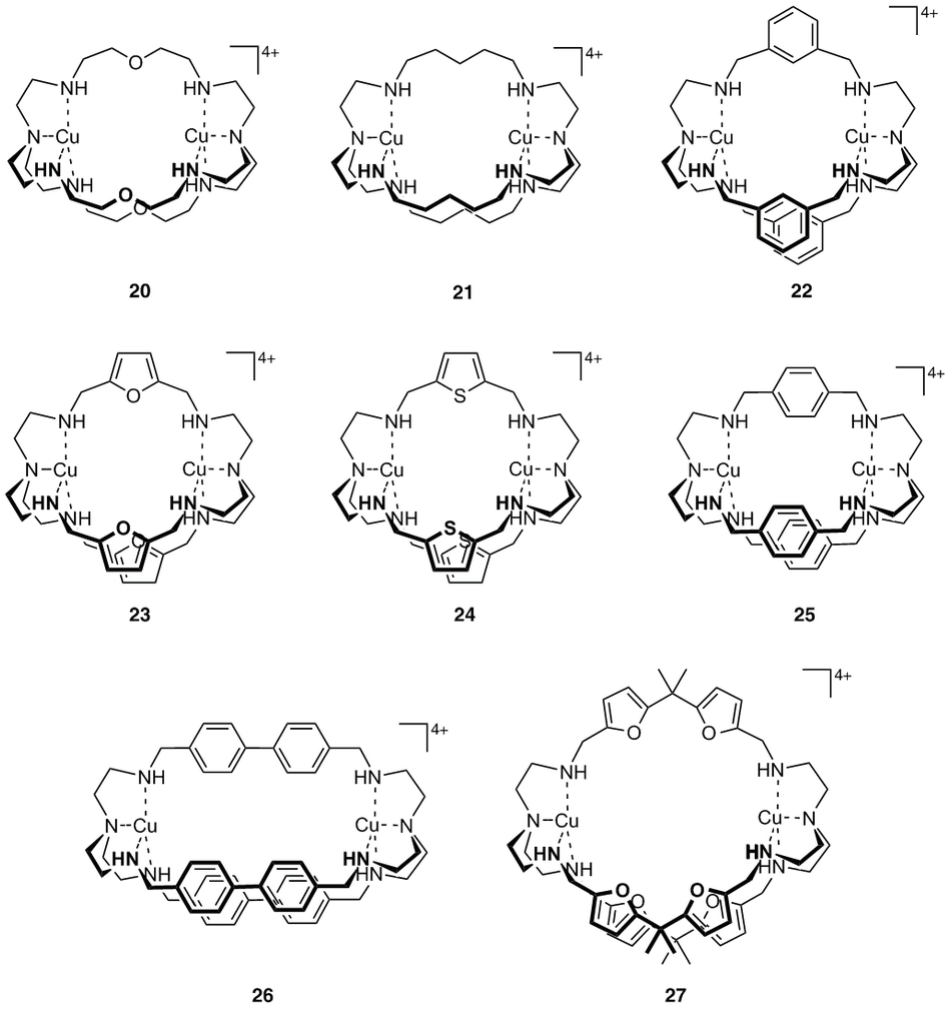

Scheme 1.18 Dinuclear copper(II) complexes of polyamine cryptands used as receptors for anions. Coordinated solvent was omitted for simplicity.

In 1977 Lehn *et al.* had preliminary indications that cryptate **20** could form cascade complexes with H_2O, CN^-, and N_3^- as substrates in aqueous solution.[99] Later Martell *et al.* noticed that a hydroxocomplex formed at unusual low pH in **20**, evidencing a strongly bound bridging OH^-.[136] Afterwards it was determined by

potentiometry a binding constant of 11.56 log units for the binding of OH^- by **20**.[137] This exceptionally high value has been justified by the possibility of additional hydrogen bonding of OH^- to an ether oxygen. Indeed receptor **21** without the ether oxygens has a lower association constant with a value of 6.2 log units.[109] Eventually a crystal structure of [**20**(μ_2-OH)]$^{3+}$ was obtained, confirming the existence of hydrogen bonding of OH^- to an ether oxygen of the cryptand.[138] Binding of the halide anions by **20** is much weaker but still very significant, with association constants of 4.71 log units for F^-, 2.11 log units for Cl^- and 3.2 for I^-. Br^- is apparently not bound by the cryptate.[139] The F^- is favoured by its higher charge density, however it seems that I^- fits better into the cavity of **20** as its association constant is higher than that of Cl^-.

Fabbrizzi *et al.* studied the interaction of cryptate **22** with several anions by spectrophotometric titrations in an aqueous solution.[83] In all cases, anion addition caused a sharp spectral change and 1:1 stoichiometry was found. Among the linear anions, N_3^-, OCN^- and SCN^-, the receptor prefers N_3^- and OCN^- with association constants of 4.78 and 4.60 log units, respectively. The SCN^- is bound less strongly (log K = 2.95) in agreement with its longer “bite length” relatively to the other two anions. The HCO_3^- is also strongly bound (log K = 4.56) due to its appropriate length.

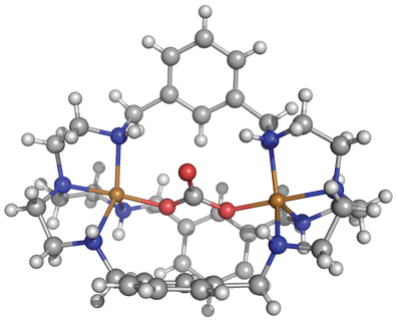

Figure 1.19 Crystal structure of the cascade complex of **22** with CO_3^{2-} anion.

The crystal structures of the [**22**(μ_2-CO_3)]$^{2+}$ (Figure 1.19)[140,141] and of [**22**(μ_2-OCN)]$^{3+}$[142] indeed reveal a good fit of these anions between the two copper centres. Cryptate **22** failed to encapsulate halide anions even when added in

excess, which was attributed to the inability of the rigid framework of the receptor to adjust its cavity to the size requirements of the halides.[143]

Cryptate **23** with furan spacers has a $Cu^{2+}\cdots Cu^{2+}$ distance shorter than that observed for cryptate **22** which prompted Fabbrizzi *et al.* to investigate whether **23** has a selectivity pattern different from that of **22** and thus be able to encapsulate halide anions.[143] Indeed, it was found by potentiometric and spectrophotometric titrations that the cryptate **23** is able to bind F^-, Cl^-, Br^- and I^-, in aqueous solution, with log *K* values of 3.20, 3.98, 3.01 and 2.39, respectively, thus showing some preference for Cl^-. Larger anions N_3^- and NCS^- are also bound with log *K* values of 4.70 and 4.28, respectively. The determined association constants are not too different from one another meaning that the cryptate **23** is not selective for any anion. The authors claimed that **23** is flexible enough to contract and expand its cavity to encapsulate anions of several sizes from the small F^- to the large SCN^-.

Curiously cryptate **24**, in which the furan spacers have been replaced by thiofurane ones, has a binding behaviour that is completely different from **23** and very similar to that of **22**[144] (the cryptate **24** binds N_3^-, OCN^- and SCN^- in aqueous solution with log *K* values of 6.75, 4.79 and 2.72, respectively, while halide anions are not encapsulated). The reason for such behaviour stems from the increased atomic radius of the S atom relative to the O atom that enhances length of the cage such that the cryptate **24** is less flexible than **23**, thus behaving more like **22** as suggested by the authors.

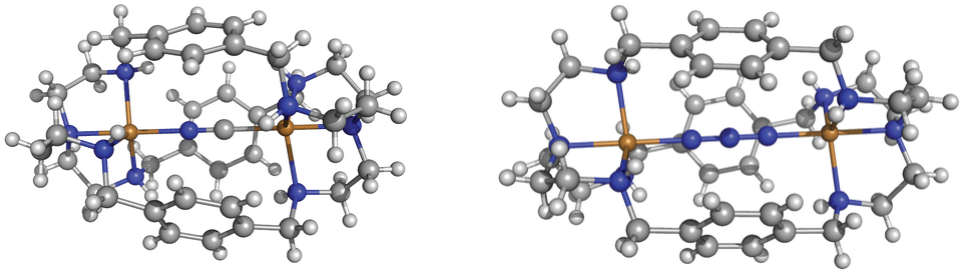

(a) (b)

Figure 1.20 Crystal structures of the cascade complexes of **25** with CN^- (a) and N_3^- (b).

Although there are no quantitative studies of the binding of anions by cryptate **25** crystal structures of its associations with CN^- and N_3^- (Figure 1.20) showed a better fit of the latter into the cavity while with CN^- the *p*-xylyl spacers twist in order to decrease the distance between the two tren subunits, which should lead to a drop in the association constant.[145,146] Thus it seems reasonable to assume that the binding behaviour of **25** will be close to that of **22** and **24**, and different from **23**.

Although strong binding was achieved in highly competitive aqueous solutions by the cryptates discussed so far, as well as very interesting selectivity patterns observed, complexes **20**-**27** are not selective for any particular anion. Inspired by the work of Inouye *et al.*[147], Fabbrizzi *et al.* have taken advantage of the indicator displacement approach to overcome this fact.[148] This method consists on the use of an indicator bound to a receptor by non-covalent interactions, which is then displaced from the receptor by a substrate with a high enough binding constant. This displacement induces a drastic change in the optical properties of the released indicator. In order to have a selective detection of given analyte the binding constant of the indicator should be distinctly lower than that of the substrate of interest and considerably higher than that of the competitors. With this method it is possible to use poorly selective receptors (in the thermodynamic sense) and convert them into selective sensors. This was demonstrated for the cryptate **22**. As discussed above, although this receptor showed clear preference for N_3^-, OCN^- and HCO_3^- over NCS^-, NO_3^-, SO_4^{2-}, HPO_4^{2-}, $HCOO^-$ and CH_3COO^-, it failed to be selective. Fabbrizzi *et al.* showed that only N_3^-, OCN^- and HCO_3^- can displace the indicator coumarine 343 from the cavity of **22** while the competitors were unable to do so.[148]

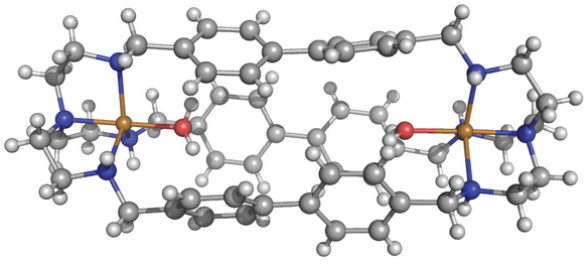

Figure 1.21 Crystal structure of the dinuclear Cu^{2+} complex **26**.

The same approach was used with cryptates having longer rigid spacers which obviously offer the possibility of binding larger anionic substrates. Cryptate **26** (Figure 1.21) in association with 6-carboxy-tetramethylrhodamine is able to discriminate L-glutamate from other amino acid neurotransmitters in aqueous solution, such as L-aspartate, L-glycine, δ-aminopentanoate, L-alanine and γ-aminobutanoate.[149] Selectivity arises from the fact that glutamate possesses two negatively charged carboxylate groups at a distance that match the metal–metal distance within the cage. Such requirements are not met by other neurotransmitters and related amino acids which consequently cannot displace the indicator from the cavity of **26**. Using the same premise and the same cryptate-indicator ensemble it was also possible to discriminate tph^{2-} from its isomers ph^{2-} and iph^{2-} and from aliphatic dicarboxylates of the general formula $^{-}OOC\text{-}(CH_2)_n\text{-}COO^{-}$ in aqueous solution.[150]

Very recently cryptate **27** has been explored as receptor for nucleoside monophosphates in mixed H_2O/MeOH (1:1 v/v) solutions also by using the indicator displacement approach. However the large size of the cryptate and substrates gave rise to complicated equilibria due to the formation receptor:indicator 2:1 stoichiometries thus, although a preference for guanosine monophosphate was found over other nucleoside monophosphates, no selective discrimination was achieved.[151]

1.4 Aims of the present work and its contribution to the field of anion recognition

The objective of this work was the development of new receptors able to selectively bind anions in aqueous solution. As aforementioned this is a highly challenging task, requiring the use of charged receptors with multiple binding sites well positioned in an organic scaffold in such way that they can work cooperatively.

With this in mind the work aimed to explore the amine functionality in conjunction with the macrobicyclic architecture. This choice stemmed from both

the versatility of the amine functional group and the encapsulating capabilities of the macrobicyclic architecture (see 1.3.5.2.1 and 1.2.6.1).

As shown in 1.3.5.2.2.2, the vast majority of polyamine macrobicycles used as anion receptors in their protonated forms or as their Cu^{2+} complexes are bis-tren cryptands, with the exception of compounds **6**-**9** (Scheme 1.15) that were insufficiently explored. Although bis-tren cryptands have very interesting anion binding properties and are extremely versatile compounds, the reported cases of true selectivity, that is, those where one analyte is bound without any interference from all possible competitors, are scarce. This fact is probably related to the flexibility conferred by the tren subunit which allows the receptors to adapt to the stereochemical requirements of the substrate by distorting its structure or rearranging its conformation, thus losing selectivity. In addition many of the existing studies did not provide thorough quantitative characterization of these binding systems in solution, relying mainly on solid state studies of the supermolecules formed. Clearly there is still much work to be done for the improvement of polyamine macrobicycles.

The intent of this work was to take advantage of the ease of modification of the macrobicyclic architecture and by small structural modifications try to rigidify the structure of the compounds in order to increase their preorganization. This was done by using 2,4,6-triethylbenzene as caps instead of tren. In addition we also expected that the 2,4,6-triethylbenzene capped cryptands would be more lipophilic than the tren derived ones, a characteristic of importance for extraction and transport applications.

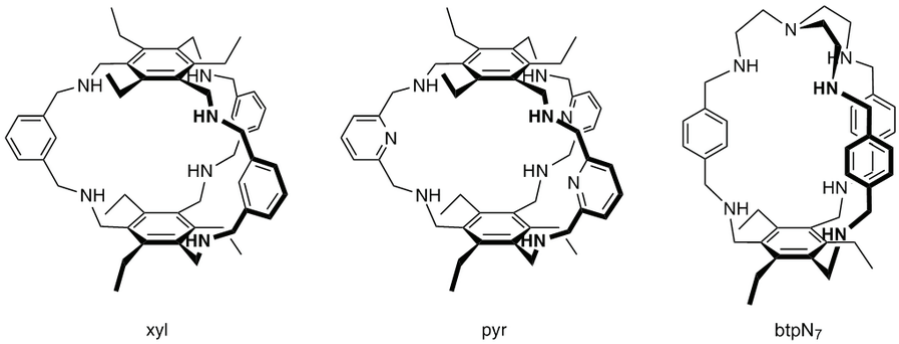

Scheme 1.19 Polyaza cryptands synthesized and studied in this work.

By doing so, the family of almost unexplored benzene capped polyamine cryptands (compounds **6**-**9**, Scheme 1.15) was enlarged and their new members (Scheme 1.19) were thoroughly studied as anion receptors in aqueous solution and in the solid state.

Mixed oxa-aza compounds were also envisioned in the work plan of this thesis with the assumption that these would be interesting for the binding in aqueous solution of highly elusive zwitterionic amino acids, a very important class of anion containing substrates (Scheme 1.20). It should be noted that by the time this work started there was no account on the anion binding behaviour of mixed oxa-aza compounds and even today the information available is practically limited to crystallographic studies.

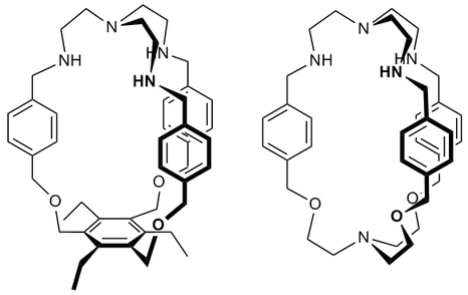

Scheme 1.20 Mixed polyazapolyaza cryptands synthesized and studied in this work.

1.5 References

[1] J.-M. Lehn, *Supramolecular Chemistry: Concepts and Perspectives*, VCH, Weinheim, **1995**; J.-M. Lehn, *Química Supramolecular: Conceitos e Perspectivas*, (translated to portuguese by M. J. Calhorda, R. Delgado, A. M. Martins, V. G. Machado, N. Miranda), IST Press, Lisboa, **2007**.

[2] J. W. Steed, J. L. Atwood, *Supramolecular Chemistry*, 2nd ed., John Wiley & Sons, Ltd, West Sussex, **2009**.

[3] J. W. Steed, D. R. Turner, K. J. Wallace, *Core Concepts in Supramolecular Chemistry and Nanochemistry*, John Wiley & Sons, Ltd, West Sussex, **2007**.

[4] H.-J. Schneider, *Angew. Chem. Int. Ed.* **2009**, *48*, 3924–3977.

[5] D. J. Cram, *Angew. Chem. Int. Ed.* **1986**, *25*, 1039–1134.

[6] B. L. Haymore, J. D. Lamb, R. M. Izatt, J. J. Christensen, *Inorg. Chem.* **1982**, *21*, 1598–1602.

[7] B. G. Cox, H. Schneider, J. Stroka, *J. Am. Chem. Soc.* **1978**, *100*, 4746–4749.

[8] B. G. Cox, P. Firman, H. Horst, H. Schneider, *Polyhedron* **1983**, *2*, 343–347.

[9] R. G. Pearson, *J. Am. Chem. Soc.* **1963**, *85*, 3533–3539.

[10] H. K. Frensdorff, *J. Am. Chem. Soc.* **1971**, *93*, 600–606.

[11] F. P. Schmidtchen, *Chem. Soc. Rev.* **2010**, *39*, 3916–3935.

[12] A. E. Martell and R. J. Motekaitis, *The determination and use of stability constants*, Wiley-VCH, **1992**.
[13] *Analytical Methods in Supramolecular Chemistry*, Ed.: C. A. Schalley,Wiley-VCH Verlag, Weinheim, **2007**.
[14] M. T. Albelda; M. A. Bernardo, E. Garcia-España, M. L. Godino-Salido, S. V. Luis, M. J. Melo, F. Pina, C. Soriano, *J. Chem. Soc., Perkin Trans. 2* **1999**, 2545–2549.
[15] H.-J. Schneider, A. K. Yatsimirsky, *Chem. Soc. Rev.* **2008**, *37*, 263–277.
[16] F. P. Schmidtchen, *Coord. Chem. Rev.* **2006**, *250*, 2918–2928.
[17] A. Bencini, A. Bianchi, M. I. Burguete, P. Dapporto, A. Doménech, E. García-España, S. V. Luis, P. Paoli, J. A. Ramírez, *J. Chem. Soc. Perkin Trans. 2* **1994**, 569–577.
[18] F. Vögtle, E. Weber, *Angew. Chem. Int. Ed.* **1979**, *18*, 753–776.
[19] J. J. Christensen, D. J. Eatough, R. M. Izatt, *Chem. Rev.* **1974**, *74*, 351–384.
[20] J.-M. Lehn, *Pure Appl. Chem.* **1977**, *49*, 857 – 870.
[21] D. J. Cram, T. Kaneda R. C. Helgeson, G. M. Lein, *J. Am. Chem. Soc.* **1979**, *101*, 6752–6754.
[22] S. M. Biros, J. Rebek, Jr., *Chem. Soc. Rev.* **2007**, *36*, 93–104.
[23] J. C. Sherman, *Tetrahedron* **1995**, *51*, 3395–3422.
[24] F. Sansone, L. Baldini, A. Casnati, R. Ungaro, *New J. Chem.* **2010**, *34*, 2715–2728.
[25] T. Brotin, J.-P. Dutasta, *Chem. Rev.* **2009**, *109*, 88–130.
[26] B. Dietrich, J.-M. Lehn, J. P. Sauvage, *Tetrahedron Lett.* **1969**, *10*, 2885–2888.
[27] B. Dietrich, J.-M. Lehn, J. P. Sauvage, *Tetrahedron Lett.* **1969**, *10*, 2889–2892.
[28] J.-M. Lehn, *Struct. Bonding* **1973**, *16*, 1–271.
[29] S. N. Yurgel, M. L. Kahn, *FEMS Microbiol. Rev.* **2004**, *28*, 489–501.
[30] I. G. Janausch, E. Zientz, Q. H. Tran, A. Kröger, G. Unden, *Biochim. Biophys. Acta* **2002**, *1553*, 39–56.
[31] R. Hyde, P. M. Taylor, H. S. Hundal, *Biochem. J.* **2003**, *373*, 1–18.
[32] D. N. Sheppard, M. J. Welsh, *Physiol. Rev.*, **1999**, *79*, 23–45.
[33] M. Brunetti, L. Timio, P. Saronio, E. Capodicasa, *J. Nephephrol.*, **2001**, *14*, 27–31.
[34] I. Fernandes, D. Laouari, P. Tutt, G. Hampson, G. Friedlander, C. Silve, *Kidney Int.*, **2001**, *59*, 210–221.
[35] D. H. Williams, B. Bardsley, *Angew. Chem. Int. Ed.* **1999**, *38*, 1172–1193.
[36] B. A. Moyer, L. H. Delmau, C. J. Fowler, A. Ruas, D. A. Bostick, J. L. Sessler, E. Katayev, G. D. Pantos, J. M. Llinares, M. A. Hossain, S. O. Kang, K. Bowman-James in *Advances in Inorganic Chemistry, vol. 59: Template Effects and Molecular Organization*, Eds. R. van Eldik and K. Bowman-James, Elsevier, Oxford, **2007**, p. 175–204.
[37] *Themed issue: Supramolecular chemistry of anionic species*, Eds. P. A. Gale, T. Gunnlaugsson, in *Chem. Soc. Rev.* **2010**, *39*.
[38] *Anion Coordination Chemistry II*, Ed. P. A. Gale, in *Coord. Chem. Rev.* **2006**, *250*.
[39] *35 years of Synthetic Anion Receptor Chemistry*, Ed. P. A. Gale, in *Coord. Chem. Rev.* **2003**, *240*.
[40] *Supramolecular Chemistry of Anions*, Eds. A. Bianchi, K. Bowman-James and E. Garcia-España, Pergamon, Oxford, Wiley-VCH, NY, **1997.**
[41] C. J. Pedersen, *J. Am. Chem. Soc.* **1967**, *89*, 2495–2496.
[42] C. H. Park, H. E. Simmons, *J. Am. Chem. Soc.* **1968**, *90*, 2431–2432.
[43] E. Graf, J.-M. Lehn, *J. Am. Chem. Soc.* **1976**, *98*, 6403–6405.
[44] J.-M. Lehn, E. Sonveaux, A. K. Willard, *J. Am. Chem. Soc.* **1978**, *100*, 4914–4916.
[45] J.-M. Lehn, A. Moradpour, *Helv. Chim. Acta* **1978**, *61*, 2407–2418.

[46] B. Dietrich, T. M. Fyles, J.-M. Lehn, L. G. Pease, D. L. Fyles, *J. Chem. Soc. Chem. Commun.* **1978**, 934–936.
[47] B. Dietrich, D. L. Fyles, T. M. Fyles, J.-M. Lehn, *Helv. Chim. Acta* **1979**, *62*, 2763–2787.
[48] P. Baret, J.-L. Pierre, *Bull. Soc. Chim. Fr.* **1983**, *II*, 367.
[49] R. Dutzler, E. B. Campbell, M. Cadene, B. T. Chait, R. MacKinnon, *Nature* **2002**, *415*, 287–294.
[50] J. W. Pflugrath, F. A. Quiocho, *Nature* **1985**, *314*, 257–260.
[51] H. Luecke, F. A. Quiocho, *Nature* **1990**, *347*, 402–406.
[52] B. L. Jacobson, F. A. Quiocho, *J. Mol. Biol.* **1988**, *204*, 783–787.
[53] N. M. Koropatkin, H. B. Pakrasi, T. J. Smith, *PNAS* **2006**, *103*, 9820–9825.
[54] N. M. Koropatkin, D. W. Koppenaal, H. B. Pakrasi, T. J. Smith, *J. Biol. Chem.* **2007**, *282*, 2606–261.
[55] Y.-F. Zhou, B. Nan, J. Nan, Q. Ma, S. Panjikar, Y.-H. Liang, Y. Wang, X.-D. Su, *J. Mol. Biol.* **2008**, *383*, 49–61.
[56] T. M. Tomasiak, T. L. Archuleta, J. Andréll, C. Luna-Chávez, T. A. Davis, M. Sarwar, A. J. Ham, W. H. McDonald, V. Yankovskaya, H. A. Stern, J. N. Johnston, E. Maklashina, G. Cecchini, T. M. Iverson, *J. Biol. Chem.* 2011, *286*, 3047–3056.
[57] C. A. Ilioudis, J. W. Steed, *J. Supramol. Chem.* **2001**, *1*, 165–187.
[58] J. M. Llinares, D. Powell, K. Bowman-James, *Coord. Chem. Rev.* **2003**, *240*, 57–75.
[59] E. García-España, P. Díaz, J. M. Llinares, A. Bianchi, *Coord. Chem. Rev.* **2006**, *250*, 2952–2986
[60] M. D. Best, S. L. Tobey, E. V. Anslyn, *Coord. Chem. Rev.* **2003**, *240*, 3–15.
[61] C. Schmuck, *Coord. Chem. Rev.* **2006**, *250*,3053–3067.
[62] V. Amendola, L. Fabbrizzi, C. Mangano, P. Pallavicini, A. Poggi, A. Taglietti, *Coord. Chem. Rev.* **2001**, *219–221*, 821–837.
[63] L. Fabbrizzi, M. Licchelli, A. Taglietti, *Dalton Trans.* **2003**, 3471–3479.
[64] E. J. O'Neil, B. D. Smith, *Coord. Chem. Rev.* **2006**, *250*, 3068–3080.
[65] V. Amendola, L. Fabbrizzi, *Chem. Commun.* **2009**, 513–531.
[66] D. J. Mercer, S. J. Loeb, *Chem. Soc. Rev.* **2010**, *39*, 3612–3620.
[67] C. R. Bondy, S. J. Loeb, *Coord. Chem. Rev.* **2003**, *240*, 77–99.
[68] K. Choi, A. D. Hamilton, *Coord. Chem. Rev.* **2003**, *240*, 101–110.
[69] S. O. Kang, M. Alamgir Hossain, K. Bowman-James, *Coord. Chem. Rev.* **2006**, *250*, 3038–3067.
[70] A.-F. Li, J.-H. Wang, F. Wang, Y.-B. Jiang, *Chem. Soc. Rev.* **2010**, *39*, 3729–3745.
[71] V. Amendola, L. Fabbrizzi, L. Mosca, *Chem. Soc. Rev.* **2010**, *39*, 3889–3915.
[72] B. M. Rambo, J. L. Sessler, *Chem. Eur. J.* **2011**, *17*, 4946–4959.
[73] P. Dydio, D. Lichosyt, J. Jurczak, *Chem. Soc. Rev.* **2011**, *40*, 2971–2985.
[74] M. M. G. Antonisse, D. N. Reinhoudt, *Chem. Commun.* **1998**, 443–448.
[75] R. A. Pascal, J. Spergel, D. V. Engbersen, *Tetrahedron Lett.* **1986**, *27*, 4099–4102.
[76] C. Raposo, M. Almaraz, M. Martín, V. Weinrich, M. L. Mussóns, V. Alcázar, M. C. Caballero, J. R.Morán, *Chem. Lett.* **1995**, 759–760.
[77] K. H. Lee, J.-I. Hong, *Tetrahedron Lett.* **2000**, *41*, 6083–6087.
[78] V. Král, H. Furuta, K. Shreder, V. Lynch, J. L. Sessler, *J. Am. Chem. Soc.* **1996**, *118*, 1595–1607.
[79] S. J. Brooks, P. A. Gale, M. E. Light, *Chem. Commun.* **2006**, 4344–4346.
[80] P. A. Gale, J. R. Hiscock, S. J. Moore, C. Caltagirone, M. B. Hursthouse, M. E. Light, *Chem.–Asian J.* **2010**, *5*, 555–561.

[81] B. Dietrich, M. W. Hosseini, J.-M. Lehn, R. B. Sessions, *J. Am. Chem. Soc.* **1981**, *103*, 1282–1283.
[82] A. Metzger, V. M. Lynch, E. V. Anslyn, *Angew. Chem. Int. Ed.* **1997**, *36*, 862–865.
[83] L. Fabbrizzi, P. Pallavicini, L. Parodi, A. Taglietti, *Inorg. Chim. Acta* **1995**, *238*, 5–8.
[84] S. L. Tobey, B. D. Jones, E. V. Anslyn, *J. Am. Chem. Soc.* **2003**, *125*, 4026–4027.
[85] H. Aït-Haddou, J. Sumaoka, S. L.Wiskur, J. F. Folmer-Andersen, E. V. Anslyn, *Angew. Chem. Int. Ed.* **2002**, *41*, 4013–4016.
[86] L. Lomozik, A. Gasowska, R. Bregier-Jarzebowska, R. Jastrzab, *Coord. Chem. Rev.* **2005**, *249*, 2335–2350.
[87] A. Bencini, A. Bianchi, E. García-España, M. Micheloni, J. A. Ramirez, *Coord. Chem. Rev.* **1999**, *188*, 97–156.
[88] N. Lomadze, H.-J. Schneider, T. Albelda, E. García-España, B. Verdejo, *Org. Biomol. Chem.* **2006**, *4*, 1755–1759.
[89] E. Kimura, Y. Kuramoto, T. Koike, H. Fujioka, M. Kodama, *J. Org. Chem.* **1990**, *55*, 42–46.
[90] S. Carvalho, R. Delgado, M. G. B. Drew, V. Calisto, V. Félix, *Tetrahedron* **2008**, *64*, 5392–5403.
[91] J.-M. Lehn, R. Méric, J. Vigneron, I. Bkouche-Waksman, C. Pascard, *J. Chem. Soc. Chem. Commun.* **1991**, 62–64.
[92] T. Fujita, J.-M. Lehn, *Tetrahedron Lett.* **1988**, *29*, 1709–1712.
[93] B. Sarkar, P. Mukhopadhyay, P. K. Bharadwaj, *Coord. Chem. Rev.* **2003**, *236*, 1–13.
[94] V. McKee, J. Nelson, R. M. Town, *Chem. Soc. Rev.* **2003**, *32*, 309–325.
[95] S. O. Kang, J. M. Llinares, V. W. Day, K. Bowman-James, *Chem. Soc. Rev.* **2010**, *39*, 3980–4003.
[96] C. A. Ilioudis, J. W. Steed, *J. Supramol. Chem.* **2001**, *1*, 165–187.
[97] *Macrocycle Synthesis: A Practical Approach*, (Ed.: D. Parker), Oxford University Press, Oxford, **1996**.
[98] J. Richman, T. J. Atkins, *J. Am. Chem. Soc.* **1974**, *96*, 2268–2270.
[99] J.-M. Lehn, S. H. Pine, E.-i. Watanabe, A. K. Willard, *J. Am. Chem. Soc.* **1977**, *99*, 6766–6768.
[100] B. Dietrich, M. W. Hosseini, J.-M. Lehn, R. B. Sessions, *Helv. Chim. Acta* **1985**, *68*, 289–299.
[101] D. McDowell, J. Nelson, Tetrahedron Lett. 1988, 29, 385–386.
[102] D. Chen, A. E. Martell, Tetrahedron 1991, 47, 6895–6902.
[103] P. Mateus, N. Bernier, R. Delgado, *Coord. Chem. Rev.* **2010**, *254*, 1726–1747.
[104] B. Dietrich, B. Dilworth, J.-M. Lehn, J.-P. Souchez, M. Cesario, J. Guilhem, C. Pascard, *Helv. Chim. Acta* **1996**, *79*, 569–587.
[105] B. Dietrich, J.-M. Lehn, J. Guilhem, C. Pascard, *Tetrahedron Lett.* **1989**, *30*, 4125–4128.
[106] M. A. Hossain, J. M. Llinares, N. W. Alcock, D. Powell, K. Bowman-James, *J. Supramol. Chem.* **2002**, *2*, 143–149.
[107] M. A. Hossain, J. M. Llinares, C. A. Miller, L. Seib, K. Bowman-James, *Chem. Commun.* **2000**, 2269–2270.
[108] M. Arunachalam, E. Suresh, P. Ghosh, *Tetrahedron* **2007**, *63*, 11371–11376.
[109] R. J. Motekaitis, A. E. Martell, I. Murase, J.-M. Lehn, M. W. Hosseini, *Inorg. Chem.* **1988**, *27*, 3630–3636.
[110] B. Dietrich, J. Guilhem, J.-M. Lehn, C. Pascard, E. Sonveaux, *Helv. Chim. Acta* **1984**, *67*, 91–104.
[111] M. W. Hosseini, J.-M. Lehn, *Helv. Chim. Acta* **1988**, *71*, 749–756.

[112] D. Heyer, J.-M. Lehn, *Tetrahedron Lett.* **1986**, *27*, 5869–5872.
[113] C. A. Iloudis, D. A. Tocher, J. W. Steed, *J. Am. Chem. Soc.* **2004**, *126*, 12395–12402.
[114] D. Chen, A. E. Martell, *Tetrahedron* **1991**, *47*, 6895–6902.
[115] J. Nelson, M. Nieuwenhuyzen, I. Pál, R. M. Town, *Chem. Commun.* **2002**, 2266–2267.
[116] J. Nelson, M. Nieuwenhuyzen, I. Pál, R. M. Town, *Dalton Trans.* **2004**, 229–235.
[117] J. Nelson, M. Nieuwenhuyzen, I. Pál, R. M. Town, *Dalton Trans.* **2004**, 2303–2308.
[118] S. O. Kang, M. A. Hossain, D. Powell, K. Bowman-James, *Chem. Commun.* **2005**, 328–330.
[119] M. J. Hynes, B. Maubert, V. McKee, R. M. Town, J. Nelson, *J. Chem. Soc. Dalton Trans.* **2000**, 2853–2859
[120] T. Clifford, A. Danby, J. M. Llinares, S. Mason, N. W. Alcock, D. Powell, J. A. Aguilar, E. García-España, K. Bowman-James, *Inorg. Chem.* **2001**, *40*, 4710–4720.
[121] S. Mason, J. M. Llinares, M. Morton, T. Clifford, K. Bowman-James, *J. Am. Chem. Soc.* **2000**, *122*, 1814–1815.
[122] R. Menif, J. Reibenspies, A. E. Martell, Inorg. Chem. **1991**, *30*, 3454–3461.
[123] I. Ravikumar, P. S. Lakshminarayanan, E. Suresh, P. Ghosh, *Inorg. Chem.* **2008**, *47*, 7992–7999.
[124] M. A. Saeed, F. R. Fronczek, M. A. Hossain, *Chem. Commun.* **2009**, 6409–6411.
[125] M. A. Saeed, F. R. Fronczek, M.-J. Huanga, M. A. Hossain, *Chem. Commun.* **2010**, *46*, 404–406.
[126] M. A. Hossain, J. M. Llinares, S. Mason, P. Morehouse, D. Powell, K. Bowman-James, *Angew. Chem. Int. Ed.* **2002**, *41*, 2335–2338.
[127] M. A. Hossain, P. Morehouse, D. Powell, K. Bowman-James, *Inorg. Chem.* **2005**, *44*, 2143–2149.
[128] P. S. Lakshminarayanan, D. K. Kumar, P. Ghosh, *Inorg. Chem.* **2005**, *44*, 7540–7546.
[129] M.-P. Teulade-Fichou, J.-P. Vigneron, J.-M. Lehn, *J. Chem. Soc. Perkin Trans. 2* **1996**, 2169–2175.
[130] S. Carvalho, R. Delgado, V. Félix, *Tetrahedron* **2010**, *66*, 8714–8721.
[131] M. C. Das, P. K. Bharadwaj, *Eur. J. Inorg. Chem.* **2007**, 1229–1232.
[132] M. C. Das, S. K. Ghosh, P. K. Bharadwaj, *Dalton Trans.* **2009**, 6496–6506.
[133] M. C. Das, S. K. Ghosh, P. K. Bharadwaj, *CrystEngComm*, **2010**, *12*, 413–419.
[134] M. C. Das, S. K. Ghosh, S. Sen, P. K. Bharadwaj, *CrystEngComm*, **2010**, *12*, 2967–2974.
[135] J.-M. Lehn, *Pure Appl. Chem.* **1980**, *52*, 2441–2459.
[136] R. J. Motekaitis, A. E. Martell, J.-M. Lehn, E. Watanabe, *Inorg. Chem.* **1982**, *21*, 4253–4257.
[137] R. J. Motekaitis, A. E. Martell, B. Dietrich, J.-M. Lehn, *Inorg. Chem.* **1984**, *23*, 1588–1591.
[138] R. J. Motekaitis, P. R. Rudolf, A. E. Martell, A. Clearfield, *Inorg. Chem.* **1989**, *28*, 112–115.
[139] R. J. Motekaitis, A. E. Martell, I. Murase, *Inorg. Chem.* **1986**, *25*, 938–944.
[140] R. Menif, J. Reibenspies, A. E. Martell, *Inorg. Chem.* **1991**, *30*, 3446–3454.
[141] Y. Dussart, C. Harding, P. Dalgaard, C. McKenzie, R. Kadirvelraj, V. McKee, J. Nelson, *J. Chem. Soc. Dalton Trans.* **2002**, 1704–1713.
[142] C. J. Harding, F. E. Mabbs, E. J. L. MacInnes, V. McKee, J. Nelson, *J. Chem. Soc. Dalton Trans.* **1996**, 3227–3230.

[143] V. Amendola, E. Bastianello, L. Fabbrizzi, C. Mangano, P. Pallavicini, A. Perotti, A. M. Lanfredi, F. Ugozzoli, *Angew. Chem. Int. Ed.* **2000**, *122*, 3039–3042.
[144] V. Amendola, L. Fabbrizzi, C. Mangano, P. Pallavicini, M. Zema, *Inorg. Chim. Acta* **2002**, *337*, 70–74.
[145] A. D. Bond, S. Derossi, C. J. Harding, E. J. L. McInnes, *Dalton Trans.* **2005**, 2403–2409.
[146] I. Ravikumar, E. Suresh, P. Ghosh, *Inorg. Chem.* **2006**, *45*, 10046–10048.
[147] M. Inouye, K. Hashimoto, K. J. Isagawa, *J. Am. Chem. Soc.* **1994**, *116*, 5517–5518.
[148] L. Fabbrizzi, A. Leone, A. Taglietti, *Angew. Chem. Int. Ed.* **2001**, *40*, 3066–3069.
[149] M. Bonizzoni, L. Fabbrizzi, G. Piovani, A. Taglietti, *Tetrahedron* **2004**, *60*, 11159–11162.
[150] M. Boiocchi, M. Bonizzoni, L. Fabbrizzi, G. Piovani, A. Taglietti, *Angew. Chem. Int. Ed.* **2004**, *43*, 3847–3852.
[151] V. Amendola, G. Bergamaschi, A. Buttafava, L. Fabbrizzi, E. Monzani, *J. Am. Chem. Soc.* **2010**, *132*, 147–156.

Chapter 2

Selective recognition of tetrahedral dianions by a hexaaza cryptand receptor

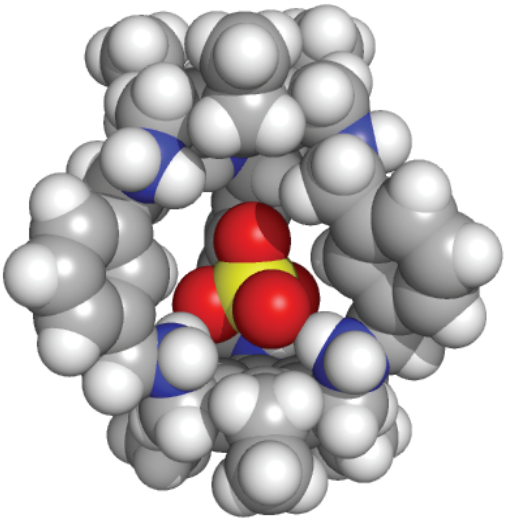

Work featured in: P. Mateus, R. Delgado, P. Brandão, S. Carvalho, V. Félix, *Org. Biomol. Chem.* **2009**, *7*, 4661–4673.

2.1 Summary

A hexamine cage was synthesised in good yield by a [2+3] Schiff-base condensation followed by sodium borohydride reduction to be used as a receptor for the selective binding of anionic species. The protonation constants of the receptor, as well as its association constants with Cl^-, I^-, NO_3^-, AcO^-, ClO_4^-, $H_2PO_4^-$, SO_4^{2-}, SeO_4^{2-} and $S_2O_3^{2-}$ were determined by potentiometry at 298.2±0.1 K in H_2O/MeOH (50:50 v/v) and at ionic strength 0.10±0.01 mol dm^{-3} in KTsO. These studies revealed a remarkable selectivity for dianionic tetrahedral anions by the protonated receptor, with association constants ranging 5.03–5.30 log units for the dianionic species and 1.49–2.97 log units for monoanionic ones. Single crystal X-ray determination of $[(H_6xyl)(SO_4)(H_2O)_6](SO_4)_2.9.5H_2O$ showed that one sulfate anion is encapsulated into the receptor cage sited between the two 2,4,6-triethylbenzene caps establishing three N–H···O hydrogen bonds with two adjacent N–H binding sites and additional O–H···O hydrogen bonding interactions with five crystallization water molecules. Four water molecules of the $(SO_4)(H_2O)_6$ cluster interact with $[H_6xyl]^{6+}$ through N–H···O hydrogen bonds. Molecular dynamics simulations (MD) carried out with SO_4^{2-} and Cl^- anions in H_2O/MeOH (50:50 v/v) allowed the full understanding of anion molecular recognition, the selectivity of the protonated receptor for SO_4^{2-} and the role played by the methanol and water solvent molecules.

2.2 Introduction

Achieving selective recognition, strong binding and transport of anions by synthetic receptors is a goal pursued by many researchers working in the supramolecular chemistry field, as a variety of potential applications can be devised in biomedical and environmental areas.[1] For instance, it as been pointed out that the disease cystic fibrosis is related to a dysfunction of chloride channels and that phosphate and sulfate homeostasis is difficult to maintain in chronic renal disease patients.[2,3] Moreover, the removal of anionic pollutants such as nitrate and phosphate from waterways, the treatment of wastewaters containing

toxic anions (pertechnetate, arsenate, selenate and chromate) and the removal of sulfate from nitrate rich nuclear wastes are also desirable developments.[4]

Despite the considerable effort put in the design of new synthetic receptors, the task of achieving high affinity and selectivity in aqueous media has been quite challenging due to the intrinsic characteristics of anions (larger sizes as compared to isoelectronic metal ions, variety of shapes, hydration energy and pH dependency), and of the receptor that may not be able to confer the necessary rigidity and complementarity for the recognition of the partner. In fact, if the receptor is flexible enough to adapt to the stereochemical requirements of the substrate by distorting its structure or rearranging its conformation, it loses selectivity.

Bearing this in mind we decided to take advantage of the well known ability of tren [tris(2-aminoethyl)amine] derived polyammonium cryptands to strongly bind anions in aqueous media by combining electrostatic and hydrogen bonding interactions,[5] aiming to obtain a more rigid structure by using 2,4,6-triethylbenzene as caps instead of tren. In addition we also expect that the 2,4,6-triethylbenzene capped cryptands will be more lipophilic than the tren derived ones, a characteristic of importance for extraction and transport applications.[6] Therefore, a receptor with *m*-xylyl groups as spacers was synthesised and its binding ability to encapsulate anions of different shape, size and charge was carried out.

Although the tren derived polyammonium cryptands have been extensively studied as receptors for anions, the benzene capped analogs are practically unexplored. In fact, besides an early article by Lehn describing the synthesis and anion binding properties of two benzene capped polyammonium cryptands with aliphatic spacers,[7] only one such cryptand has been reported so far but has been explored for its carbohydrate recognition rather than for anion recognition.[8] It was not until very recently, and when our studies were under progress, that an almost identical cryptand has been studied as halide receptor in DMSO-d_6 by ^{1}H-NMR, although with no quantitative binding information.[9]

2.3 Results and discussion

2.3.1 Synthesis of the cryptand

The cryptand was prepared through a modification of the general synthetic method reported by Chen and Martell,[10] as outlined in Scheme 2.1. Reaction between 1,3,5-tris(aminomethyl)-2,4,6-triethylbenzene and isophthaldehyde in 2:3 ratio in MeCN, yielded the desired hexaimine cage in surprising good yield, taking into account the simultaneous formation of six bonds. The preorganization of both caps and spacers greatly facilitated the synthesis: the alternating substitution pattern in 1,3,5-tris(aminomethyl)-2,4,6-triethylbenzene ensures that the amine groups are oriented on the same face of the aromatic ring[11] while the *meta* positions of the carbonyl groups in isophthaldehyde provide the right angle for the mutual complementarity of the reagents. We found that under the same conditions, the reactions of 1,3,5-tris(aminomethyl)benzene with isophthaldehyde and of 1,3,5-tris(aminomethyl)-2,4,6-triethylbenzene with terephthalaldehyde gave mostly insoluble polymeric materials and less than 5% of the desired hexaimines. Reduction of the hexaimine with $NaBH_4$ resulted in the corresponding hexaamine.

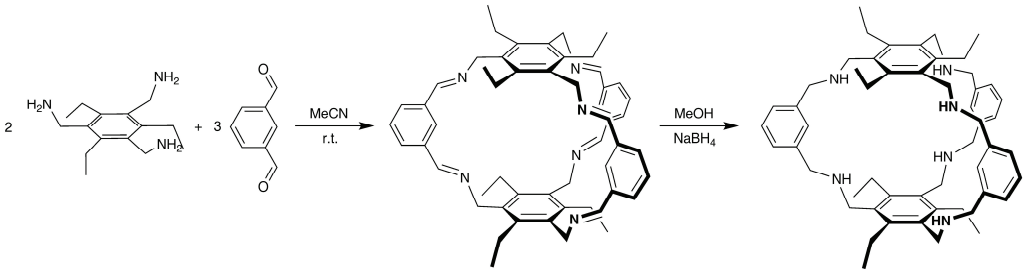

Scheme 2.1 Synthetic procedure of xyl.

2.3.2 Potentiometric studies

2.3.2.1 Acid-base behaviour

The choice of the appropriate background electrolyte to maintain the ionic strength is the first decision to take before the potentiometric measurements for the determination of protonation or association constants were undertaken. The electrolyte salt cannot contain anions that may interact with the receptor, because

it is present in very large concentration compared to the receptor and the substrate species. The bulky potassium tosylate (KTsO) was chosen based on the assumption that it does not appreciably interact with the receptor, as also observed for the tren-capped cryptands.[5b,5e,12] The determined constants are conditional values that only hold for the specific medium used.

The determination of the protonation constants of xyl and all the studied substrates alone and in the same medium is the next step. The measurements were carried out at 298.2±0.1 K in H_2O/MeOH (50:50 v/v) and at ionic strength 0.10±0.01 mol dm^{-3} in KTsO, and the results are shown in Table 2.1 and Table A2.1 (in Appendix).

Table 2.1 Overall (β_i^H) and stepwise protonation (K_i^H) constants of xyl in H_2O/MeOH (50:50 v/v).[a]

Equilibrium reaction	log β_i^{H} [b]	Equilibrium reaction	log K_i^H
$xyl + H^+ \rightleftharpoons Hxyl^+$	8.7[c]	$xyl + H^+ \rightleftharpoons Hxyl^+$	8.7
$xyl + 2\,H^+ \rightleftharpoons H_2xyl^{2+}$	16.56(1)	$Hxyl^+ + H^+ \rightleftharpoons H_2xyl^{2+}$	7.86
$xyl + 3\,H^+ \rightleftharpoons H_3xyl^{3+}$	23.77(1)	$H_2xyl^{2+} + H^+ \rightleftharpoons H_3xyl^{3+}$	7.21
$xyl + 4\,H^+ \rightleftharpoons H_4xyl^{4+}$	30.32(1)	$H_3xyl^{3+} + H^+ \rightleftharpoons H_4xyl^{4+}$	6.55
$xyl + 5\,H^+ \rightleftharpoons H_5xyl^{5+}$	36.29(1)	$H_4xyl^{4+} + H^+ \rightleftharpoons H_5xyl^{5+}$	5.97
$xyl + 6\,H^+ \rightleftharpoons H_6xyl^{6+}$	41.28(1)	$H_5xyl^{5+} + H^+ \rightleftharpoons H_6xyl^{6+}$	4.99

[a] T = (298.2±0.1) K; I = (0.10±0.01) mol dm^{-3} in KTsO. [b] Values in parenthesis are standard deviations in the last significant figures. [c] Estimated value, see text.

The first protonation constant of xyl could not be accurately determined due to precipitation at pH 7.75. Thus the value was estimated at 8.7 assuming that the difference between the first and second protonation constants is mainly due to both statistical factor and electrostatic repulsions. Taking this into account, six protonation constants were found for the xyl cryptand in the working pH region (2.90–7.75) corresponding to the successive protonation of the secondary amines, with the values decreasing steadily with increasing protonation state due to the build up of positive charges.

The corresponding species distribution diagram, represented in Figure 2.1, shows that the hexaprotonated form, H_6xyl^{6+}, exists as the main species up to pH

of about 4.5, at which value all the studied substrates are deprotonated, except dihydrogen phosphate and acetate anions.

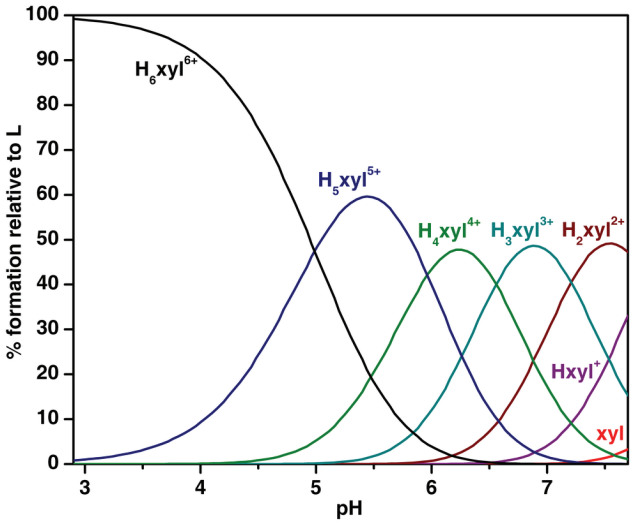

Figure 2.1 Species distribution diagram for the protonation of xyl. C_{xyl}=1.0×10^{-3} mol dm^{-3}.

The overall basicity of the receptor is lower than expected for secondary amines due to the electron withdrawing effect of the *m*-xylyl rings and the 2,4,6-triethylbenzene caps. Indeed the tren derived cryptand with *m*-xylyl spacers[5f] is more basic than xyl in each protonation step and the related cryptand with five –CH_2– groups bridging the two tren caps[5c] is the most basic one.

2.3.2.2 Binding studies

The association constants of the protonated forms of xyl with several anions differing in shape, size and charge were determined in H_2O/MeOH (50:50 v/v) solutions at 298.2 K and 0.10 mol dm^{-3} KTsO. The values obtained are collected in Table 2.2.

A better way to visualise the affinity of the receptor for each anion along the pH region is provided by plots of the effective association constant (Figure 2.2), K_{eff}, in function of the pH. The K_{eff} value is defined as the quotient between the total amount of supramolecular species formed and the total amounts of the free receptor and free substrate: $K_{eff} = \Sigma[(H_{i+j}A)R]/\Sigma[H_iA]\times\Sigma[H_jR]$.[13] This value takes into consideration the different basicities of receptors and substrates thus

Table 2.2 Overall (log $\beta_{H_hL_lA_a}$) and stepwise (log $K_{H_hL_lA_a}$) association constants for the indicated equilibria in H_2O/MeOH (50:50 v/v).[a]

Equilibrium [b]	Cl^-	I^-	NO_3^-	ClO_4^-	AcO^-	SO_4^{2-}	SeO_4^{2-}	$S_2O_3^{2-}$	HPO_4^{2-}
					log $\beta_{H_hL_lA_a}$ [c]				
$7\ H^+ + L + A \rightleftharpoons H_7LA$	–	–	–	–	–	–	–	–	50.86(5)
$6\ H^+ + L + A \rightleftharpoons H_6LA$	43.29(4)	42.77(7)	43.33(4)	43.07(6)	–	46.31(1)	46.32(1)	46.58(1)	46.72(2)
$5\ H^+ + L + A \rightleftharpoons H_5LA$	–	–	–	–	38.57(2)	40.03(1)	40.13(1)	40.36(1)	40.41(2)
$4\ H^+ + L + A \rightleftharpoons H_4LA$	–	–	–	–	32.52(3)	33.01(3)	33.00(1)	33.12(3)	33.66(2)
$3\ H^+ + L + A \rightleftharpoons H_3LA$	–	–	–	–	26.03(3)	–	–	–	–
$2\ H^+ + L + A \rightleftharpoons H_2LA$	–	–	–	–	18.86(4)	–	–	–	–
$H^+ + L + A \rightleftharpoons HLA$	–	–	–	–	10.8(1)	–	–	–	–
					log $K_{H_hL_lA_a}$				
$H_6L^{6+} + A' \rightleftharpoons H_6LA'$	2.01	1.49	2.05	1.79	–	5.03	5.04	5.30	2.12
$H_5L^{5+} + A' \rightleftharpoons H_5LA'$	–	–	–	–	2.28	3.74	3.84	4.07	2.97
$H_4L^{4+} + A' \rightleftharpoons H_4LA'$	–	–	–	–	2.20	2.69	2.67	2.80	2.63
$H_3L^{3+} + A' \rightleftharpoons H_3LA'$	–	–	–	–	2.27	–	–	–	2.43
$H_2L^{2+} + A' \rightleftharpoons H_2LA'$	–	–	–	–	2.30	–	–	–	–
$HL^+ + A' \rightleftharpoons HLA'$	–	–	–	–	2.1	–	–	–	–

[a] T = 298.2±0.1 K; I = 0.10×0.01 mol dm^{-3} in KTsO. [b] L = xyl, A = Cl^-, I^-, NO_3^-, ClO_4^-, AcO^-, SO_4^{2-}, SeO_4^{2-}, $S_2O_3^{2-}$ and HPO_4^{2-} (because only $H_2PO_4^-$ and HPO_4^{2-} are important in the pH range studied this anion was considered diprotic), A' = A in all cases except for phosphate where A' = $H_2PO_4^-$. Charges were omitted in species involving A for simplicity. [c] Values in parentheses are standard deviations for the last significant figure.

provides a suitable way to derive selectivity trends. Furthermore, whenever there is overlapping protonation equilibria between receptors and anions, it is possible to distinguish the stepwise equilibria that effectively occur from all those that can be established for each case.

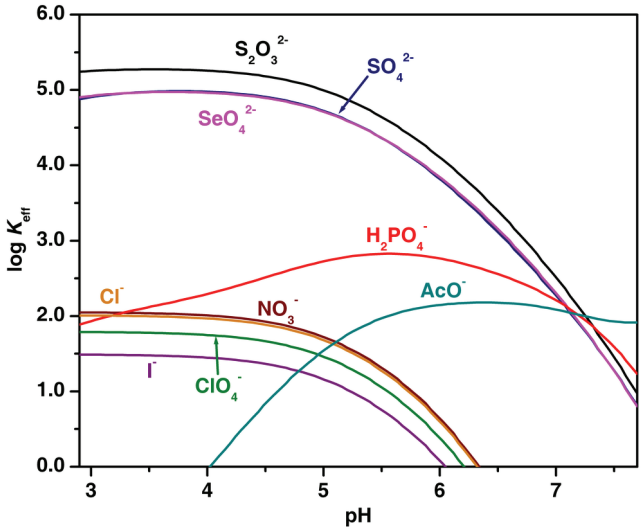

Figure 2.2 Plots of the effective association constant K_{eff} (in log units) *versus* pH for the supramolecular species formed between protonated xyl and the anions studied. $C_{xyl} = C_A = 1\times10^{-3}$ mol dm^{-3}.

Only species of 1:1 (receptor to anionic substrate) stoichiometry were found for all the cases and at different protonation states of xyl. As expected, the association constants increase with increasing positive charge on the receptor and increasing negative charge on the anionic substrate suggesting that the main interactions are of electrostatic nature although contributions of hydrogen bonding are not to be ruled out. In fact, the mononegative and poor hydrogen bond acceptor anions, I^- and ClO_4^-, have the lowest association constants.

Due to the pK_a value of acetate, there is no interaction between this anion and the fully protonated receptor. Furthermore, the association constants do not vary appreciably with decreasing protonation of the receptor. This indicates that acetate is bound to the receptor by only one or two donor centres.

The binding constant of dihydrogen phosphate with H_6xyl^{6+}, is smaller than that with H_5xyl^{5+}. This probably is due to the fact that in the pH region where

these species are formed, H_6xyl^{6+} species coexists in solution partly with H_3PO_4 and H_6xyl^{6+} has no hydrogen bond acceptors to interact with the protons of the substrate. On the other hand, in the H_5xyl^{5+} form, one of the amines can act as hydrogen bond acceptor of the OH groups in dihydrogen phosphate which accounts for the larger constant. However, because the interactions are mainly of electrostatic nature, the association constants progressively drop with the decrease of protonation state of the receptor, although in less extension then in the cases of sulfate, selenate and thiosulfate, indicating that the hydrogen bond donating/accepting abilities of dihydrogen phosphate are still playing a role. This behaviour somewhat recalls the sulfate-binding protein, as its low affinity to phosphate is mainly attributed to the lack of hydrogen bond acceptors in the binding site.[14]

However the most interesting point of the behaviour of the receptor under study it is its remarkable selectivity for dinegative anions over the mononegative ones, although the receptor fails to discriminate between anionic substrates of the same charge and shape. Selenate and sulfate exhibit the same binding affinities, within experimental error, whereas thiosulfate is the most strongly bound. Although the mean S–O distance in thiosulfate should be comparable to that of sulfate and selenate, the long S–S bond and the larger radius of the sulfur atom should account for the enhanced binding constant. This has been found to be true in the crystal structure of tren derived analog with *m*-xylyl spacers in which thiosulfate is the only anion that is able to bind directly to all six protonated amines *via* hydrogen bonds.[15]

The remarkable high selectivity of the receptor for dinegative anions over all mononegative anions studied can be better visualised by a competitive binding diagram, in which the overall percentages of the associated species as a function of pH are displayed for systems containing the receptor and several anions in equimolar amounts.[16] It is quite clear in Figure 2.3 that at pH values bellow 5 the receptor binds exclusively sulfate in a mixture of equimolar amounts chloride, iodide, nitrate, perchlorate, dihydrogen phosphate and acetate.

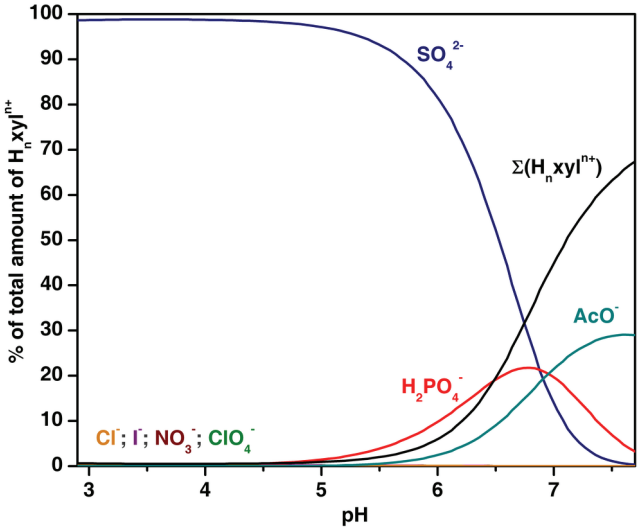

Figure 2.3 Distribution diagram of the overall amounts of supramolecular species formed between the receptor, H_nxyl^{n+}, and each anion. Where SO_4^{2-}, $H_2PO_4^-$, AcO^-, Cl^-, I^-, NO_3^- and ClO_4^- represent $\Sigma[H_nxylA]$, being A the indicated anion. $C_{xyl} = C_A/3 = 1\times10^{-3}$ mol dm^{-3}.

2.3.3 NMR studies

The ^{1}H NMR spectra of xyl were acquired in D_2O at pD = 3.80 and 298.2 K, see Figure 2.4. At this pD value the receptor is expected to be completely protonated (see Figure 2.1).

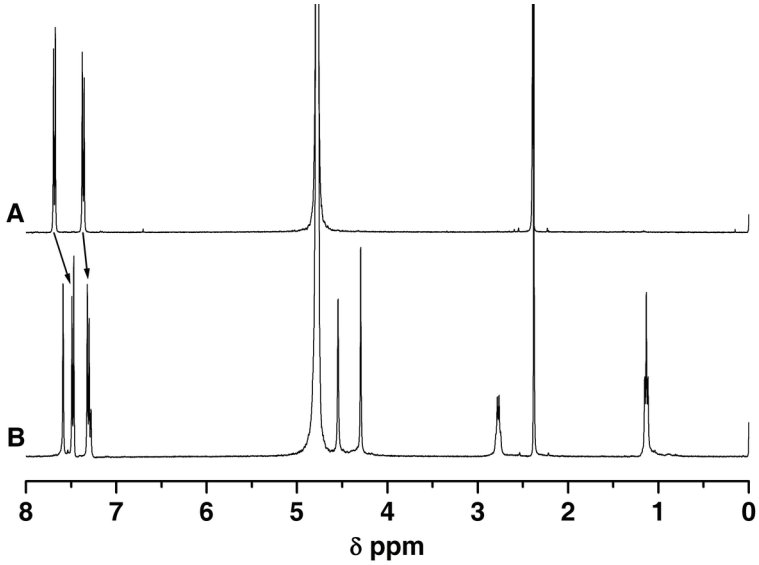

Figure 2.4 ^{1}H NMR spectra of KTsO (A) and of $H_6xyl(TsO)_6$ (B) in D_2O at pD = 3.80 and 298.2 K.

The number and integration of the signals observed in the ^{1}H NMR spectra of H_6xyl^{6+} suggest a highly symmetric structure in solution, consistent with the presence of a C_3 symmetry axis and a horizontal symmetry plane. Another interesting feature is that the tosylate resonances in H_6xyl$(TsO)_6$ are shifted upfield in relation to their free form at the same pD. Moreover, the biggest shift is observed for the doublet resonance corresponding to the hydrogen atoms in the *ortho* position relative to the sulfonate group, while the doublet assigned to the ones in the *meta* position are less shifted and the methyl hydrogen atoms have almost no shift. This indicates that the sulfonate groups are at the entrance of the cavity, with the methyl groups pointing outwards, suggesting that the tosylate is bound in a cleft manner, most likely interacting with the protonated amines that should, on the other hand, be turned outside the cavity. These observations are in close agreement with the reported crystal structure of the hexaprotonated tren derived analog with *m*-xylyl spacers, having tosylate as counter-ion.[12d]

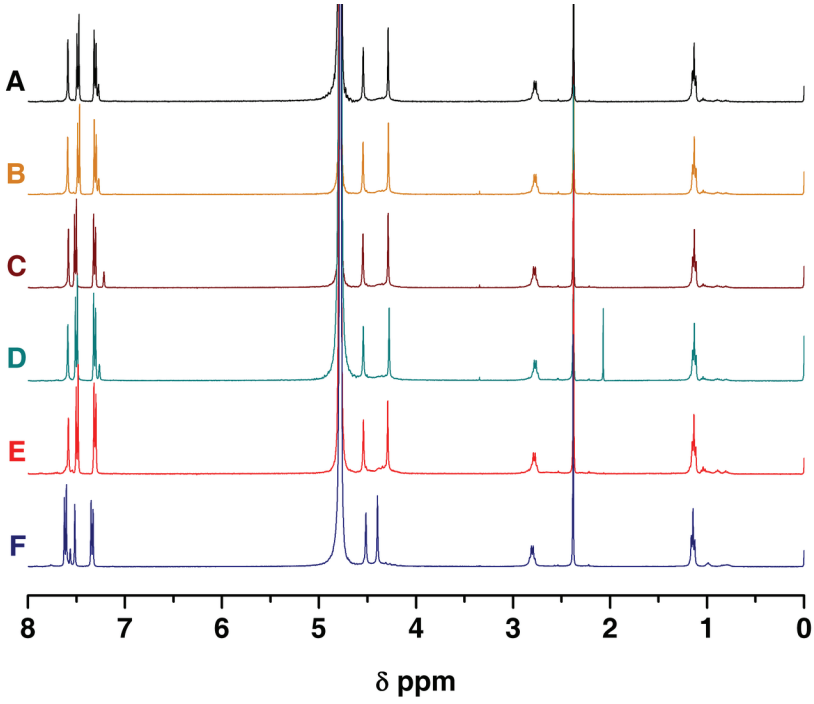

Figure 2.5 ^{1}H NMR spectra of solutions of the H_6xyl$(TsO)_6$ receptor (A) and of the receptor with each anionic substrate in equimolar amounts, Cl^- (B), NO_3^- (C), AcO^- (D), $H_2PO_4^-$ (E) and SO_4^{2-} (F), respectively, in D_2O at pD = 3.80 and 298.2 K.

The ^{1}H-NMR spectra of solutions of equimolar amounts of the receptor and the anionic substrates in D_2O at pD = 3.80 were also recorded (see Figure 2.5). In all cases, only one set of signals was observed for the free receptor and for the associated entities, indicating fast receptor-substrate exchanges on the NMR time scale. As shown in Figure 2.5, in these conditions the shifts of resonances are only significant for sulfate.

The stoichiometry of the H_6xyl^{6+}–SO_4^{2-} associated species was confirmed by performing a Job's plot[17] in which the induced shift was plotted against the mole fraction of the receptor. One-to-one binding was indicated by the maximum value at the host mole fraction of 0.5 (Figure 2.6).

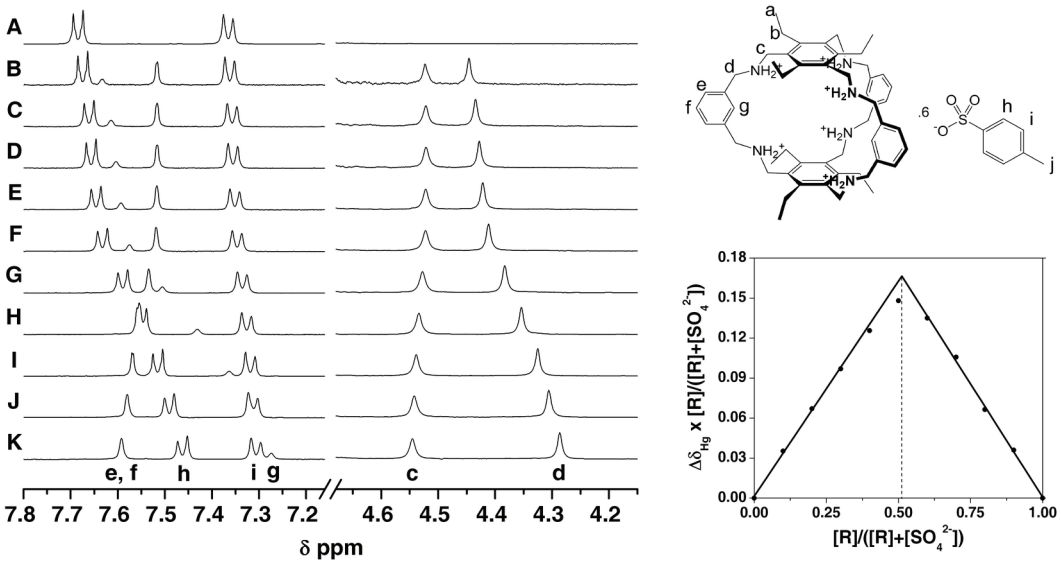

Figure 2.6 Job's plot between H_6xyl^{6+} (R) and sulfate in D_2O at pD = 3.80 and 298.2 K. X = [R]/([R]+[SO_4^{2-}]), being in each spectrum the amount of X: 0 (A), 0.1 (B), 0.2 (C), 0.3 (D), 0.4 (E), 0.5 (F), 0.6 (G), 0.7 (H), 0.8 (I), 0.9 (J), and 1.0 (K), respectively. In all the recorded spectra [R] + [SO_4^{2-}] = 2×10^{-3} mol dm^{-3}. Changes of chemical shifts of H_g resonance in the receptor was monitored (lower right corner).

The set of spectra obtained for the Job's plot also carried additional structural information on the binding event. First of all, it is very clear that the tosylate is excluded from the proximity of the receptor in presence of sulfate, as its chemical shift values tend to those of the free tosylate as the amount of sulfate increases. Furthermore, except for the small upfield shift of the benzylic protons **c**, no

significant shifts were observed for protons related to the caps, namely, protons **a** and **b**, indicating that, as expected, the caps function as rigid scaffolds and that the binding event affects mostly the spacers. In this regard, it can be seen that the proton resonances **d** and **g** undergo the biggest shifts. Surprisingly, downfield shifts are observed for these two protons, which could be attributable to a rearrangement of the receptor upon binding, probably the rotation of the protonated amines to the inside of the cavity. All these observations strongly suggest that the sulfate anion is encapsulated within the receptor cavity.

2.3.4 Electrospray mass spectrometry studies on sulfate cryptate

The ESI mass spectra acquired in positive polarity mode using solutions of 1:1receptor to sulfate stoichiometry in H_2O/MeOH (50:50 v/v) at pH 3.80 (Figure 2.7), showed peaks corresponding to the free receptor and to the sulfate cryptate.

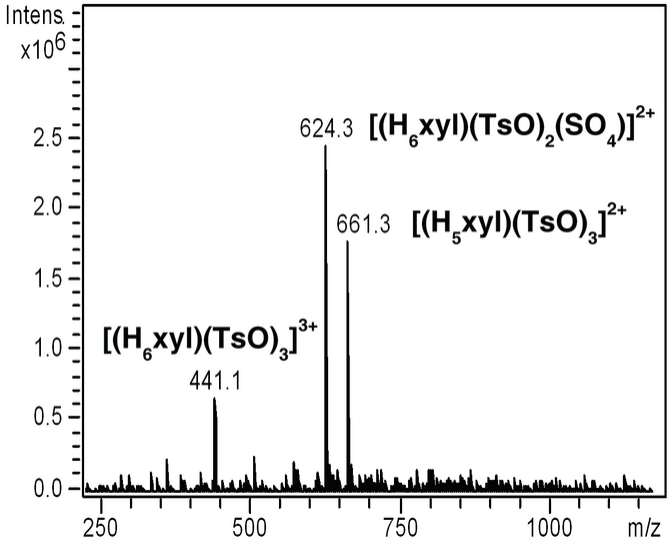

Figure 2.7 ESI mass spectra of a solution of 1:1 receptor to sulfate stoichiometry in H_2O/MeOH (50:50 v/v) at pH = 3.80.

Only one species formed between the association of the hexaprotonated xyl and sulfate was found, $[(H_6xyl)(TsO)_2(SO_4)]^{2+}$ at m/z 624.3, along with two other peaks at m/z 661.3 and 441.1, corresponding to penta and hexaprotonated species of the free receptor, $[(H_5xyl)(TsO)_3]^{2+}$ and $[(H_6xyl)(TsO)_3]^{3+}$, respectively.

These results are in agreement with the potentiometric and ^{1}H-NMR studies, where the hexaprotonated species give rise to more stable cryptates and the binding stoichiometry is 1:1. In a competition experiment using a solution of 1:1:1 receptor/sulfate/nitrate stoichiometry in H_2O/MeOH (50:50 v/v) at pH 3.80 (Figure 2.8) the spectra is identical to the one obtained with solutions of 1:1 receptor to sulfate stoichiometry, demonstrating the high sulfate/nitrate selectivity.

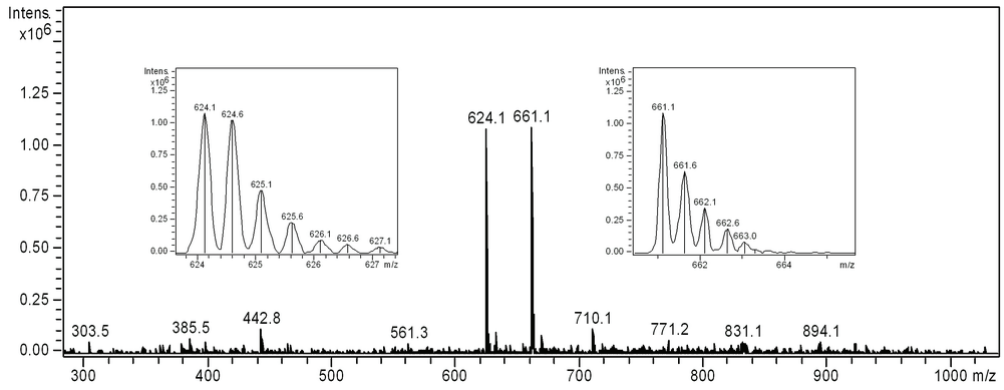

Figure 2.8 ESI mass spectra of a solution of 1:1:1 receptor/sulfate/nitrate stoichiometry in H_2O/MeOH (50:50 v/v) at pH = 3.80.

2.3.5 Crystallographic studies

The crystal structure of the sulfate cryptate is built from an asymmetric unit composed of H_6xyl^{6+} hexaprotonated receptor, three sulfate anions and sixteen water molecules, two of them with half occupancies, which is consistent with the molecular formula $[(H_6xyl)(SO_4)(H_2O)_6](SO_4)_2.9.5H_2O$. One sulfate anion is entirely encapsulated into the macrobicyclic cage as shown in Figure 2.9 in two different views, (a) and (b).

The sulfate anion is sited between the two 2,4,6-triethylbenzene caps at 1.156 Å from the mass centre of the cage determined by the six nitrogen atoms, leading to distances between the centroids of 2,4,6-triethylbenzene rings and the sulfur atom of 5.504 and 3.604 Å, Figure 2.9a. Accordingly, the SO_4^{2-} anion establishes only three straight N–H···O hydrogen bonds with three adjacent N–H binding sites at N···O distances of 2.703(8), 2.809(4) and 2.849(4) Å and N–H···O corresponding angles of 166, 167 and 175º, respectively. Furthermore, the

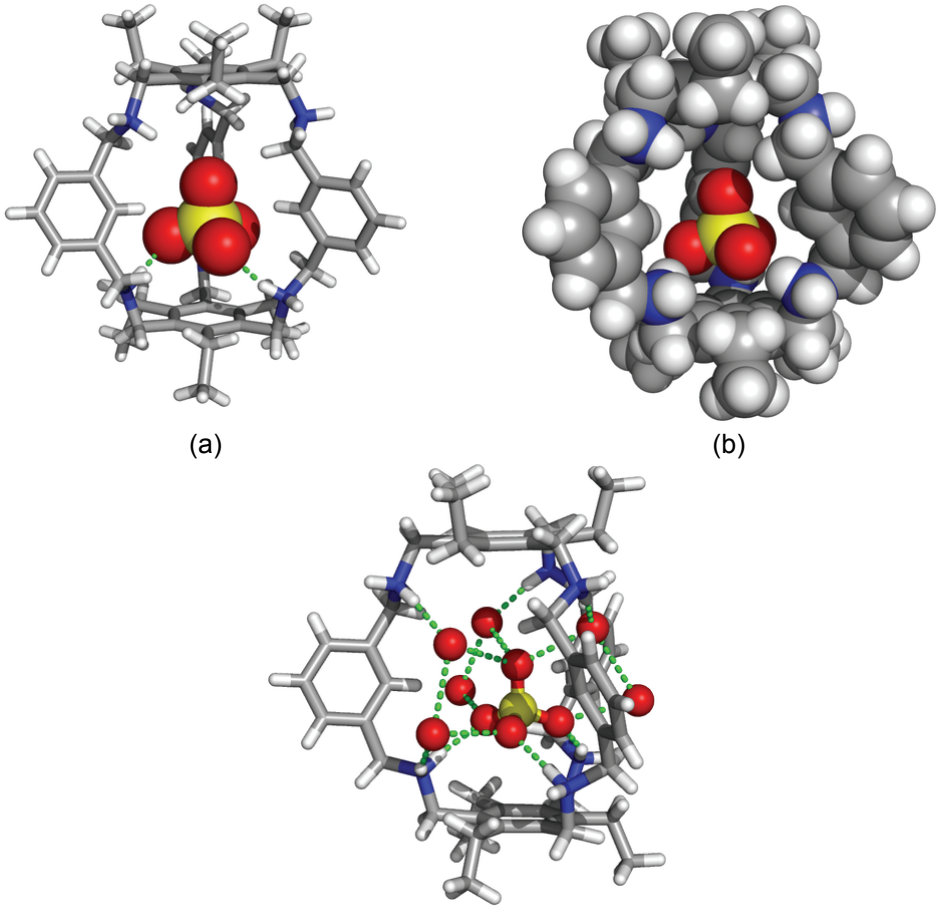

Figure 2.9 Perspective views illustrating different structural features in the associated entity formed between SO_4^{2-} and H_6xyl^{6+} receptor: (a) view showing the sulfate anion inserted into the receptor cavity and its relative position towards to the two 2,4,6-triethylbenzene rings; (b) space-filling view emphasizing the complete encapsulation of sulfate into the cage; (c) hydrogen bonding interactions of the $(SO_4)(H_2O)_6$ cluster with receptor N–H binding centres. The disordered water molecule was shown only in one position. Sulfur, carbon, nitrogen, hydrogen and oxygen atoms are shown in yellow, gray, blue, white and red, respectively. N–H···O hydrogen bonds are drawn as green dashed lines.

perspective view presented in Figure 2.9c indicates that the sulfate anion is also assembled with six crystallization water molecules on a network of O–H···O hydrogen bonding interactions with O···O distances ranging from 2.715(4) to 2.868(4) Å. Four water molecules of the $(SO_4)(H_2O)_6$ cluster interacts with H_6xyl^{6+} through N–H···O hydrogen bonds with N···O distances between 2.820(4) and 2.858(4) Å. In other words, the molecular recognition of the sulfate anion involves

multiple and cooperative N–H···O and O–H···O hydrogen bonding interactions. Another interesting feature revealed by Figure 2.9a and 2.9b is that the 2,4,6-triethylbenzene substituents are positioned above of the corresponding arene rings leaving the binding pocket unlocked for the sulfate entrance.

The H_6xyl^{6+} receptor displays an almost C_3 symmetry, see Figure 2.9b with 3-fold axis perpendicular to the two parallel 2,4,6-triethylbenzene ring caps with lines determined by the centroids of *m*-xylyl spacers and mass centre of the cage intercepting at α angles of 120.6, 122.2 and 117.7º. Comparable binding arrangements were found in the cryptates of the hexaprotonated related 2,4,6-trimethylbenzene-capped hexaazacryptand with *m*-xylyl spacers with iodide and $Cl_3(H_2O)_5$ cluster recently reported.[9] In the first case, the iodide is also inside of the cryptand cage as well as disordered water bounded in a cleft fashion, while in the $Cl_3(H_2O)_5$ cryptate only two water molecules of the cluster are inside of the pocket. The intramolecular distance between the centroids of the two benzene caps of 9.157 Å (β distance) in the sulfate cryptate is slightly shorter than the 9.336 and 9.357 Å found in the I^- and $Cl_3(H_2O)_5$ cryptates, respectively. By contrast, in the corresponding deprotonated cryptand this distance is significantly reduced to 7.582 Å. Thus, these comparisons indicate that the 2,4,6-trialkylbenzene-capped hexaazacryptands have flexibility to enlarge their binding pockets supplying enough room to accommodate large single anion or anions forming supramolecular entities.

In the crystal structure of $[(H_6xyl)(SO_4)(H_2O)_6](SO_4)_2{\cdot}9.5H_2O$, five water molecules as well as one sulfate counter-ion are disordered over two positions (see above). This fact associated with the water hydrogen atoms absence (see above) in the final structure refinement, limited a complete analysis of the hydrogen bonding interactions. However, the crystal packing diagram shows that the five N–H hydrogen bonding sites, not involved in the molecular recognition of $(SO_4)(H_2O)_6$ participates with sulfate counter-anions and water molecules in a extensive network of N–H···O and O–H···O hydrogen bonds, at least with 1-D dimension.

2.3.6 Molecular mechanics and molecular dynamics calculations

The binding mode of sulfate and chloride by the H_6xyl^{6+} receptor was also investigated by means of molecular mechanics (MM) and molecular dynamics (MD) simulations using the Amber10[18] software with the GAFF force field.[19] No bond or angle terms were included in the calculations consequently the attractive interactions between anions and the NH binding sites of H_6xyl^{6+} were primarily electrostatic.

The lowest energy conformations for H_6xyl^{6+} and its associations with SO_4^{2-} and Cl^- obtained in gas phase through quenching molecular dynamics, as described in the experimental section, are shown in Figure 2.10.

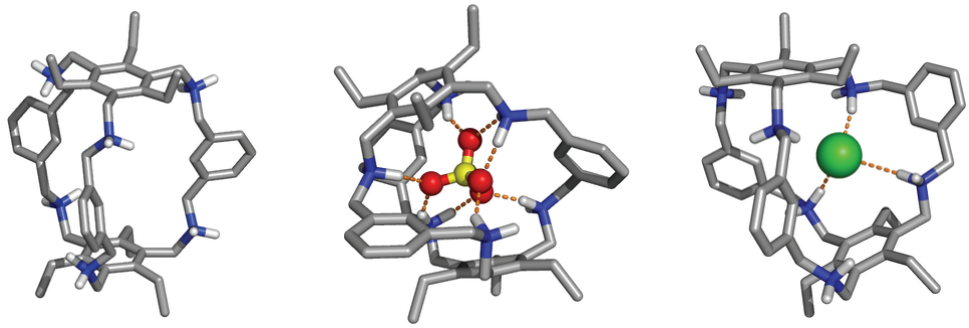

(a) (b) (c)

Figure 2.10 Lowest energy conformations of H_6xyl^{6+} (left), $[(H_6xyl)(SO_4)]^{4+}$ (centre) and $[(H_6xyl)(Cl)]^{5+}$ (right) found in the conformational analyses. C–H hydrogen atoms have been omitted for clarity. Chloride atom in green and hydrogen bonds are drawn as dashed orange lines. The colour scheme of the remaining atoms is given in Figure 2.9.

The free protonated receptor exhibits a symmetric cage with a perfect C_3 symmetry axis with α angles of 120º and β distance of 9.138 Å. This conformation resembles the one found in the crystal structure, $[(H_6xyl)(SO_4)(H_2O)_5]^{4+}$. In contrast, the gas phase structure of $[(H_6xyl)(SO_4)]^{4+}$ does not have a C_3 symmetry exhibiting α angles between 112.8 and 134.7º and a β distance of only 7.617 Å. The sulfate anion is in the middle of the cage at 3.875 Å of both 2,4,6-triethylbenzene caps and all four oxygen atoms are bound to N–H sites from different nitrogen centres, as shown in Figure 2.10 (centre). All nitrogen centres are involved in the molecular recognition of the sulfate with H···O

distances ranging from 1.79 to 1.99 Å. The structure of the association with chloride is also deprived of this symmetry having α angles varying from 91.7 to 147.2º and β distance of 8.355 Å. The chloride is inside of the binding pocket, but it is only hydrogen bonded to three N–H sites with H···Cl distances of 2.12, 2.15 and 2.82 Å. These results indicate that the apparently rigid H_6xyl^{6+} has enough flexibility and space to accommodate anions with different binding requirements and sizes.

The lowest energy structures found for $[(H_6xyl)(SO_4)]^{4+}$ and $[(H_6xyl)(Cl)]^{5+}$ associations were solvated with H_2O:MeOH (50:50 v/v), the solvent used in the potentiometric experiments. The dynamic behaviours of these two associations were investigated in this solvent *via* two independent MD runs carried out at 300 K for long 15 ns using a NPT ensemble. The cage of the H_6xyl^{6+} receptor upon recognition of sulfate exhibits many different conformational shapes with the 2,4,6-triethylbenzene caps adopting different poses including an almost parallel arrangement comparable to that found in the $[(H_6xyl)(SO_4)(H_2O)_6]^{4+}$ crystal structure. These conformational changes are accompanied by variations on the cavity size-binding pocket with the distance between the two caps ($C_A\cdots C_A$ distance) ranging from 7.52 to 9.55 Å. The distance of the six nitrogen binding centres to the mass centre of H_6xyl^{6+}, defined by the atomic positions of these atoms ($N\cdots C_N$ distances), ranges between 3.22–5.84 Å, leading to corresponding average values of 4.43(33) Å.

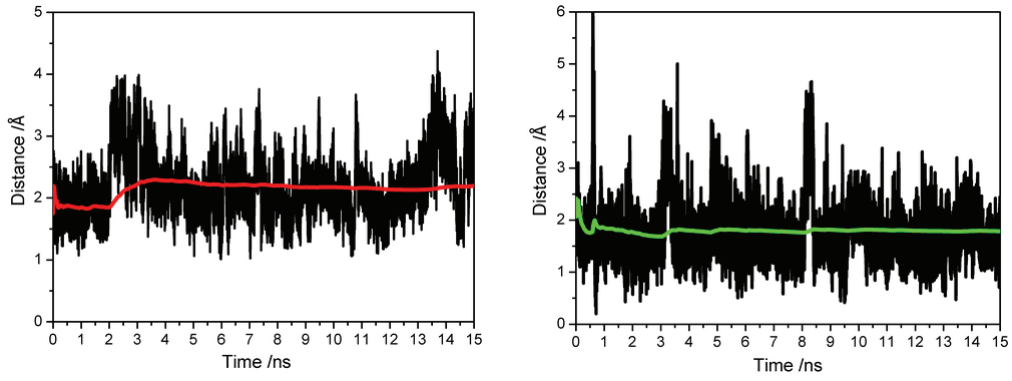

Figure 2.11 Evolution of the sulfate (left) and chloride (right) distances to the binding pocket centre in H_2O:MeOH solution. The red and green lines correspond to the $S\cdots C_N$ and $Cl\cdots C_N$ accumulated average distances, respectively.

The evolution of the sulfate anion distance to the binding pocket centre ($S\cdots C_N$) along the MD simulations, plotted in Figure 2.11, indicates that the sulfate anion remains encapsulated during the entire course of the simulations, establishing with H_6xyl^{6+} weak and multiple exchangeable N–H···O binding interactions consistent with substantial variations on the receptor conformation accompanied of a significant anion movement into the cage. Indeed, occasionally the sulfate anion reaches the pocket boundaries, but never leaving the cage. These structural features are illustrated in Figure 2.12 with two snapshots taken from the simulation.

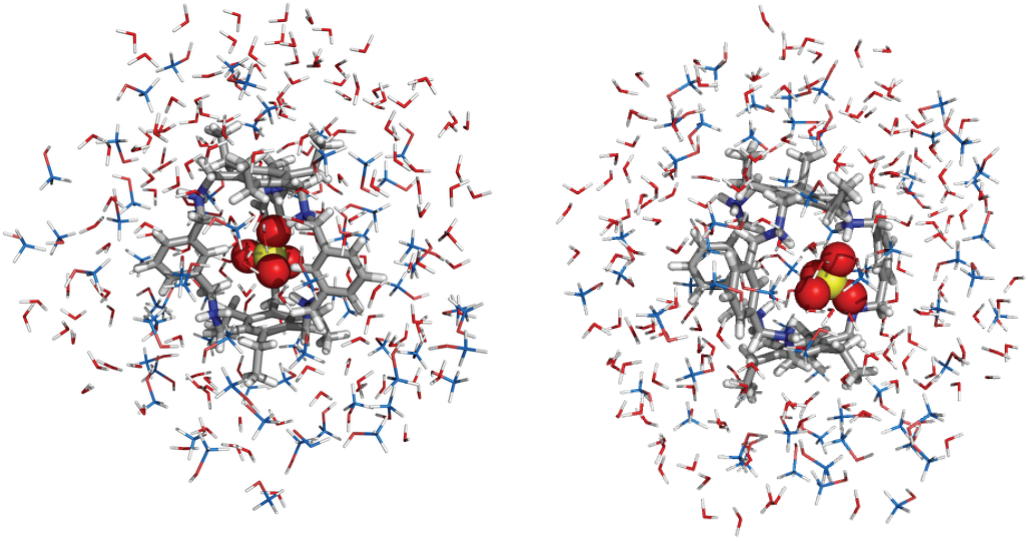

Figure 2.12 Snapshots of $[(H_6xyl)(SO_4)]^{4+}$ taken at 6 ns (left) and 13.7 ns (right) of MD simulation showing the anion located at the centre (left) and at the entrance (right) of the receptor pocket. Only the closest solvent molecules within 8 Å distance from H_6xyl^{6+} are shown. Colour scheme used as given in previous figures apart of the carbon atoms of MeOH, which are drawn in blue.

The variations in the six S···N intermolecular distances reported during the course of simulations are listed in Table 2.3 together with the corresponding average values. Two S···N distances are much longer than the remaining four showing that the receptor recognizes the sulfate anion *via* only four NH_2 binding groups. Moreover, the plot of the S···N distances along the entire time of the simulation presented in Figure A2.1 (see Appendix), indicates that the sulfate anion forms concomitantly hydrogen bonds with N–H groups from three or four

nitrogen centres. Furthermore, all four sulfate oxygen atoms are involved in these interactions with the N···O distances showing large variations between 2.47–7.86 Å, which indicates an exchange of the oxygen donors involved in the N–H···O hydrogen bonds.

Table 2.3 Variations in N···X distances (Å) of $[(H_6xyl)(A)]^{n+}$ (A = SO_4^{2-}, n = 4; A = Cl^-, n =5) over the MD simulations in H_2O:MeOH (50:50 v/v) solution at r.t.

Distances[a]	SO_4^{2-} [b]	Cl^-
N_1···X	4.48–8.99, 6.33(28)	3.00–6.04, 4.56(99)
N_2···X	4.23–8.98, 6.29(25)	3.05–5.95, 4.57(83)
N_3···X	3.06–6.62, 4.34(26)	3.10–5.86, 4.46(44)
N_4···X	3.08–6.62, 4.15(22)	3.17–5.89, 4.60(24)
N_5···X	3.02–6.34, 3.96(19)	2.98–5.89, 4.49(52)
N_6···X	3.11–6.29, 3.90(16)	3.22–6.05, 4.60(50)

[a] The range of distances is followed by the average distance with standard deviations calculated with N = 75000. [b] X = S for the sulfate anion and X = Cl for the chloride anion.

Insights into the solvent effect on the anion recognition were obtained from the radial distributions (rdfs) of the O–H···C_N and O–H···O=S distances between the water or methanol molecules and the mass centres of the receptor and sulfate (defined by the four oxygen atoms), which are plotted in Figure 2.13. The H_6xyl^{6+} presents a first water coordination shell centred at *ca.* 2.85 Å, while the anion exhibits three well defined water shells, the first one at 1.75 Å followed by the second and third ones at 2.95 Å and 3.75 Å, respectively. The water molecules solvate the receptor and the anion in a much higher extension than the methanol molecules, which form around the receptor and anion first coordination shells centred at 2.85 and 1.65 Å, respectively. This fact is consistent with the different numbers of water and methanol molecules that encompass the receptor and sulfate listed in Table 2.4. These numbers were calculated using a cut-off distances of 4.2 Å and 3.5 Å from the receptor and anion mass centres, respectively, and therefore including the number of the solvent molecules inside of the pocket and hydrogen bonded to the anion.

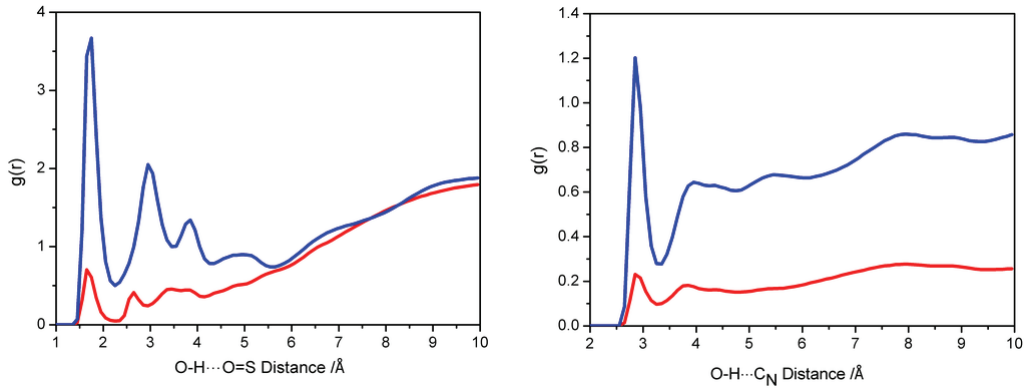

Figure 2.13 Rdfs for O–H···O=S and O–H···C_N distances between the water (blue) and methanol (red) molecules and the centre of mass of the receptor (left) and the anion (right).

Table 2.4 Variations in the number of water and methanol enclosing the receptor and anion estimated with cut-off radius of 4.2 Å and 3.5 Å, respectively.

Cryptate		Methanol[a]	Water[a]
$[(H_6xyl)(SO_4)]^{4+}$	$(H_6xyl)^{6+}$	0–16 (7)	7–30 (19)
	SO_4^{2-}	0–5 (1)	2–12 (7)
$[(H_6xyl)(Cl)]^{5+}$	$(H_6xyl)^{6+}$	0–17 (7)	7–33 (19)
	Cl^-	0–4 (1)	0–8 (3)

[a] In parenthesis are the average number of solvent molecules.

The charge balance of $[(H_6xyl)(SO_4)]^{4+}$ in solution under periodic frontier conditions was achieved by the addition of four chloride anions. The Cl···C_N distances together with N···Cl distances found indicate that these counter-ions never enter into the binding pocket. In addition, as expected, some of the chloride counter-ions interact with N–H binding groups pointing to outside of the macrobicyclic cavity with shortest N···Cl distances of 4.4 Å. Therefore, chloride counter-ions have a marginal effect on the dynamic behaviour of $[(H_6xyl)(SO_4)]^{4+}$ association.

As reported for the sulfate recognition, the receptor upon chloride binding also undergoes a large conformational change accompanied of wide variations on the C_A···C_A, between 7.16 and 9.79 Å, and C_N···N distances from 3.00 to 6.05 Å for 15 ns of simulation. The evolution of the chloride anion distance to the binding pocket centre (Cl···C_N) during the course of simulation is also plotted in Figure 2.11 (right). The chloride remains encapsulated into the binding pocket

during almost the entire time of the simulation leaving sporadically the receptor for few picoseconds.

The wide variations found in all Cl···N intermolecular distances, listed in Table 2.3, indicate that all six nitrogen centres are involved in the anion binding with chloride swapping between them. It is also noteworthy that the chloride anion interacts simultaneously only with two amine groups. In addition it shares occasionally the cage room with one of the five chloride counter-ions added to the periodic system for the charge balance of $[(H_6xyl)(Cl)]^{5+}$. These structural findings show that the receptor cage cavity is large enough to accommodate well one or two chloride anions. The Figure 2.14 presents two snapshots taken from the simulation showing one chloride inside of the binding pocket and two chlorides accommodated into the receptor.

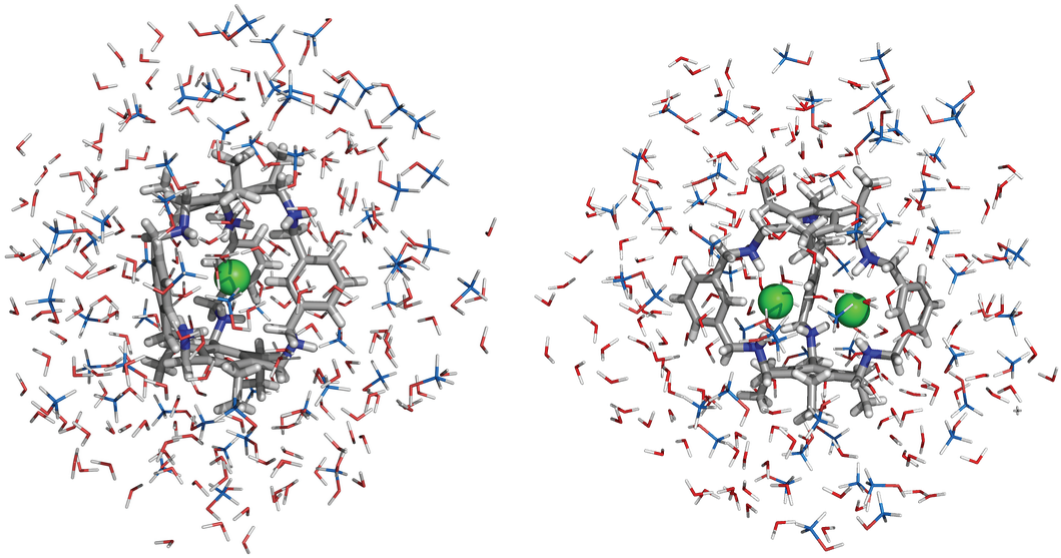

Figure 2.14 Snapshots of the association between H_6xyl^{6+} and chloride taken at 3.0 ns (left) and 1.6 ns (right) of MD simulation showing one and two chloride anions accommodated into the cryptand cage. The other four chloride anions are omitted. Remaining details as given in previous figures.

The rdfs for O–H···Cl and C_N···O–H distances presented in Figure A2.2 (see Appendix) once more shows that the receptor and the chloride anion, are solvated in much higher extension by the water than the methanol molecules, which is corroborated by the number of estimated solvent molecules that enclose both species in H_2O:MeOH solvent mixture (Table 2.4).

In summary, the conventional MD simulations undertaken allowed a full understanding of the receptor binding preference for sulfate relatively to chloride based on structural findings reported.

2.4 Conclusions

Solution studies revealed that the receptor is remarkably selective for dinegative anions over mononegative ones at pH values below 5. In fact, in this pH region, the protonated receptor is able to exclusively bind any of the dinegative anions in the presence of equimolar amounts of all the mononegative ones. Therefore the receptor selectively uptakes sulfate in a mixture of sulfate and nitrate, making xyl an attractive candidate to be used in nuclear waste remediation.[4]

Sulfate, selenate and thiosulfate have the same charge, geometry and about the same size thus the receptor is unable to discriminate them, a characteristic shared by most natural transporters.[20]

The potentiometric studies revealed that the main interaction are of electrostatic nature although contributions of hydrogen bonding are not to be ruled out, as it was found that the poor hydrogen bond acceptor anions, I^- and ClO_4^-, have the lowest association constants. The importance of hydrogen bonds was also highlighted by the fact that when the receptor is fully protonated it lacks hydrogen bond acceptors for dihydrogen phosphate OH groups, which accounts for the low association constant found for $[(H_6xyl)(H_2PO_4)]^{5+}$, resembling the sulfate binding protein.[14] Single crystal X-ray studies showed that in the solid state one sulfate anion is encapsulated into the receptor cage trough three N–H···O hydrogen bonding interactions. The molecular recognition process was investigated in solution theoretically by MD simulations, which also indicated that the sulfate and chloride binding is dictated by electrostatic interactions complemented by multiple N–H···O or N–H···Cl hydrogen bonds. MD simulations allowed understanding of the receptor binding preference for sulfate relatively to chloride.

2.5 Experimental

2.5.1 General considerations

All solvents and chemicals were commercially purchased reagent grade quality and used as supplied without further purification, except 1,3,5-tris(aminomethyl)-2,4,6-triethylbenzene which was prepared according to literature methods.[21] Potassium or sodium salts of the anions were purchased as analytical grade and were used without further purification. Potassium *p*-toluenesulfonate (KTsO) was prepared by the neutralization of *p*-toluenesulfonic acid (HTsO) with KOH in water, followed by recrystallization from H_2O/MeOH. All the solutions were prepared using demineralised water (obtained by a Millipore/Milli-Q system) and methanol purified by standard methods.[22] NMR spectra used for characterization of products and binding experiments were recorded on a Bruker Avance 400 instrument. The reference used for the ^1H NMR measurements in $CDCl_3$ was TMS and in D_2O the 3-(trimethylsilyl)-propanoic acid-d_4-sodium salt. Peak assignments are based on peak integration and multiplicity for 1D ^1H spectra and on COSY, NOESY and HMQC experiments (Figures A2.3-A2.9 in Appendix). Microanalyses were carried out by the ITQB Microanalytical Service.

2.5.2 Synthesis

2.5.2.1 Schiff's base of xyl

A solution of 1,3,5-tris(aminomethyl)-2,4,6-triethylbenzene (300 mg, 1.2 mmol) in MeCN (30 cm^3) was added dropwise over 15 minutes to a magnetically stirred solution of isophthaldehyde (242 mg, 1.8 mmol) in MeCN (30 cm^3). The mixture was left under stirring during the night and a white precipitate formed which was separated by filtration and washed with MeCN (about 100 cm^3) to remove any unreacted starting materials. The precipitate was suspended in $CHCl_3$ (100 cm^3), ultrasonicated for 1 hour and filtered. Evaporation of the solvent yielded the desired hexaimine which was dried in vacuum. Yield: 90%, ^1H NMR (400 MHz, $CDCl_3$, 25 ºC, TMS): δ = 8.08 (d, ^3J (H,H) = 8.0 Hz, 6 H, H4, H6, *m*-xylyl), 7.72 (s, 6 H, HC=N), 7.42 (t, ^3J (H,H) = 7.6 Hz, 3 H, H5, *m*-xylyl), 6.99 (s, 3

H, H2, *m*-xylyl), 5.01 (s, 12 H, CH_2Bz), 2.25 (q, ^3J (H,H) = 8.0 Hz, 12 H, $BzCH_2CH_3$), 1.15 ppm (t, ^3J (H,H) = 8.0 Hz, 18H, $BzCH_2CH_3$); ^{13}C NMR (100 MHz, $CDCl_3$, 25 ºC, TMS): δ = 157.95 (C=N), 144.41 (C1, C3, C5, Bz), 136.80 (C1, C3, *m*-xylyl), 131.36 (C2, C4, C6, Bz), 130.71 (C2, *m*-xylyl), 129.42 (C5, *m*-xylyl), 128.68 (C6, C4, *m*-xylyl), 54.82 (CH_2Bz), 23.70 ($BzCH_2CH_3$), 16.11 ppm ($BzCH_2CH_3$).

2.5.2.2 xyl

Solid $NaBH_4$ (1.226 g, 32.4 mmol) was added in small portions to a magnetically stirred suspension of the hexaimine (432 mg, 0.54 mmol) in methanol (65 cm^3). After the addition was completed, the mixture was left under stirring at room temperature for two hours, and under reflux overnight. The solution was evaporated under vacuum almost to dryness, then 1 mol dm^{-3} HCl (10 cm^3) was added and the entire methanol was evaporated. The solution was made strongly basic with 6 mol dm^{-3} KOH and extracted with $CHCl_3$ (3×50 cm^3). The organic portions were collected in an Erlenmeyer flask, dried over anhydrous sodium sulfate, filtered, evaporated to dryness and dried under vacuum. Yield: 80%; m.p. 146 ºC (decomp.), ^1H NMR (400 MHz, $CDCl_3$, 25 ºC, TMS): δ = 7.26 (s, 3 H, H2, *m*-xylyl), 7.14 (t, 3 H, ^3J (H,H) = 4.0, H5, *m*-xylyl), 7.01 (d, 6 H, ^3J (H,H) = 8.0, H6, H4, *m*-xylyl), 3.89 (s, 12 H, *m*-xylyl-CH_2), 3.76 (s, 12 H, CH_2Bz), 2.70 (q, 12 H, ^3J (H,H) = 8.0 Hz, $BzCH_2CH_3$), 1.35 (bs, NH + H_2O), 1.18 ppm (t, 18H, ^3J (H,H) = 8.0 Hz, $BzCH_2CH_3$); ^{13}C NMR (100 MHz, $CDCl_3$, 25 ºC, TMS): δ = 141.37 (C1, C3, C5, Bz), 139.87 (C1, C3, *m*-xylyl), 133.15 (C2, C4, C6, Bz) 126.55 (C5, *m*-xylyl), 124.72 (C4, C6, *m*-xylyl), 122.23 (C2, *m*-xylyl), 54.01 (*m*-xylyl-CH_2), 47.37 (CH_2Bz), 21.70 ($BzCH_2CH_3$), 15.63 ppm ($BzCH_2CH_3$); ESI-MS (MeOH): m/z (%): 805.6 $[M+H]^+$, 403.3 $[M+2H]^{2+}$; elemental analysis calcd (%) for $C_{54}H_{72}N_6.CHCl_3.H_2O$: C 70.08, H 8.02, N 8.92; found: C 69.85, H 8.31, N 8.82.

2.5.2.3 Crystals of $[(H_6xyl)(SO_4)(H_2O)_6](SO_4)_2 \cdot 9.5H_2O$

xyl (4.03 mg, 5 μmol) was dissolved in acetone (500 μL) and 97% H_2SO_4 (0.833 μL) was added. Immediately a white precipitate was formed. Water (140

μL) was added and the solution heated until it was clear, then the mixture was allowed to slowly cool to r.t. Single colourless crystals suitable for X-ray crystallography were obtained over night.

2.5.3 Potentiometric measurements

2.5.3.1 Reagents and solutions

All solutions were prepared in water/methanol (50:50 v/v) mixed solvent. A stock solution of the receptor was prepared at *ca*. 1.5×10^{-3} mol dm^{-3}. Anion solutions were prepared at 0.10 mol dm^{-3} from the corresponding potassium salts and the concentrations were checked by titration with standard 0.1 mol dm^{-3} KOH solutions. Carbonate-free solutions of the KOH titrant were prepared from a Merck ampoule diluted to 500 cm^3 of water (freshly boiled for about 2 hours and allowed to cool under nitrogen) to which 500 cm^3 of methanol was added. These solutions were discarded every time carbonate concentration was about 0.5% of the total amount of base. The titrant solutions were standardized (tested by Gran's method).[23]

2.5.3.2 Equipment and working conditions

The potentiometric setup consisted of a 50 cm^3 glass-jacketed titration cell sealed from the atmosphere and connected to a separate glass-jacketed reference electrode cell by salt bridge containing 0.10 mol dm^{-3} KTsO solution. An Orion 720A measuring instrument fitted with a Metrohm 6.0150.100 glass electrode and a Mettler Toledo InLab 301 Ag/AgCl reference electrode was used for the measurements. The ionic strength of the experimental solutions was kept at 0.10 ± 0.01 mol dm^{-3} with KTsO, temperature was controlled at 298.2± 0.1 K using a Huber Polystat cc1 thermostatic system and atmospheric CO_2 was excluded from the titration cell during experiments by passing purified nitrogen across the top of the experimental solution. Titrant solutions were added through capillary tips at the surface of the experimental solution by a Metrohm Dosimat 665 automatic burette. Titration procedure is automatically controlled by software after selection of suitable parameters. The glass electrode was pre-treated by

soaking it in the water–methanol (50:50 v/v) solution over a period of 2 days, in order to prevent erratic responses.

2.5.3.3 Measurements

The $[H^+]$ of the solutions was determined by the measurement of the electromotive force of the cell, $E = E^{o\prime} + Q \log [H^+] + E_j$. The term pH is defined as $-\log [H^+]$. $E^{o\prime}$, Q, E_j and K_w were determined by titration of a solution of known hydrogen-ion concentration at the same ionic strength, using the acid pH range of the titration. The liquid-junction potential, E_j, was found to be negligible under the experimental conditions used. The value of K_w was determined from data obtained in the alkaline range of the titration, considering $E^{o\prime}$ and Q valid for the entire pH range and found to be equal to $10^{-13.91}$ in our experimental conditions. Before and after each set of titrations the glass electrode was calibrated as a $[H^+]$ probe by titration of 1.0×10^{-3} mol dm^{-3} standard HCl solution with standard KOH. The potentiometric equilibrium measurements were carried out using 20.00 cm^3 of $\approx 1.50\times10^{-3}$ mol dm^{-3} ligand solution diluted to a final volume of 30.00 cm^3, in the absence of any anions, then in the presence of each anion at 1:3 R:A ratios (R = receptor and A = anion). Care has been taken to maintain unaltered the methanol–water ratio in measured solution. The exact amount of ligand was obtained by determination of the excess of acid present in a mixture of xyl and standard *p*-toluenesulfonic acid 1.0×10^{-2} mol dm^{-3} by titration with standard KOH solution.

2.5.3.4 Calculation of equilibrium constants

Overall protonation constants, β_i^H, of both ligand and anions, were calculated by fitting the potentiometric data obtained for all the performed titrations in the same experimental conditions with the HYPERQUAD program.[24] All these constants were taken as fixed values to obtain the equilibrium constants of the new species from the experimental data corresponding to all the titrations at 1:3 R:A ratio, also using the HYPERQUAD program. The initial computations were obtained in the form of overall stability constants, β_{HhLlAa} values, β_{HhLlAa} =

$[H_hL_lA_a]/[H]^h[L]^l[A]^a$. The errors quoted are the standard deviations of the overall association constants given directly by the program for the input data, which include all the experimental points of all titration curves. The HYSS program[25] was used to calculate the concentration of equilibrium species from the calculated constants from which distribution diagrams were plotted. The species considered in a particular model were those that could be justified by the principles of supramolecular chemistry.

2.5.4 NMR studies

2.5.4.1 ^{1}H-NMR of the cryptates

Solutions of the $(H_6xyl)(TsO)_6$ and respective cryptates where prepared in D_2O (≈ 2.0×10^{-3} mol dm^{-3}) and the pD was adjusted to 3.80 by addition of DTsO or KOD with a Orion 420A instrument fitted with a combined Ingold 405M3 microelectrode. The pH*, the reading of the pH meter previously calibrated with two standard aqueous buffers at pH 4 and 8, was measured directly in the NMR tube. The final pD was calculated from pD = pH* + (0.40 ± 0.02).[26]

2.5.4.2 Job's Plots

Stock solutions of 2.0×10^{-3} mol dm^{-3} $(H_6xyl)(TsO)_6$ and K_2SO_4 were prepared in D_2O. Ten NMR tubes were prepared having a total concentration of $(H_6xyl)(TsO)_6$ and of K_2SO_4 maintained at 2.0×10^{-3} mol dm^{-3}. The pD value was adjusted to 3.80 with DTsO or KOD. The chemical shift changes for each solution were measured, and the product between the increment in chemical shift and receptor concentration versus the molar fraction of the receptor was plotted. A curve is generated where the maximum point indicates the stoichiometry of the association by use of the equation, $[C] = [R]_0\times(\delta_{obs}-\delta_R)/(\delta_{max}-\delta_R)$, where $[R]_0$ is the total receptor concentration, δ_{obs} is the observed chemical shift, δ_R is the chemical shift of the free receptor, and δ_{max} is the chemical shift of the cryptate. Because $\delta_{max}-\delta_R$ is a constant, the concentration of the associated entity is proportional to $\Delta\delta\times[R]_0$ (where $\Delta\delta = \delta_{obs}-\delta_R$). Plots of $\Delta\delta X_R$ as a function of X_R (where X_R is the

molar fraction of the receptor) that exhibit a maximum at X_R = 0.5, indicate a 1:1 association.

2.5.5 Mass spectrometry studies

Two solutions were prepared, one containing $(H_6xyl)(TsO)_6$ and K_2SO_4 diluted to a concentration of 1.0×10^{-5} mol dm^{-3} in water/methanol (50:50 v/v) and another containing $(H_6xyl)(TsO)_6$, K_2SO_4 and KNO_3 diluted to a concentration of 1.0×10^{-5} mol dm^{-3} also in water/methanol (50:50 v/v). Mass spectra for both solutions have been acquired in the positive polarity mode, after their direct injection into the mass spectrometer using a syringe pump, in a Bruker Daltonics Esquire 3000plus mass spectrometer equipped with ESI source. The following tune conditions were used: ion spray voltage, 30–80 V ramp range capillary exit and temperature of the heated capillary, 100 ºC. Nitrogen was used as drying gas at a flow rate of 5 L/min and at a constant pressure of 15 psi.

2.5.6 Crystallography

Crystal data of $[(H_6xyl)(SO_4)(H_2O)_6](SO_4)_2.9.5H_2O$. Mr = 1383.63. Triclinic, space group $P\bar{1}$, Z = 2, *a* = 12.5490(5), *b* = 15.0384(6), *c* = 19.0959(7) Å, α = 99.510(2) β = 99.578(2), γ = 98.598(2)º, V = 3446.1(2) $Å^3$, ρ(calc) = 1.333 Mg m^{-3}, 0.192 mm^{-1}. 55623 reflections were collected and subsequently merged to 16070 unique reflections with a R_{int} of 0.0365.

The single crystal X-ray data were collected on a CCD Bruker APEX II at 150(2) K using graphite monochromatized Mo-Kα radiation (λ = 0.71073 Å). The crystal of the complex was positioned at 40 mm from the CCD and the spots were measured using a counting time of 120 s. Data reduction including a multi-scan absorption correction was carried out using the SAINT-NT from Bruker AXS. The structure was solved by direct methods and by subsequent difference Fourier syntheses and refined by full matrix least squares on F^2 using the SHELX-97 suite.[27] One SO_4^{2-} counter-ion was found to be disordered with the sulfur and four oxygen atoms occupying two alternative positions, which were included in the model refinement with refined occupancies of *x* and 1-*x*, being *x*

equal to 0.590(4). Among sixteen crystallization water solvent molecules, five were found disordered over two or three positions (one molecule), with occupation factors ranging from 0.25 to 0.75. Anisotropic thermal parameters were used for all non-hydrogen atoms. The N–H and C–H hydrogen atoms were refined with U_{iso} = 1.2U_{eq} of the parent atom. The hydrogen atoms of the water molecules were not apparent from the last Fourier difference maps and they were not included in the structure refinement.

The final refinement of 935 parameters converged to final R and R_w indices R_1 = 0.0777 and wR_2 = 0.2247 for 10951 reflections with $I>2\sigma(I)$ and R_1 = 0.1133 and wR_2 = 0.2578 for all *hkl* data.

2.5.7 Molecular modelling simulations

MM and MD simulations were carried out using Amber10[18] suites of program, with parameters for the receptor and sulfate taken from the GAFF[19] force field. The methanol solvent molecules were described using a full atom solvent model with atomic charges and force field parameters taken from ref. 28 and the TIP3P model was used for the water.[29] The chloride ion with a charge of –1 was described with Van der Waals parameters taken from ref. 30. The atomic charges for the receptor and sulfate anion were calculated at the HF/6-31G* level using RESP methodology with Gaussian03.[31]

The structure of the protonated receptor was taken from crystal structure of $[(H_6xyl)(SO_4)(H_2O)_6](SO_4)_2.9.5H_2O$. The conformational analysis of H_6xyl^{6+} was carried out by MD using the following procedure: the MM minimized structure was subjected to a MD quenching run in gas phase at 2000 K using a time step of 1 fs. 20 000 conformations were collected over 2 ns simulation time and then they were minimized by MM using an in-house script.

The docking between the receptor and sulfate and chloride anions was also performed through quenching molecular dynamics using equivalent procedure adopted for the receptor. The anion was located inside the receptor cavity and 50 000 conformations were collect over 5 ns simulation.

The lowest energy geometric arrangements found for sulfate and chloride associations were immersed in H_2O:MeOH cubic boxes having a total of 2905 solvent molecules. The electrostatic neutrality of the periodic cubic systems was achieved with the replacement of solvent molecules by the equivalent number of chloride anions depending on the total charge of the system.

All the MD simulations started with equilibration of the system under periodic boundary conditions using a multistage protocol composed of two successive MM minimizations, to eliminate undesired short potential contacts. In the first MM minimization 10000 steps of steepest descent method followed by 10000 steps of conjugate gradient methods was done keeping a positional restrain of 500 kcal mol^{-1} $Å^{-2}$ on the associations. In the second MM minimization the positional restrain was removed and 1000 steps by the steepest descent method followed by 10000 steps of conjugate gradient methods were made. Next, a MD-NVT simulation with weak positional restrain of 10 kcal mol^{-1} $Å^{-2}$ on the associations was run for 50 ps to bring the temperature to 300 K. Then, the positional restrain was removed and the equilibration process proceed with a MD-NPT simulation run of 500 ps to adjust the solvent density given rise to a cubic boxes with final sizes between 38.9 and 40.0 Å. At this stage the average value of the density remained constant at least during the last 100 ps of the NPT simulation and in agreement with the experimental density at r.t. for H_2O/MeOH (50:50 v/v). Finally, MD data collection run was produced at 300 K and 1 atm for 15 ns using a NPT assemble. All the bonds involving hydrogen atoms were constrained using SHAKE,[32] which allowed the use of a time step of 2 fs. The particle mesh Ewald method[33] was used to describe long range electrostatic interactions and the nonbonded van der Waals interactions were subjected to a 12 Å cutoff.

2.6 Acknowledgements

The authors acknowledge FCT and POCI, with co-participation of the European Community funds FEDER, for the financial support under projects PTDC/QUI/56569/2004 and PTDC/QUI/68582/2006. The NMR spectrometers are part of the National NMR Network and were acquired with funds from FCT and

FEDER. M. C. Almeida is acknowledged for providing elemental analysis and ESI-MS data from the Elemental Analysis and Mass Spectrometry Service at the ITQB. Pedro Mateus thanks FCT for the grant, SFRH/BD/36159/2007.

2.7 References

[1] a) Anion Coordination Chemistry II, ed. P. A. Gale, in *Coord. Chem. Rev.* **2006**, *250*; b) 35 years of Synthetic Anion Receptor Chemistry, ed. P. A. Gale, in *Coord. Chem. Rev.* **2003**, *240*; c) J. L. Sessler, P. I. Sansom, A. Andrievsky, V. Kral in *Supramolecular Chemistry of Anions*, eds.: A. Bianchi, K. Bowman-James and E. Garcia-España, Pergamon, Oxford, Wiley-VCH, **1997**, pp. 355–419.

[2] D. N. Sheppard, M. J. Welsh, *Physiol. Rev.* **1999**, *79*, 23–45.

[3] a) M. Brunetti, L. Timio, P. Saronio, E. Capodicasa, *J. Nephephrol.* **2001**, *14* , 27–31; b) I. Fernandes, D. Laouari, P. Tutt, G. Hampson, G. Friedlander, C. Silve, *Kidney Int.* **2001**, *59*, 210–221.

[4] B. A. Moyer, L. H. Delmau, C. J. Fowler, A. Ruas, D. A. Bostick, J. L. Sessler, E. Katayev, G. D. Pantos, J. M. Llinares, M. A. Hossain, S. O. Kang, K. Bowman-James in *Advances in Inorganic Chemistry, vol. 59: Template Effects and Molecular Organization*, Eds.: R. van Eldik and K. Bowman-James, Elsevier, Oxford, **2007**, p. 175–204.

[5] a) V. McKee, J. Nelson, R. M. Town, *Chem. Soc. Rev.* **2003**, *32*, 309–325, and references therein; b) R. J. Motekaitis, A. E. Martell, J-M. Lehn, E-I. Watanabe, *Inorg. Chem.* **1982**, *21*, 4253–4251; c) R. J. Motekaitis, A. E. Martell, I. Murase, J-M. Lehn, M. W. Hosseini, *Inorg. Chem.* **1988**, *27*, 3630–3636; d) S. Mason, J. M. Llinares, M. Morton, T. Clifford, K. Bowman-James, *J. Am. Chem. Soc.* **2000**, *122*, 1814–1815; e) J. Aguilar, T. Clifford, A. Danby, J. M. Llinares, S. Mason, E. Garcia-España, K. Bowman-James, *Supramol. Chem.* **2001**, *13*, 405–417; f) J. Nelson, M. Nieuwenhuyzen, I. Pál, R. M. Town, *Dalton Trans*. **2004**, 2303–2308.

[6] K. Gloe, H. Stephan, M. Grotjahn, *Chem. Eng. Technol.* **2003**, *26*, 1107–1117.

[7] D. Heyer, J.-M. Lehn, *Tetrahedron Lett.* **1986**, *27*, 5869–5872.

[8] O. Francesconi, A. Ienco, G. Moneti, C. Nativi, S. Roelens, *Angew. Chem. Int. Ed.* **2006**, *45*, 6693–6696.

[9] M. Arunachalam, I. Ravikumar, P. Ghosh, *J. Org. Chem.* **2008**, *73*, 9144–9147.

[10] D. Chen, A. E. Martell, *Tetrahedron* **1991**, *47*, 6895–6902.

[11] G. Hennrich, E. V. Anslyn*, Chem. Eur. J.* **2002**, *8*, 2218–2224.

[12] a) B. Dietrich, J. Guilhem, J-M., Lehn, C. Pascard, E. Sonveau, *Helv. Chim. Acta* **1984**, *67*, 91–104; b) D. Heyer, J-M., Lehn, *Tettrahedron Lett.* **1986**, *27*, 5869–5672; c) M. J. Hynes, B. Maubert, V. McKee, R. M. Town, J. Nelson, *J. Chem. Soc., Dalton Trans.* **2000**, 2853–2859; d) T. Clifford, A. Danby, J. M. Llinares, S. Mason, N. W. Alcock, D. Powell, J. A. Aguilar, E. Garcia-España, K. Bowman-James, *Inorg. Chem.* **2001**, *40*, 4710–4720.

[13] M. T. Albelda; M. A. Bernardo, E. Garcia-España, M. L. Godino-Salido, S. V. Luis, M. J. Melo, F. Pina, C. Soriano, *J. Chem. Soc., Perkin Trans. 2* **1999**, 2545–2549.

[14] B. L. Jacobson, F. A. Quiocho, *J. Mol. Biol.* **1988**, *204*, 783–787.

[15] B. M. Maubert, J. Nelson, V. McKee, R. M. Town, I. Pál, *J. Chem. Soc., Dalton Trans.* **2001**, 1395–1397.

[16] A. Bianchi, E. Garcia-España, *J. Chem. Educ.* **1999**, *76*, 1727–1732.

[17] K. Hirose, *J. Inclusion Phenom. Macrocyclic Chem.* **2001**, *39*, 193–209.

[18] AMBER 10, D. A. Case, T. A. Darden, T. E. Cheatham III, C. L. Simmerling, J. Wang, R. E. Duke, R. Luo, M. Crowley, R. C. Walker, W. Zhang, K. M. Merz, B.Wang, S. Hayik, A. Roitberg, G. Seabra, I. Kolossváry, K. F. Wong, F. Paesani, J. Vanicek, X. Wu, S. R. Brozell, T. Steinbrecher, H. Gohlke, L. Yang, C.Tan, J. Mongan, V. Hornak, G. Cui, D. H. Mathews, M. G. Seetin, C. Sagui, V. Babin, P. A. Kollman, University of California, San Francisco, **2008**.
[19] J. Wang, R. M. Wolf, J. W. Caldwell, P. A. Kollmann, D. A. Case, *J. Comput. Chem.* **2004**, *25*, 1157–1174.
[20] D. Markovich, *Physiol. Rev.* **2001**, *81*, 1499–1533.
[21] K. J. Wallace, R. Hanes, E. V. Anslyn, J. Morey, K. V. Kilway, J. Siegel, *Synthesis* **2005**, 2080–2083.
[22] D. D. Perrin, W. L. F. Armarego, *Purification of Laboratory Chemicals*, Pergamon, Oxford, 3rd. ed., **1988**, p. 217.
[23] F. J. Rossotti, H. J. Rossotti, *J. Chem. Educ.* **1965**, *42*, 375–378.
[24] P. Gans, A. Sabatini, A. Vacca, *Talanta* **1996**, *43*, 1739–1753.
[25] L. Alderighi, P. Gans, A. Ienco, D. Peters, A. Sabatini, A. Vacca, *Coord. Chem. Rev.* **1999**, *184*, 311–318.
[26] R. Delgado, J. J. R. F. da Silva, M. T. S. Amorim, M. F. Cabral, S. Chaves, J. Costa, *Anal. Chim. Acta* **1991**, *245*, 271–282.
[27] G. M.Sheldrick, Shelx-97, Program for the Solution of Crystal Structures, University of Göttingen, Göttingen (Germany), **1997**.
[28] J. W. Caldwell, P. A. Kollman, *J. Phys. Chem.* **1995**, *99*, 6208–6219.
[29] W. L. Jorgensen, J. Chandrasekhar, J. D. Madura, R. W. Impey, M. L. Klein, *J. Chem. Phys.* **1983**, *79*, 926–935.
[30] I. S. Joung, T. E. Cheatham III, *J. Phys. Chem. B* **2008**, *112*, 9020–9041.
[31] Gaussian 03, Revision C.02, M. J. Frisch, G. W. Trucks, H. B. Schlegel, G. E. Scuseria, M. A. Robb, J. R. Cheeseman, J. A. Montgomery Jr., T. Vreven, K. N. Kudin, J. C. Burant, J. M. Millam, S. S. Iyengar, J. Tomasi, V. Barone, B. Mennucci, M. Cossi, G. Scalmani, N. Rega, G. A. Petersson, H. Nakatsuji, M. Hada, M. Ehara, K. Toyota, R. Fukuda, J. Hasegawa, M. Ishida, T. Nakajima, Y. Honda, O. Kitao, H. Nakai, M. Klene, X. Li, J. E. Knox, H. P. Hratchian, J. B. Cross, V. Bakken, C. Adamo, J. Jaramillo, R. Gomperts, R. E. Stratmann, O. Yazyev, A. J. Austin, R. Cammi, C. Pomelli, J. W. Ochterski, P. Y. Ayala, K. Morokuma, G. A. Voth, P. Salvador, J. J. Dannenberg, V. G. Zakrzewski, S. Dapprich, A. D. Daniels, M. C. Strain, O. Farkas, D. K. Malick, A. D. Rabuck, K. Raghavachari, J. B. Foresman, J. V. Ortiz, Q. Cui, A. G. Baboul, S. Clifford, J. Cioslowski, B. B. Stefanov, G. Liu, A. Liashenko, P. Piskorz, I. Komaromi, R. L. Martin, D. J. Fox, T. Keith, M. A. Al-Laham, C. Y. Peng, A. Nanayakkara, M. Challacombe, P. M. W. Gill, B. Johnson, W. Chen, M. W. Wong, C. Gonzalez, J. A. Pople, Gaussian, Inc., Wallingford CT, **2004**.
[32] J. P. Ryckaert, G. Cicotti, H. J. C. Berendsen, *J. Comput. Phys.* **1977**, *23*, 327–341.
[33] U. Essmann, L. Perera, M. L. Berkowitz, T. Darden, H. Lee, L. G. Perdensen, *J. Chem. Phys.* **1995**, *103*, 8577–8593.

Chapter 3

Polyaza cryptand receptor selective for dihydrogen phosphate

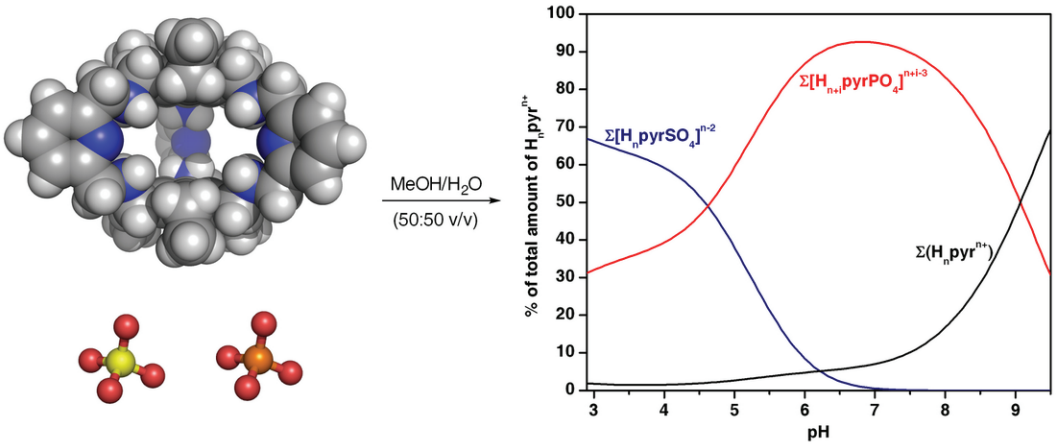

Work featured in: P. Mateus, R. Delgado, P. Brandão, V. Félix, *J. Org. Chem.* **2009**, *74*, 8638–8646.

3.1 Summary

A hexaamine cage with pyridyl spacers was synthesised in good yield by a [2+3] Schiff-base condensation followed by sodium borohydride reduction. The protonation constants of the receptor as well as its association constants with Cl^-, NO_3^-, AcO^-, ClO_4^-, SO_4^{2-}, $H_2PO_4^-$ and $H_2AsO_4^-$ were determined by potentiometry at 298.2±0.1 K in H_2O/MeOH (50:50 v/v) and at ionic strength 0.10±0.01 mol dm^{-3} in KTsO. These studies revealed that although dihydrogen phosphate is less charged than SO_4^{2-}, it is still appreciably bound by the receptor at low pH, suggesting that the pyridyl nitrogen is accepting hydrogen bonds from $H_2PO_4^-$. It is also shown that $H_2PO_4^-$ is capable of effectively competing with SO_4^{2-} for the receptor at higher pH, the latter being selective for hydrogen phosphate at pH about 7.0. ^{31}P NMR experiments supported these findings. The fact that the receptor shows such a marked preference for hydrogen phosphate based mainly in its hydrogen bond accepting/donating ability in a highly competitive medium such as water/methanol mixed solvent is quite remarkable. Single crystal X-ray diffraction determinations of anion associations between H_6pyr^{6+} receptor and nitrate, sulfate and phosphate are consistent with the existence of $[(H_6pyr)(NO_3)_3(H_2O)_3]^{3+}$, $[(H_6pyr)(SO_4)_2(H_2O)_4]^{2+}$ and $[(H_6pyr)(HPO_4)_2(H_2PO_4)(H_2O)_2]^+$ cations. One nitrate anion is embedded into the H_6pyr^{6+} cage of the first supermolecule whereas in the second and third ones the anions are located in the periphery of the macrobicycle.

3.2 Introduction

The important role played by anions in environmental and natural processes have triggered the interest in the development of synthetic receptor molecules for their selective recognition and transport. Among anionic substrates, phosphate and sulfate are of special interest due to their ubiquitous presence in biological systems and also because their well known deleterious effects on the environment.[1]

In Nature, the sulfate-binding protein (SBP) and the phosphate-binding protein (PBP) take advantage of the backbone amide NH groups to tightly bind

their respective substrates with a network of several hydrogen bonds in the interior of a deep cleft completely inaccessible to the solvent.[2,3] The most striking difference between these two proteins is the presence of the carboxylate group of an aspartate residue that functions as a hydrogen bond acceptor for the phosphate OH in PBP. This feature allows PBP to discriminate phosphate from other similar tetrahedral oxyanions such as SO_4^{2-}, which in normal pH lacks OH groups and additionally is repelled by the carboxylate negative charge. Conversely SBP has no hydrogen bond acceptors making it unsuitable for protonated oxyanions.[4]

Polyamines are one of the most successful group of compounds used as receptors for the binding of anions in aqueous medium, due to the versatile nature of the amino group.[5] Amines can be protonated to provide the necessary positive charge to interact with anions and to impart water solubility. The amino group can also act as hydrogen bond donor and as hydrogen bond acceptor if not protonated, which may be useful for the binding of protonated anions such as phosphates. Indeed, several examples of phosphate binding by polyammonium receptors have been reported.[6]

In Chapter 2 a 2,4,6-triethylbenzene capped polyamine cryptand with *m*-xylyl spacers (xyl, Scheme 3.1) was described which in its protonated forms showed remarkable affinity and selectivity for tetrahedral dianionic species in water/methanol mixed solvent. This study suggested that the discrimination of sulfate from phosphate resulted from the fact that at high degree of protonation the receptor lacks hydrogen bond acceptors for dihydrogen phosphate OH groups, resembling the natural systems. It has been pointed out that the introduction of hydrogen bond acceptors for the OH groups of phosphate into an anion receptor should lead to selective recognition of di- or monohydrogen phosphate.[7] Pyridyl moieties have been used in this regard and selectivity for dihydrogen phosphate was achieved by the hydrogen bond acceptor of the pyridyl group.[8] Bearing this in mind it was decided to take advantage of the same macrobicyclic architecture as before and incorporate on its framework

pyridyl spacers (pyr, Scheme 3.1) in order to have a cavity with hydrogen bond acceptors and evaluate the effect on the selectivity pattern.

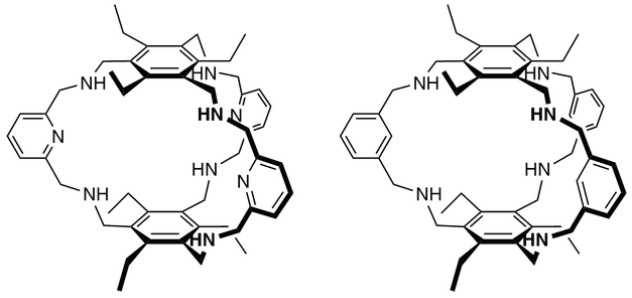

pyr xyl

Scheme 3.1 Polyaza cryptands discussed in this work.

3.3 Results and Discussion

3.3.1 Synthesis of pyr

The hexaamine cryptand containing pyridyl spacers was prepared by reaction between 1,3,5-tris(aminomethyl)-2,4,6-triethylbenzene and 2,6-pyridinedicarbaldehyde in 2:3 ratio in MeCN, followed by addition of sodium borohydride for the reduction of imines to amines. This compound is the hexaamine version of the polyamide bicyclic cyclophane reported by Anslyn *et al.* obtained by a [2+3] reaction between 1,3,5-tris(aminomethyl)-2,4,6-triethylbenzene and 2,6-pyridinedicarbonyl chloride.[9] The pyr cryptand was obtained in 55% yield suggesting that the preorganization of caps and spacers is not the only factor controlling the cyclization process. In fact, as in this type of synthesis the reversible imine condensation is driven towards the formation of the [2+3] product by precipitation, the hexaimine being the kinetically favored product, it is likely that the solubility of the final product in the solvent used may also affect the yield.

3.3.2 Potentiometric studies

3.3.2.1 Acid-base behaviour

As in the work described in the previous chapter, potassium tosylate was chosen as the electrolyte to maintain the ionic strength as this bulky anion did not appreciably interact with the receptor. The studies were performed in H_2O/MeOH

(50:50 v/v) due to the precipitation of the receptor at pH 7.22 in pure water, preventing the determination of the first two protonation constants in that medium, and also to allow direct comparison with the related compound xyl (see Scheme 3.1). The protonation constants of pyr were thus determined at ionic strength 0.10 mol dm^{-3} in KTsO and at 298.2 K in H_2O/MeOH (50:50 v/v). The results are collected in Table 3.1.

Table 3.1 Overall (β_i^H) and stepwise protonation (K_i^H) constants of pyr in H_2O/MeOH (50:50 v/v).[a]

Equilibrium	log β_i^{H} [b]	Equilibrium	log K_i^H
$pyr + H^+ \rightleftharpoons Hpyr^+$	8.72(1)	$pyr + H^+ \rightleftharpoons Hpyr^+$	8.72
$pyr + 2\ H^+ \rightleftharpoons H_2pyr^{2+}$	16.61(1)	$Hpyr^+ + H^+ \rightleftharpoons H_2pyr^{2+}$	7.89
$pyr + 3\ H^+ \rightleftharpoons H_3pyr^{3+}$	23.76(1)	$H_2pyr^{2+} + H^+ \rightleftharpoons H_3pyr^{3+}$	7.15
$pyr + 4\ H^+ \rightleftharpoons H_4pyr^{4+}$	30.16(1)	$H_3pyr^{3+} + H^+ \rightleftharpoons H_4pyr^{4+}$	6.40
$pyr + 5\ H^+ \rightleftharpoons H_5pyr^{5+}$	35.85(1)	$H_4pyr^{4+} + H^+ \rightleftharpoons H_5pyr^{5+}$	5.70
$pyr + 6\ H^+ \rightleftharpoons H_6pyr^{6+}$	40.39(1)	$H_5pyr^{5+} + H^+ \rightleftharpoons H_6pyr^{6+}$	4.54

[a] T = (298.2 ± 0.1) K and I = (0.10 ± 0.01) mol dm^{-3} in KTsO. [b] Values in parenthesis are standard deviations in the last significant figure.

Six protonation constants were found for pyr in the working pH region (2.9–9.5), corresponding to the successive protonations of the secondary amines. The stepwise values decrease steadily with increasing protonation state of the receptor due to both increasing electrostatic repulsion between positive charges and to statistical factors. In this pH region there is no protonation of the pyridyl nitrogens, which should be very acidic. The overall basicity of the receptor is lower than expected for secondary amines due to the electron withdrawing effect of the pyridyl rings and the 2,4,6-triethylbenzene caps. The corresponding distribution curve diagram, represented in Figure 3.1, shows that the hexaprotonated form, H_6pyr^{6+}, exists as the main species at pH values lower than 4.0.

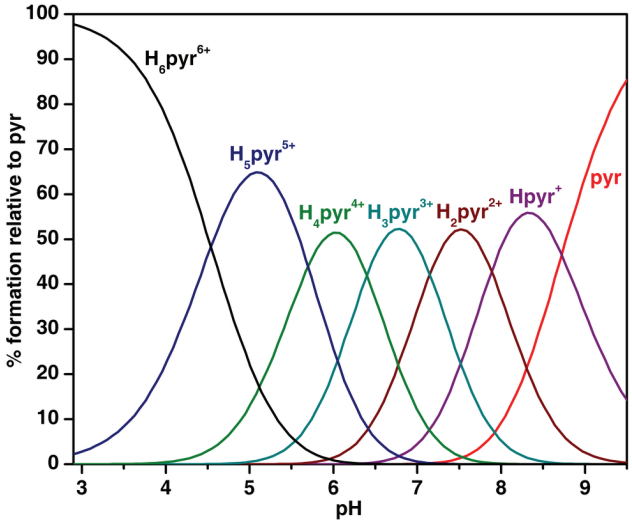

Figure 3.1 Species distribution diagram for the protonation of pyr. C_{pyr}=1.0×10^{-3} mol dm^{-3}.

3.3.2.2 Binding studies

The association constants of the protonated forms of pyr, H_npyr^{n+}, with several anions differing in geometry, size and charge were determined in MeOH/H_2O (50:50 v/v) solutions at 298.2 K and 0.10 mol dm^{-3} KTsO. The protonation constants of the anions have been previously determined in the same experimental conditions (Table A2.1 in Appendix) with the exception of those of arsenate which were found to be 3.01(1), 7.34(1) and 11.33(1). The overall values obtained are collected in Table A3.1 (in Appendix) and in Table 3.2 the stepwise constants, along with those determined for the related cryptand xyl (see Scheme 3.1) for comparison purposes.

The direct comparison of stepwise constants of both receptors with each anion can lead to erroneous conclusions and to incorrect selectivity attributions, especially when there are overlapping protonation equilibria between receptors and anions. The K_{eff} values, defined as the quotient between the total amount of supramolecular species formed and the total amounts of the free receptor and free substrate at a given pH (K_{eff} = Σ[H_{i+j}AL]/Σ[H_iA] Σ[H_jL], L is the ligand and A the anion),[10] not only allow comparisons between different supramolecular systems studied under the same experimental conditions as it takes into consideration the different basicities of receptors and substrates, but also makes

Table 3.2 Stepwise association constants (log K_{HhLlAa}) for the indicated equilibria in H_2O/MeOH (50:50 v/v).[a]

Equilibrium	L = pyr[b]	L = xyl
$H_6L^{6+} + Cl^- \rightleftharpoons [H_6L(Cl)]^{5+}$	2.37(4)	2.01
$H_6L^{6+} + NO_3^- \rightleftharpoons [H_6L(NO_3)]^{5+}$	2.54(1)	2.05
$H_6L^{6+} + ClO_4^- \rightleftharpoons [H_6L(ClO_4)]^{5+}$	–[c]	1.79
$H_6L^{6+} + SO_4^{2-} \rightleftharpoons [H_6L(SO_4)]^{4+}$	4.34(1)	5.03
$H_5L^{5+} + SO_4^{2-} \rightleftharpoons [H_5L(SO_4)]^{3+}$	3.23(1)	3.74
$H_4L^{4+} + SO_4^{2-} \rightleftharpoons [H_4L(SO_4)]^{2+}$	2.20(3)	2.69
$H_5L^{5+} + HAcO \rightleftharpoons [H_5L(HAcO)]^{5+}$	1.78(3)	–
$H_5L^{5+} + AcO^- \rightleftharpoons [H_5L(AcO)]^{4+}$	2.04(2)	2.28
$H_4L^{4+} + AcO^- \rightleftharpoons [H_4L(AcO)]^{3+}$	2.06(2)	2.20
$H_3L^{3+} + AcO^- \rightleftharpoons [H_3L(AcO)]^{2+}$	1.74(2)	2.27
$H_2L^{2+} + AcO^- \rightleftharpoons [H_2L(AcO)]^{+}$	1.42(6)	2.30
$HL^{+} + AcO^- \rightleftharpoons [HL(AcO)]$	–	2.10
$H_6L^{6+} + H_2PO_4^- \rightleftharpoons [H_6L(H_2PO_4)]^{5+}$	4.05(2)	2.12
$H_5L^{5+} + H_2PO_4^- \rightleftharpoons [H_5L(H_2PO_4)]^{4+}$	3.99(2)	2.98
$H_4L^{4+} + H_2PO_4^- \rightleftharpoons [H_4L(H_2PO_4)]^{3+}$	4.01(2)	2.62
$H_3L^{3+} + H_2PO_4^- \rightleftharpoons [H_3L(H_2PO_4)]^{2+}$	4.00(2)	2.43
$H_2L^{2+} + H_2PO_4^- \rightleftharpoons [H_2L(H_2PO_4)]^{+}$	4.00(2)	–
$H_2L^{2+} + HPO_4^{2-} \rightleftharpoons [H_2L(HPO_4)]$	3.68(1)	–
$HL^{+} + HPO_4^{2-} \rightleftharpoons [HL(HPO_4)]^-$	3.17(1)	–
$H_6L^{6+} + H_2AsO_4^- \rightleftharpoons [H_6L(H_2AsO_4)]^{5+}$	3.53(2)	–
$H_5L^{5+} + H_2AsO_4^- \rightleftharpoons [H_5L(H_2AsO_4)]^{4+}$	3.58(2)	–
$H_4L^{4+} + H_2AsO_4^- \rightleftharpoons [H_4L(H_2AsO_4)]^{3+}$	3.61(2)	–
$H_3L^{3+} + H_2AsO_4^- \rightleftharpoons [H_3L(H_2AsO_4)]^{2+}$	3.64(2)	–
$H_2L^{2+} + H_2AsO_4^- \rightleftharpoons [H_2L(H_2AsO_4)]^{+}$	3.69(2)	–
$H_2L^{2+} + HAsO_4^{2-} \rightleftharpoons [H_2L(HAsO_4)]$	3.37(1)	–
$HL^{+} + HAsO_4^{2-} \rightleftharpoons [HL(HAsO_4)]^-$	2.89(1)	–

[a] T = (298.2 ± 0.1) K and I = (0.10 ± 0.01) mol dm^{-3} in KTsO. [b] Values in parenthesis are standard deviations in the last significant figure. [c] Too small to be determined.

it possible to distinguish the stepwise equilibria that effectively occur from all those that can be established for each case. In Figure 3.2 the plots of the effective association constant K_{eff} *versus* pH for the supramolecular associations between the protonated forms of pyr and the studied anions, along with those determined for of the protonated forms of xyl for comparison are shown.

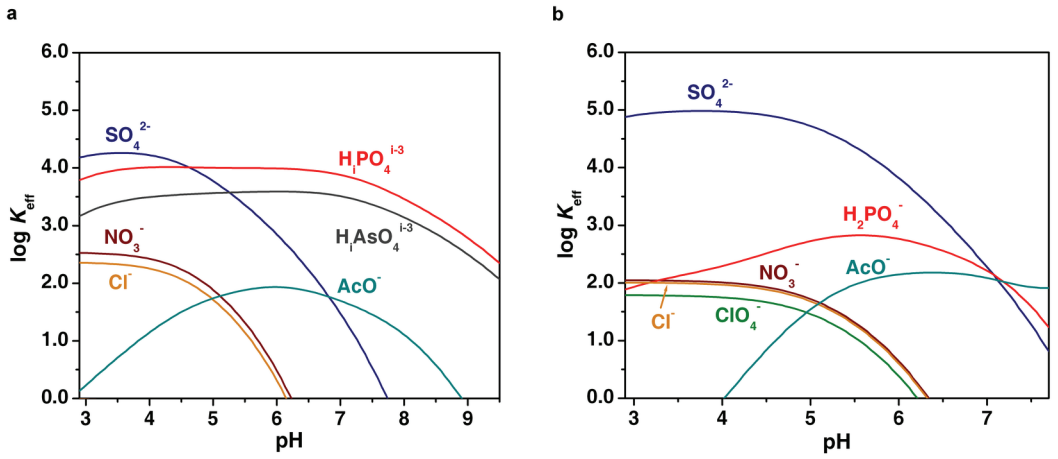

Figure 3.2 Plots of the effective association constant K_{eff} (in log units) *versus* pH for the supramolecular associations between H_npyr^{n+} (a), H_nxyl^{n+} (b) and the studied anions. $C_{pyr} = C_{xyl} = C_A = 1.0\times10^{-3}$ mol dm^{-3}.

Only species of 1:1 receptor to anion stoichiometry were found for the different protonation states of pyr. For fully ionized anions such as chloride, nitrate and sulfate the association constants increase with increasing positive charge on H_npyr^{n+}, the main interaction being of electrostatic nature. Perchlorate showed virtually no binding to the receptor. Although we have found no differences in the selectivity pattern of H_npyr^{n+} and H_nxyl^{n+} for the series of fully ionized anions (SO_4^{2-} >> NO_3^- > Cl^- > ClO_4^-), the H_npyr^{n+} receptor showed a slightly lower affinity for sulfate and also a lower sulfate to nitrate selectivity. Acetate is weakly bound to both receptors, however the binding of H_npyr^{n+} with the protonated form of acetate occurs at lower pH.

The most interesting feature of H_npyr^{n+} is that it binds hydrogen phosphate strongly than does H_nxyl^{n+}, and the effect is more evident at lower pH values. This result can be ascribed to the presence of hydrogen bond acceptors in the cavity, namely the pyridyl nitrogen atoms. Moreover, the association constants for hydrogen phosphate do not vary much in the entire pH region studied. This is due to the fact that hydrogen phosphate and polyammonium receptors can be involved in the formation of several hydrogen bonds in which both the anions and the receptors can act as acceptors or donors.[6e] Hydrogen bonds of the type –N^+–H···$^-$O–, –N^+–H···OH– and –N:···HO– are expected to be formed at low pH. As

deprotonation of the receptor occurs, $–N^{+}–H\cdots{}^{-}O–$ hydrogen bonds will become less important while those of type –N–H···⁻O–, –N–H···OH– and –N:···HO– are expected to dominate.

Arsenate, being structurally similar to phosphate and having very close protonation constants, presents binding constants slightly lower than phosphate despite having a binding behaviour that is completely parallel.

Competitive binding diagrams, in which the overall percentages of the associated species as a function of pH for systems containing the receptor and equimolar amounts of several anions are displayed,[11] give a better overview of the selectivity trends.

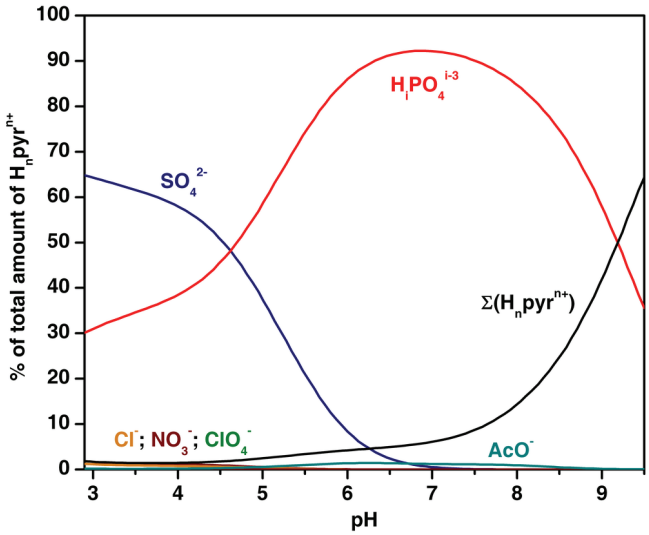

Figure 3.3 Distribution diagram of the overall amounts of supramolecular species formed between the receptor, H_npyr^{n+}, and each anion. Where SO_4^{2-}, $H_iPO_4^{i-3}$, AcO^-, Cl^-, NO_3^- and ClO_4^- represent the total amount of the anion bound to the receptor $\Sigma[H_npyrA]$, being A the indicated anion. $C_{pyr} = C_{anion}/3 = 1\times10^{-3}$ mol dm^{-3}.

As shown in Figure 3.3, at lower pH values the receptor preferably binds sulfate in a mixture of equimolar amounts of chloride, nitrate, perchlorate, dihydrogen phosphate and acetate, even though it is not selective due to strong competition of dihydrogen phosphate. In fact, it is quite remarkable that dihydrogen phosphate, being less charged that sulfate, is still appreciably bound by the receptor, showing the importance of hydrogen bonding formation. Above

pH 4.6 the selectivity is reversed and the receptor preferably binds hydrogen phosphate, due to the fact that it is the only anion that does not rely exclusively on electrostatic interactions and on $–N^{+}–H\cdots{}^{-}O–$ hydrogen bonds. At pH 7 the receptor becomes selective for phosphate.

Defining selectivity as the difference between the log K_{eff} values for the associations of phosphate and sulfate [log K_{eff} (PO_4)–log K_{eff} (SO_4)] in function of the pH, a phosphate/sulfate selectivity profile can be plotted for H_npyr^{n+} and other known polyamine compounds for which binding constants determined in aqueous solution for both anions exist in the literature: obisdien,[6b,12] [21]aneN$_7$,[6e,13] Me$_2$[18]aneN$_6$,[6e,13] Me$_3$[21]aneN$_7$,[6e,13] Me$_4$[18]aneN$_6$,[6e,13] Ph$_2$Me$_6$N$_6$,[6e,13] obistren[6a] and [18]aneN$_6$[6e,13] (see Figure 3.4). The plot clearly shows that H_npyr^{n+} is to the best of our knowledge the artificial polyamine compound with highest reported phosphate/sulfate selectivity in aqueous solutions at pH about 7.0. It should be noted however that for pyr H_2O/MeOH (50:50 v/v) was the solvent used, while in all the other cases the solvent is water.

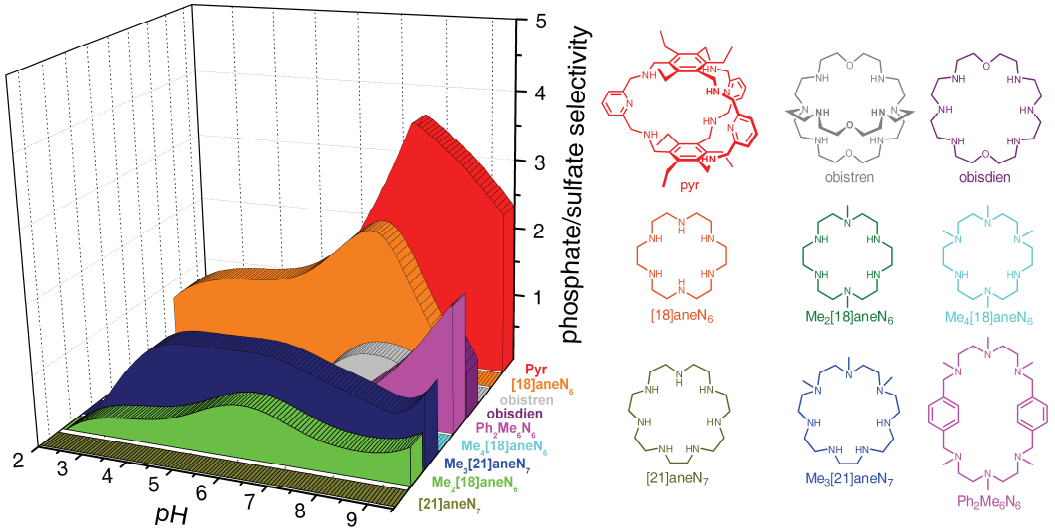

Figure 3.4 Plot of phosphate/sulfate selectivity profile as a function of pH for H_npyr^{n+} and other polyamine compounds: obisdien,[6b,12] [21]aneN$_7$,[6e,13] Me$_2$[18]aneN$_6$,[6e,13] Me$_3$[21]aneN$_7$,[6e,13] Me$_4$[18]aneN$_6$,[6e,13] Ph$_2$Me$_6$N$_6$,[6e,13] obistren[6a] and [18]aneN$_6$.[6e,13]

3.3.3 ^{31}P-NMR studies.

^{31}P-NMR spectra provide a way of getting further insights on the type of hydrogen bonds involved in the binding of phosphate, as the hydrogen bonding interactions in which phosphate acts as hydrogen bond acceptor causes upfield shifts,[14] as it corresponds to a partial protonation of phosphate, whereas when phosphate acts as hydrogen bond donor results in a shift in the opposite direction.

^{31}P NMR spectra of 1:1 H_npyr^{n+} to hydrogen phosphate solutions (H_2O/MeOH 50/50 v/v) were recorded at pH = 3.8 and 7.2. Spectra of hydrogen phosphate solutions alone in the same experimental conditions were also recorded for comparison. The results compiled in Figure 3.5 clearly show that the protonation equilibria of the substrate are disturbed in presence of H_npyr^{n+}. At pH = 3.8, the ^{31}P NMR signal of the 1:1 H_npyr^{n+} to hydrogen phosphate solution shifted upfield relative to the free hydrogen phosphate at the same pH, in agreement with phosphate accepting hydrogen bonds. Under the same conditions, the 1:1 mixture of H_nxyl^{n+} and hydrogen phosphate ^{31}P NMR resonance yields a larger upfield shift than the previous case in spite of its lower K_{eff} value at this pH.

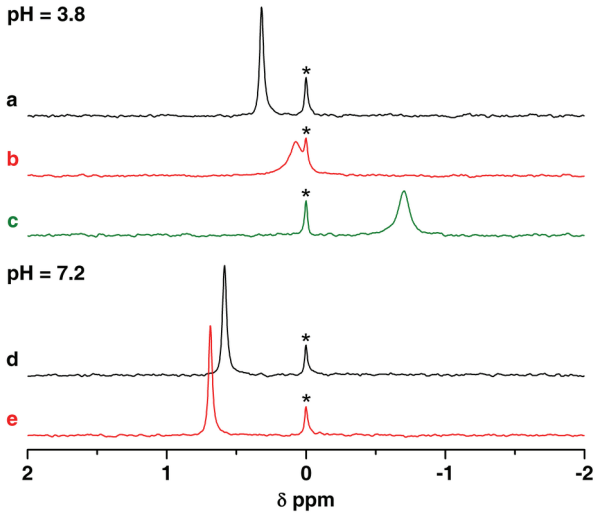

Figure 3.5 ^{31}P-NMR spectra of 1:1 H_npyr^{n+}:hydrogen phosphate solutions in H_2O/MeOH at pH = 3.8 (b) and 7.2 (e), and for free hydrogen phosphate (a) and (d) at 298.2 K. For comparison the ^{31}P-NMR spectrum of hydrogen phosphate in the presence of 1 equivalent of H_nxyl^{n+} (c) is also given in the same experimental conditions. The signal centered at 0 ppm (*) corresponds to H_3PO_4 used as external reference. $C_{pyr} = C_{xyl} = C_{H_nPO_4^{(3-n)-}} = 8.3\times10^{-4}$ mol dm^{-3}. The pH was adjusted to 3.8 or 7.2 by adding small amounts of HTsO or KOH solutions (see Experimental Section).

This result derives from the fact that H_nxyl^{n+} only can act as hydrogen bond donor to the substrate, as at this pH the cavity lacks hydrogen bond acceptors, consequently an upfield shift is observed. In the case of H_npyr^{n+} at the same pH value (3.8) both hydrogen bond donors and acceptors are present and the observed chemical shift is an average between the two effects working in opposite ways, in which the hydrogen bond accepting is predominant. In the two cases the broad linewidth suggests slower receptor-substrate exchanges on the NMR time scale, which is a strong indication of the encapsulation of hydrogen phosphate substrate. Differently, at pH 7.2 the ^{31}P NMR signal of the 1:1 mixture of H_npyr^{n+} and hydrogen phosphate is shifted downfield relative to the free hydrogen phosphate, indicating that the hydrogen bond donating from hydrogen phosphate to the receptor is predominant, in agreement with the partial deprotonation of the receptor at this pH with the concomitant –N:···HO– hydrogen bonds significance.

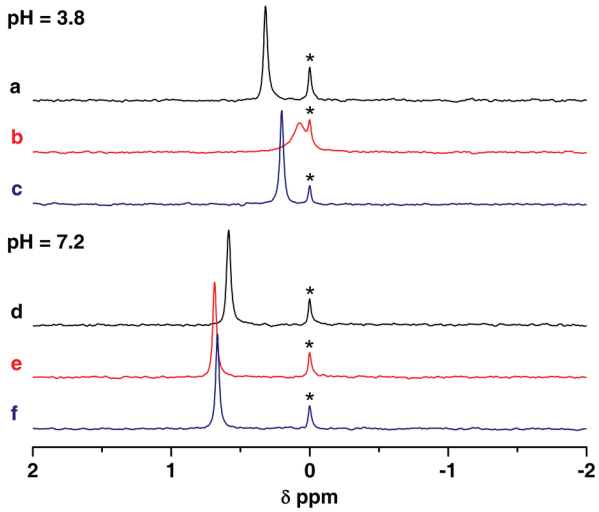

Figure 3.6 ^{31}P-NMR spectra of 1:1:1 H_npyr^{n+}:hydrogen phosphate:sulfate solutions in H_2O/MeOH at pH = 3.8 (c) and 7.2 (f) at 298.2 K. For comparison, the ^{31}P-NMR spectra of 1:1 H_npyr^{n+}:hydrogen phosphate (b) and (e) and of free hydrogen phosphate (a) and (d) in the same experimental conditions already shown in Figure 3.5 were added. The signal centered at 0 ppm (*) corresponds to H_3PO_4 used as external reference. C_{pyr} = $C_{H_nPO_4^{(3-n)-}}$ = $C_{SO_4^{2-}}$ = 8.3×10^{-4} mol dm^{-3}. The pH was adjusted to 3.8 or 7.2 by adding small amounts of HTsO or KOH solutions (see Experimental Section).

A competitive experiment also followed by ^{31}P NMR was performed in which to the 1:1 mixture of H_npyr^{n+} and hydrogen phosphate one equivalent of sulfate was added. The spectra shown in Figure 3.6, revealed that at pH 3.8 sulfate displaces hydrogen phosphate from the receptor, although not completely, while at pH 7.2 the presence of sulfate has almost no influence on the binding of hydrogen phosphate. These results are in excellent agreement with those determined by potentiometry and expressed in Figure 3.3.

3.3.4 Crystallographic studies

Single crystal structures of anion associations of H_6pyr^{6+} receptor with nitrate, sulfate and phosphate were determined by X-ray diffraction and they are consistent with the existence of $[(H_6pyr)(NO_3)_3(H_2O)_3]^{3+}$, $[(H_6pyr)(SO_4)_2(H_2O)_4]^{2+}$ and $[(H_6pyr)(HPO_4)_2(H_2PO_4)(H_2O)_2]^{+}$ cations.

The asymmetric unit of the nitrate association is composed of one hexaprotonated H_6pyr^{6+} receptor, six nitrate anions and seven water molecules, which is consistent with molecular formula $[(H_6pyr)(NO_3)_3(H_2O)_3](NO_3)_3{\cdot}4H_2O$. The structure of $[(H_6pyr)(NO_3)_3(H_2O)_3]^{3+}$ association, presented in Figure 3.7, shows one nitrate anion inserted into the macrobicyclic cage adopting an almost parallel disposition to the 2,4,6-triethylbenzene caps. The nitrate is located at 3.31 and 3.22 Å from these two aromatic rings suggesting that the encapsulated anion is stabilized by π–π interactions. This nitrate anion is also involved in a network of hydrogen bonds with three bridging water molecules and NH_2 binding groups, as shown in Figure 3.7(b) and 3.7(c). The nitrate is 1.25 Å deviated from the N_6 center binding cage establishing only three straight N–H···O hydrogen bonds with two N–H neighbor binding sites at H···O distances of 2.22, 2.30 and 2.38 Å, drawn as green dashed lines in Figures 3.7(b) and 3.7(c). Each bridging water molecule is hydrogen bonded to the included nitrate oxygen and two N–H binding sites from adjacent NH_2 binding groups leading to O···O distances of 2.767(7), 2.797(6) and 2.823(7) Å, respectively, and O···N distances between 2.816(7) and 3.002(7) Å. Two water molecules are also stabilized by further hydrogen bonds formed with two nitrate anions, located at the periphery of the

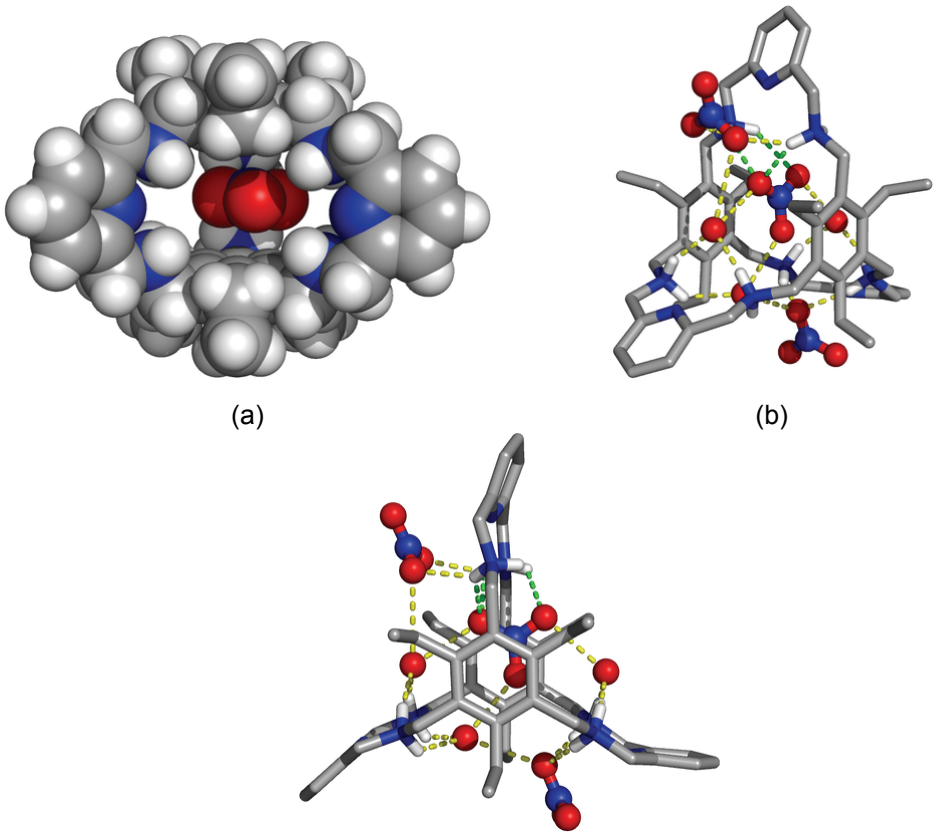

Figure 3.7 Perspective views illustrating different structural features of the association between nitrate and the H_6pyr^{6+} receptor: (a) Space-filling model showing the nitrate anion inserted into the macrobicyclic cavity and its relative position towards to the two 2,4,6-triethylbenzene rings; (b) and (c) views emphasize the N–H···O hydrogen bonding network and the receptor conformation adopted. N–H···O hydrogen bonds are represented in yellow and green dashed lines. C–H hydrogen atoms have been omitted for clarity.

cage, at O···O distances of 2.895(7) and 2.874(7) Å. These two nitrate anions interact with receptor NH_2 binding sites with N···O distances ranging between 2.9717(7) and 3.041(7) Å. The dimensions of all N–H···O bonds in $[(H_6pyr)(NO_3)_3(H_2O)_3](NO_3)_3{\cdot}4H_2O$ are given in Table A3.2 in Appendix. The analysis of hydrogen bonds is consistent with the existence of a $\{(NO_3)_3(H_2O)_3\}^{3-}$ cluster with a nitrate embedded into the cage and stabilized by means of multiple hydrogen bonds and electrostatic interactions formed with the highly charged H_6pyr^{6+} receptor.

In the case of the sulfate association, the asymmetric unit is composed of ten crystallization water molecules, four sulfate anions and one H_6pyr^{6+} cation. The charge balance of the asymmetric unit content requires necessarily the existence of two protons, which can be accommodated by one H_2SO_4 neutral species or more likely by two hydrogen sulfate anions (HSO_4^-). The main structural features of sulfate association are presented in Figure 3.8.

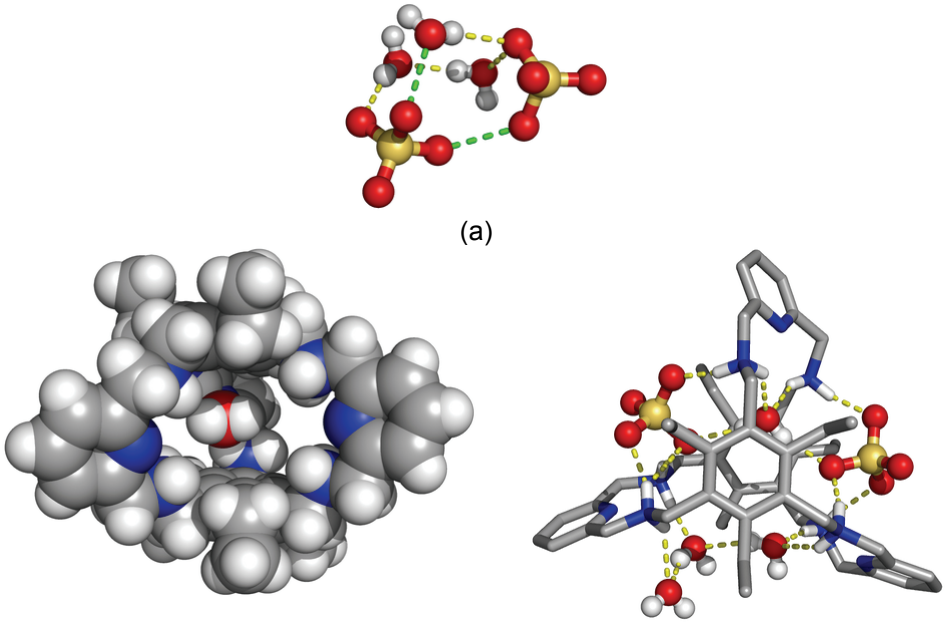

Figure 3.8 Three views illustrating different structural features of the association of sulfate with H_6pyr^{6+} receptor: (a) view of $\{(HSO_4)_2(H_2O)_3\}^{2-}$ hydrogen bonded cluster with yellow dashed lines showing the potential location of HSO_4^- protons; (b) space-filling model showing one crystallization water molecule inserted into the macrobicyclic cavity; (c) view showing the receptor conformation and N–H···O hydrogen bond network formed between sulfate anions, water molecules and twelve receptor N–H binding sites. The remaining details are given in Figure 3.7.

Although the atomic positions of some water hydrogen atoms were discernible from the last difference Fourier maps, these two extra protons were not. However their location can be inferred from the S–O distances pattern. Indeed, two sulfate anions display one S–O distance of 1.560(2) and 1.566(2) Å longer than the remaining ones ranging between 1.462(2) and 1.439(2) Å. By contrast in the other two sulfate counter-ions, the all four S–O distances are

equivalent varying only from 1.472(2) to 1.494(2) Å. This structural feature suggests that the two protons are bonded to oxygen atoms of two sulfate anions with S–O longer distances. Furthermore, the crystal packing diagram shows that these two anions are hydrogen bonded by three water molecules and by the two protons with one S=O–H···O=S distance of 2.632(3) Å and S=O–H···OH_2 distance of 2.559(3) Å, green dashed lines in Figure 3.8(a). Furthermore, the two HSO_4^- anions do not interact directly with the receptor, while the two SO_4^{2-} anions are assembled together with four water molecules as shown in Figures 3.8(b) and 3.8(c). This associated entity contains a water molecule hydrogen bonded to two sulfate anions with H···O distances of 2.01 and 2.03 Å as well as a trimer of water molecules with H···O distances of 1.99 and 2.17 Å. The $\{(SO_4)_2(H_2O)\}^{4-}$ and $\{(H_2O)\}_3$ entities are stabilized through multiple and cooperative N–H···O hydrogen bonds with the receptor, as shown in Figure 3.8(c). The dimensions of all N–H···O and O–H···O hydrogen bonding interactions found in $[(H_6pyr)(SO_4)_2(H_2O)_4](HSO_4)_2{\cdot}6H_2O$ are given in Table A3.3 in Appendix. The water molecule that bridge both sulfate anions, see Figure 3.8(b) is completely encapsulated into the macrobicyclic cage and hydrogen bonded to two N–H binding sites from adjacent amino-alkyl linkages with N···O distances of 2.849(2) and 2.945(2) Å. The two sulfate anions interact with H_6pyr^{6+} through three N–H···O hydrogen bonds with N···O distances between 2.773(2) and 2.872(2) Å. This binding arrangement contrasts with that of $\{(SO_4)(H_2O)_6\}^{2-}$ in $[(H_6xyl)(SO_4)(H_2O)_6]^{4+}$ described in the previous chapter, where the sulfate anion is entirely embedded inside of the macrocyclic cage.

In the phosphate assembled molecule the asymmetric unit is composed of one H_6pyr^{6+} cation, four phosphate anions and eighteen water molecules. The most relevant structural features of phosphate association are illustrated in Figure 3.9. The charge balance of the molecular formula is consistent with the existence of two $H_2PO_4^-$ and two HPO_4^{2-} independent anions, taking into account the conditions used to grow the crystals. These protons were not revealed by single crystal X-ray determination, and similarly to what was done for the sulfate association, the protons to the phosphate species were tentatively assigned from

P–O distances. Two phosphate anions exhibit one P–O distance of 1.582(3) and 1.581(3) Å, respectively, which are slightly larger than the remaining three ones ranging from 1.540(3) and 1.513(3) Å. This suggests that these two anions are the HPO_4^{2-}. The third phosphate, that is not directly involved in hydrogen bonds with H_6pyr^{6+}, contains two P–O distances of 1.579(3) and 1.583(3) Å longer than the remaining two 1.496(4) and 1.501(3) Å, which seems to indicate that this species is $H_2PO_4^-$. Finally, taking into account this analysis, the forth counter anion is necessarily $H_2PO_4^-$, and has P–O distances varying between 1.496(3) and 1.547(4), which are apparently not consistent with such species. Two water molecules, three phosphate anions (two HPO_4^{2-} and eventually one $H_2PO_4^-$) and H_6pyr^{6+} are assembled in the $[(H_6pyr)(HPO_4)_2(H_2PO_4)(H_2O)_2]^+$ cation, shown in Figure 3.9.

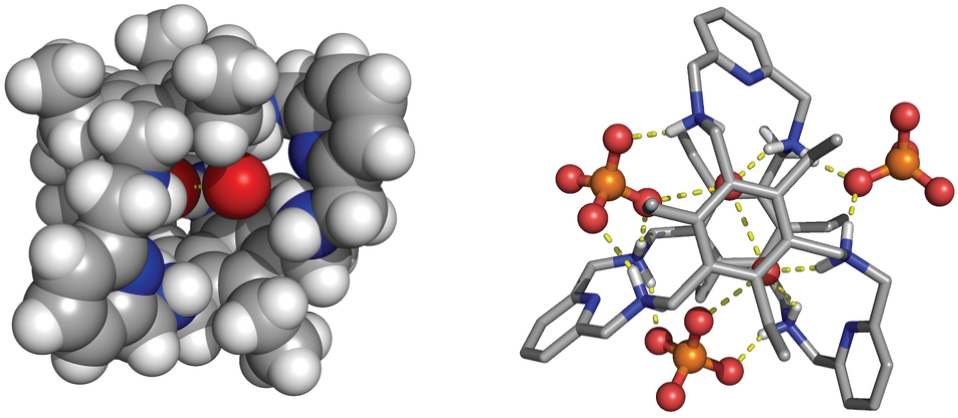

(a) (b)

Figure 3.9 Two views illustrating different structural features of the association between phosphate and H_6pyr^{6+} receptor: a) space-filling model showing two crystallization water molecules inserted into the macrobicyclic cavity; b) view showing the receptor conformation and the N–H···O hydrogen bonding interactions formed. The remaining details are given in Figure 3.7.

Two water molecules, separated by O···O distance of 2.945(4) Å are hydrogen bonded and located inside of the cage, see Figure 3.9(a). Both water molecules are linked to one phosphate oxygen acceptor with O···O distances of 2.623(4) and 2.620(4) Å and two N–H binding sites from adjacent amino-alkyl linkages with N···O distances of 2.866(4), 2.999(4), 2.873(5) and 2.973(4) Å. The three anions surround the macrobicycle, two of them (HPO_4^{2-} species) are linked

by three short N–H···O bonding interactions to N–H binding sites while the third one ($H_2PO_4^-$) establishes only two N–H···O hydrogen bonds. The dimensions of all hydrogen bonds found in $[(H_6pyr)(HPO_4)_2(H_2PO_4)(H_2O)_2](H_2PO_4)\cdot 16H_2O$ are also listed in Table A3.4 in Appendix.

The comparison of the structures of the three associations provides further information on the possible conformations of the receptor. In fact, the H_6pyr^{6+} receptor in $[(H_6pyr)(NO_3)_3(H_2O)_3]^{3+}$ displays nearly a C_3 symmetry with 3-fold axis perpendicular to parallel 2,4,6-triethylbenzene caps as apparent from the Figure 3.7(b), which shows a view of the nitrate supermolecule along these aromatic rings. Indeed, the lines determined by the centroids of pyridine spacers and mass center of the cage make angles (α angles) of 114.0, 122.8 and 123.3º. The interplanar distance between the two caps (β distance) is 6.543 Å. In the sulfate association the α angles are 113.2, 121.2 and 125.2º and β distance is 6.939 Å, but the molecular diagram presented in Figure 3.8(c) indicates an evident absence of C_3 symmetry motivated by the spatial disposition of pyridine rings and staggered arrangement of 2,4,6-triethylbenzene substituents. A comparable macrobicyclic conformation was observed for the association with phosphate, Figure 3.9(b), but the α angles 103.6, 115.5 and 140.0º are more deviated from the ideal value of 120º and the β distance of 7.353 Å is longer. Equivalent conformations were found in the crystal structures of associations of related benzene-capped hexaprotonated cryptands with halide[15] and sulfate anions. However, in all cases the reported distances between the two parallel benzene caps are much longer *c.a*. 9 Å. For example, in the $[(H_6xyl)(SO_4)(H_2O)_6]^{4+}$ crystal structure shown in the previous chapter, the β distance is 9.157 Å and α angles range from 117.7 to 120.6º. This comparison indicates that this cryptand receptor type has apparent rigid structures, but with enough flexibility to trap water molecules assembled or not with anions in their cages. In particular, in the three anion supramolecular associations reported here, the H_6pyr^{6+} conformation is determined by the N–H···O hydrogen bonding interactions established with anions as counter-ions located in the cryptand cavity periphery, rather than by the mismatch of sizes between the cage and the encapsulated substrate.

3.4 Conclusions

Solution studies revealed that H_npyr^{n+} receptor is able to discriminate dinegative sulfate from mononegative anions NO_3^-, Cl^- and ClO_4^-, the main interaction being of electrostatic nature, as the association constants increase with increasing positive charges on H_npyr^{n+}. This means that the association is only governed by the charge and hydrogen bond donating ability of the receptor, and in this sense H_npyr^{n+} has a behavior similar to H_nxyl^{n+}. However, the present work also shows how the selectivity pattern can be modulated by slight changes in the framework of the receptor. In fact, the change of the *m*-xylyl spacers of H_nxyl^{n+} to pyridyl ones in H_npyr^{n+} led to remarkable differences on the association behavior of the receptor with anions. Apparently, like in phosphate binding protein (PBP), the presence of hydrogen bond acceptors in H_npyr^{n+} receptor enhances the affinity for hydrogen phosphate. Therefore, at low pH dihydrogen phosphate has an affinity of the order of sulfate, in spite of the higher charge of the latter anion and it is capable to effectively compete with sulfate with the receptor at higher pH. At pH about 7.0 the H_npyr^{n+} receptor is selective for hydrogen phosphate. Furthermore, the fact that the receptor shows such a marked preference for hydrogen phosphate based mainly in its hydrogen bond accepting/donating ability in a highly competitive media such as water/methanol mixed solvent is quite remarkable.

The crystallographic studies reported here are apparently in contradiction with the solution studies, namely, sulfate and phosphate anions located outside of the cavity and no evidence of the –N:···HO– hydrogen bonds formation, which are important features in light of the solution studies. However, considering the crystal structure as the unique in solution is a broad simplification of a complex process, where only a collection of individual arrangements represents the structural ensemble, even when the configuration of the assembled molecule observed in the crystal is the most stable one in solution.[16] Thus the crystal structures should best viewed as snapshots of the binding event. Despite this, the reported crystal structures provided important information on the different possible conformations of the receptor.

The present study allowed us to conclude that, although H_npyr^{n+} is not as efficient in discriminating hydrogen phosphate from sulfate as the PBP, it is to the best of our knowledge the artificial polyamine compound with highest reported phosphate/sulfate selectivity in aqueous solutions at pH about 7.0.

3.5 Experimental

3.5.1 General considerations

All solvents and chemicals were reagent grade quality and commercially purchased and used as supplied, except 1,3,5-tris(aminomethyl)-2,4,6-triethylbenzene and 2,6-pyridinedicarbaldehyde which where prepared according to literature methods.[17,18] Potassium or sodium salts of the anions were purchased as analytical grade and were used without further purification. Potassium *p*-toluenesulfonate (KTsO) was prepared by the neutralization of *p*-toluenesulfonic acid (HTsO) with KOH in water, followed by recrystallization from MeOH/H_2O. All the solutions used in the potentiometric measurements were prepared with demineralised water and methanol purified by standard methods.[19] The references used for the ^1H NMR measurements were TMS in $CDCl_3$ and 3-(trimethylsilyl)-propanoic acid-d_4-sodium salt in D_2O. Resonance assignments were based on peak integration and multiplicity for 1D ^1H spectra and on COSY, NOESY and HMQC experiments (Figures A3.1-A3.5 in Appendix).

3.5.2 Synthesis

3.5.2.1 Schiff base of pyr

A solution of 1,3,5-tris(aminomethyl)-2,4,6-triethylbenzene (300 mg, 1.2 mmol) in MeCN (30 cm^3) was added dropwise over 7 minutes to a magnetically stirred solution of 2,6-pyridinedicarbaldehyde (244 mg, 1.8 mmol) dissolved in MeCN (30 cm^3) and the mixture was left under stirring overnight. A white precipitate formed which was separated by filtration and washed with MeCN (about 100 cm^3) to remove any unreacted starting materials. The precipitate was suspended in $CHCl_3$ (100 cm^3), ultrasonicated for 1 hour and filtered. Evaporation of the solvent yielded the desired hexaimine which was dried in vacuum.Yield:

60 %; ^{1}H NMR (400 MHz, $CDCl_3$, 298.2 K, TMS): δ = 8.07 (d, 6 H, ^{3}J (H,H) = 8.0 Hz, , H3, H5, py), 7.91 (s, 6 H, HC=N), 7.70 (t, 3 H, ^{3}J (H,H) = 7.6 Hz, H4, py), 5.07 (s, 12 H, CH_2Ph), 2.22 (q, 12 H, ^{3}J (H,H) = 8.0 Hz, PhC$H_2$$CH_3$), 1.18 (t, 18 H, ^{3}J (H,H) = 8.0 Hz, $PhCH_2CH_3$) ppm; ^{13}C NMR (100 MHz, $CDCl_3$, 298.2 K, TMS): δ = 159.5 (C=N), 154.8 (C2, C6, py), 144.3 (C1, C3, C5, Ph), 136.7 (C4, py), 131.1 (C2, C3, C4, Ph), 121.8 (C3, C5, py), 54.4 (CH_2Ph), 23.8 (PhCH_2CH_3), 16.0 ($PhCH_2CH_3$) ppm.

3.5.2.2 pyr

Solid $NaBH_4$ (1.226 g, 32.4 mmol) was added in small portions to a magnetically stirred suspension of the hexaimine (428 mg, 0.54 mmol) in MeOH (65 cm^3). The mixture stirred at r.t. for two hours, and under reflux overnight. Then the solution was evaporated under vacuum to almost dryness, then H_2O (20 cm^3) was added and the methanol was evaporated. The solution was made strongly basic with 6 mol dm^{-3} KOH and extracted $CHCl_3$ (3×50 cm^3). The organic portions were collected, dried over anhydrous sodium sulfate, filtered, evaporated to dryness and dried under vacuum. Yield: 90%; m.p. 110 ºC (decomp.), ^{1}H NMR (400 MHz, $CDCl_3$, 298.2 K, TMS): δ = 7.46 (t, 3 H, ^{3}J (H,H) = 8.0 Hz, H4, py), 6.99 (d, 6 H, ^{3}J (H,H) = 8.0 Hz, H3, H5, py), 3.85 (s, 12 H, $pyCH_2$), 3.71 (s, 12 H, CH_2Ph), 2.70 (q, 12 H, ^{3}J (H,H) = 8.0 Hz, PhC$H_2$$CH_3$), 1.03 (t, 18 H, ^{3}J (H,H) = 8.0 Hz, $PhCH_2CH_3$) ppm; ^{13}C NMR (100 MHz, $CDCl_3$, 298.2 K, TMS): δ = 157.6 (C2, C6, py) 141.7 (C1, C3, C5, Ph), 135.5 (C4, py), 132.6 (C2, C3, C4, Ph), 119.5 (C3, C5, py), 54.5 ($pyCH_2$), 46.6 (CH_2Ph), 21.6 (PhCH_2CH_3), 15.7 ppm ($PhCH_2CH_3$); ESI-MS (MeOH): m/z (%): 808.6 $[M+H]^+$. Elem. Anal. calcd (%) for $C_{51}H_{69}N_9.0.5CHCl_3.2.5H_2O$: C 67.76, H 8.23, N 13.81; found: C 67.93, H 8.34, N 13.71.

3.5.2.3 Crystals of $[(H_6pyr)(NO_3)_3(H_2O)_3](NO_3)_3 \cdot 4H_2O$

The pyr compound (4.04 mg, 5 μmol) was dissolved in acetone (500 μL) and 65% HNO_3 (2.077 μL) was added. Immediately a white precipitate was formed. Water (90 μL) was added and the solution heated until it was clear, then the

mixture was allowed to slowly cool to r.t. Single colourless crystals suitable for X-ray crystallography were grown overnight.

3.5.2.4 Crystals of $[(H_6pyr)(SO_4)_2(H_2O)_4](HSO_4)_2 \cdot 6H_2O$

The pyr compound (4.04 mg, 5 μmol) was dissolved in acetone (500 μL) and 97% H_2SO_4 (1.658 μL) was added. Water (90 μL) was added and the solution was treated as in the latter case. Single colourless crystals suitable for X-ray crystallography were grown overnight.

3.5.2.5 Crystals of $[(H_6pyr)(HPO_4)_2(H_2PO_4)(H_2O)_2](H_2PO_4) \cdot 16H_2O$

The pyr compound (4.04 mg, 5 μmol) was dissolved in acetone (500 μL) and 85% H_3PO_4 (2.053 μL) was added. To the white precipitate formed water (60 μL) was added, and the solution was treated as before. Single colorless crystals suitable for X-ray crystallography were grown overnight.

3.5.3 Potentiometric measurements

3.5.3.1 Reagents and solutions

All solutions were prepared in water/methanol (50:50 v/v) solvent. A stock solution of the receptor was prepared at *ca*. 1.5×10^{-3} mol dm^{-3}. Anion solutions were prepared at 0.10 mol dm^{-3} from the corresponding potassium salts and the concentrations were checked by titration with standard 0.100 mol dm^{-3} KOH solutions. Carbonate-free solutions of the KOH titrant were prepared as described the previous chapter. These solutions were discarded every time carbonate concentration was about 0.5% of the total amount of base. The titrant solutions were standardized (tested by Gran's method).[20]

3.5.3.2 Equipment and working conditions

The equipment used was described in the previous chapter. The ionic strength of the experimental solutions was kept at 0.10±0.01 mol dm^{-3} with KTsO, temperature was maintained at 298.2±0.1 K. Atmospheric CO_2 was excluded from the titration cell during experiments by passing purified nitrogen across the

top of the experimental solution. The glass electrode was pre-treated by soaking it in the water–methanol (50:50 v/v) solution over a period of 2 days, in order to prevent erratic responses.

3.5.3.3 Measurements

The $[H^+]$ of the solutions was determined by the measurement of the electromotive force of the cell, $E = E^{o\prime} + Q \log [H^+] + E_j$. The term pH is defined as $-\log [H^+]$. $E^{o\prime}$, Q, E_j and K_w were determined by titration of a solution of known hydrogen-ion concentration at the same ionic strength, using the acid pH range of the titration. The liquid-junction potential, E_j, was found to be negligible under the experimental conditions used. The value of K_w was determined from data obtained in the alkaline range of the titration, considering $E^{o\prime}$ and Q valid for the entire pH range and found to be equal to $10^{-13.91}$ in our experimental conditions. Before and after each set of titrations the glass electrode was calibrated by titration of 1.0×10^{-3} mol dm^{-3} standard HCl solution with standard KOH. The potentiometric equilibrium measurements were carried out using 20.00 cm^3 of $\approx$ 1.56×10^{-3} mol dm^{-3} of pyr solution diluted to a final volume of 30.00 cm^3, in the absence of anions, then in the presence of each anion at 1:3 R:A ratios (R = receptor and A = anion). In each titration 85 to 120 points were collected, and a minimum of two titration curves were performed. Care has been taken to maintain unaltered the methanol–water ratio in measured solution. The exact concentration of pyr was obtained by determination of the excess of acid present in a mixture of pyr and standard *p*-toluenesulfonic acid 1.0×10^{-2} mol dm^{-3} by titration with standard KOH solution.

3.5.3.4 Calculation of equilibrium constants

Overall protonation constants, β_i^H, of both ligand and anions in the same experimental conditions, were calculated by fitting the potentiometric data obtained for all the performed titrations with the HYPERQUAD program.[21] All these constants were taken as fixed values to obtain the equilibrium constants of the new species from the experimental data corresponding to all titrations at 1:3

R:A ratio, using also the HYPERQUAD program. The initial computations were obtained in the form of overall stability constants, β_{HhLlAa} values, $\beta_{HhLlAa} = [H_hL_lA_a]/[H]^h[L]^l[A]^a$. The errors quoted are the standard deviations of the overall association constants given directly by the program for the input data, which include all the experimental points of all titration curves. Distribution diagrams were plotted from the calculated constants with the HYSS program.[22] The species considered in a particular model were those that could be justified by the principles of supramolecular chemistry.

3.5.4 ^{31}P-NMR studies

Solutions of the hydrogen phosphate associations with $(H_6pyr)(TsO)_6$ and $(H_6xyl)(TsO)_6$ were prepared in H_2O/MeOH 50:50 v/v at 8.30×10^{-4} mol dm^{-3} (1:1 receptor to anion ratio). The pH was adjusted to 3.8 or 7.2 by adding small amounts of HTsO or KOH solutions. Hydrogen phosphate solutions in the absence of receptors were also prepared at the same concentration and at the same pH values.

Competition experiments were carried out by mixing equimolar amounts of potassium dihydrogen phosphate, potassium sulfate and $(H_6pyr)(TsO)_6$ (8.30×10^{-4} mol dm^{-3}) in H_2O/MeOH 50:50 v/v and the pH was adjusted to 3.8 or 7.2 by adding small amounts of HTsO or KOH solutions.

In all cases an internal capillary tube containing D_2O and H_3PO_4 was used for locking and referencing purposes during spectra acquisition.

3.5.5 Crystallography

The single crystal X-ray data of the anion binding complexes were collected on a CCD Bruker APEX II at 150(2) K using graphite monochromatized Mo-Kα radiation (λ = 0.71073 Å). The pertinent crystallographic data are given in Table A3.5 (in Appendix). Data reduction including a multi-scan absorption correction was carried out using the SAINT-NT from Bruker AXS. The structures were solved by direct methods and by subsequent difference Fourier syntheses and refined by full matrix least squares on F^2 using the SHELX-97 suite.[23]

Anisotropic thermal parameters were used for all non-hydrogen atoms. One nitrate counter-ion of $[(H_6pyr)(NO_3)_3(H_2O)_3](NO_3)_3{\cdot}4H_2O$ displays high thermal displacements, which were ascertained to thermal disorder. The N–H and C–H hydrogen atoms were introduced in the structure refinement at calculated positions. The hydrogen atomic positions of water molecules were obtained from the last Fourier difference maps for sulfate association while for phosphate and nitrate anion association they were not found and therefore they were not included in the structure refinement. The protons required by the charge balance of the molecular formulas of sulfate and phosphate associations were not taken into account. All hydrogen atoms were refined $U_{iso} = 1.2U_{eq}$ of the parent atom. Molecular diagrams were drawn with PyMOL.[24]

3.6 Acknowledgements

The authors acknowledge FCT, with co-participation of the European Community funds FEDER, for the financial support under projects PTDC/QUI/56569/2004 and PTDC/QUI/68582/2006. The NMR spectrometers are part of the National NMR Network and were acquired with funds from FCT and FEDER. We also acknowledge M. C. Almeida for providing elemental analysis and ESI-MS data from the Elemental Analysis and Mass Spectrometry Service at the ITQB. Pedro Mateus thanks FCT for the grant, SFRH/BD/36159/2007.

3.7 References

[1] a) *Supramolecular Chemistry of Anions*, Eds.: A. Bianchi, K. Bowman-James, E. Garcia-España, Pergamon, Oxford, Wiley-VCH, New York, **1997**, b) J. W. Steed, J. L. Atwood, *Supramolecular Chemistry*; 2nd Ed., John Wiley & Sons, Ltd, **2009**.
[2] J. W. Pflugrath, F. A. Quiocho, *Nature* **1985**, *314*, 257–260.
[3] H. Luecke, F. A. Quiocho, *Nature* **1990**, *347*, 402–406.
[4] B. L. Jacobson, F. A. Quiocho, *J. Mol. Biol.* **1988**, *204*, 783–787.
[5] a) C. A. Ilioudis, J. W. Steed, *J. Supramol. Chem.* **2001**, *1*, 165–187; b) J. M. Llinares, D. Powell, K. Bowman-James, *Coord. Chem. Rev.* **2003**, *240*, 57–102; c) E. García-España, P. Díaz, J. M. Llinares, A. Bianchi, *Coord. Chem. Rev.* **2006**, *250*, 2952–2986; d) V. McKee, J. Nelson, R. M. Town, *Chem. Soc. Rev.* **2003**, *32*, 309–325.
[6] a) B. Dietrich, J. Guilhem, J.-M. Lehn, C. Pascard, E. Sonveaux, *Helv. Chim. Acta* **1984**, *67*, 91–104; b) R. J. Motekaitis, A. E. Martell, *Inorg. Chem.* **1992**, *31*, 5534–5542; c) D. A. Nation, J. Reibenspies, A. E. Martell, *Inorg. Chem.* **1996**, *35*, 4597–

4603; d) Q. Lu, J. H. Reibenspies, R. I. Carroll, A. E. Martell, A. Clearfiled, *Inorg. Chim. Acta* **1998**, *270*, 207–215; e) C. Bazzicalupi, A. Bencini, A. Bianchi, M. Cecchi, B. Escuder, V. Fusi, E. García-España, C. Giorgi, S. V. Luis, G. Maccagni, V. Marcelino, P. Paoletti, B. Valtancoli, *J. Am. Chem. Soc.* **1999**, *121*, 6807–6815; f) P. D. Beer, J. Cadman, J. M. Lloris, R. Martínez-Máñez, M. E. Padilla, T. Pardo, D. K. Smith, J. Soto, *J. Chem. Soc., Dalton Trans.* **1999**, 127–133; g) C. Anda, C. Bazzicalupi, A. Bencini, E. Berni, A. Bianchi, P. Fornasari, A. Llobet, C. Giorgi, P. Paoletti, B. Valtancoli, *Inorg. Chim. Acta* **2003**, *356*, 167–178.

[7] a) E. A. Katayev, N. V. Boev, E. Myshkovskaya, V. N. Khrustalev, Y. A. Ustynyuk, *Chem. Eur. J.* **2008**, *14*, 9065–9073; b) E. A. Katayev, J. L. Sessler, V. N. Khrustalev, Y. A. Ustynyuk, *J. Org. Chem.* **2007**, *72*, 7244–7252; c) K. S. Moon, N. Singh, G. W. Lee, D. O. Jang, *Tetrahedron* **2007**, *63*, 9106–9111.

[8] a) T. H. Kwon, K. Jeong, *Tetrahedron Lett.* **2006**, *47*, 8539–8541; b) S. Kondo, Y. Hiraoka, N. Kurumatani, Y. Yano, *Chem. Commun.* **2005**, 1720–1722.

[9] a) A. P. Bisson, V. M. Lynch, M.-K. C. Monahan, E. V. Anslyn, *Angew. Chem., Int. Ed.* **1997**, *36*, 2340–2342. b) K. Niikura, A. P. Bisson, E. V. Anslyn, *J. Chem. Soc., Perkin Trans. 2* **1999**, 1111–1114.

[10] M. T. Albelda; M. A. B. E. Garcia-España, M. L. Godino-Salido, V. L. Santiago, M. J. Melo, F. Pina, C. Soriano, *J. Chem. Soc. Perkin Trans. 2* **1999**, 2545–2549.

[11] A. Bianchi, E. Garcia-España, *J. Chem. Educ.* **1999**, *76*, 1727–1732.

[12] R. J. Motekaitis, W. B. Utley, A. E. Martell, *Inorg. Chim. Acta* **1993**, *212*, 15–21.

[13] P. Arranz, A. Bencini, A. Bianchi, P. Diaz, E. García-España, C. Giorgi, S. V. Luis, M. Querol, B. Valtancoli, *J. Chem. Soc., Perkin Trans. 2* **2001**, 1765–1770.

[14] a) V. Král, H. Furuta, K. Shreder, V. Lynch, J. L. Sessler, *J. Am. Chem. Soc.* **1996**, *118*, 1595–1607; b) P. J. Cozzoner, O. Jardetzky, *Biochemistry* **1976**, *15*, 4853–4859.

[15] M. Arunachalam, I. Ravikumar, P. Ghosh, *J. Org. Chem.* **2008**, *73*, 9144–9147.

[16] F. P. Schmidtchen, *Coord. Chem. Rev.* **2006**, *250*, 2918–2928.

[17] K. J. Wallace, R. Hanes, E. V. Anslyn, J. Morey, K. V. Kilway, J. Siegel, *Synthesis* **2005**, 2080–2083.

[18] N. W. Alcock, R. G. Kingston, P. Moore, C. Pierpoint, *J. Chem. Soc., Dalton Trans.* **1984**, 1937–1943.

[19] D. D. Perrin, W. L. F. Armarego, *Purification of Laboratory Chemicals*, Pergamon, Oxford, 3rd. ed., **1988**, p. 217.

[20] F. J. Rossotti, H. J. Rossotti, *J. Chem. Educ.* **1965**, *42*, 375–378.

[21] P. Gans, A. Sabatini, A. Vacca, *Talanta* **1996**, *43*, 1739–1753.

[22] L. Alderighi, P. Gans, A. Ienco, D. Peters, A. Sabatini, A. Vacca, *Coord. Chem. Rev.* **1999**, *184*, 311–318.

[23] M. Sheldrick, *Shelx-97, Program for the Solution of Crystal Structures*, University of Göttingen, Göttingen (Germany), 1997.

[24] W. L. DeLano, *The PyMOL Molecular Graphics System DeLano Scientific*, San Carlos, CA, USA, **2002**. http://www.pymol.org.

Chapter 4

A trinuclear copper(II) cryptate and its μ_3-CO_3 cascade complex: thermodynamics, structural and magnetic properties

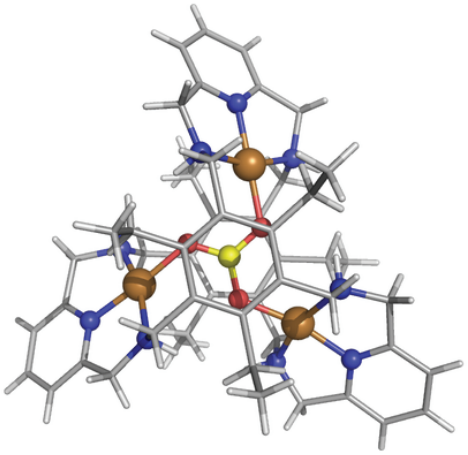

Work featured in: P. Mateus, R. Delgado, F. Lloret, J. Cano, P. Brandão, V. Félix, *Chem. Eur. J.* **2011**, 17, 11193–11203.

4.1 Summary

The 2,4,6-triethylbenzene capped hexaamine macrobicycle with pyridyl spacers (pyr) was able to coordinate three copper(II) ions within its cavity. Potentiometric studies performed at 298.2 K in MeOH/H_2O (50:50 v/v) and at ionic strength 0.10 mol dm^{-3} in KNO_3 revealed that trinuclear species predominate in solution from pH 5.0, the hydroxo complexes being the main species, which start forming at unusual very low pH. The single crystal X-ray determination of the trinuclear complex showed that the three copper centres have square-planar geometry, arranged in an almost equilateral triangle, having carbonate bridging the three metal centres. The presence of carbonate resulted from fixation of atmospheric CO_2. The present study represents the first μ_3-CO_3-bridged trinuclear copper(II) complex located in the interior of a macrobicyclic cavity. The magnetic data of $[Cu_3pyr(\mu_3\text{-}CO_3)](ClO_4)_4$ showed ferromagnetic intramolecular interactions [J = 3.80 cm^{-1}, based on the Hamiltonian $H = -J(S_1S_2 + S_2S_3 + S_1S_3)$] yielding a spin quartet, S = 3/2, ground state. *DFT* calculations on the experimental geometry of the trinuclear complex showed that the ferromagnetic nature of the magnetic coupling can be attributed to the *syn-anti* conformation of the carbonato-bridge and a magneto-structural correlation, based on the different conformations (*syn-anti*, *syn-syn* and *anti-anti*), is presented. The interesting properties observed, namely the lowering the pK_a of coordinated water molecules to unusual values and the good fit of the carbonate anion between the copper centres, derive from the special architecture of pyr.

4.2 Introduction

Trinuclear copper clusters with trigonal symmetry play a central role in fundamental steps of biological catalysis by ubiquitous multicopper oxidases.[1] The study of model complexes of these systems should not only provide better understanding of the biological molecules but also assist in the development of new low molecular weight catalysts[2] and of new types of magnetic materials.[3]

Macrocyclic and macrobicyclic compounds with several donor atoms and cavities of suitable dimensions constitute a viable approach to coordinate two or

more metal ions and bring them into close proximity so that the metal centres can be able to interact magnetically or electronically, giving rise to new properties or reactivities. Moreover, it is well documented that dinuclear copper(II) complexes are useful in the recognition and binding of anionic substrates.[4] However, few complexes of macrocyclic ligands with three copper(II) centres accommodated within the cyclic framework have been described[5] and only one involving a macrobicycle was reported.[6]

In the previous chapter it was shown that the protonated forms of the 2,4,6-triethylbenzene capped hexaamine macrobicycle with pyridyl spacers (pyr, Scheme 4.1) is an interesting anion receptor selective for dihydrogen phosphate. The structural motifs of this compound, the C_3 symmetry and the three pyridyl spacers, prompted us to study its copper(II) complexes in solution and in the solid state. Unexpectedly, the crystal X-ray diffraction characterization of the trinuclear copper(II) complex revealed the presence of a carbonate ion bridging the three copper(II) centres, formed *via* atmospheric CO_2 fixation. Although a few examples of μ_3-CO_3-bridged trinuclear copper(II) complexes formed upon CO_2 absorption were reported, in all cases the trinuclear assembly is composed of three individual mononuclear complexes bound by carbonate.[7] The present study represents the first μ_3-CO_3-bridged trinuclear copper(II) assembly located into a macrobicyclic cavity.

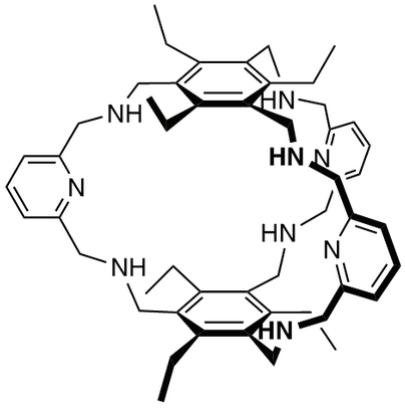

Scheme 4.1 pyr compund.

4.3 Results and Discussion

4.3.1 Potentiometric studies

4.3.1.1 Acid-base behaviour

The protonation constants of pyr were determined at ionic strength 0.10 mol dm^{-3} in KNO_3 and at 298.2 K in H_2O/MeOH (50:50 v/v), and the results are collected in Table 4.1. The mixed solvent system was chosen due to the precipitation of the compound at pH 7.22 in pure water, which prevented the determination of all the protonation constants in that medium. The present values agree well with those reported in Chapter 2, obtained in tosylate medium, except K_5^H and K_6^H, which are higher due to the association of nitrate with the most protonated forms of pyr (log $K_{H_6pyrNO_3}$ = 2.54 in H_2O/MeOH (50:50 v/v), T = 298.2 K and I = 0.10 mol dm^{-3} in KTsO).

Table 4.1 Overall (β_i^H) and stepwise (K_i^H) protonation constants of pyr in H_2O/MeOH (50:50 v/v).[a]

Equilibrium	log $\beta_i^{H\,[b]}$	Equilibrium	log $K_i^{H\,[c]}$
$pyr + H^+ \rightleftharpoons Hpyr^+$	8.76(1)	$pyr + H^+ \rightleftharpoons Hpyr^+$	8.76 [8.72]
$pyr + 2\,H^+ \rightleftharpoons H_2pyr^{2+}$	16.70(1)	$Hpyr^+ + H^+ \rightleftharpoons H_2pyr^{2+}$	7.94 [7.89]
$pyr + 3\,H^+ \rightleftharpoons H_3pyr^{3+}$	23.86(1)	$H_2pyr^{2+} + H^+ \rightleftharpoons H_3pyr^{3+}$	7.16 [7.15]
$pyr + 4\,H^+ \rightleftharpoons H_4pyr^{4+}$	30.44(1)	$H_3pyr^{3+} + H^+ \rightleftharpoons H_4pyr^{4+}$	6.59 [6.40]
$pyr + 5\,H^+ \rightleftharpoons H_5pyr^{5+}$	36.44(1)	$H_4pyr^{4+} + H^+ \rightleftharpoons H_5pyr^{5+}$	5.99 [5.70]
$pyr + 6\,H^+ \rightleftharpoons H_6pyr^{6+}$	41.76(1)	$H_5pyr^{5+} + H^+ \rightleftharpoons H_6pyr^{6+}$	5.32 [4.54]

[a] T = (298.2 ± 0.1) K; I = (0.10 ± 0.01) mol dm^{-3} in KNO_3. [b]Values in parenthesis are standard deviations in the last significant figure. [c] Values in brackets were determined in H_2O/MeOH (50:50 v/v), I = 0.10 mol dm^{-3} in KTsO and T = 298.2 K, see Chapter 2.

4.3.1.2 Complexation studies

The stability constants of pyr with copper(II) were also determined at ionic strength 0.10 mol dm^{-3} in KNO_3 and at 298.2 K in H_2O/MeOH (50:50 v/v). The results are collected in Table 4.2.

When pyr is titrated in the presence of 0.5 equiv. of copper(II) only mononuclear complexes were found (Figure 4.1a). At low pH copper coordinates

Table 4.2 Overall (log β_{MmHhLl}) and stepwise (log K_{MmHhLl}) stability constants of the copper(II) complexes of pyr in H_2O/MeOH (50:50 v/v).[a]

Equilibrium	log β_{MmHhLl} [b]	Equilibrium	log K_{MmHhLl}
$Cu^{2+} + 5H^+ + pyr \rightleftharpoons [CuH_5pyr]^{7+}$	41.06(5)	$[CuH_4pyr]^{6+} + H^+ \rightleftharpoons [CuH_5pyr]^{7+}$	2.56
$Cu^{2+} + 4H^+ + pyr \rightleftharpoons [CuH_4pyr]^{6+}$	38.50(1)	$[CuH_3pyr]^{5+} + H^+ \rightleftharpoons [CuH_4pyr]^{6+}$	5.37
$Cu^{2+} + 3H^+ + pyr \rightleftharpoons [CuH_3pyr]^{5+}$	33.13(3)	$[CuH_2pyr]^{4+} + H^+ \rightleftharpoons [CuH_3pyr]^{5+}$	6.28
$Cu^{2+} + 2H^+ + pyr \rightleftharpoons [CuH_2pyr]^{4+}$	26.86(3)	$[CuHpyr]^{3+} + H^+ \rightleftharpoons [CuH_2pyr]^{4+}$	6.82
$Cu^{2+} + H^+ + pyr \rightleftharpoons [CuHpyr]^{3+}$	20.04(3)	$[Cupyr]^{2+} + H^+ \rightleftharpoons [CuHpyr]^{3+}$	7.67
$Cu^{2+} + pyr \rightleftharpoons [Cupyr]^{2+}$	12.37(3)	$pyr + Cu^{2+} \rightleftharpoons [Cupyr]^{2+}$	12.37
$Cu^{2+} + pyr \rightleftharpoons [CupyrOH]^{+} + H^+$	3.50(5)	$[CupyrOH]^{+} + H^+ \rightleftharpoons [Cupyr]^{2+}$	8.87
$2Cu^{2+} + 2H^+ + pyr \rightleftharpoons [Cu_2H_2pyr]^{6+}$	33.69(2)	$[Cu_2Hpyr]^{5+} + H^+ \rightleftharpoons [Cu_2H_2pyr]^{6+}$	5.12
$2Cu^{2+} + H^+ + pyr \rightleftharpoons [Cu_2Hpyr]^{5+}$	28.57(2)	$[Cu_2pyr]^{4+} + H^+ \rightleftharpoons [Cu_2Hpyr]^{5+}$	6.57
$2Cu^{2+} + pyr \rightleftharpoons [Cu_2pyr]^{4+}$	22.00(3)	$[Cupyr]^{2+} + Cu^{2+} \rightleftharpoons [Cu_2pyr]^{4+}$	9.63
$2Cu^{2+} + pyr \rightleftharpoons [Cu_2pyrOH]^{3+} + H^+$	14.52(4)	$[Cu_2pyrOH]^{3+} + H^+ \rightleftharpoons [Cu_2pyr]^{4+}$	7.48
$3Cu^{2+} + H^+ + pyr \rightleftharpoons [Cu_3Hpyr]^{7+}$	32.01(3)	$[Cu_3pyr]^{6+} + H^+ \rightleftharpoons [Cu_3Hpyr]^{7+}$	5.7
$3Cu^{2+} + pyr \rightleftharpoons [Cu_3pyr]^{6+}$	26.3(1)	$[Cu_2pyr]^{4+} + Cu^{2+} \rightleftharpoons [Cu_3pyr]^{6+}$	4.3
$3Cu^{2+} + pyr \rightleftharpoons [Cu_3pyrOH]^{5+} + H^+$	21.84(2)	$[Cu_3pyrOH]^{5+} + H^+ \rightleftharpoons [Cu_3pyr]^{6+}$	4.4
$3Cu^{2+} + pyr \rightleftharpoons [Cu_3pyr(OH)_2]^{4+} + 2H^+$	15.14(3)	$[Cu_3pyr(OH)_2]^{4+} + H^+ \rightleftharpoons [Cu_3pyrOH]^{5+}$	6.70
$3Cu^{2+} + pyr \rightleftharpoons [Cu_3pyr(OH)_3]^{3+} + 3H^+$	6.33(5)	$[Cu_3pyr(OH)_3]^{3+} + H^+ \rightleftharpoons [Cu_3pyr(OH)_2]^{4+}$	8.81

[a] T = (298.2 ± 0.1) K and I = (0.10 ± 0.01) mol dm^{-3} in KNO_3. [b] Values in parenthesis are standard deviations in the last significant figure.

to one of the pyridyl groups, the two contiguous amines and one or more solvent molecules. As pH increases, the successive deprotonation of the remaining ammonium groups takes place; however, due to the presence of the metal ion the basicity of the amines is decreased by an average of 1.06 log units. With the increase of the amount of copper to 1.0 equiv. (Figure 4.1b), dinuclear species start to form and they are the predominant species at Cu^{2+}:pyr 2:1 ratio (Figure 4.1c). The stability constant corresponding to the addition of Cu^{2+} to $[Cupyr]^{2+}$ is lower than the stability constant of $[Cupyr]^{2+}$ by 2.74 log units due to the charge repulsion between the two metal ions, which are in close proximity, besides the statistical factor. Insertion of a third copper ion is even more disfavoured due to the build up of positive charge, resulting in a formation constant of only 4.3 log units. Nonetheless, at 3:1 Cu:pyr ratio (Figure 4.1d), trinuclear species

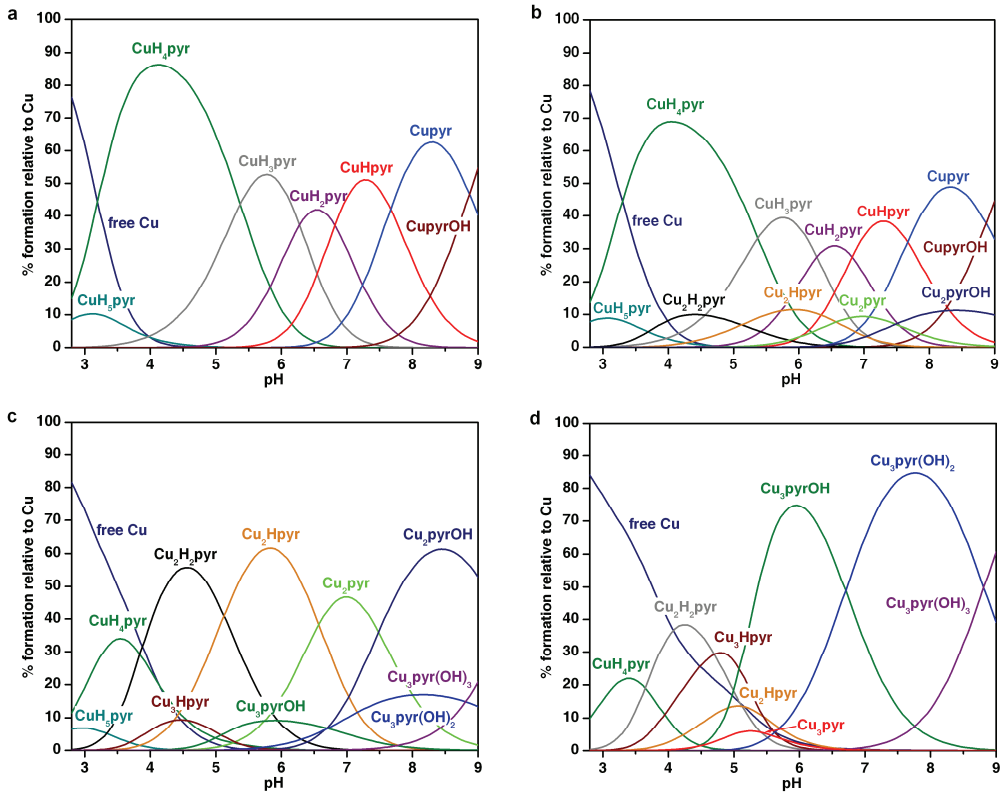

Figure 4.1 Species distribution diagram calculated for copper(II):pyr solutions: (a) at 0.5:1 ratio, $C_{Cu} = 1/2C_{pyr} = 0.5 \times 10^{-3}$ mol dm^{-3}, (b) at 1:1 ratio, $C_{Cu} = C_{pyr} = 1.0 \times 10^{-3}$ mol dm^{-3}, (c) at 2:1 ratio, $C_{Cu} = 2C_{pyr} = 2.0 \times 10^{-3}$ mol dm^{-3} and (d) at 3:1 ratio, $C_{Cu} = 3C_{pyr} = 3.0 \times 10^{-3}$ mol dm^{-3}. Charges were omitted for clarity.

predominate starting from pH 5.0 but exist mainly in form of hydroxo complexes. These hydroxo complexes start to form at a very low pH, likely to lower the amount of positive charge within the cryptand cavity in order to minimize electrostatic repulsions. The 1:1 ratio of hydroxide to copper ions was found, suggesting a four coordinate environment for each metal centre. However, based only in the potentiometric measurements it is not possible to establish whether the hydroxo groups bridge two copper centres.

4.3.2 Crystallographic studies

Crystals of the trinuclear copper complex were grown from H_2O/MeOH at pH ≈ 6, by mixing pyr with 3 equiv. of $Cu(NO_3)_2$ [or $Cu(ClO_4)_2$] followed by slow evaporation. The production of $[Cu_3pyr(\mu_3\text{-}CO_3)]^{4+}$ in different crystallization conditions, *i.e.* in presence of NO_3^- or ClO_4^- counter ions, indicates that carbonate bridging ligand formed by absorption of CO_2 from the atmosphere is preferred to nitrate in spite of the same geometry of both anions and the higher concentration of nitrate in solution. Interestingly, in another example of CO_2 fixation by a dinuclear copper(II) cryptate,[8] the authors reported that in the presence of acetate and nitrate, these anions bridged two copper centres forming dinuclear complexes instead of the carbonate-bridged complex.

The two single crystal X-ray structure determinations of the copper complex revealed unit cell contents consistent with molecular formulas $[Cu_3pyr(\mu_3\text{-}CO_3)](ClO_4)_4\cdot(MeOH)\cdot 2H_2O$ **1** and $[Cu_3pyr(\mu_3\text{-}CO_3)](NO_3)_4\cdot 9H_2O$ **2**. In the nitrate salt **2**, the copper complex displays a 2 fold crystallographic axis perpendicular to the CO_3^{2-} bridging ligand plane intercepting its carbon atom and the 2,4,6-triethylbenzene ring caps. Consequently, in the crystal structure, the CO_3^{2-} was found disordered over two positions with the same probability. However, in both salts, the $[Cu_3pyr(\mu_3\text{-}CO_3)]^{4+}$ has comparable distances and angles subtend at the copper centres as can be seen from their dimensions given in Table 4.3. The molecular structure of $[Cu_3pyr(\mu_3\text{-}CO_3)]^{4+}$ in **1** is shown in Figure 4.2 with the labeling scheme adopted while its structure in **2** is presented in Figure 4.3.

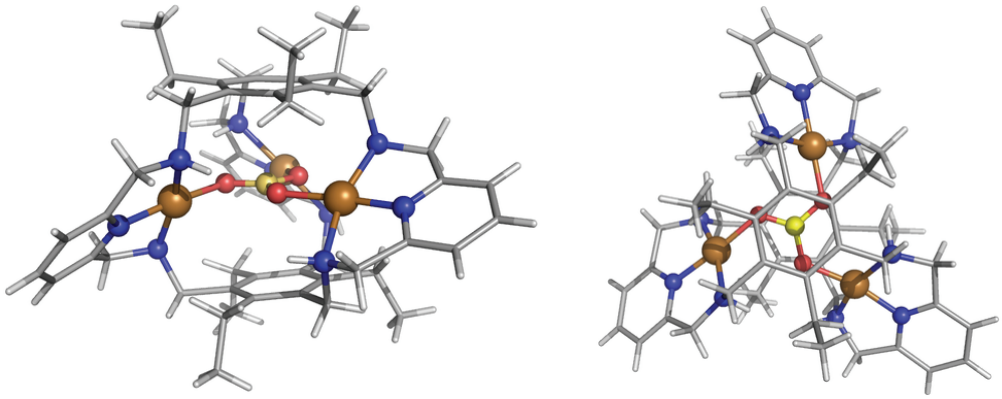

(a) (b)

Figure 4.2 Molecular structure of $[Cu_3pyr(\mu_3\text{-}CO_3)]^{4+}$ in complex salt **1** with $Cu_3(\mu_3\text{-}CO_3)$ central core drawn in ball stick style. The perspective view (a) shows the overall structure of the complex with the CO_3^{2-} trapped in macrobicyclic cavity while the top view (b) emphasis the pseudo C_3 symmetry of the complex cation. The carbon atom of CO_3^{2-} is represented in yellow.

The two structures are equivalent regarding the dimensions of the most relevant structural parameters associated with metal coordination spheres and henceforth the subsequent discussion of the complex $[Cu_3pyr(\mu_3\text{-}CO_3)]^{4+}$ is focused on the crystal structure of **1**. Each copper centre exhibits a distorted square planar coordination environment composed of three nitrogen donors from pyr macrobicycle an one oxygen atom of the μ_3-CO_3 ligand. Cu–O distances are comparable to those found previously for μ_3-CO_3-bridged trinuclear copper(II) complexes (see Table 4.4). The Cu–N distances are also in agreement with those found for macrocyclic complexes containing 2,6-bis(aminomethyl)pyridine clefts and the distances to the pyridine rings are slightly shorter than to the aliphatic amines, as would be expected for metal complexes incorporating this structural unit.[9] The CO_3^{2-} is encapsulated into the macrobicyclic cavity almost equidistant from two 2,4,6-triethylbenzene caps with the carbon atom located at 2.923(4) and 3.060(4) Å from benzene ring least square planes. Furthermore, the three CuN_3O coordination planes intercept the carbonate plane at angles ranging from 46.27(3) to 54.49(4)º. The intramolecular distances between the three copper centers (4.9263(8), 4.8492(7) and 4.8381(7) Å) indicate the absence of metal-metal bonds. The top view of the complex presented in Figure 4.2b shows

that the 2,4,6-triethylbenzene caps adopt a roughly eclipsed arrangement with an average rotation angle around the centroids of the benzene ring of 17.0º.

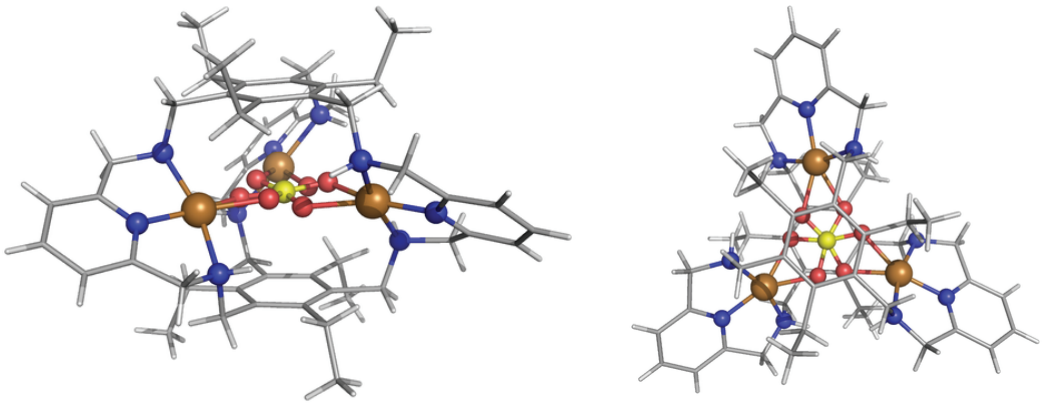

(a) (b)

Figure 4.3 Molecular structure of $[Cu_3pyr(\mu_3\text{-}CO_3)]^{4+}$ in complex salt **2** with $Cu_3(\mu_3\text{-}CO_3)$ central core drawn in ball stick style. The perspective (left) view shows the overall structure of the complex with the CO_3^{2-} trapped in macrobicyclic cavity while the top view (right) depicts the CO_3^{2-} anion disorder. The carbon atom of CO_3^{2-} is represented in yellow.

Obviously, in both nitrate and perchlorate salts, the $[Cu_3pyr(\mu_3\text{-}CO_3)]^{4+}$ complex cation participates with the anions (NO_3^- or ClO_4^-) and mother liquor solvent molecules in extensive hydrogen bonds, which are not described here. Indeed, the detailed analysis of these bonding interactions is not significant to understanding the $[Cu_3pyr(\mu_3\text{-}CO_3)]^{4+}$ chemistry reported.

4.3.3 CO_2 fixation

CO_2 fixation should derive from the nucleofilic attack of the hydroxo group of the $[Cu_3pyrOH]^{5+}$ complex (the main species present at pH ≈ 6) on the electrophilic carbon of CO_2 (see Scheme 4.2), as observed in mono[7,10] and dinuclear complexes[8,11] of copper(II) and other metal centres.

In every μ_3-CO_3-bridged trinuclear complex reported, CO_2 fixation occurs in alkaline media (pH > 7.5). Curiously, the only exception to this was observed with a dinuclear copper(II) complex of a macrobicyclic compound,[8] which is also able to form hydroxo complexes at a pH lower than usual. Apparently, the ability of macrobicyclic compounds to bring into close proximity several metal ions plays a

Table 4.3 Selected bond distances (Å) and angles (°) for $[Cu_3pyr(\mu_3\text{-}CO_3)]^{4+}$ in salt complexes **1** and **2**.

Complex **1**[a]					
Cu(1)–O(101)	1.902(3)	Cu(2)–O(103)	1.907(3)	Cu(3)–O(102)	1.907(3)
Cu(1)–N(8)	1.914(4)	Cu(2)–N(44)	1.930(4)	Cu(3)–N(26)	1.917(4)
Cu(1)–N(1)	2.072(4)	Cu(2)–N(37)	2.027(4)	Cu(3)–N(28)	2.099(4)
Cu(1)–N(10)	2.077(4)	Cu(2)–N(46)	2.056(4)	Cu(3)–N(19)	2.070(4)
N(1)–Cu(1)–N(10)	164.8(2)	N(8)–Cu(1)–O(101)	173.3(2)	N(37)–Cu(2)–N(46)	163.0(1)
N(44)–Cu(2)–O(103)	168.3(2)	N(37)–Cu(3)–N(46)	163.0(1)	N(26)–Cu(3)–O(102)	173.1(1)
Complex **2**[a]					
Cu(1)–O(103)	1.978(4)	Cu(1)–N(10)	2.098(3)	Cu(2)–N(24)	1.903(4)
Cu(1)–N(8)	1.925(3)	Cu(1)–O(101)	1.987(5)	Cu(2)–N(19)	2.061(3)
Cu(1)–N(1)	2.088(3)	Cu(2)–O(102)	1.984(5)		
N(1)–Cu(1)–N(10)	165.7(1)	N(19)–Cu(2)–N(19)[b]	164.4(2)	N(8)–Cu(1)–O(101)	154.5(1)
N(24)–Cu(2)–O(102)	154.8(1)	N(8)–Cu(1)–O(103)	158.7(1)		

[a] Nitrogen atoms labelled N(8), N(26) and N(44) in **1** and N(8) and N(24) in **2** are pyridine nitrogen atoms. The remaining nitrogen atoms belong to the amine groups. [b] denotes the symmetry operation: 1-*x*, *y*, 1.5-*z*

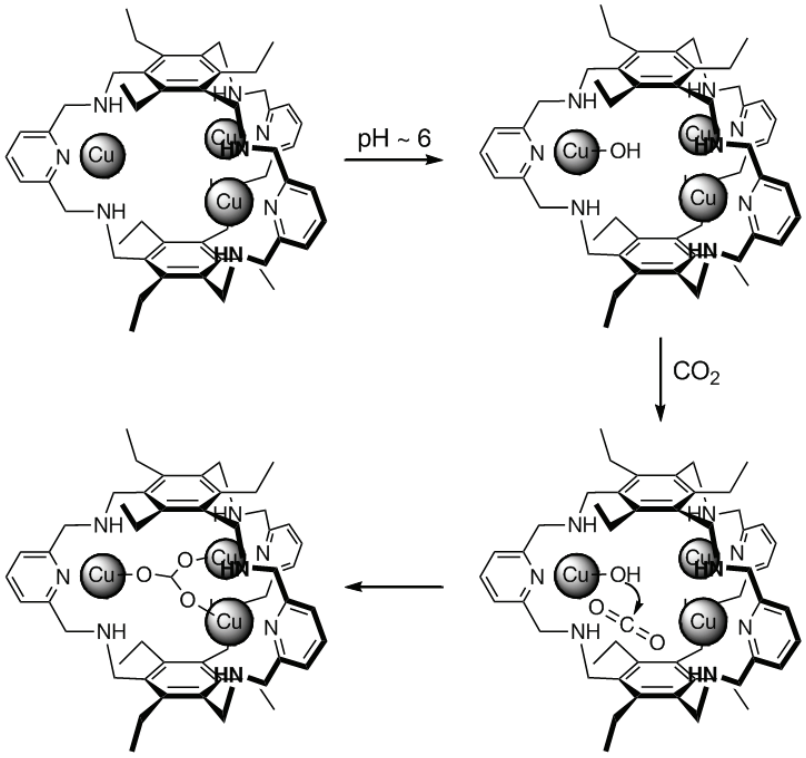

Scheme 4.2 Proposed mechanism for CO_2 fixation by $[Cu_3pyr]^{6+}$. Coordinated water molecules and charges are omitted for simplicity.

crucial role in lowering the pK_a of coordinated water molecules, which allows hydroxo complexes to be formed in slightly acid media that in turn permits CO_2 fixation to occur at lower pH. This is similar, although with a different metal ion, to what happens in the hydration of carbon dioxide to yield bicarbonate by carbonic anhydrase, whose catalytic activity requires a zinc-bound water molecule with a pK_a near 7, a lower than usual value which results not only from zinc coordination but also from assistance of nearby amino acid residues.[12] However, unlike the carbonic anhydrase that has low affinity for the bicarbonate anion and thus readily liberates it, the $[Cu_3pyr]^{6+}$ keeps CO_3^{2-} tightly bound between the three copper(II) ions.

Dinuclear metal complexes able to fix atmospheric CO_2 can also further promote the reaction of the bridged carbonate with primary alcohols to yield monoalkylcarbonates.[8,11b,11c] However, in the case of the trinuclear copper(II) cryptate the esterification reaction did not take place in spite of the crystals being

grown in methanol solution, due to the fact that the carbonate is held tightly by the three copper ions and kept inside the cryptand cavity.

4.3.4 IR and ESI mass spectra

The bands corresponding to the ring stretching vibrations of the pyridine ν(C=C) and ν(C=N) observed at 1594, 1577 cm^{-1} for the free ligand (Figure A4.1 in Appendix) are shifted to higher frequencies in the complex (1613, 1587 cm^{-1}, see Figure A4.2 in Appendix), which is characteristic of pyridyl nitrogen coordination.[13] The strong broad absorption band centred at 1100 cm^{-1}, the very weak absorption at 941 cm^{-1} and the strong sharp band at 626 cm^{-1}, along with the absence of a second band near 650 cm^{-1}, are consistent with the presence of non coordinate perchlorate ions,[14] as observed in the crystal structure.

Carbonate species, as the free ion, exhibits a D_{3h} space group, displays three bands in the infrared spectrum corresponding to the anti-symmetrical stretching, the out-of-plane bending, and the in-plane bending modes. However, changes will occur due to coordination, namely the lowering of symmetry to C_{2v} or C_s and consequent loss of degeneracy of the bands.[13] The carbonate related bands are somewhat difficult to assign unambiguously, due to overlap of ligand related bands. Nonetheless, the strong band observed at 1456 cm^{-1}, along with two shoulders at 1479 and 1497 cm^{-1}, should correspond to the C–O anti-symmetrical stretching of carbonate, although the CH_2 in-plane bending of the ligand also occurs in this region (1452 cm^{-1}). The out-of-plane bending mode appears as weak band at 814 cm^{-1} with a shoulder at 820 cm^{-1} and the in-plane bending as two weak bands at 793 and 772 cm^{-1}.

The ESI mass spectrum acquired in positive polarity mode using a solution of the crystals of $[Cu_3pyr(\mu_3\text{-}CO_3)]\cdot(ClO_4)_4\cdot H_2O$ dissolved in H_2O/MeOH (50:50 v/v) at pH 6.0 (Figure A4.3 in Appendix), showed only one peak at 1357.0 m/z corresponding to the $\{[Cu_3pyr(\mu_3\text{-}CO_3)]\cdot(ClO_4)_3\}^+$ ion, indicating that the structure of the complex is retained in solution.

4.3.5 Magnetic properties

The magnetic properties of $[Cu_3pyr(\mu_3\text{-}CO_3)]\cdot(ClO_4)_4\cdot H_2O$, under the form of $\chi_M T$ *versus* T plot, are shown in Figure 4.4 (χ_M being the magnetic susceptibility per three copper(II) ions).

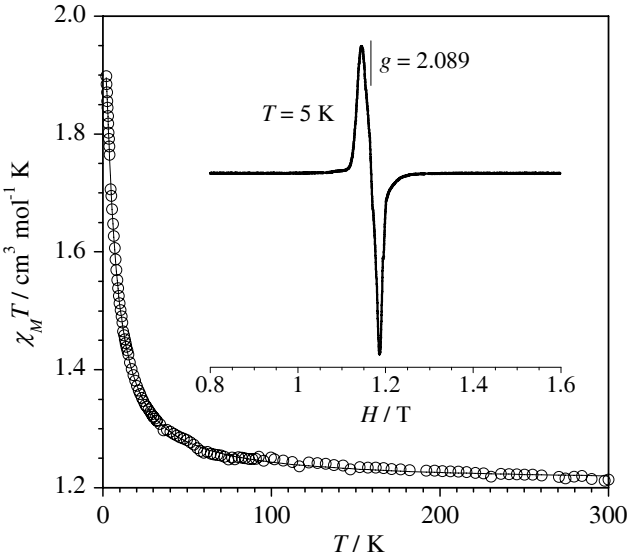

Figure 4.4 Temperature dependence of the product of the magnetic susceptibility with temperature for $[Cu_3pyr(\mu_3\text{-}CO_3)]^{4+}$. The solid line is the theoretical curve based on the equation (1). The inset shows the Q-Band EPR spectrum of a powder sample of $[Cu_3pyr(\mu_3\text{-}CO_3)]^{4+}$ at 5 K.

At r.t. $\chi_M T$ is 1.21 cm^3 mol^{-1} K, a value which is expected for three magnetically isolated spin doublets. Upon cooling, $\chi_M T$ increases monotonically to attain a value of 1.90 cm^3 mol^{-1} K at 2.0 K. The shape of this plot clearly shows the occurrence of intramolecular ferromagnetic interactions and so, a spin quartet (S = 3/2) as ground state is expected. Having in mind the triangular topology of the three crystallographically independent copper(II) ions in $[Cu_3pyr(\mu_3\text{-}CO_3)]^{4+}$ (see Figure 4.2), three different exchange pathways through *syn-anti* carbonato bridge could be expected (J_{12}, J_{13} and J_{23}). However, because of the similarity of the structural parameters for all these three independent Cu(II) ions, we can assume $J_{12} = J_{13} = J_{23} = J$. Taking into account this coupling scheme and considering that the zero-field splitting of the ground spin quartet is axial (2D is

the energy gap between the ±3/2 and ±1/2 Kramers doublets), the derived expression for the magnetic susceptibility could be given by Equation (1).[5g]

$$\chi_M = \frac{N\beta^2 g^2}{4k(T-\theta)}\left\{\frac{(3+2/d)+(3-2/d)\exp(-2d)]+2\exp(-j)}{1+\exp(-2d)+2\exp(-j)}\right\} \qquad (1)$$

where θ is the Weiss parameter for the intermolecular interactions, $d = D/kT$ and $j = 3J/2kT$ (for $|D| < |J|$). We have assumed the same value of g for all three copper(II) ions with $g_{\parallel} = g_{\perp} = g$. Least-squares fit of the magnetic data of $[Cu_3pyr(\mu_3\text{-}CO_3)]^{4+}$ through eq (1) leads to J = +3.80(2) cm^{-1} and g = 2.08(1). The parameters D and θ are strongly correlated and they can be vary in the range $|D|$ = 0 – 0.1 cm^{-1} and $-\theta$ = 0.1 – 0.14 K, indicating that both the intermolecular interactions (θ) and the zero-field splitting effects (D) of the low-lying spin quartet (S = 3/2) are very small. At this respect, Q-band ($h\nu \approx 35$ Ghz ≈ 1.2 cm^{-1}) EPR spectrum on a polycrystalline sample of $[Cu_3pyr(\mu_3\text{-}CO_3)]^{4+}$ at 5 K (see inset of Figure 4.4) shows a quasi-isotropic signal at g = 2.089 indicating that $D \approx 0$.[15]

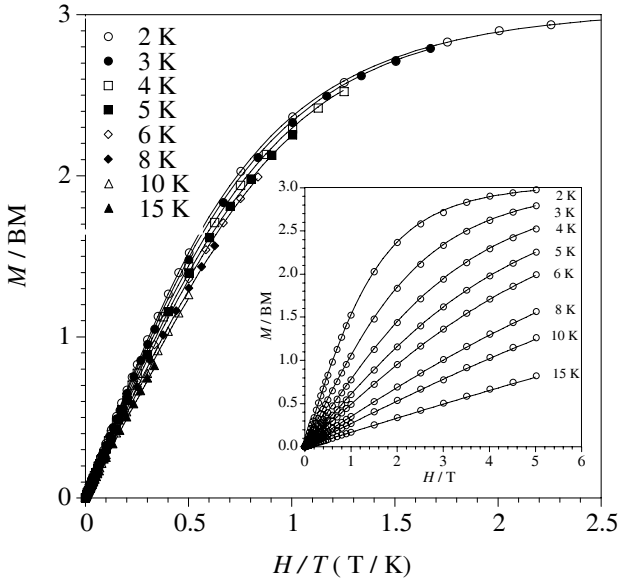

Figure 4.5 Magnetization curves for $[Cu_3pyr(\mu_3\text{-}CO_3)]^{4+}$ at different temperatures. The solid lines are the theoretical curves using the best-fit parameters (see text).

In Figure 4.5 the experimental isothermal magnetization curves at different temperatures (2 – 15 K) are shown. The saturation magnetization tends to 3 BM, as expected for a S = 3/2 ground state. The plot of the *M versus H*/*T* ratio shows that the different isothermal curves do not collapse on a unique master curve. This fact is not due to the existence of a zero-field splitting of the S = 3/2 ground state but to the different population of the excited spin doublets (S = 1/2) which are separated from ground state by $3J/2 \approx 5.7$ cm^{-1} (see Figure 4.6).

In fact, we can fit these experimental magnetization curves by using the isotropic Hamiltonian (2). The best-fit parameters obtained from a numerical matrix diagonalization method through the Hamiltonian of Equation (2) are J = 4.20(3) cm^{-1} and g = 2.07(1).

$$\hat{H} = -J(\hat{S}_1\hat{S}_2 + \hat{S}_2\hat{S}_3 + \hat{S}_1\hat{S}_3) + g\beta H\sum_{i=1}^{3}\hat{S}_i \qquad (2)$$

A fit taking into account both the experimental magnetization and $\chi_M T$ curves simultaneously through Equation (2) yields J = 4.0 (1) cm^{-1} and g = 2.07(1) with D and θ equal to zero.

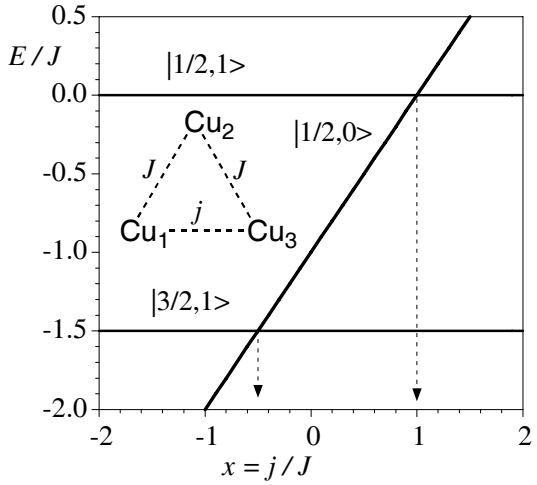

Figure 4.6 Variation of the spin state energies (*E/J versus* the x = *j/J* ratio) for an isosceles triangle with local spins $S_1 = S_2 = S_3 = 1/2$, using the common notation $|S,S^*>$, where S is the total spin ($S = S_1 + S_2 + S_3$) and $S^* = S_1 + S_3$.

4.3.6 DFT Calculations and Magneto-Structural Correlations

DFT calculations on the experimental geometry of the trinuclear complex were done to estimate the three magnetic coupling constants present. The values obtained for them (J = +5.2, +5.6 and +6.5 cm^{-1}) are close to those found from the experimental data (J = +4.0 cm^{-1}) and they are included in Table 4.4 with some of their more relevant structural parameters. It deserves to be noted that these values are also close to each other since there are small geometrical differences. The ferromagnetic nature of the interactions leads to a spin quartet (S = 3/2) ground state. However, the magnetic couplings are weak enough to allow the nearby presence of the excited doublet states (see Figure 4.6) accounting for the observed thermal dependence of the magnetization curves (Figure 4.5). The ferromagnetic nature of the magnetic coupling can be attributed to the *syn-anti* conformation of the carbonato-bridge (Scheme 4.3c) as known for other copper(II) complexes where a carboxylate[16] or carbonate[7b,d,e,f,g,h,j,k,m,o,p,17] group adopts the *syn-anti* conformation.

In order to study the influence of the different carbonato-bridge conformations (*syn-anti*, *syn-syn* or *anti-anti*) on the nature and magnitude of the magnetic coupling (J) we have considered a copper(II) dinuclear model (see Experimental Section).

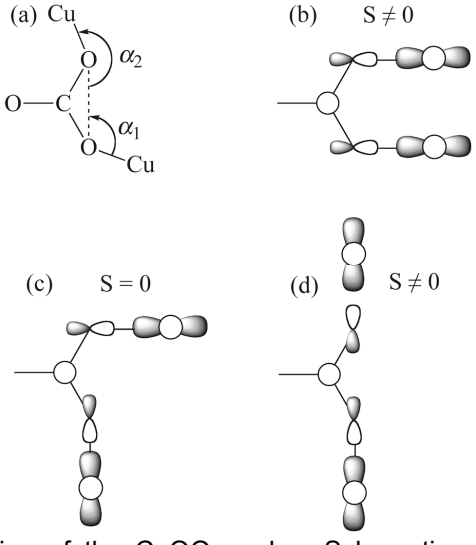

Scheme 4.3 (a) Definition of the CuOO angles. Schematic views of the overlapping between magnetic orbitals in the (b) *syn-syn*, (c) *syn-anti* and (d) *anti-anti* conformations.

Table 4.4 Magneto-structural data for the compounds where a carbonate group acts as bridge between three copper(II) ions through only the OCO pathway.

Label	Compound[a]	J[b]	Cu–O[c]	Cu_1OO[d]	Cu_2OO[d]	θ [e]	Refcode[f]	Ref.
1				77.0	204.5			
1'	$[Cu_3(L^4)_6(\mu_3\text{-}CO_3)](BF_4)_4$	29.3	1.98	79.5	222.0	1.8	MOGPUT	7j
1"				96.3	220.9			
2	$[Cu_3(L^5)_3(\mu_3\text{-}CO_3)\ (ClO_4)_3](ClO_4)$	18.0	1.97	81.0	219.0	2.1	RAMVIL	7m
3	$[Cu_3(L^{10})_3(\mu_3\text{-}CO_3)](ClO_4)_4$	17.2	2.00	82.1	217.9	0.0	NOJZOB	7f
4	$[Cu_3(L^2)_3(\mu_3\text{-}CO_3)\ (ClO_4)_3](ClO_4)$	12.6	1.97	88.7	211.7	5.5	ZOKDIM	7d
5				89.1	213.3			
5'	$[Cu_3(L^6)_3(\mu_3\text{-}CO_3)(ClO_4)_2(H_2O)](ClO_4)$	12.6	1.99	110.4	211.8	2.3	OGEHIR	7k
5"				87.0	199.0			
6	$[Cu_3(L^1)_3(\mu_3\text{-}CO_3)](ClO_4)_4$	11.3	1.98	87.8	212.2	1.2	IFIDOR	7p
7				88.4	223.5			
7'	$[Cu_3(L^8)_6(\mu_3\text{-}CO_3)](BF_4)_4$	10.6	2.02	81.0	212.7	12.4	WOJSOD	7h
7"				78.5	218.7			
8	$[Cu_3(L^9)_3(\mu_3\text{-}CO_3)(H_2O)_3](NO_3)_4$	9.6	1.96	–[g]	–[g]	–[g]	COPYCU	7b
9	$[Cu_3(L^3)_3(\mu_3\text{-}CO_3)](ClO_4)_4$	8.2	1.93	97.2	204.3	8.7	ZINXAV	7e
10	$[Cu_3(L^7)_6(\mu_3\text{-}CO_3)_2(ClO_4)_2(CH_3OH)_{0.5}]_n$	6.2	1.95	77.6	222.4	0.2	WANLED	7o
11				92.1	205.1			
11'	$[Cu_3(L^{11})(\mu_3\text{-}CO_3)](ClO_4)_4\cdot H_2O$	4.0	1.90	91.3	208.6	5.0	–	this work
11"				94.7	209.3			
12	$[Cu_3(L^{12})_3(\mu_3\text{-}CO_3)](ClO_4)_4$	-1.2	1.95	–[g]	–[g]	–[g]	MUWWOQ	7g

[a] L^1 = *N*-(2-thiophenoethyl)-*N,N*-bis(3-aminopropyl)amine. L^2 = bis(3-aminopropyl) methylamine. L^3 = 1,4-dioxa-7,10,13-triazacyclopentadecane. L^4 = 4,4'-dimethyl-2,2'-bipyridine. L^5 = methyl[2-(2-pyridyl)ethyl](2-pyridylmethyl)amine. L^6 = bis(3-aminopropyl)amine. L^7 = 4-aminopyridine. L^8 = 2,2'-bipyridine. L^9 = 2-[2-(2-pyridyl)ethyliminomethyl]pyridine. L^{10} = 1,4.7.10-tetraazabicyclo[5.5.3]pentadecane. L^{11} = pyr. L^{12} = tris-pyridylmethyl)amine. [b] In cm^{-1}. [c] Average distance in angstroms. [d] In degrees. [e] Angle (in degrees) that measure the planarity of the fragment Cu-carbonate, which takes a null value when all atoms in the fragment are placed in the same plane. [f] Code from Cambridge Data Base. [g] No data available from Cambridge Data Base.

The CuOO angles (see Scheme 4.3a) were chosen to visualize the way that *syn-syn* is transformed into *syn-anti* and *anti-anti* conformations. In this model, the carbonate group and copper atoms were kept in the same plane. Thus, an ideal *syn-syn* conformation is found when the CuOO angle is 90º for both metal ions (see Scheme 4.3b).

The magnetic coupling parameters (*J*) calculated through this model are displayed in Figure 4.7 as a contour map for each value of *J* as a function of the CuOO angle of both copper(II) ions.

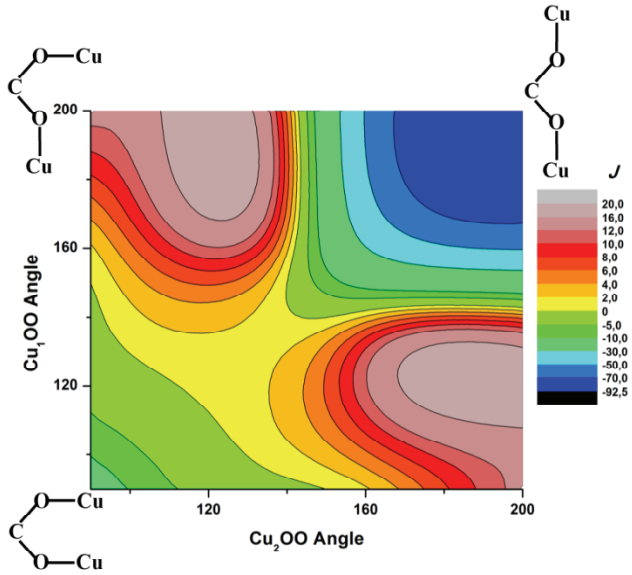

Figure 4.7 Contour map showing the dependence of the magnetic coupling constant *J* (in cm^{-1}) on the CuOO angles (in degrees). The *syn-syn*, *syn-anti* and *anti-anti* conformations are shown in the corresponding corners of the plot. Antiferro- and ferromagnetic couplings are represented in blue and red shades, respectively.

These results show that antiferromagnetic couplings prevail in a *syn-syn* conformation because the overlapping between the magnetic orbitals is far to be canceled (Scheme 4.3b). This overlap increases for an *anti-anti* conformation [180º for both CuOO angles] (Scheme 4.3d) yielding a stronger antiferromagnetic interaction.

As shown by Figure 4.7, the ferromagnetic coupling can be observed for the *syn-anti* conformation (about 90º for one CuOO angle and about 180º for the other one) and it can be explained by an accidental orthogonality between the

magnetic orbitals (Scheme 4.3c). Table 4.4 shows the most relevant magnetic (*J*) and structural (CuOO angles) parameters for the μ_3-carbonato tricopper(II) complexes whose magnetism and structure have been studied as far as we know. A label has been assigned to each complex according to the magnitude of the magnetic coupling (a stronger magnetic coupling receives a lower label) and they are placed in the contour map of Figure 4.8 as a function of their CuOO angles. Figure 4.8 is similar to Figure 4.7 but only for the narrow domain of CuOO known angles of the complexes (Table 4.4).

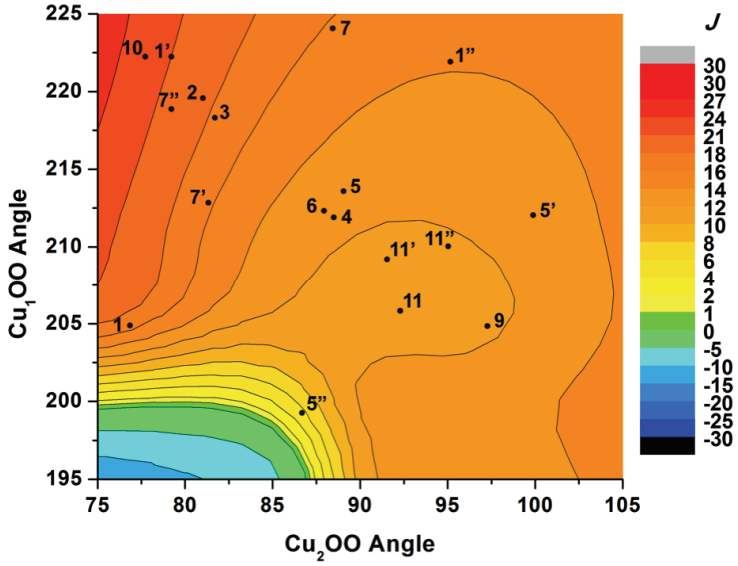

Figure 4.8 Contour map showing the dependence of the magnetic coupling constant *J* (in cm^{-1}) on the CuOO angles (in degrees). The experimental points are marked with a dot and a label identifying the compound. Compounds 1, 5, 7 and 11 (see Table 4.4) have a low symmetry and each copper present two angles, therefore these compounds are represented by three dots but the same label with different quotes.

However, it is not easy to establish a good magneto-structural correlation due to the following reasons: (i) the magnetic coupling depends at least on two CuOO angles, (ii) in many cases the copper(II) ions are structurally independent (three different CuOO angles) but only a magnetic coupling has been considered in the analysis of the experimental magnetic data and (iii) the number of compounds reported in the literature is scarce (only 10 complexes are fully characterized). In any case, when Figure 4.8 is carefully examined, a good agreement is evidenced

between the experimental and theoretical results. Nevertheless, the experimental couplings for 7 and 10 are much weaker than those expected from the theoretical study. Although generally the copper(II) ions are placed in the same plane of the carbonate group (see θ angle in Table 4.4), it is not the case for complex $[Cu_3(L^8)_6(\mu_3\text{-}CO_3)](BF_4)_4$ (7) which presents the larger values of θ (12.4º) and Cu-O bond length in this family. Clearly, both factors induce a decrease of the antiferromagnetic coupling because the spin delocalization and the overlapping between magnetic orbitals are reduced. On the other hand, the structure of the compound $[Cu_3(L^7)_6(\mu_3\text{-}CO_3)_2(ClO_4)_2(CH_3OH)_{0.5}]_n$ (10) is a complicated 2D network whose law to simulate the magnetic behavior being unknown at present the authors have fitted the experimental data using a law developed for a simpler hexagonal network.

4.4 Conclusions

Solution studies of the copper(II) complexes of the macrobicyclic ligand showed that the trinuclear species predominate from pH 5.0, the main species being the hydroxo complexes. The stepwise stability constants of the complexes formed between copper(II) and pyr decrease in the order $[Cupyr]^{2+} > [Cu_2pyr]^{4+} > [Cu_3pyr]^{6+}$ mainly due to the build up of positive charge in the macrobicyclic cavity. In order to lower this positive charge and minimize the electrostatic repulsions, the hydroxo complexes start forming at very unusual low pH.

Crystals of the trinuclear copper complex grown at pH ≈ 6, revealed the presence of carbonate (formed by spontaneous CO_2 uptake from air) bridging the three copper centres. CO_2 fixation is likely to derive from the nucleofilic attack of the hydroxo group of the $[Cu_3pyrOH]^{5+}$ complex on the electrophilic carbon of CO_2. Apparently, the ability of pyr to bring into close proximity three metal ions plays a crucial role in lowering the pK_a of coordinated water molecules, which allows hydroxo complexes to be formed in slightly acid media that in turn permits CO_2 fixation to occur without need for high pH. The Cu–Cu distances of the $[Cu_3pyr(\mu_3\text{-}CO_3)]^{4+}$ complex are comparable to those of the known examples of

μ_3-CO_3-bridged trinuclear copper(II) complexes formed by assembly of three individual mononuclear complexes[7] where no special constraints exists.

The magnetic data of $[Cu_3pyr(\mu_3\text{-}CO_3)]^{4+}$ showed the existence of ferromagnetic intramolecular interactions through the carbonato bridge in *anty-syn* conformation. The Q-band EPR spectrum at 5 K clearly shows that the spin quartet, S = 3/2, ground state is basically degenerated ($D \approx 0$). *DFT* calculations indicated that the ferromagnetic nature of the magnetic coupling can be attributed to the *syn-anti* conformation of the carbonato-bridge.

In conclusion, the architecture of pyr is responsible for the interesting properties observed, namely the lowering the pK_a of coordinated water molecules to unusual values and the good fit of the carbonate anion between the copper centres that allows its encapsulation.

4.5 Experimental

4.5.1 General considerations

The pyr compound was synthesized from 1,3,5-tris(aminomethyl)-2,4,6-triethylbenzene and 2,6-pyridinedicarbaldehyde as described in Chapter 2. All solvents and chemicals were reagent grade quality and commercially purchased and used as supplied, except 1,3,5-tris(aminomethyl)-2,4,6-triethylbenzene and 2,6-pyridinedicarbaldehyde which were prepared according to literature methods.[18] KNO_3, $Cu(NO_3)_2{\cdot}2.5H_2O$ and $Cu(ClO_4)_2{\cdot}6H_2O$ were analytical grade quality, commercially purchased and used as supplied. All the solutions were prepared using demineralised water (obtained by a Millipore/Milli-Q system) and methanol purified by standard methods.[19] IR spectra were recorded in the 4000–450 cm^{-1} region at room temperature by using KBr pellets and a UNICAM Mattson 7000 spectrometer. Microanalyses were carried out by the ITQB Microanalytical Service.

4.5.2 Synthesis of crystals

4.5.2.1 $[Cu_3pyr(\mu_3\text{-}CO_3)](NO_3)_4\cdot 9H_2O$

The pyr compound (2 mg, 2.5 μmol) was dissolved in MeOH (50 μL) and 0.05 mol dm^{-3} $Cu(NO_3)_2$ (150 μL) was added. Immediately a blue precipitate was formed. MeOH (500 μL) was added and the solution slightly heated until it was clear, then the mixture was left exposed to the atmosphere for three days, after which blue single crystals suitable for X-ray crystallography were obtained.

4.5.2.2 $[Cu_3pyr(\mu_3\text{-}CO_3)](ClO_4)_4\cdot H_2O$

The pyr compound (82 mg, 0.1 mmol) was dissolved in MeOH (2 cm^3) and 0.05 mol dm^{-3} $Cu(ClO_4)_2$ (6 cm^3) was added. Immediately a blue precipitate was formed. MeOH (20 cm^3) was added and the solution slightly heated until it was clear, then the mixture was placed inside a box in CO_2 atmosphere (dry ice) where it was allowed to stand for three days. Blue single crystals suitable for X-ray crystallography were filtered and washed with cold water. Yield: 70%. IR spectrum (KBr pellet), v (cm^{-1}): 3450br v(N–H); 2966m, 2931m, 2912m, 2870m v(CH_2); 1613m v(C=C, py); 1587m v(C=N, py); 1497sh, 1479sh, 1455s ν_d(C–O); 1100br ν_a(Cl–O); 941w ν_s(Cl–O); 820sh, 814w $\pi(CO_3)$; 793w, 772w δ_d(OCO); 626 δ(Cl–O). ESI-MS (H_2O/MeOH): m/z (%): 1357.0 $\{[Cu_3pyr(\mu_3\text{-}CO_3)]\cdot 3ClO_4\}^+$; Elem. Anal. calcd (%) for $[Cu_3pyr(\mu_3\text{-}CO_3)]4ClO_4.H_2O$: C 42.35, H 4.85, N 8.55; found: C 42.40, H 4.84, N 8.44.

4.5.3 Potentiometric measurements

4.5.3.1 Reagents and solutions

All solutions were prepared in water/methanol (50:50 v/v) solvent. A stock solution of the receptor was prepared at *ca*. 2.0×10^{-3} mol dm^{-3}. Carbonate-free solutions of the KOH titrant were prepared as described in Chapter 2. These solutions were discarded every time carbonate concentration was about 0.5% of the total amount of base. The titrant solutions were standardized (tested by Gran's method).[20]

4.5.3.2 Equipment and working conditions

The equipment used was described in Chapter 2. The ionic strength of the experimental solutions was kept at 0.10±0.01 mol dm^{-3} with KNO_3, temperature was maintained at 298.2±0.1 K. Atmospheric CO_2 was excluded from the titration cell during experiments by passing purified nitrogen across the top of the experimental solution. The glass electrode was pre-treated by soaking it in the water–methanol (50:50 v/v) solution over a period of 2 days, in order to prevent erratic responses.

4.5.3.3 Measurements

The $[H^+]$ of the solutions was determined by the measurement of the electromotive force of the cell, $E = E^{o\prime} + Q \log [H^+] + E_j$, where $E^{o\prime}$ is the formal cell potential, $Q = 2.303RT/F$ and E_j is the liquid-junction potential. The term pH is defined as $-\log [H^+]$. $E^{o\prime}$, Q, E_j and K_w (ionic product of water) were determined by titration of a solution of known hydrogen-ion concentration at the same ionic strength, using the acid pH range of the titration. E_j was found to be negligible under the experimental conditions used. The value of K_w, the ionic product of water, was determined from data obtained in the alkaline range of the titration, considering $E^{o\prime}$ and Q valid for the entire pH range and found to be equal to $10^{-13.91}$ in our experimental conditions. Before and after each set of titrations the glass electrode was calibrated as a $[H^+]$ probe by titration of 1.0×10^{-3} mol dm^{-3} standard HCl solution with standard KOH. Measurements were carried out with 0.0475 mmol of ligand in a total volume of 40 cm^3, in the absence and in the presence $Cu(NO_3)_2$ in C_{Cu}:C_{pyr} ratios of 0.5, 1.0, 2.0 and 3.0. Each titration curve consisted typically of 60–90 points in the 2.5–9.0 pH range and a minimum of two replicate titrations were performed for each C_{Cu}:C_{pyr} ratio. Backtitrations with standard HNO_3 solution were performed to confirm the values of the final $E^{o\prime}$ readings. Care has been taken to maintain unaltered the methanol–water ratio in measured solution. The exact amount of ligand was obtained by determination of the excess of acid present in a mixture of pyr and standard HNO_3 1.3×10^{-2} mol dm^{-3} by titration with standard KOH solution.

4.5.3.4 Calculation of equilibrium constants

Overall protonation constants, β_i^H of the free ligand were calculated by fitting the potentiometric data obtained for all the performed titrations in the same experimental conditions with the HYPERQUAD program.[21] Stability constants of the various species formed in solution were obtained from the experimental data corresponding to the potentiometric titration of solutions of the different metal ions, each of them with different metal to ligand ratios, also using the HYPERQUAD program. The initial computations were obtained in the form of overall stability constants, $\beta_{M_mH_hL_l} = [M_mH_hL_l]/[M]^m[H]^h[L]^l$. The errors quoted are the standard deviations of the overall stability constants given directly by the program for the input data, which include all the experimental points of all titration curves. The HYSS program[22] was used to calculate the concentration of equilibrium species from the calculated constants from which distribution diagrams were plotted. The species considered in a particular model were those that could be justified by the principles of coordination chemistry.

4.5.4 Crystallography

The X-ray data of $[Cu_3pyr(\mu_3\text{-}CO_3)](ClO_4)_4\cdot(MeOH)\cdot 2H_2O$ **1** and $[Cu_3pyr(\mu_3\text{-}CO_3)](NO_3)_4\cdot 9H_2O$ **2** were collected on a CCD Bruker APEX II at 150(2) K using graphite monochromatized Mo-Kα radiation (λ = 0.71073 Å). The selected crystal was positioned at 35 mm from the CCD and the spots were measured using a counting time of 100 s for 1 and 60 s for 2. Data reduction including a multi-scan absorption correction was carried out using the SAINT-NT software package from Bruker AXS. The structures were solved by a combination of direct methods with subsequent difference Fourier syntheses and refined by full matrix least squares on F^2 using the SHELX-97 suite.[23] Anisotropic thermal displacements were used for all non-hydrogen atoms. The hydrogen atoms of the C–H and N–H bonds were placed at geometrical positions and refined with $U_{iso} = 1.2U_{eq}$ of the atom they are attached. The OH hydrogen atom of the methanol molecule present in salt 1 was also refined in an ideal position calculated *via* a suitable AFIX instruction. The atomic positions of the hydrogen atoms of the water

crystallization molecules of both complexes were discernible from difference Fourier maps and they included in the structure refinement with individual isotropic thermal parameters. In addition in complex **1**, one perchlorate counter ion was found disordered over two tetrahedral positions, which were included in the refinement with refined occupancies of 1-*x* and *x*, being *x* 0.55(1). Molecular diagrams were drawn with PYMOL software.[24] The crystal data and refinement details are summarized in Table A4.1 given in Appendix.

CCDC 823349 and 823350 contains the supplementary crystallographic data for this paper. These data can be obtained free of charge from The Cambridge Crystallographic Data Centre via www.ccdc.cam.ac.uk/data_request/cif.

4.5.5 ESI MS

A solution of $[Cu_3pyr(\mu_3\text{-}CO_3)](ClO_4)_4 \cdot H_2O$ 1×10^{-4} mol dm^{-3} in water/methanol (50:50 v/v) at pH = 6.0, was prepared and the mass spectra was acquired in the positive polarity mode, after their direct injection into the mass spectrometer using a syringe pump, in a Bruker Daltonics Esquire 3000plus mass spectrometer equipped with ESI source. The following tune conditions were used: ion spray voltage, 50–300 V ramp range capillary exit and temperature of the heated capillary, 150 ºC. Nitrogen was used as drying gas at a flow rate of 5 L/min and at a constant pressure of 15 psi.

4.5.6 Magnetic measurements

Magnetic susceptibility measurements of polycrystalline samples were measured over the temperature range 2 – 300 K with a Superconducting Quantum interference Design (SQUID) magnetometer in the temperature range 2.0 – 300 K and under an an applied magnetic field of 0.02 T for T < 20 K in order to avoid the saturation effects and 1 T for T > 20 K. Diamagnetic corrections of the constituents atoms were estimated from Pascal's constants and a value of 60 x 10^{-6} cm^3 mol^{-1} was used for the temperature independent paramagnetism of each copper(II) ion. Q-band EPR spectrum on a polycrystalline sample of

$[Cu_3pyr(\mu_3\text{-}CO_3)]\cdot(ClO_4)_4\cdot H_2O$ was performed with a Brucker ER 200 spectrometer equipped with a helium continuous-flow cryostat.

4.5.7 Computational Details

Calculations were performed through the *Gaussian09* package using the B3LYP functional and the quadratic convergence approach.[25] Triple-ζ and double-ζ all electron basis sets proposed by Ahlrichs *et al.* were used for the metal and for the rest of atoms, respectively.[26,27] The broken symmetry approach has been employed to describe the unrestricted solutions of the antiferromagnetic spin states,[28] which have been obtained from the guess functions generated with the fragment tool implemented in Gaussian code. The full geometry has been used for $[Cu_3pyr(\mu_3\text{-}CO_3)](ClO_4)_4\cdot H_2O$. *DFT* calculations have also been done on a dinuclear model where the copper(II) ions have been perfectly placed in the carbonate plane and, to allow close positions for the metal atoms, the peripheral ligands have been put in a perpendicular plane to that built from the carbonate group. To prevent contacts between these peripheral groups from different metal ions (strong hydrogen-bonds), small fluoride groups have been chosen rather than bulkier ammonia groups. In this model, the metal-ligand distances have been optimized in the singlet spin state. The metal fragments have been shifted to reach *anti-anti* conformations from the *syn-syn* and *syn-anti* configurations.

On the other hand, the broken-symmetry methodology allows obtain all the exchange coupling constants that are present in polynuclear transition metal complexes.[28] In order to calculate the *n* J_i exchange coupling constants of a polynuclear complex, we must at least perform *n+1* energy calculations of different spin configurations that correspond to single-determinant Kohn-Sham solutions. Such spin configurations must be selected in such way that it is possible to solve a system of *n* equations with *n* unknowns, the J_i values. In this way, four calculations are necessary on the complex $[Cu_3pyr(\mu_3\text{-}CO_3)](ClO_4)_4\cdot H_2O$ in order to obtain the three possible exchange coupling constants (see Table 4.3). In this case, one of them is that where the local spin

moment is paralleling aligned leading to a quartet spin state (S = 3/2), which can be chosen as energy reference. The other spin configurations corresponds to the doublet spin states where one of the local spin moments associated with the metal ions is contrary aligned to the rest ones.

4.6 Acknowledgements

The authors acknowledge FCT, with co-participation of the European Community funds FEDER, POCI, QREN and COMPETE for the financial support under project PTDC/QUI/67175/2006. The authors also thank the MICINN (Spain) (Projects CTQ2010-15364 and the Consolider Ingenio in Molecular Nanoscience CSD2007-00010) and the Generalitat Valenciana (Spain) (Project PROMETEO/2009/108). The NMR spectrometers are part of The National NMR Network (REDE/1517/RMN/2005), supported by "Programa Operacional Ciência e Inovação (POCTI) 2010" and Fundação para a Ciência e a Tecnologia (FCT). We also acknowledge M. C. Almeida for providing elemental analysis and ESI-MS data from the Elemental Analysis and Mass Spectrometry Service at the ITQB. Pedro Mateus thanks FCT for the grant, SFRH/BD/36159/2007.

4.7 References

[1] J. Yoon, E. I. Solomon, *Coord. Chem. Rev.* **2007**, *251*, 379–400.
[2] W. B. Tolman, *J. Biol. Inorg. Chem.* **2006**, *11*, 261–271.
[3] a) L. K. Thompson, *Coord. Chem. Rev.* **2002**, *233–234*, 193–206; b) S. Ferrer, F. Lloret, I. Bertomeu, G. Alzuet, J. Borrás, S. García-Granda, M. Liu-González, J. G. Hasnoot, *Inorg. Chem.* **2002**, *41*, 5821–5830.
[4] a) A. E. Martell, R. J. Motekaitis, *J. Am. Chem. Soc*. **1988**, *110*, 8059–8064; b) R. J. Motekaitis, A. E. Martell, *Inorg. Chem.* **1991**, *30*, 694–700; c) L. Fabbrizzi, P. Pallavicini, L. Parodi, A. Taglietti, *Inorg. Chim. Acta* **1995**, *238*, 5–8; d) Q. Lu, J. J. Reibenspies, A. E. Martell, R. J. Motekaitis, *Inorg. Chem.* **1996**, *35*, 2630–2636; e) L. Fabbrizzi, I. Faravelli, G. Francese, M. Licchelli, A. Perotti, A. Taglietti, *Chem. Commun.* **1998**, 971–972; f) C. Bazzicalupi, A. Bencini, A. Bianchi, V. Fusi, E. García-España, C. Giorgi, J. M. Llinares, J. A. Ramirez, B. Valtancoli, *Inorg. Chem.* **1999**, *38*, 620–621; g) L. Fabbrizzi, A. Leone, A. Taglietti, *Angew. Chem. Int. Ed.* **2001**, *40*, 3066–3069; h) L. Fabbrizzi, N. Marcotte, F. Stomeo, A. Taglietti, *Angew. Chem. Int. Ed.* **2002**, *41*, 3811–3814; i) N. Marcotte, A. Taglietti, *Supramol. Chem.* **2003**, *15*, 617–625; j) S. Carvalho, C. Cruz, R. Delgado, M. G. B. Drew, V. Félix, *Dalton Trans.* **2003**, 4261–4270; k) M. Boiocchi, M. Bonizzoni, L. Fabbrizzi, G. Piovani, A. Taglietti, *Angew. Chem. Int. Ed.* **2004**, *43*, 3847–3852; l) M. Bonizzoni, L. Fabbrizzi, G. Piovani, A. Taglietti, *Tetrahedron* **2004**, *60*, 11159–11162; m) F. Li, R.

Delgado, V. Félix, *Eur. J. Inorg. Chem.* **2005**, 4550–4561; n) B. Verdejo, J. Aguilar, A. Doménech, C. Miranda, P. Navarro, H. R. Jiménez, C. Soriano, E. García-España, *Chem. Commun.* **2005**, 3086–3088; o) L. Fabbrizzi, F. Foti, A. Taglietti, *Org. Lett.* **2005**, *7*, 2603–2606; p) M. Boiocchi, M. Bonizzoni, A. Moletti, D. Pasini, A. Taglietti, *New J. Chem.* **2007**, *31*, 352–356; q) S. Carvalho, R. Delgado, M. G. B. Drew, V. Félix, M. Figueira, R. T. Henriques, *Polyhedron* **2008**, *27*, 679–687.

[5] a) J. Comarmond, B. Dietrich, J.-M. Lehn, R. Louis, *J. Chem. Soc., Chem. Commun.* **1985**, 74–76; b) A. Bencini, A. Bianchi, E. García-España, M. Micheloni, P. Paoletti, *Inorg. Chem.* **1988**, *27*, 176–180; c) H. Adams, N. A. Bailey, M. J. S. Dwyer, D. E. Fenton, P. C. Hellier, P. D. Hempstead, J. M. Latour*, J. Chem. Soc. Dalton Trans.* **1993**, 1207–1216; d) M. P. Suh, M. Y. Han, J. H. Lee, K. S. Min, C. Hyeon, *J. Am. Chem. Soc.* **1998**, *120*, 3819–3820; e) M. del C. Fernández-Fernández, R. Bastida, A. Macías, P. Pérez-Lourido, L. Valencia, *Cryst. Growth Des.* **2008**, *8*, 3924–3926; f) B. Verdejo, S. Blasco, J. González, E. García-España, P. Gaviña, S. Tatay, A. Doménech, M. T. Doménech-Carbó, H. R. Jiménez, C. Soriano, *Eur. J. Inorg. Chem.* **2008**, 84–97; g) A. González-Alvarez, I. Alfonso, J. Cano, P. Díaz, V. Gotor, V. Gotor-Fernández, E. García-España, S. García-Granda, H. R. Jiménez, F. Lloret, *Angew. Chem. Int. Ed.* **2009**, *48*, 6055–6058.

[6] Q.-Y. Chen, Z.-Q. Pan, Q.-H. Luo, L.-M. Zhen, X.-L. Hu, Z.-L. Wang, Z-Y. Zhou, C.-H. Yeung, *J. Chem. Soc., Dalton Trans.* **2002**, 1315–1318.

[7] a) N. F. Curtis, R. W. Hay, Y. M. Curtis, *J. Chem. Soc. (A)* **1968**, 182–187; b) G. Kolks, S. J. Lippard, J. V. Waszczak, *J. Am. Chem. Soc.* **1980**, *102*, 4832–4833; c) C. Bazzicalupi, A. Bencini, A. Bianchi, V. Fusi, P. Paoletti, B. Valtancoli, *J. Chem. Soc., Chem. Commun.* **1995**, 1555–1556; d) A. Escuer, R. Vicente, E. Peñalba, X. Solans, M. Font-Bardía, *Inorg. Chem.* **1996**, *35*, 248–251; e) C. Bazzicalupi, A. Bencini, A. Bencini, A. Bianchi, F. Corana, V. Fusi, C. Giorgi, P. Paoli, P. Paoletti, B. Valtancoli, C. Zanchini, *Inorg. Chem.* **1996**, *35*, 5540–5548; f) J. Springborg, J. Glerup, I. Søtofte, *Acta Chem. Scand.* **1997**, *51*, 832–838; g) S. Yan, J. Cui, X. Liu, P. Cheng, D. Liao, Z. Jiang, G. Wang, H. Wang, X. Yao, *Sci. China (Ser. B)* **1999**, *42,* 535–542; h) G. A. van Albada, I. Mutikainen, O. S. Roubeau, U. Turpeinen, J. Reedijk, *Eur. J. Inorg. Chem.* **2000**, 2179–2184; i) Z.-W. Mao, G. Liehr, R. van Eldik, *J. Chem. Soc., Dalton Trans.* **2001**, 1593–1600; j) G. A. van Albada, I. Mutikainen, O. Roubeau, U. Turpeinen, J. Reedijk, *Inorg. Chim. Acta* **2002**, *331*, 208–215; k) M. Rodríguez, A. Llobet, M. Corbella, P. Müller, M. A. Usón, A. E. Martell, J. Reibenspies, *J. Chem. Soc., Dalton Trans.* **2002**, 2900–2906; l) W. Huang, P.-Y. Sun, J.-L. Fang, Y.-F. Sun, S.-H. Gou, *Transition Met. Chem.* **2003**, *28*, 925–929; m) J. Mukherjee, R. Gupta, T. Mallah, R. Mukherjee, *Inorg. Chim. Acta* **2005**, *358*, 2711–2717; n) J. Mukherjee, V. Balamurugan, M. S. Hundal, R. Mukherjee, *J. Chem. Sci.* **2005**, *117*, 111–116; o) A. Majumder, C. R. Choudhury, S. Mitra, G. M. Rosair, M. S. El Fallah, J. Ribas, *Chem. Commun.* **2005**, 2158–2160; p) D. Hu, L. Chen, Z.-Q. Pan, H. Liu, X.-G. Meng, Y. Song, *J. Coord. Chem.* **2008**, *61*, 1973–1982.

[8] J.-M. Chen, W. Wei, X.-L. Feng, T.-B. Lu, *Chem. Asian J.* **2007**, *2*, 710–719.

[9] F. H. Allen, *Acta Cryst.* **2002**, *B58*, 380–388.

[10] a) M. Kato, T. Ito, *Inorg. Chem.* **1985**, *24*, 504–508; b) N. Kitajima, K. Fujisawa, T. Koda, S. Hikichi, Y. Moro-oka, J*. Chem. Soc., Chem. Commun.* **1990**, 1357–1358; c) N. N. Murthy, K. O. Karlin, *J. Chem. Soc., Chem. Commun.* **1993** 1236–1238; d) N. Kitajima, S. Hikichi, M. Tanaka, Y. Moro-oka *J. Am. Chem. Soc.* **1993**, *115*, 5496–5508; (e) X.-M. Chen, Q.-Y. Deng, G. Wang, Y.-J. Xu, *Polyhedron* **1994**, *13*, 3085–3089; f) A. Escuer, R. Vicente, S. B. Kumar, X. Solans, M. Font-Bardía, A. Caneschi, *Inorg. Chem.* **1996**, *35*, 3094–3098; g) A. Schrodt, A. Neubrand, R. van Eldik, *Inorg. Chem.* **1997**, *36*, 4579–4584; h) A. Escuer, R. Vicente, S. B. Kumar, X.

Solans, M. Font-Bardía, *J. Chem. Soc., Dalton Trans.* **1997**, 403–407; i) Z.-W. Mao, F. W. Heinemann, G. Liehr, R. van Eldik, *J. Chem. Soc., Dalton Trans.* **2001**, 3652–3662; j) X. Liang, J. A. Parkinson, S. Parsons, M. Weishäupl, P. J. Sadler, *Inorg. Chem.* **2002**, *41*, 4539–4547; k) H. Fu, W.-L. Chen, D.-G. Fu, M.-L. Tong, X.-M. Chen, L.-N. Ji, Z.-W. Mao, *Inorg. Chem. Commun.* **2004**, *7*, 1285–1288; l) L.-Y. Kong, H.-F. Zhu, Y.-Q. Huang, T.-A. Okamura, X.-H. Lu, Y. Song, G.-X. Liu, W.-Y. Sun, N. Ueyama, *Inorg. Chem.* **2006**, *45*, 8098–8107; m) D. E. Janzen, M. E. Botros, D. G. VanDerveer, G. J. Grant, *Dalton Trans.* **2007**, 5316–5321; n) J. Notni, S. Schenk, H. Görls, H. Breitzke, E. Anders, *Inorg. Chem.* **2008**, *47*, 1382–1390; o) P. Mukherjee, M. G. B. Drew, M. Estrader, A. Ghosh, *Inorg. Chem.* **2008**, *47*, 7784–7791; p) J. C. Anderson, A. J. Blake, R. B. Moreno, G. R., J. van Slageren, *Dalton Trans.* **2009**, 9153–9156; q) H. Ke, L. Zhao, G.-F. Xu, Y.-N. Guo, J. Tang, X.-Y. Zhang, H.-J. Zhang, *Dalton Trans.* **2009**, 10609–10613.

[11] a) R. Menif, J. Reibenspies, A. E. Martell, *Inorg. Chem.* **1991**, *30*, 3446–3454; b) B. Kersting, *Angew. Chem. Int. Ed.* **2001**, *40*, 3987–3990; c) Y. Dussart, C. Harding, P. Dalgaard, C. McKenzie, R. Kadirvelraj, V. McKee, J. Nelson, *J. Chem. Soc., Dalton Trans.* **2002**, 1704–1713; d) B. Verdejo, J. Aguilar, E. García-España, *Inorg. Chem.* **2006**, *45*, 3803–3815; e) A. Company, J.-E. Jee, X. Ribas, J. M. Lopez-Valbuena, L. Gómez, M. Corbella, A. Llobet, J. Mahía, J. Benet-Buchholz, M. Costas, R. van Eldik, *Inorg. Chem.* **2007**, *46*, 9098–9110.

[12] D. W. Christianson, C. A. Fierke, *Acc. Chem. Res.* **1996**, *29*, 331–339.

[13] K. Nakamoto, *Infrared Spectra of Inorganic and Coordination Compounds*, 4th ed. Wiley-Interscience, New York, **1986**.

[14] a) D. L. Lewis, E. D. Estes, D. J. Hodgson, *J. Cryst. Mol. Struct.* **1975**, *5*, 67–74; b) B. J. Hathaway, A. E. Underhill, *J. Chem. Soc.*, **1963**, 4586–4589.

[15] a) R. Boča, *Coord. Chem. Rev.* **2004**, *248*, 757–815; b) F. E. Mabbs, D. Collison, *Electron Paramagnetic Resonance of d Transition Metal Compounds*, Elsevier Science Publishers B. V., Amsterdam, **1992**, p. 605–715.

[16] a) F. S. Delgado, F. Lahoz, F. Lloret, M. Julve, C. Ruiz-Perez, *Cryst. Growth Des.* **2008**, *8*, 3219–3232; b) J. Pasan, J. Sanchiz, C. Ruiz-Perez, J. Campo, F. Lloret, M. Julve, *Chem. Commun.* **2006**, 2857–2859; c) J. Pasan, J. Sanchiz, C. Ruiz-Perez, F. Lloret, M. Julve, *New J. Chem.* **2003**, *27*,1557–1562; d) F. S. Delgado, J. Sanchiz, C. Ruiz-Perez, F. Lloret, M. Julve, *Inorg. Chem.* **2003**, *42*, 5938–5948, e) J. Pasan, F. S. Delgado, Y. Rodriguez-Martin, M. Hernandez-Molina, C. Ruiz-Perez, J. Sanchiz, F. Lloret, M. Julve, *Polyhedron* **2003,** *22*, 2143–2153; f) C. Ruiz-Perez, J. Sanchiz, M. H. Molina, F. Lloret, M. Julve, *Inorg. Chem.* **2000**, *39*, 1363–1370.

[17] a) D. Armentano, N. Marino, T. F. Mastropietro, J. Martinez-Lillo, J. Cano, M. Julve, F. Lloret, G. De Munno, *Inorg. Chem.* **2008**, *47*, 10229–10231; b) J. Sertucha, A. Luque, O. Castillo, P. Roman, F. Lloret, M. Julve, *Inorg. Chem. Commun.* **1999**, *2*, 14–16.

[18] a) K. J. Wallace, R. Hanes, E. V. Anslyn, J. Morey, K. V. Kilway, J. Siegel, *Synthesis* **2005**, 2080–2083; b) N. W. Alcock, R. G. Kingston, P. Moore, C. Pierpoint, *J. Chem. Soc., Dalton Trans.* **1984**, 1937–1943.

[19] D. D. Perrin, W. L. F. Armarego, *Purification of Laboratory Chemicals*, Pergamon, Oxford, 3rd. ed., 1988, p. 217.

[20] F. J. Rossotti, H. J. Rossotti, *J. Chem. Educ.* **1965**, *42*, 375–378.

[21] P. Gans, A. Sabatini, A. Vacca, *Talanta* **1996**, *43*, 1739–1753.

[22] L. Alderighi, P. Gans, A. Ienco, D. Peters, A. Sabatini, A. Vacca, *Coord. Chem. Rev.* **1999**, *184*, 311–318.

[23] G. M. Sheldrick, Acta Cryst. **2008**, *A64*, 112–122.

[24] W. L. Delano, The Pymol Molecular Graphics System, **2002**, on World Wide Web http://www.pymol.org.

[25] a) A. D. Becke, *Phys. Rev. A* **1988**, *38*, 3098–3100; (b) C. Lee, W. Yang, R. G. Parr, *Phys. Rev. B*, **1988**, *37*, 785–789; b) A. D. Becke, *J. Chem. Phys.* **1993**, *98*, 5648–5652.

[26] a) A. Schaefer, A. Horn, R. Ahlrichs, *J. Chem. Phys.* **1992**, *97*, 2571–2577; b) A. Schaefer, C. Huber, R. Ahlrichs, *J. Chem. Phys.* **1994**, *100*, 5829–5835.

[27] *GAUSSIAN 09*; Gaussian, Inc.: Pittsburg, PA, **2009**.

[28] a) E. Ruiz, J. Cano, S. Alvarez, P. Alemany, *J. Am. Chem. Soc.,* **1998**, *120*, 11122–11129; b) E. Ruiz, J. Cano, S. Alvarez, P. Alemany, *J. Comput. Chem*. **1999**, *20*, 1391–1400; c) E. Ruiz, A. Rodríguez-Fortea, J. Cano, S. Alvarez, P. Alemany, *J. Comput. Chem.* **2003**, *24*, 982–989; d) E. Ruiz, J. Cano, S. Alvarez, V. Polo, *J. Phys. Chem B* **2006**, *110*, 115–118.

Chapter 5

Recognition of oxalate by a new copper(II) polyaza macrobicyclic complex

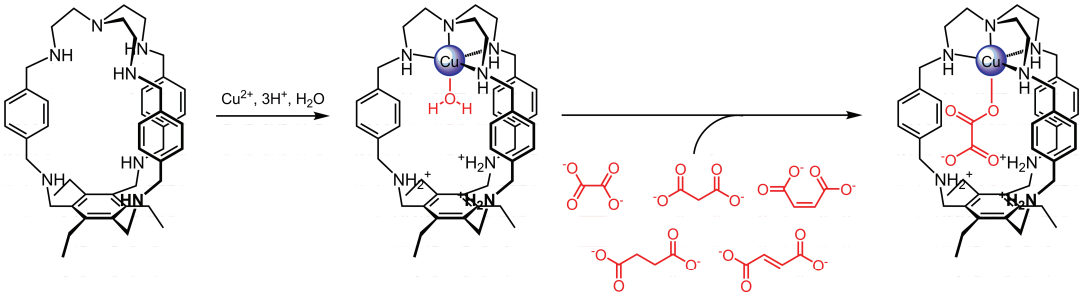

Work featured in: P. Mateus, R. Delgado, P. Brandão, V. Félix, *Chem. Eur. J.* **2011**, *17*, 7020–7031.

5.1 Summary

A new polyamine macrobicyclic compound was synthesized through a [1+1] "tripod-tripod coupling" strategy and using the Schiff-base condensation reaction, followed by sodium borohydride reduction. The resulting compound is a heteroditopic cage ($btpN_7$) in which one of the head units is appropriate for the coordination of copper(II) while the other head is available for additional hydrogen bonding and electrostatic interactions with substrates. The acid-base behaviour of the new compound, the stability constants of its complex with Cu^{2+} ion and the association constants of the copper(II) cryptate with oxalate (oxa^{2-}), malonate (mal^{2-}), succinate (suc^{2-}), maleate ($male^{2-}$) and fumarate (fum^{2-}) were determined by potentiometry at 298.2 K in aqueous solution and at ionic strength 0.10 mol dm^{-3} in KNO_3. These studies revealed a clear preference of the receptor $[CuH_hbtpN_7H_2O]^{(2+h)+}$ for oxa^{2-} over the other dicarboxylate substrates, arising from cooperativity between metal-anion coordination, electrostatic and hydrogen bonding interactions, in accordance with the ideal size of this dicarboxylate, which allows it to take full advantage of the potential binding sites of the receptor. A qualitative indicator-displacement study, in agreement with the potentiometric studies, demonstrated that the copper cryptate receptor can be used as a selective visual sensor for oxalate.

5.2 Introduction

The carboxylate functionality is part of a wide range of biologically active entities, and in many cases is responsible for their biochemical properties.[1] The recognition and transport of carboxylate containing substrates is of great biological and medicinal relevance. For instance, the specific recognition and transport of dicarboxylates across biological membranes is crucial in the metabolism of cells,[2] the sensing and signalling of amino acids play important roles in regulating cell functions[3] and the mechanism of action of the vancomycin antibiotics is highly dependant on carboxylate binding.[4] Not surprisingly, since the early days of the supramolecular chemistry of anions much work has been devoted to the design of new synthetic receptors for carboxylates, which resulted

in a plethora of compounds that take advantage of binding sites such as ammonium, guanidinium, urea, amide groups and metal ions.[5]

Two common approaches have been used in the design of synthetic receptors for carboxylate binding in aqueous solution: the incorporation of polyammonium groups and of Lewis-acid centres.[6] Thus polyamine groups have been included in macrocyclic and macrobicyclic architectures to be used in the protonated form for the direct interaction with carboxylates,[7] or in the neutral form for the coordination to metal ions and subsequent formation of cascade complexes.[8] A few examples exist in the literature that combine both ammonium groups (or other positively charged groups) and metal centres in macrocyclic or tripodal architectures, in which the two sites cooperatively bind the carboxylates.[9,8a,c,d] However, to the best of our knowledge, this approach was never explored using macrobicyclic compounds.

Herein we present a new heteroditopic macrobicyclic compound ($btpN_7$), which combines two different head units, a tren derived and a 2,4,6-triethylbenzene derived one, separated by relatively long and rigid *p*-xylyl spacers. The present compound is the third member of a family of heteroditopic heptaamine cryptands, the first one described by Heyer and Lehn [10] and the second by Steed *et al.* (cryptands **8** and **9**, in Scheme 1.15, Chapter 1, respectively) [11] however the framework of our compound forms the larger cavity of the series, see Scheme 5.1.

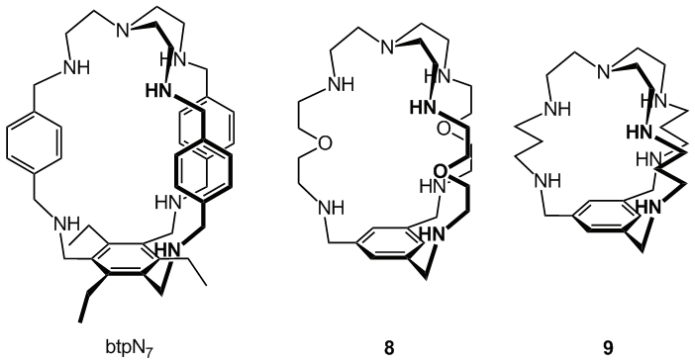

Scheme 5.1 The new compound $btpN_7$, and the two heteroditopic heptaamine cryptands already reported.[10,11]

In the design of $btpN_7$, the tren derived head unit was chosen due to its tendency to coordinate copper(II) in a trigonal bipyramidal geometry, leaving a vacant apical position for further coordination to a substrate, while the 2,4,6-triethylbenzene-derived head unit provides a rigid organic scaffold containing three ammonium sites in the right position for hydrogen bonding and electrostatic interactions with the substrate. In a somewhat similar approach heteroditopic macrobicycles containing a crown ether subunit and amide functionalities have been developed to bind alkali metal-halide ion pairs in organic solvents.[12]

We expected that the cryptate formed by coordination of copper(II) with $btpN_7$ would be suitable for interaction with dicarboxylates, thus in the present work we seek the selective uptake of the substrate with appropriate size to take full advantage of cooperativity between the copper site and the ammonium binding sites (Scheme 5.2).

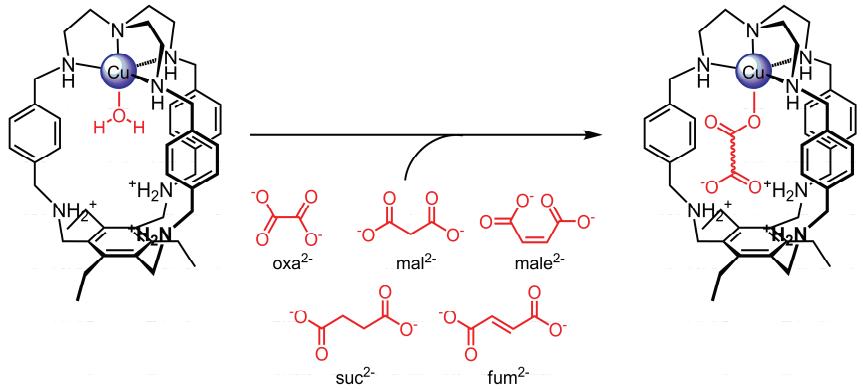

Scheme 5.2 Copper(II) cryptate of $btpN_7$ and its cascade species formed with the studied dicarboxylates.

A tren derived tripodal compound (tbN_4, Scheme 5.3) was also studied as a model of the copper(II) binding part of the $btpN_7$ cryptand.

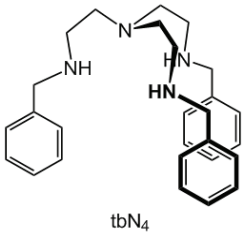

Scheme 5.3 Tripodal compound used for comparison purposes.

5.3 Results and Discussion

5.3.1 Synthesis of the cryptand

The synthesis of heteroditopic macrobicyclic compounds requires two critical steps: formation of a tripodal intermediate and macrobicyclization through a [1+1] "tripod-tripod coupling" strategy.[13] The new polyamine macrobicyclic compound was prepared as outlined in Scheme 5.4.

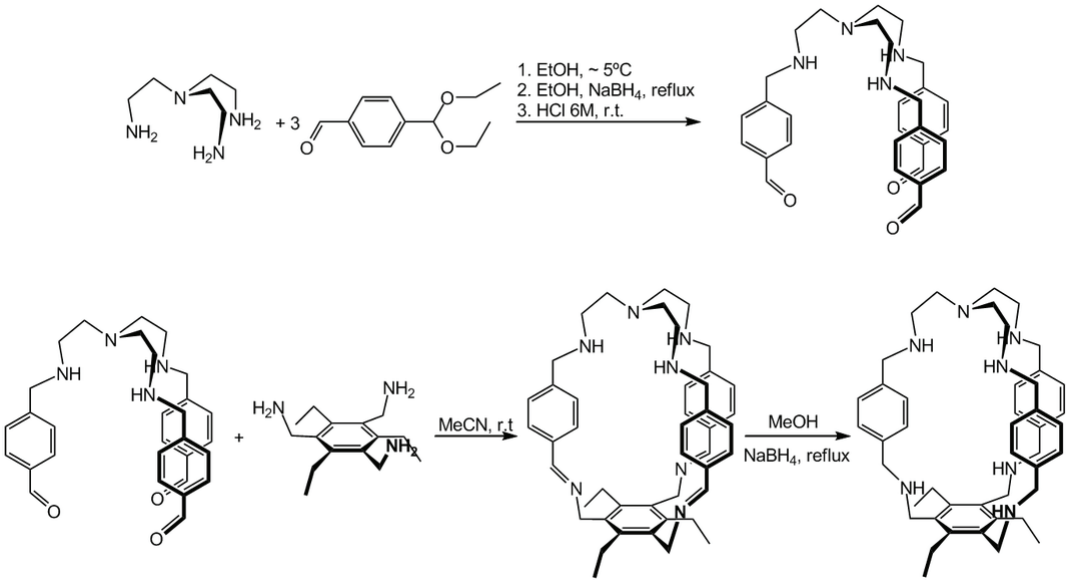

Scheme 5.4 Synthetic procedure of $btpN_7$.

A key element in this synthesis was the 4-(diethoxymethyl)benzaldehyde, in which one of the aldehyde groups is protected in the form of diethylacetal and the other is available to react with tren. After *"in situ"* sodium borohydride reduction followed by acid hydrolysis of the acetal groups, a tripodal trialdehyde intermediate was obtained in good yield. This intermediate was then reacted with 1,3,5-tris(aminomethyl)-2,4,6-triethylbenzene (again through Schiff-base condensation and without high dilution conditions) to afford a triimine compound, which after sodium borohydride reduction resulted in the desired polyamine macrobicycle in overall very good yield.

5.3.2 Acid-base behaviour of the synthesized compounds

The protonation constants of $btpN_7$ and tbN_4 were determined by potentiometry in aqueous solution at 298.2 K and ionic strength 0.10 mol dm^{-3} in KNO_3. The results are collected in Table 5.1 and the corresponding species distribution diagrams represented in Figure 5.1.

Table 5.1 Overall (β_i^H) and stepwise protonation (K_i^H) constants of $btpN_7$ and tbN_4 in H_2O.[a]

Equilibrium reaction	log β_i^H [b]		Equilibrium reaction	log K_i^H	
	$btpN_7$	tbN_4		$btpN_7$	tbN_4
$L + H^+ \rightleftharpoons HL^+$	9.05(1)	9.27(1)	$L + H^+ \rightleftharpoons HL^+$	9.05	9.27
$L + 2\,H^+ \rightleftharpoons H_2L^{2+}$	17.57(1)	17.66(1)	$HL^+ + H^+ \rightleftharpoons H_2L^{2+}$	8.52	8.39
$L + 3\,H^+ \rightleftharpoons H_3L^{3+}$	25.22(1)	24.68(1)	$H_2L^{2+} + H^+ \rightleftharpoons H_3L^{3+}$	7.65	7.02
$L + 4\,H^+ \rightleftharpoons H_4L^{4+}$	32.08(1)	–	$H_3L^{3+} + H^+ \rightleftharpoons H_4L^{4+}$	6.86	–
$L + 5\,H^+ \rightleftharpoons H_5L^{5+}$	38.75(1)	–	$H_4L^{4+} + H^+ \rightleftharpoons H_5L^{5+}$	6.67	–
$L + 6\,H^+ \rightleftharpoons H_6L^{6+}$	44.68(1)	–	$H_5L^{5+} + H^+ \rightleftharpoons H_6L^{6+}$	5.93	–

[a] T = (298.2±0.1) K; I = (0.10±0.01) mol dm^{-3} in KNO_3. [b] Values in parenthesis are standard deviations in the last significant figures.

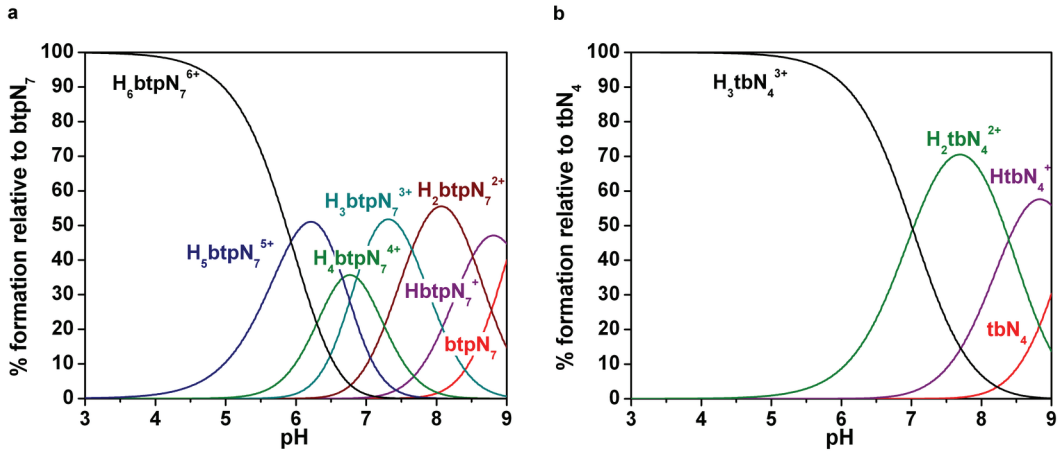

Figure 5.1 Species distribution diagrams of the protonation of $btpN_7$ (a) and tbN_4 (b). $C_{btpN_7} = C_{tbN_4} = 1.0\times10^{-3}$ mol dm^{-3}.

Six protonation constants were found for $btpN_7$ in the working pH region (2.9–9.0), corresponding to the successive protonation of the secondary amines. The stepwise values decrease with increasing protonation state of the receptor due to

both increasing electrostatic repulsion between positive charges and to statistical factors. In studied pH region the protonation constant of the tertiary amine of the tren derived head unit was not obtained, which should be very acidic due to the nearby presence of three positive charges. The same was found for tbN_4, for which only three protonation constants were determined that correspond to the successive protonation of the secondary amines.

5.3.3 Crystal structure

The single crystal X-ray diffraction of the protonated $btpN_7$ receptor revealed that the asymmetric unit is composed of one $[H_7btpN_7]^{7+}$ receptor cation, eight chloride anions, four methanol and five water molecules. The molecular diagram presented in Figure 5.2 shows that one water molecule, together with a methanol molecule and two halide anions are located inside of the cryptand cage. Furthermore, the charge balance requires that one water molecule is protonated leading to the molecular formula $[H_7btpN_7(H_2O)(MeOH)Cl_2]Cl_6\cdot(H_3O)\cdot3(H_2O)\cdot3MeOH$. This formulation is expected taking into account that the crystals suitable for X-ray determination were grown only from a very acidic hydrochloride water/methanol solution.

One external chloride counter-ion and the hydroxyl group of the encapsulated methanol were found disordered (see Experimental Section). In addition only the hydrogen atoms of the encapsulated water molecule were located. In these circumstances, the detailed analysis of the hydrogen bonding interactions is somewhat limited and will be discussed as follows. The $\{(H_2O)(MeOH)Cl_2\}^{2-}$ assembly is held into the large cavity through multiple hydrogen bonds as shown in Figure 5.2. The corresponding hydrogen bond dimensions are listed in Table A5.1 in Appendix. The water molecule is concomitantly hydrogen bonded to the N–H tertiary amine (N···O distance of 2.726(5) Å and N–H···O angle of 170(4)º) and two chloride anions (Cl···O distances of 3.206(4) and 3.189(3) Å and O–H···Cl angles of 157(4) and 163(3)º respectively), which establish two independent hydrogen bonds each with adjacent N–H binding groups from the three secondary amines linked to the 2,4,6-triethylbenzene cap. The

corresponding N···Cl distances ranges from 3.189(3) to 3.294(3) Å. The methanol molecule forms two hydrogen bonds with the remaining two N–H binding sites of this structural unit with N···O distances of 2.978(4) and 2.970(6) Å and corresponding N–H···O angles of 159(4) and 165(4)º, respectively. Five chloride counter anions surround the receptor forming with the NH_2 binding sites of the tren moiety a total of six N–H···Cl hydrogen bonds with N···Cl distances ranging from 2.988(4) to 3.113(4) Å. Furthermore, all chloride anions (including the disordered one) and the surrounded solvent molecules (methanol and water) interact at Cl···O and O···O short distances, which are consistent with the existence of a 3-D network of hydrogen bonds. The receptor adopts approximately a C_3 symmetry with pseudo-three fold axis perpendicular to the benzene ring and bisecting the N–H tertiary amine (see right view, Figure 5.2). It is interesting to notice that the secondary amines of the tren subunit are apart from each other, turning to the outside of the cavity, due to the electrostatic repulsions.

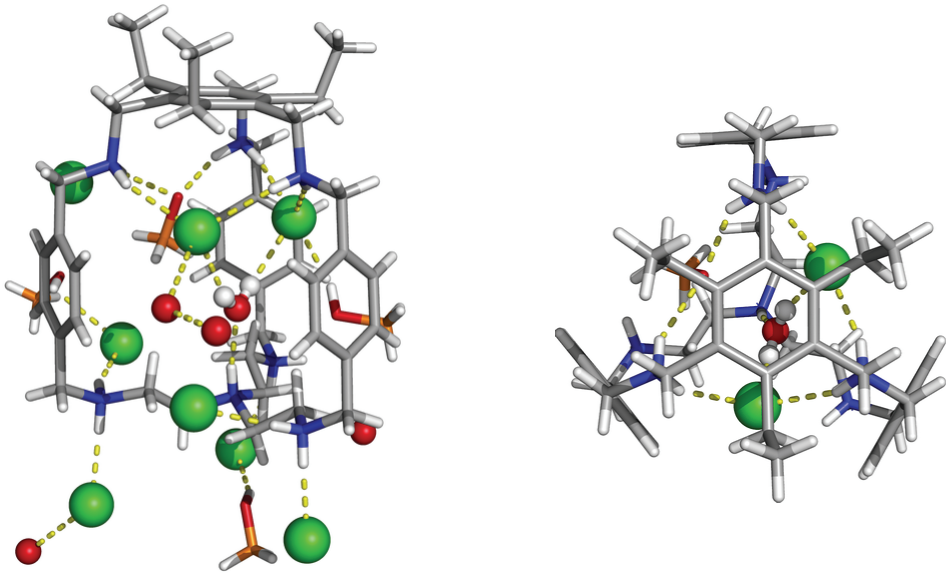

Figure 5.2 X-ray crystal structure in two different views depicting $[H_7btpN_7(H_2O)(MeOH)Cl_2]Cl_6{\cdot}(H_3O){\cdot}3(H_2O){\cdot}3MeOH$: the left view shows the $[H_7btpN_7]^{7+}$ cation interacting with chloride anions solvent water molecules through hydrogen bonds and, in the right view, the encapsulation of $\{(H_2O)(MeOH)Cl_2\}^{2-}$ assembly together with the approximately C_3 cryptand symmetry are emphasized.

5.3.4 Binding affinity of the protonated forms of $btpN_7$ towards dicarboxylates

The association constants of the protonated forms of $btpN_7$ with several dicarboxylates that differ in chain length were determined by potentiometry in aqueous solution at 298.2 K and 0.10 mol dm^{-3} KNO_3. The values are collected in Table 5.2. The protonation constants of the dicarboxylates were also determined in the same experimental conditions and used in the calculations (Table A5.2 in Appendix).

Table 5.2 Overall ($\beta_{H_hL_lA_a}$) and stepwise ($K_{H_hL_lA_a}$) association constants for the indicated equilibria in H_2O.[a]

Equilibrium reaction[b]	oxa^{2-}	mal^{2-}	suc^{2-}	fum^{2-}	$male^{2-}$
			$\log \beta_{H_hL_lA_a}$ [c]		
$7\,H^+ + L + A^{2-} \rightleftharpoons H_7LA^{5+}$	51.12(5)	–	–	50.74(5)	–
$6\,H^+ + L + A^{2-} \rightleftharpoons H_6LA^{4+}$	47.34(2)	46.81(3)	46.69(2)	47.10(2)	46.86(4)
$5\,H^+ + L + A^{2-} \rightleftharpoons H_5LA^{3+}$	40.60(6)	–	–	40.57(5)	–
			$\log K_{H_hL_lA_a}$		
$H_6L^{6+} + H^{A-} \rightleftharpoons H_7LA^{5+}$	2.61	–	–	1.96	–
$H_6L^{6+} + A^{2-} \rightleftharpoons H_6LA^{4+}$	2.66	2.13	2.01	2.42	2.18
$H_5L^{5+} + A^{2-} \rightleftharpoons H_5LA^{3+}$	1.85	–	–	1.82	–

[a] T = (298.2±0.1) K; I = (0.10±0.01) mol dm^{-3} in KNO_3. [b] A^{2-} indicates in general the dicarboxylate anion. [c] Values in parenthesis are standard deviations in the last significant figures.

The association constant values are low for all the studied dicarboxylates, with the highest values corresponding to the association of $H_6btpN_7^{6+}$ with the fully ionized dicarboxylates. Oxa^{2-} and fum^{2-} display slightly higher association constants than the rest of the substrates. It is unlikely that oxa^{2-}, due to its small size, can take advantage of the ditopic nature of the cryptand, thus its higher association constant should arise from binding of both carboxylate groups to one of the head units and to its higher charge density, whereas in the case of fum^{2-} the higher association constant should be due to the better fit into the cavity and its rigidity.

The general low association constants of the protonated receptor with the dicarboxylate anions derive from the degree of flexibility of the receptor and its lack of preorganization. Indeed the crystal structure of $[H_7btpN_7]^{7+}$ (Figure 5.2) shows the secondary ammonium groups of the tren head unit turned to the outside of the cavity due to mutual electrostatic repulsions, suggesting that a rearrangement of the receptor conformation is needed for the binding of dicarboxylate anions (Scheme 5.5), with consequent energy penalty and loss of selectivity. It is also likely that nitrate present in the supporting electrolyte may compete with the dicarboxylates, contributing to the low association constants observed.

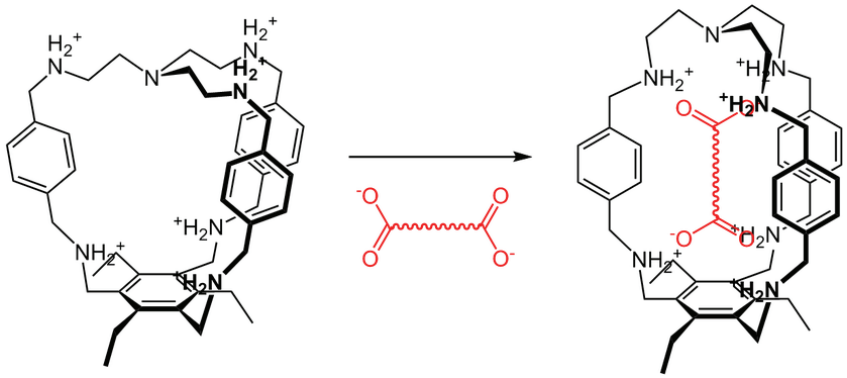

Scheme 5.5 Representation of possible conformational rearrangement of $H_6btpN_7^{6+}$ needed for dicarboxylate binding.

5.3.5 Copper(II) coordination studies

The stability constants of the copper(II) complexes of $btpN_7$ and tbN_4 were determined by potentiometry in aqueous solution at 298.2 K and 0.10 mol dm^{-3} KNO_3. The results are collected in Table 5.3 and the corresponding species distribution diagrams represented in Figure 5.3.

Only mononuclear species were found for $btpN_7$, even when two equivalents of copper were added. This fact indicates that the 2,4,6-triethylbenzene unit is not able to coordinate copper(II), and instead acts as a rigid organic scaffold to hold the three additional ammonium sites that are capable of establishing hydrogen bonding and electrostatic interactions with anionic substrates. Unlike tbN_4, for which protonated copper complexes were not found, $btpN_7$ forms three

protonated complexes that correspond to the protonation of the three secondary amines of the 2,4,6-triethylbenzene head unit (see Table 5.3).

The stability constant corresponding to the formation of $[CubtpN_7]^{2+}$ is almost three log units lower than that for $[CutbN_4]^{2+}$. This is due, at least in part, to constraints in the conformation of $btpN_7$ that increase the energetic cost of rearrangement of the secondary amine groups of the tren head unit for the coordination of the metal ion in comparison to what happens with tbN_4, which has higher freedom of motion. Thus, the coordination to copper(II), besides affording a favourable enthalpic contribution to the binding of dicarboxylates, preorganize also the receptor for the encapsulation of anionic substrates.

Also interesting to note is that the water molecule bound to the copper cryptate deprotonates at a higher pH (9.57) than that of the tripodal copper complex (8.28), which indicates that the coordinated water molecule is less susceptible to deprotonation when encapsulated into the framework of the cryptand, possible due to the network of hydrogen bonds formed into the cavity (see Figure 5.3).

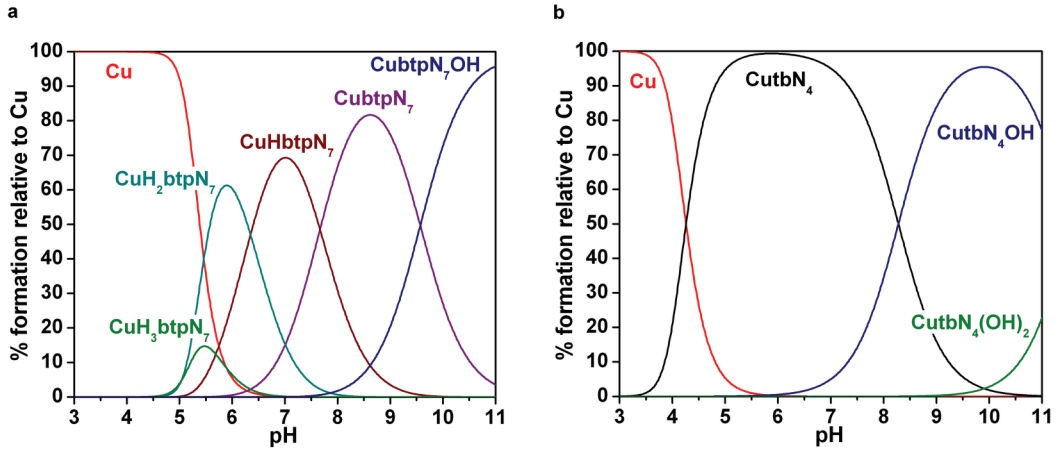

Figure 5.3 Species distribution diagram calculated for the complexes of Cu^{2+} with of $btpN_7$ (a) and tbN_4 (b). C_{btpN_7} = C_{tbN_4} =. C_{Cu} = 1.0×10^{-3} mol dm^{-3}. Charges were omitted for simplicity.

Table 5.3 Overall (β_{MmHhLl}) and stepwise (K_{MmHhLl}) stability constants of the copper(II) complexes of $btpN_7$ and tbN_4 in aqueous solution.[a]

Equilibrium	log β_{MmHhLl}[b]		Equilibrium	log K_{MmHhLl}	
	$btpN_7$	tbN_4		$btpN_7$	tbN_4
$Cu^{2+} + 3\ H^+ + L \rightleftharpoons [CuH_3L]^{5+}$	31.39(1)	–	$[CuH_2L]^{4+} + H^+ \rightleftharpoons [CuH_3L]^{5+}$	5.03	–
$Cu^{2+} + 2\ H^+ + L \rightleftharpoons [CuH_2L]^{4+}$	26.36(1)	–	$[CuHL]^{3+} + H^+ \rightleftharpoons [CuH_2L]^{4+}$	6.35	–
$Cu^{2+} + H^+ + L \rightleftharpoons [CuHL]^{3+}$	20.01(1)	–	$[CuL]^{2+} + H^+ \rightleftharpoons [CuHL]^{3+}$	7.66	–
$Cu^{2+} + L \rightleftharpoons [CuL]^{2+}$	12.35(1)	15.20(1)	$Cu^{2+} + L \rightleftharpoons [CuL]^{2+}$	12.35	15.20
$Cu^{2+} + L \rightleftharpoons [CuLOH]^{+} + H^+$	2.78(1)	6.92(1)	$[CuLOH]^{+} + H^+ \rightleftharpoons [CuL]^{2+}$	9.57	8.28
$Cu^{2+} + L \rightleftharpoons [CuL(OH)_2] + 2\ H^+$	–	-4.61(3)	$[CuL(OH)_2] + H^+ \rightleftharpoons [CuLOH]^{+}$	–	11.53

[a] T = (298.2±0.1) K; I = (0.10±0.01) mol dm^{-3} in KNO_3. [b] Values in parenthesis are standard deviations in the last significant figure.

5.3.6 Cascade species formed by the copper(II) complexes of $btpN_7$ and tbN_4 with dicarboxylate substrates

The association constants of copper(II) complexes of $btpN_7$ and tbN_4 with the dicarboxylate substrates were determined in aqueous solution at 298.2 K and 0.10 mol dm^{-3} KNO_3. The results are collected in Table 5.4. The stability constants of the copper(II) complexes of the studied dicarboxylates were also determined in the same experimental conditions and used in the calculations (Table A5.3 in Appendix).

The association constants of the copper(II) complexes of $btpN_7$ with the dicarboxylate anions are much higher than when only the cryptand is the receptor (Tables 5.2 and 5.4). In all cases the association constants are larger at the triprotonated state of the cryptate and decrease with decreasing protonation of the cryptate which provides evidence of the existence of electrostatic and possibly hydrogen bonding interactions. Oxa^{2-} is clearly the preferred dicarboxylate, presenting the highest association constants, followed by mal^{2-}. The species distribution diagram for the system $[CuH_hbtpN_7(oxa)]^{h+}$ (Figure 5.4) shows that the $[CuH_3btpN_7(oxa)]^{3+}$ is the predominant species, reaching a maximum at pH 6.2.

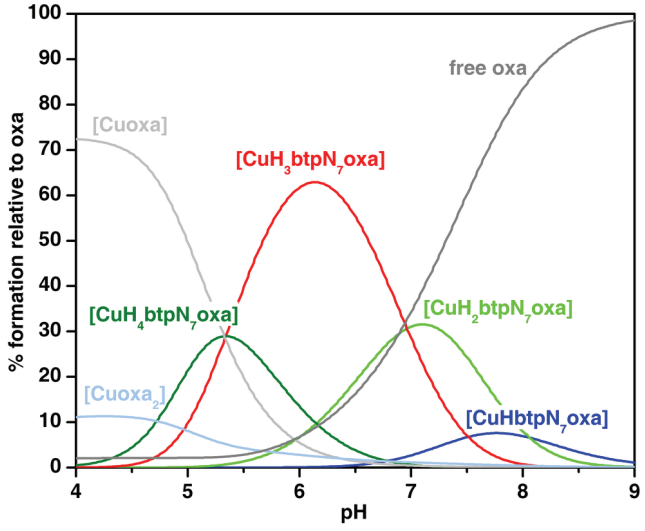

Figure 5.4 Species distribution diagram calculated for the system $[CuH_hbtpN_7(oxa)]^{h+}$. $C_{btpN_7} = C_{Cu} = C_{oxa} = 1.0\times10^{-3}$ mol dm^{-3}. Charges were omitted for simplicity.

Table 5.4 Overall ($\beta_{M_mH_hL_lA_a}$) and stepwise ($K_{M_mH_hL_lA_a}$) association constants for the indicated equilibria in H_2O.[a]

Equilibrium reaction[b]	oxa^{2-}		mal^{2-}		suc^{2-}		fum^{2-}	$male^{2-}$
	$btpN_7$	tbN_4	$btpN_7$	tbN_4	$btpN_7$	tbN_4	$btpN_7$	$btpN_7$
				log $\beta_{M_mH_hL_lA_a}$ [c]				
$Cu^{2+} + 4\ H^+ + L + A^{2-} \rightleftharpoons CuH_4LA^{4+}$	42.88(3)	–	41.81(3)	–	–	–	–	–
$Cu^{2+} + 3\ H^+ + L + A^{2-} \rightleftharpoons CuH_3LA^{3+}$	37.54(1)	33.67(3)	35.84(1)	–	34.94(2)	–	34.79(2)	35.30(3)
$Cu^{2+} + 2\ H^+ + L + A^{2-} \rightleftharpoons CuH_2LA^{2+}$	30.58(3)	29.11(3)	29.59(3)	–	29.26(2)	–	29.53(1)	29.58(2)
$Cu^{2+} + H^+ + L + A^{2-} \rightleftharpoons CuHLA^{+}$	22.5(1)	24.14(3)	22.48(4)	22.80(5)	22.58(2)	22.88(2)	22.56(4)	22.67(6)
$Cu^{2+} + L + A^{2-} \rightleftharpoons CuLA$	–	17.75(5)	–	17.69(3)	–	17.71(3)	–	–
				log $K_{M_mH_hL_lA_a}$				
$CuH_3L^{5+} + A^{2+} \rightleftharpoons CuH_3LA^{3+}$	6.15	–	4.45	–	3.55	–	3.40	3.91
$CuH_2L^{4+} + A^{2+} \rightleftharpoons CuH_2LA^{2+}$	4.22	–	3.23	–	2.90	–	3.17	3.22
$CuHL^{3+} + A^{2+} \rightleftharpoons CuHLA^{+}$	2.49	–	2.47	–	2.57	–	2.55	2.66
$CuL^{2+} + A^{2+} \rightleftharpoons CuLA$	–	2.55	–	2.49	–	2.51	–	–

[a] T = (298.2±0.1) K; I = (0.10±0.01) mol dm^{-3} in KNO_3. [b] A^{2-} denote in general the dicarboxylate anion and L the cryptand or the tripodal compounds. [c] Values in parenthesis are standard deviations in the last significant figures.

However in the absence of oxa^{2-}, the relative percentage of $[CuH_3btpN_7]^{5+}$ species is low (Figure 5.3a) due to the build up of positive charge in the interior of the cavity. This indicates that the binding of oxa^{2-} helps to relieve the electrostatic repulsions stabilizing the supercryptate, $[CuH_3btpN_7(oxa)]^{3+}$. With all the other studied dicarboxylates, the $[CuH_3btpN_7(A)]^{3+}$ species is not so dominant suggesting that in those cases the fit of the anions is not as good as for oxa^{2-}. It is also noteworthy that the decrease of binding constants with decreasing protonation state of the cryptate is much more marked for oxa^{2-} and mal^{2-} whereas for suc^{2-}, fum^{2-} and $male^{2-}$ the decrease is relatively small. This indicates that oxa^{2-} and mal^{2-} fit better than the other studied anions into the cryptate cavity taking advantage of both the coordination to copper(II) and the electrostatic and hydrogen bonding interactions with the ammonium groups of the 2,4,6-triethylbenzene head unit. In all cases the association constants corresponding to the formation of neutral and deprotonated cascade species, $[CubtpN_7(A)]$, is too low to be determined and the hydroxide ion is able to displace the dicarboxylates from the cavity at pH higher than 9.0. This clearly indicates that the electrostatic and possibly also the hydrogen bonding formation with the ammonium groups of the 2,4,6-triethylbenzene head unit contribute for the stabilization of the anions into the cryptate cavity.

On the other hand the association constants of the copper(II) complexes of the noncyclic receptor, tbN_4, with oxa^{2-}, mal^{2-} and suc^{2-}, determined also for comparison reasons, revealed that the values are of about 2.5 log units for all the dicarboxylate anions studied. These low and similar values of binding constants mean that all dicarboxylates bind to the copper(II) complex of tbN_4 by the same mode, and in the absence of any other binding sites, the receptor cannot distinguish the substrates. These data support our conclusion that the discrimination of the dicarboxylate anions by the protonated forms of the copper(II) cryptate is consequence of the inclusion of oxa^{2-} and mal^{2-} into the cryptate cavity derived from the additional stabilization of the carboxylate moiety not coordinated to the copper(II), by electrostatic and possible hydrogen bonding formation with the ammonium groups of the 2,4,6-triethylbenzene head unit.

5.3.7 Study of selective uptake of oxa^{2-} anion from protonated forms of the cryptate over other dicarboxylate anions

The previous studies demonstrated that the oxa^{2-} is the anion most strongly bound to the protonated species of the copper(II) cryptate, followed by mal^{2-}. However the values listed in Table 5.4 do not give a simple snapshot of what happens when all the studied anions are mixed with the copper(II) cryptate along the pH in aqueous solution. In order to evaluate the competition of the various anions for the receptor a binding diagram was plotted, representing the overall percentages of the associated species as a function of the pH, for equimolar amounts of the studied dicarboxylates and of copper cryptate,[14] see Figure 5.5.

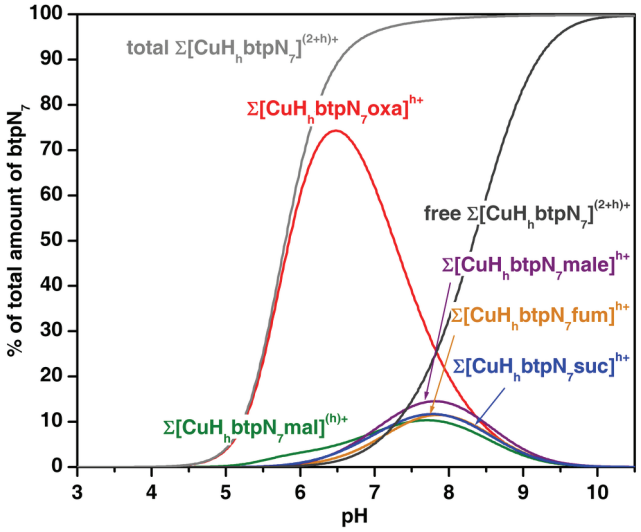

Figure 5.5 Distribution diagram of the overall amounts of supramolecular species formed between $[CuH_hbtpN_7]^{(2+h)+}$ and each dicarboxylate. $C_{btpN_7} = C_{Cu} = C_A/3 = 1.0\times10^{-3}$ mol dm^{-3}.

At pH = 6.2 the copper cryptate receptor clearly prefers oxa^{2-} in the presence of equimolar amounts of all the other studied dicarboxylates, with the $\Sigma[CuH_hbtpN_7(oxa)]^{h+}$ supercryptate representing 88% of the total $\Sigma[CuH_hbtpN_7(A)]^{h+}$ species.

5.3.8 Spectroscopic studies

In order to get further insight on the binding event and on the characteristics of the copper binding site the absorption and EPR spectra of $[CuH_hbtpN_7]^{(2+h)+}$ (Figure 5.6) and $[CuH_hbtpN_7(oxa)]^{h+}$ (Figure 5.7) were recorded in the 6.3-11.4 pH region. The results are summarized in Table 5.5.

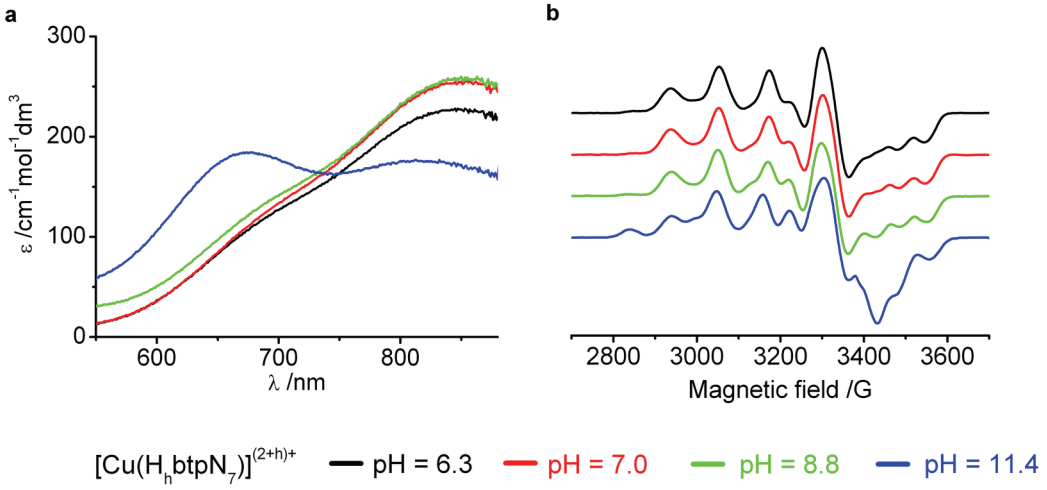

Figure 5.6 Absorption and X-band EPR spectra of $[CuH_hbtpN_7]^{(2+h)+}$ at several pH values. The complexes were prepared at 1.0×10^{-3} mol dm^{-3} in water for the spectrophotometric and at 5.0×10^{-4} mol dm^{-3} in water/ethylene glycol solutions (1:1 vol) for the EPR measurements. The EPR spectra were recorded at a microwave power of 2.0 mW, frequency (n) 9.67 GHz, T=89 K.

The absorption spectra of $[CuH_hbtpN_7]^{(2+h)+}$ at pH values ranging from 6.3 to 8.8 (Figure 5.6a) shows a maximum at 850 nm and a shoulder at 705 nm indicative of trigonal bipyramidal geometry,[15] which can be assigned to the $d_{xy},d_{x^2-y^2} \rightarrow d_{z^2}$ and $d_{xz},d_{yz} \rightarrow d_{z^2}$ transitions, respectively, and agree well with those of copper complexes of tren and other tren derived compounds found in the literature.[16,17] On increasing the pH the higher energy band becomes more intense than the lower energy one, indicating that the geometry distorts from trigonal bipyramidal to a square pyramidal structure due to the formation of $[CubtpN_7(OH)]^+$.[15] Simulation of the EPR spectra (Table 5.5, Figure A5.1 in Appendix) recorded in the 6.3-8.8 pH range indicated three different principal values of g, with $(g_1+g_2)/2 > g_3$ and the lowest value smaller that 2.04 indicative of five-coordinate copper complexes with a geometry intermediate between trigonal

Table 5.5 X-band EPR[a] and absorption spectra[b] data for the Cu^{2+} complexes of $btpN_7$ and respective associations with oxalate.

Complex	pH	Species	g_1	g_2	g_3	A_1	A_2	A_3	R	λ /nm
						$\times 10^4$ cm^{-1}				(ε /$cm^{-1}mol^{-1}dm^3$)
$[CuH_hbtpN_7]^{(2+h)+}$	6.3-8.8	1	2.217	2.153	2.002	124	87	60	2.4	705 (130); 850 (226)
		2	2.248	2.094	2.010	156	12	8	0.5	
	11.4	1	2.219	2.153	1.995	127	85	61	2.4	678 (184); 820 (175)
		2	2.253	2.072	2.013	154	12	1	0.3	
$[CuH_hbtpN_7oxa]^{h+}$	6.3		2.254	2.087	2.032	160	37	17	0.3	674 (103)

[a] All the complexes were prepared at 5.0×10^{-4} mol dm^{-3} in H_2O/ethylene glycol (1:1) and the spectra were recorded at a microwave power of 2.0 mW, frequency (v) 9.67 GHz, T = 89 K. [b] All the complexes were prepared at 1.0×10^{-3} mol dm^{-3} in H_2O.

bipyramidal and square pyramidal geometries.[17] For complexes of this type, a parameter R can be indicative of the predominance of the d_{z^2} or $d_{x^2-y^2}$ orbital in the ground state, R = $(g_2-g_3)/(g_1-g_2)$ with $g_1 > g_2 > g_3$. If R > 1, the greater contribution to the ground state arises from d_{z^2} orbital and the geometry is closer to a trigonal bipyramidal geometry; if R < 1, the greater contribution to the ground state arises from $d_{x^2-y^2}$ orbital and the geometry approaches more a square pyramidal geometry.[18] In the case of the spectra recorded from pH 6.3-8.8 the parameter R has a value of 2.4 in agreement with a trigonal bipyramidal geometry. The hyperfine splitting values are also in the range expected for trigonal bipyramidal complexes.[17] It is also noticeable the presence in small amount of a second species with $g_1 > (g_2 + g_3)/2$, R = 0.5, which should correspond to a distorted square pyramidal geometry. On increasing the pH this second species becomes predominant, in agreement with what was observed in the absorption spectrum upon formation of the $[CubtpN_7(OH)]^+$ species (Figure 5.6b and Figure A5.2 in Appendix).

The absorption spectra of $[CuH_hbtpN_7(oxa)]^{h+}$ at pH = 6.3 and 8.8 (Figure 5.7a) shows a maximum at 674 nm, tailing into the low energy region of the spectrum. This band occurs in the same wavelength as the maximum of the $[CubtpN_7(OH)]^+$ species, suggesting that both species should have approximately the same distorted square pyramidal geometry. Also, it is clear that as the pH increases from 6.3 to 11.4 the spectra resemble more those of the $[CuH_hbtpN_7]^{(2+h)+}$, in agreement with what was observed by potentiometry that the association constants are larger at the triprotonated state of the cryptate and decrease with decreasing protonation of the cryptate. Simulation of the EPR spectrum of $[CuH_hbtpN_7(oxa)]^{h+}$ recorded at pH 6.3 (Table 5.5, Figure A5.3 in Appendix), indicated three different principal values of g, with $g_1 > (g_2 + g_3)/2$ and R = 0.3, corresponding to a geometry closer to a square pyramid. The hyperfine splitting values are also in the range expected for square pyramidal complexes.[16] As in the case of the absorption spectra it is also clear that as the pH increases the spectra resemble more those of the $[CuH_hbtpN_7]^{(2+h)+}$ system (Figure 5.7b), agreeing well with the potentiometric studies.

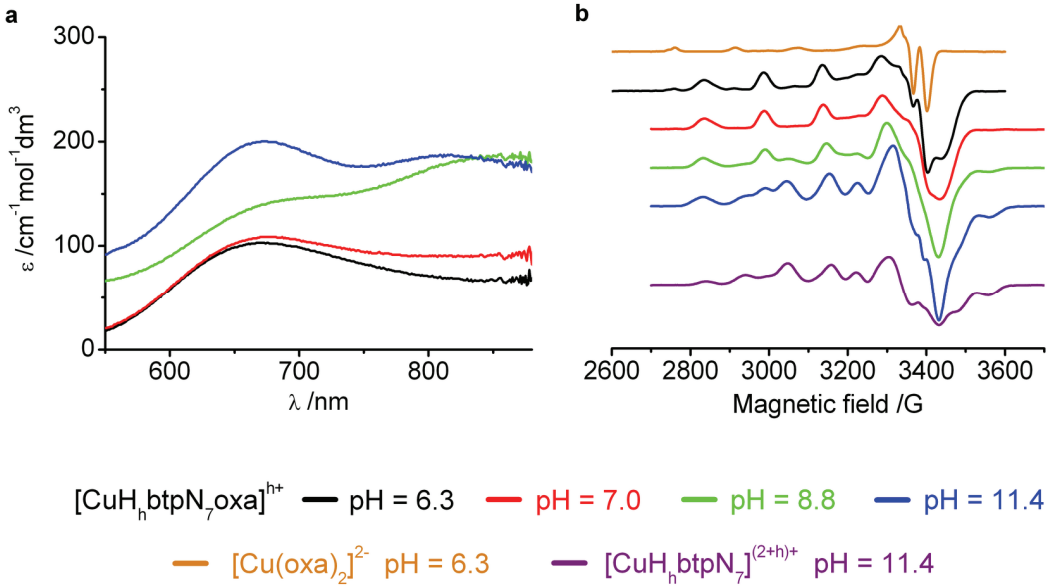

Figure 5.7 Absorption and X-band EPR spectra of $[CuH_hbtpN_7(oxa)]^{h+}$ at several pH values. The complexes were prepared at 1.0×10^{-3} mol dm^{-3} in water for the spectrophotometric and at 5.0×10^{-4} mol dm^{-3} in water/ethylene glycol solutions (1:1 vol) for the EPR measurements. The EPR spectra were recorded at a microwave power of 2.0 mW, frequency (v) 9.67 GHz, *T* = 89 K.

The results of the spectroscopic studies suggest that the binding of oxa^{2-} to the $[CuH_hbtpN_7]^{(2+h)+}$ receptor is accompanied by a rearrangement of the conformation of the copper cryptate such that a change from trigonal bipyramidal to square pyramidal geometry of the copper site occurs. This should happen by increasing the angle N^1–Cu—N^2 until N^1, N^2, N^4 and O are almost coplanar (see Scheme 5.6).

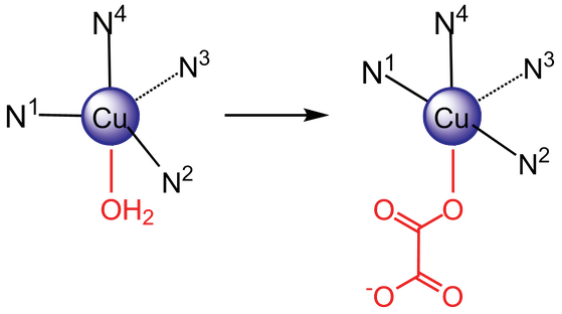

Scheme 5.6 Proposed change of geometry of the copper site upon oxa^{2-} binding.

5.3.9 Indicator-displacement assay

To further reveal the selectivity of the $[CuH_hbtpN_7]^{(2+h)+}$ receptor for the studied dicarboxylate anions, in a qualitative and more visual manner, an indicator-displacement assay was carried out. This method, first introduced in the supramolecular field by Inouye et al.[19] and later popularized by Anslyn et al.,[20] consists on the use of an indicator bound to a receptor by means of non-covalent interactions, which is then displaced from the receptor by a substrate with a high enough binding constant. This displacement induces a drastic change in the optical properties of the released indicator. The adaptation of this methodology to our system is illustrated in Scheme 5.7.

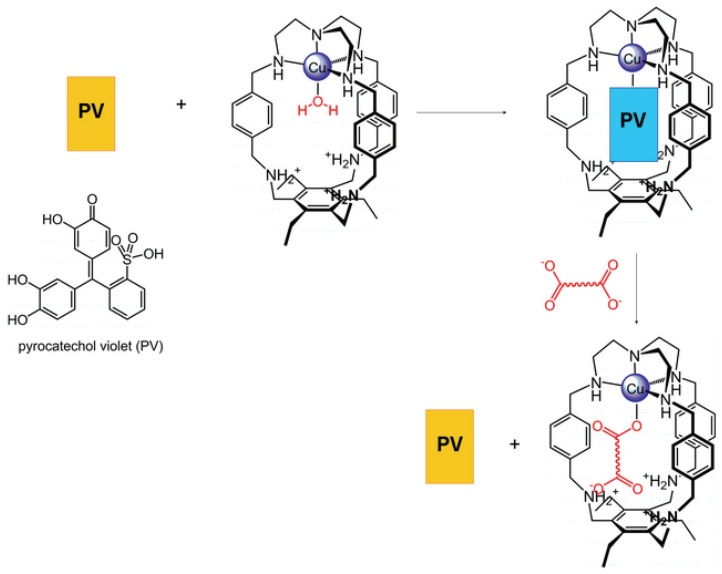

Scheme 5.7 Indicator-displacement assay.

In the current assay, pyrocatechol violet (PV) was used as the indicator. First the spectrum in the visible region of PV was recorded in the presence of $btpN_7$ at pH = 6.2 (Figure 5.8a), showing that the indicator is not affected by the presence $btpN_7$ in the absence of copper(II) and retains its yellow colour. In the concentration used and in the absence of indicator the absortion the copper(II) cryptate in the 350–800 nm region is negligible. Upon addition of copper to a

mixture of PV and $btpN_7$ (Figure 5.8b) at the same pH a drastic change in colour takes place and the solution turns blue due to the formation of $[CuH_hbtpN_7]^{(2+h)+}$-PV complex.

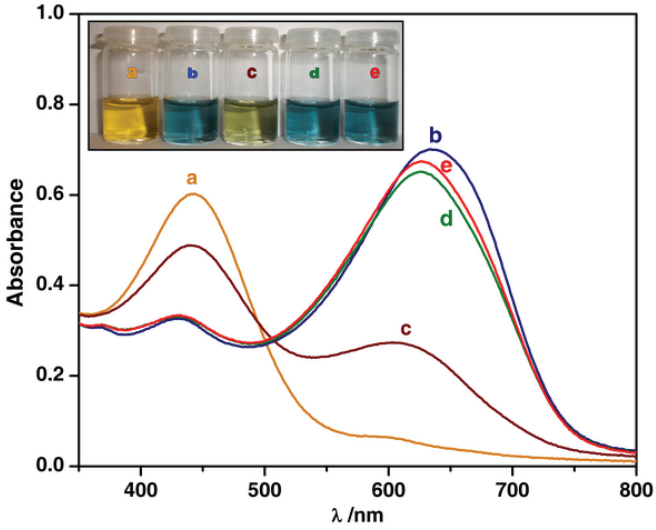

Figure 5.8 Vis absorbance spectra of aqueous solutions of PV in the following conditions: a) $C_{PV} = C_{btpN_7}/2 = 5.0\times10^{-5}$ mol dm^{-3}, b) $C_{PV} = C_{btpN_7}/2 = C_{Cu} = 5.0\times10^{-5}$ mol dm^{-3}, c) $C_{PV} = C_{btpN_7}/2 = C_{Cu} = C_{oxa}/3 = 5.0\times10^{-5}$ mol dm^{-3}, d) $C_{PV} = C_{btpN_7}/2 = C_{Cu} = C_{mal}/3 = 5.0\times10^{-5}$ mol dm^{-3}, e) $C_{PV} = C_{btpN_7}/2 = C_{Cu} = C_{suc}/3 = 5.0\times10^{-5}$ mol dm^{-3}. All spectra recorded at T = (298.2±0.1) K and pH = 6.2.

In Figure 5.8 is clearly shown that only oxalate can displace the indicator from the receptor, yielding a change of colour to green (not yellow because under the conditions used the indicator is not fully displaced), in perfect agreement with the potentiometric studies.

5.4 Conclusions

A new heteroditopic macrobicyclic heptamine compound was prepared in good yield through a new [1+1] “tripod-tripod coupling” strategy using the Schiff-base condensation reaction.

Aqueous solution studies revealed that the values of the association constants of the protonated cryptand, $H_nbtpN_7^{n+}$, with all the studied dicarboxylate anions are very low. These low constants and lack of selectivity of the various

anions for the receptor was attributed to the flexibility and lack of preorganization of the receptor. The copper(II) complex of the tripodal compound, [Cu$tbN_4(H_2O)$], which is related to the part of the cryptand coordinated to the copper(II) centre, exhibited also small binding constants and no selectivity for the series of studied anions. These features emphasize that polyammonium and metal binding sites working independently are unable to provide neither strong interaction nor selectivity.

When the copper(II) complex of $btpN_7$ is the receptor for the same series of dicarboxylate anions much higher association constants are found. In addition, the constants are higher for the tri protonated state of the cryptate and decrease with decreasing protonation of the receptor, which provides evidence of complementary electrostatic and possibly hydrogen bonding interactions. These cooperative effects between coordination to the copper(II) centre, electrostatic and hydrogen bonding interactions are particularly evident when oxa^{2-} is the anionic substrate.

At pH = 6.2 the copper cryptate receptor clearly prefers oxa^{2-} in the presence of equimolar amounts of all the other studied dicarboxylates, suggesting that this dicarboxylate has the ideal size to take full advantage of the potential binding sites of the receptor. The qualitative study provided by the indicator-displacement assay, using pyrocatechol violet as the indicator, is in excellent agreement with the potentiometric studies, demonstrated that the copper cryptate receptor can be used as a selective visual sensor for oxalate. It should be noted that the development of optical oxalate detectors is of great interest in the analysis of food, natural waters and urine, due to its detrimental effects on the human body and its importance in the diagnosis of a number of diseases.[21]

5.5 Experimental

5.5.1 General considerations

All solvents and chemicals were commercially purchased reagent grade quality and used as supplied without further purification, except 1,3,5-tris(aminomethyl)-2,4,6-triethylbenzene and tbN_4 which were prepared according

to literature methods.[22,23] NMR spectra used for characterization of products and binding experiments were recorded on a Bruker Avance 400 instrument. TMS was used as reference for the ^{1}H NMR measurements in $CDCl_3$. Peak assignments are based on peak integration and multiplicity for 1D ^{1}H spectra and on COSY, NOESY and HMQC experiments (See Figures A5-A14 in Appendix). Microanalyses were carried out by the ITQB Microanalytical Service. The absorption spectra were recorded with a UNICAM UV-vis spectrophotometer model UV-4. EPR spectroscopy measurements were recorded with a Bruker ESP 380 spectrometer equipped with continuous-flow cryostat for liquid nitrogen, operating at X-band.

5.5.2 Synthesis

5.5.2.1 Tripodal trialdehyde

A solution of 4-(diethoxymethyl)benzaldehyde (2.320 g, 11.14 mmol) in EtOH (10 cm^3) was added dropwise over 15 minutes to a magnetically stirred solution of tren (536 mg, 3.66 mmol) in EtOH (10 cm^3) at ~5 ºC. The mixture was left under stirring at r.t. during the night. Solid $NaBH_4$ (832 mg, 22.1 mmol) was added in small portions to avoid excessive foaming. After the addition was completed, the mixture was left under stirring at r.t. until the bubbling ceased, and under reflux for 3 hours. The solution was filtered and evaporated under vacuum almost to dryness, then water was added (20 cm^3) and the rest of the ethanol was evaporated. The solution was made strongly basic with 6 mol dm^{-3} KOH (20 cm^3) and extracted with $CHCl_3$ (3 × 50 cm^3). The organic portions were collected and extracted with 6 mol dm^{-3} HCl (20 cm^3). The aqueous phase was separated, washed with $CHCl_3$ (3×50 cm^3) and left under stirring during the night. The solution was then put in an ice bath and 6 mol dm^{-3} KOH (30 cm^3) was slowly added. The solution was extracted with diethyl ether (3 × 50 cm^3), the organic portions were collected in an Erlenmeyer flask, dried over anhydrous sodium sulfate, filtered and evaporated to dryness to give the crude tripodal trialdehyde (1.666 g, 90%) as a pale yellow viscous oil. The product was further purified by column chromatography using CH_2Cl_2/MeOH/NH_3(aq) (90:9:1) as eluent. ^{1}H NMR

(400 MHz, $CDCl_3$, 298 K; TMS) δ=9.90 (3 H, s, *H*C=O), 7.70 (6 H, d, ^3J (H,H) = 8.0 Hz, *H3*/*H5* of *p*-xylyl), 7.36 (6 H, d, *J* = 8.0 Hz, *H2*/*H6* of *p*-xylyl), 3.76 (6 H, s, CH_2*p*-xylyl), 2.63 (6 H, t, ^3J (H,H) = 8.0 Hz, NCH_2CH_2NH), 2.55 (6 H, t, ^3J (H,H) = 8.0 Hz, NCH_2CH_2NH), 2.04 ppm (br s, 3H; N–H); ^{13}C NMR (100 MHz; $CDCl_3$; 298 K; Me_4Si) δ=191.86 (C=O), 147.31 (*C1* of *p*-xylyl), 135.42 (*C4* of *p*-xylyl), 129.90 (*C3*/*C5* of *p*-xylyl), 128.44 (C2/*C6* of *p*-xylyl), 54.02 (NCH_2CH_2NH), 53.63 (CH_2*p*-xylyl), 47.14 ppm (NCH_2CH_2NH).

5.5.2.2 Schiff's base of btpN_7

A solution of 1,3,5-tris(aminomethyl)-2,4,6-triethylbenzene (350 mg, 1.4 mmol) in MeCN (65 cm^3) was added dropwise over 15 minutes to a magnetically stirred solution of the tripodal trialdehyde (700 mg, 1.4 mmol) in MeCN (185 cm^3). The mixture was left under stirring overnight and a white precipitate formed, which was separated by filtration and washed with MeCN (about 100 cm^3) to remove any unreacted starting materials. The precipitate was suspended in $CHCl_3$ (100 cm^3), ultrasonicated for 1 hour and filtered off. Evaporation of the solvent yielded the desired triimine (860 mg, 88%) which was dried under vacuum. ^{1}H NMR (400 MHz, $CDCl_3$, 298 K; TMS) δ=7.22 (s, 3H; *H*C=N), 6.91 (d, ^3J (H,H) = 8.0 Hz, 6H; *H3*/*H5* of *p*-xylyl), 6.85 (d, ^3J (H,H) = 8.0 Hz, 6H; *H2*/*H6* of *p*-xylyl), 4.99 (s, 6H; CH_2bz), 3.76 (s, 6H; CH_2*p*-xylyl), 1.19 (t, ^3J (H,H) = 8.0 Hz, 9H; $bzCH_2CH_3$), 2.84 (t, ^3J (H,H) = 8.0 Hz, 6H; NCH_2CH_2NH), 2.60 (t, ^3J (H,H) = 8.0 Hz, 6H; NCH_2CH_2NH), 2.43 (q, ^3J (H,H) = 8.0 Hz, 6H; $bzCH_2CH_3$), 1.19 ppm (t, ^3J (H,H) = 8.0 Hz, 9H, $bzCH_2CH_3$); ^{13}C NMR (100 MHz; $CDCl_3$; 298 K; Me_4Si) δ=161.5 (*C*=N), 143.9 (*C1*/*C3*/*C5* of bz), 143.3 (*C1* of *p*-xylyl), 134.4 (*C4* of *p*-xylyl), 132.7 (*C2*/*C4*/*C6* of bz), 128.6 (*C3/C5* of *p*-xylyl), 127.1 (*C2*/*C6* of *p*-xylyl), 53.9 (NCH_2CH_2NH), 53.8 (CH_2*p*-xylyl), 51.3 (CH_2bz), 46.4 (NCH_2CH_2NH), 24.0 ($bzCH_2CH_3$), 16.5 ppm ($bzCH_2CH_3$),.

5.5.2.3 btpN_7

Solid $NaBH_4$ (1.200 g, 31.7 mmol) was added in small portions to a magnetically stirred suspension of the triimine (432 mg, 0.54 mmol) in methanol

(100 cm^3). After the addition was completed, the mixture was left under stirring at r.t. for two hours, and under reflux overnight. The solution was evaporated under vacuum almost to dryness, then water (20 cm^3) was added and the entire methanol was evaporated. The solution was made strongly basic with 6 mol dm^{-3} KOH and extracted with $CHCl_3$ (3 × 50 cm^3). The organic portions were collected in an Erlenmeyer flask, dried over anhydrous sodium sulfate, filtered off, evaporated to dryness to give $btpN_7$ (750 mg, 90%) as a white solid. mp 192 ºC (decomp.); ^{1}H NMR (400 MHz, $CDCl_3$, 298 K; TMS) δ=6.81 (d, ^3J (H,H) = 8.0 Hz, 6H; *H3*/*H5* of *p*-xylyl), 6.69 (d, ^3J (H,H) = 8.0 Hz, 6H; *H2*/*H6* of *p*-xylyl), 3.94 (s, 6H; CH_2bz), 3.60 (s, 6H; *p*-xylyl CH_2), 3.37 (s, 6H; CH_2*p*-xylyl), 2.96 (q, ^3J (H,H) = 8.0 Hz, 6H; bzC$H_2$$CH_3$), 2.53 (t, ^3J (H,H) = 5.0 Hz, 6H; NC$H_2$$CH_2$NH), 2.43 (q, ^3J (H,H) = 5.0 Hz, 6H; bzC$H_2$$CH_3$), 1.69 (br s, 3H; N–*H*), 1.23 (br s, 3H; N–*H*), 1.12 ppm (t, ^3J (H,H) = 8.0 Hz, 9H; bzCH_2CH_3); ^{13}C NMR (100 MHz; $CDCl_3$; 298 K; Me_4Si) δ=142.8 (*C1*/*C3*/*C5* of bz), 139.7 (*C1* of *p*-xylyl), 138.9 (*C4* of *p*-xylyl), 133.7 (*C2*/*C4*/*C6* of bz), 128.8 (*C3*/*C5* of *p*-xylyl), 128.4 (*C2*/*C6* of *p*-xylyl), 54.8 (N*C*$H_2$$CH_2$NH), 54.5 (*C*$H_2$*p*-xylyl), 51.6 (*p*-xylyl*C*H_2), 47.9 (NCH_2*C*H_2NH), 45.9 (*C*H_2bz), 22.8 (bz*C*$H_2$$CH_3$), 17.0 ppm (bz$CH_2$*C*$H_3$); ESI–MS (MeOH) m/z: 702.5 $[M+H]^+$; elemental analysis calcd. (%) for $C_{45}H_{63}N_7$: C 77.0, H 9.04, N 13.97; found: C 76.7, H 8.9, N 13.9.

5.5.2.4 Crystals of $[H_7btpN_7(H_2O)(MeOH)Cl_2]Cl_6\cdot(H_3O)\cdot3(H_2O)\cdot3MeOH$

The cryptand $btpN_7$ (4.0 mg, 5.7 μmol) was dissolved in MeOH (200 μL) and 37% HCl (29 μL) was added. Immediately a white precipitate was formed. Water (10 μL) was added and the solution heated until it was clear, then the mixture was allowed to slowly cool to r.t. Single colourless crystals suitable for X-ray crystallographic determination were obtained overnight.

5.5.3 Potentiometric measurements

5.5.3.1 Reagents and solutions

All the solutions were prepared using demineralised water (obtained by a Millipore/Milli-Q system). A stock solution of the receptor was prepared at *ca*.

2.0×10^{-3} mol dm^{-3}. Stock solutions of the dicarboxylic acids (analytical grade) were prepared at about 5.0×10^{-2} mol dm^{-3} and the concentrations were checked by titration with standard 0.100 mol dm^{-3} KOH solutions.

A stock solution of $Cu(NO_3)_2$ (analytical grade) was prepared at about 5.0×10^{-2} mol dm^{-3} and the exact concentration checked by titration with K_2H_2edta following standard methods.[24] Carbonate-free solutions of the KOH titrant were prepared from a Merck ampoule diluted with 1000 cm^{-3} of water (freshly boiled for about 2 h and allowed to cool under nitrogen). These solutions were discarded every time carbonate concentration was about 0.5% of the total amount of base. The titrant solutions were standardized (tested by Gran's method).[25]

5.5.3.2 Equipment and working conditions

The equipment used was described in Chapter 2. The ionic strength of the experimental solutions was kept at 0.10±0.01 mol dm^{-3} with KNO_3, the temperature was maintained at 298.2±0.1 K. Atmospheric CO_2 was excluded from the titration cell during experiments by passing purified nitrogen across the top of the experimental solution.

5.5.3.3 Measurements

The $[H^+]$ of the solutions was determined by the measurement of the electromotive force of the cell, $E = E^{o\prime} + Q \log [H^+] + E_j$. The term pH is defined as $-\log [H^+]$. $E^{o\prime}$, Q, E_j and K_w were determined by titration of a solution of known hydrogen-ion concentration at the same ionic strength, using the acid pH range of the titration. The liquid-junction potential, E_j, was found to be negligible under the experimental conditions used. The value of K_w, the ionic product of water, was determined from data obtained in the alkaline range of the titration, considering $E^{o\prime}$ and Q valid for the entire pH range and found to be equal to $10^{-13.76}$ in our experimental conditions. Before and after each set of titrations the glass electrode was calibrated as a $[H^+]$ probe by titration of 1.000×10^{-3} mol dm^{-3} standard HNO_3 solution with standard KOH. Every measurement was carried out with 0.050 mmol of ligand in a total volume of 40 cm^3. The exact amount of ligand

was obtained by determination of the excess of acid present in a mixture of the ligand and standard 1.4×10^{-2} mol dm^{-3} HNO_3 by titration with standard KOH solution. Copper complexation experiments were performed in the presence $Cu(NO_3)_2$ in 0.5, 1.0 and 2.0 C_{Cu}:C_L ratios. For studies of the association of the protonated forms of $btpN_7$ with the dicarboxylates anions were carried out in the presence of the dicarboxylates in 1.0 and 3.0 C_A:C_{btpN_7} ratios. The ternary systems measurements were carried out in the simultaneous presence of copper(II), ligand and dicarboxylate anions for 1:1:1 and 1:1:3 C_{Cu}:C_L:C_A ratios. Each titration curve consisting typically of one hundred points in the 3.0–10.0 pH range, with a minimum of two replicates undertaken. All the anions were independently titrated, alone and in the presence of copper(II) ion at 1:1 and 2:1 C_{Cu}:C_A ratios. Backtitrations with standard HNO_3 solution were performed to confirm the values of the final $E^{o\prime}$ readings.

5.5.3.4 Calculation of equilibrium constants

Overall protonation constants, β_i^H, of the free ligands and of the studied dicarboxylates, the overall stability constants of complexes, β_{MmHhLl} (M = Cu^{2+} and L = $btpN_7$ or tbN_4 or the studied dicarboxylate anions), and the overall association constants of the complexes of $btpN_7$ or tbN_4 with the dicarboxylates, β_{HhLlAa}, were calculated by fitting the potentiometric data obtained for all the performed titrations in the same experimental conditions with the HYPERQUAD program.[26] The initial computations were obtained in the form of overall stability constants, $\beta_{MmHhLlAa} = [M_mH_hL_lA_a]/[M]^m[H]^h[L]^l[A]^a$. The errors quoted are the standard deviations of the overall stability constants given directly by the program for the input data, which include all the experimental points of all titration curves. The HYSS program[27] was used to calculate the concentration of equilibrium species from the calculated constants from which distribution diagrams were plotted. The species considered in a particular model were those that could be justified by the principles of coordination and supramolecular chemistry.

5.5.4 Absorption and X-band EPR spectra

Solutions of $[CuH_hbtpN_7]^{(2+h)+}$ and $[CuH_hbtpN_7(oxa)]^{h+}$ were prepared in 1.0×10^{-3} mol dm^{-3} concentration and the pH was adjusted to 6.3, 7.0, 8.8 and 11.4 with small additions of either standard KOH or HNO_3 solutions. All absorption spectra were recorded from 350 to 900 nm at T = 298.2±0.1 K. To these solutions ethylene glycol was added in a 1:1 proportion and the EPR spectra recorded at a microwave power of 2.0 mW, frequency (v) 9.67 GHz, T = 89 K. EPR spectra were simulated using SpinCount software, created by Professor M. P. Hendrich at Carnegie Mellon University. SpinCount is available at http://www.chem.cmu.edu/groups/hendrich/.

5.5.5 Indicator-displacement assay

Stock solutions of pyrocatechol violet (1.50×10^{-3} mol dm^{-3}), $btpN_7$ (2.00×10^{-3} mol dm^{-3}) and $Cu(NO_3)_2$ (4.00×10^{-2} mol dm^{-3}) were prepared in aqueous solution. From the stock solutions, other five solutions were prepared having the following concentrations: a) $C_{PV} = C_{btpN_7}/2 = 5.0\times10^{-5}$ mol dm^{-3}, b) $C_{PV} = C_{btpN_7}/2 = C_{Cu} = 5.0\times10^{-5}$ mol dm^{-3}, c) $C_{PV} = C_{btpN_7}/2 = C_{Cu} = C_{oxa}/3 = 5.0\times10^{-5}$ mol dm^{-3}, d) $C_{PV} = C_{btpN_7}/2 = C_{Cu} = C_{mal}/3 = 5.0\times10^{-5}$ mol dm^{-3}, e) $C_{PV} = C_{btpN_7}/2 = C_{Cu} = C_{suc}/3 = 5.0\times10^{-5}$ mol dm^{-3}. The pH of the above solutions was adjusted to 6.2 with small additions of either standard KOH or HNO_3 solutions. All spectra were recorded from 350 to 850 nm at T = 298.2±0.1 K.

5.5.6 Crystallography

Crystal data: $C_{49}H_{97}Cl_8N_7O_8$, Mr = 1212.0; Monoclinic, space group $P2_1/c$, Z=4, a = 23.3117(11), b = 31.4728(15), c = 23.0916(11) Å, β= 117.740(2)º, V= 6337.7(5) $Å^3$, ρ(calc) = 1.251 Mg m^{-3}.

The X-ray data were collected on a CCD Bruker APEX II at 150 (2) K using graphite monochromatized Mo-Kα radiation (λ = 0.71073 Å) with the crystal positioned at 35 mm from the CCD and the spots were measured using a counting time of 60 s. Data reduction and multi-scan absorption correction

effects were carried out using the SAINT-NT software from Bruker AXS. The structure was solved by direct methods and by subsequent difference Fourier syntheses and refined by full matrix least squares on F^2 using the SHELX-97 system programs.[28] One chloride counter ion and the encapsulated methanol molecule (see above) were found disordered over two alternative positions. The methanol atomic positions were included in the structure refinement with refined ocuppancies of 1-*x* and *x*, being *x* equal to 0.31(2). Occupancy factores of two chloride alternative positions were set to 0.88 and 0.12, respectively. Anisotropic thermal parameters were used for all non-hydrogen atoms. The C–H and O–H (methanol solvent molecules) hydrogen atoms were inserted in the structure refinement in calculated positions with isotropic parameters equivalent 1.2 times those of the atom to which they are attached. The hydrogen atoms of the water encapsulated molecule as well as the N–H hydrogen atoms were obtained from the last Fourier Map and they were inserted in the structure refinment with the same thermal constrain used for the other hydrogen atoms. The hydrogen atoms of the remaining water mother liquor molecules as well the O–H of the disordered methanol molecule were not descernible from the last diference Fourier maps and consequentely were not taking into account. 44831 reflections were collected and subsequently merged to 11116 unique reflections with a R_{int} of 0.0336. The final refinement of 717 parameters converged to final *R* indices R_1 = 0.0662 and wR_2 = 0.1887 for 8832 reflections with $I>2\sigma(I)$ and R_1 = 0.0836 and wR_2 =0.2101 for all *hkl* data. Molecular diagrams presented are drawn with PyMOL.[29]

CCDC-809812 contain(s) the supplementary crystallographic data for this paper. These data can be obtained free of charge from The Cambridge Crystallographic Data Centre via www.ccdc.cam.ac.uk/data_request/cif.

5.6 Acknowledgements

The authors acknowledge FCT and POCI, with co-participation of the European Community funds FEDER, for the financial support under project PTDC/QUI/68582/2006. The NMR spectrometers are part of The National NMR

Network (REDE/1517/RMN/2005), supported by "Programa Operacional Ciência e Inovação (POCTI) 2010" and Fundação para a Ciência e a Tecnologia (FCT). We also acknowledge M. C. Almeida for providing elemental analysis and ESI-MS data from the Elemental Analysis and Mass Spectrometry Service at the ITQB and Dr. Filipe de Oliveira for help with the EPR spectra simulations. Pedro Mateus thanks FCT for the grant (SFRH/BD/36159/2007).

5.7 References

[1] J. M. Berg, J. L. Tymoczko, L. Stryer, *Biochemistry*, 5th ed., W. H. Freeman & Co Ltd, New York, **2002**, pp. 465–484.

[2] a) S. N. Yurgel, M. L. Kahn, *FEMS Microbiol. Rev.* **2004**, *28*, 489–501; b) I. G. Janausch, E. Zientz, Q. H. Tran, A. Kröger, G. Unden, *Biochim. Biophys. Acta* **2002**, *1553*, 39–56.

[3] R. Hyde, P. M. Taylor, H. S. Hundal, *Biochem. J.* **2003**, *373*, 1–18.

[4] D. H. Williams, B. Bardsley, *Angew. Chem. Int. Ed.* **1999**, *38*, 1172–1193.

[5] a) *Supramolecular Chemistry of Anions*, Eds.: A. Bianchi, K. Bowman-James, E. Garcia-España, Pergamon, Oxford, Wiley-VCH, New York, **1997**; b) R. J. Fitzmaurice, G. M. Kyne, D. Douheret, J. D. Kilburn, *J. Chem. Soc., Perkin Trans.* **2002**, *1*, 841–864; c) P. A. Gale, R. Quesada, *Coord. Chem. Rev.* 250 **2006**, *250*, 3219–3244; d) P. A. Gale, S. E. García-Garrido, J. Garric, *Chem. Soc. Rev.* **2008**, *37*, 151–190; e) C. Caltagirone, P. A. Gale, *Chem. Soc. Rev.* **2009**, *38*, 520–563; f) P. A. Gale, *Chem. Soc. Rev*. **2010**, *39*, 3746–3771.

[6] a) E. García-España, P. Díaz, J. M. Llinares, A. Bianchi, *Coord. Chem. Rev.* **2006**, *250*, 2952–2986; b) S. Kubik, C. Reyheller, S. Stüwe, *J. Inclusion Phenom. Macrocyclic Chem.* **2005**, *52*, 137–187.

[7] a) B. Dietrich, M. W. Hosseini, J.-M. Lehn, R. B. Sessions, *J. Am. Chem. Soc.* **1981**, *103*, 1282–1283; b) E. Kimura, A. Sakonaka, T. Yatsunami, M. Kodama, *J. Am. Chem. Soc.* **1981**, *103*, 3041–3045; c) M. W. Hosseini, J.-M. Lehn, *J. Am. Chem. Soc.* **1982**, *104*, 3525–3527; d) B. Dietrich, J. Guilhem, J.-M. Lehn, C. Pascard, E. Sonveaux, *Helv. Chim. Acta* **1984**, *67*, 91–104; e) M. W. Hosseini, J.-M. Lehn, *Helv. Chim. Acta* **1986**, *69*, 587–603; f) J.-M. Lehn, R. Meric, J.-P. Vigneron, B. Waksman, C. Pascard, *J. Chem. Soc., Chem. Commun.* **1991**, 62–64; g) A. Bencini, A. Bianchi, M. I. Burguete, E. García-España, S. V. Luis, J. A. Ramirez, *J. Am. Chem. Soc.* **1992**, *114*, 1919–1920; h) A. Bencini, A. Bianchi, M. I. Burguete, P. Dapporto, A. Dorménech, E. García-España, S. V. Luis, P. Paoli, J. A. Ramirez, *J. Chem. Soc., Perkin Trans.* **1994**, *2*, 569–577; i) Q. Lu, R. J. Motekaitis, J. J. Reibenspies, A. E. Martell, *Inorg. Chem*. **1995**, *34*, 4958–4964; j) M.-P. Teulade-Fichou, J.-P. Vigneron, J.-M. Lehn, *J. Chem. Soc., Perkin Trans.* **1996**, *2*, 2169–2175; k) T. Paris, J.-P. Vigneron, J.-M. Lehn, *J. Inclusion Phenom. Macrocyclic Chem.* **1999**, *33*, 191–202; l) I. Alfonso, B. Dietrich, F. Rebolledo, V. Gotor, J.-M. Lehn, *Helv. Chim. Acta* **2001**, *84*, 280–295; m) C. Miranda, F. Escartí, L. Lamarque, M. J. R. Yunta, P. Navarro, E. García-España, M. L. Jimeno, *J. Am. Chem. Soc.* **2004**, *126*, 823–833; n) C. Anda, A. Llobet, A. E. Martell, J. Reibenspies, E. Berni, X. Solans, *Inorg. Chem.* **2004**, *43*, 2793–2802; o) J. Nelson, M. Nieuwenhuyzen, I. Pál, R. M. Town, *Dalton Trans.* **2004**, 229–235; p) C. Bazzicalupi, A. Bencini, A. Bianchi, L. Borsari, C. Giorgi, B. Valtancoli, *J. Org. Chem.* **2005**, *70*, 4257–4266; q) S. Carvalho, R. Delgado, N.

Fonseca, V. Félix, *New J. Chem.* **2006**, *30*, 247–257; r) A. Arbuse, C. Anda, M. A. Martínez, J. Pérez-Mirón, C. Jaime, T. Parella, A. Llobet, *Inorg. Chem.* **2007**, *46*, 10632–10638; s) C. Cruz, R. Delgado, M. G. B. Drew, V. Félix, *J. Org. Chem.* **2007**, *72*, 4023–4034; t) C. Bazzicalupi, A. Bencini, A. Bianchi, C. Borri, A. Danesi, E. García-España, C. Giorgi, B. Valtancoli, *J. Org. Chem.* **2008**, *73*, 8286–8295; u) A. González-Álvarez, I. Alfonso, P. Díaz, E. García-España, V. Gotor-Fernández, V. Gotor, *J. Org. Chem.* **2008**, *73*, 374–382; v) S. Carvalho, R. Delgado, M. G. B. Drew, V. Calisto, V. Félix, *Tetrahedron* **2008**, *64*, 5392–5403; w) C. Cruz, V. Calisto, R. Delgado, V. Félix, *Chem. Eur. J.* **2009**, *15*, 3277– 3289, x) S. Carvalho, R. Delgado, V. Félix, *Tetrahedron* **2010**, *66*, 8714–8721.

[8] a) A. E. Martell, R. J. Motekaitis*, J. Am. Chem. Soc.* **1988**, *110*, 8059–8064; b) R. J. Motekaitis, A. E. Martell*, Inorg. Chem.* **1991**, *30*, 694–700; c) Q. Lu, J. J. Reibenspies, A. E. Martell, R. J. Motekaitis, *Inorg. Chem.* **1996**, *35*, 2630–2636; d) C. Bazzicalupi, A. Bencini, A. Bianchi, V. Fusi, E. García-España, C. Giorgi, J. M. Llinares, J. A. Ramirez, B. Valtancoli, *Inorg. Chem.* **1999**, *38*, 620–621; e) L. Fabbrizzi, A. Leone, A. Taglietti, *Angew. Chem. Int. Ed.* **2001**, *40*, 3066–3069; f) N. Marcotte, A. Taglietti, *Supramol. Chem.* **2003**, *15*, 617–625; g) S. Carvalho, C. Cruz, R. Delgado, M. G. B. Drew, V. Félix, *Dalton Trans.* **2003**, 4261–4270; h) M. Boiocchi, M. Bonizzoni, L. Fabbrizzi, G. Piovani, A. Taglietti, *Angew. Chem. Int. Ed.* **2004**, *43*, 3847–3852; i) M. Bonizzoni, L. Fabbrizzi, G. Piovani, A. Taglietti, *Tetrahedron* **2004**, *60*, 11159–11162; j) F. Li, R. Delgado, V. Félix, *Eur. J. Inorg. Chem.* **2005**, 4550–4561; k) B. Verdejo, J. Aguilar, A. Doménech, C. Miranda, P. Navarro, H. R. Jiménez, C. Soriano, E. García-España, *Chem. Commun.* **2005**, 3086–3088; l) L. Fabbrizzi, F. Foti, A. Taglietti, *Org. Lett.* **2005**, *7*, 2603–2606; m) M. Boiocchi, M. Bonizzoni, A. Moletti, D. Pasini, A. Taglietti, *New J. Chem.* **2007**, *31*, 352–356; n) S. Carvalho, R. Delgado, M. G. B. Drew, V. Félix, M. Figueira, R. T. Henriques, *Polyhedron* **2008**, *27*, 679–687.

[9] a) H. Aït-Haddou, S. L. Wiskur, V. M. Lynch, E. V. Anslyn, *J. Am. Chem. Soc.* **2001**, *123*, 11296–11297; b) L. A. Cabell, M. D. Best, J. J. Lavigne, S. E. Schneider, D. M. Perreault, M.-K. Monahan, E. V. Anslyn, *J. Chem. Soc., Perkin Trans. 2* **2001**, 315–323; c) Z. Zhong, E. V. Anslyn, *Angew. Chem. Int. Ed*. **2003**, *42*, 3005–3008; d) M. D. Best, E. V. Anslyn, *Chem. Eur. J.* **2003**, *9*, 51–57; e) S. L. Tobey, E. V. Anslyn, *J. Am. Chem. Soc.* **2003**, *125*, 10963–10970; f) A. D. Hughes, E. V. Anslyn, *Proc. Natl. Acad. Sci. U. S. A.* **2007**, *104*, 6538–6543.

[10] D. Heyer, J.-M. Lehn, *Tetrahedron Lett.* **1986**, *27*, 5869–5872.

[11] C. A. Ilioudis, D. A. Tocher, J. W. Steed, *J. Am. Chem. Soc.* **2004**, *126*, 12395–12402.

[12] a) S. S. Flack, J.-L. Chaumette, J. D. Kilburn, G. J. Langley and M. Webster, *J. Chem. Soc., Chem. Commun.* **1993**, 399–401; M. J. Deetz, M. Shang, B. D. Smith, *J. Am. Chem. Soc.* **2000**, *122*, 6201–6207; b) J. M. Mahoney, A. M. Beatty, B. D. Smith, *J. Am. Chem. Soc.* **2001**, *123*, 5847–5848; J. M. Mahoney, R. A. Marshall, A. M. Beatty, B. D. Smith, S. Camiolo, P. A. Gale, *J. Supramol. Chem.* **2001**, *1*, 289–292; C. Suksai, P. Leeladee, D. Jainuknan, T. Tuntulani, N. Muangsin, O. Chailapakul, P. Kongsaeree, C. Pakavatchai, *Tetrahedron Lett.* **2005**, *46*, 2765–2769.

[13] B. Dietrich, M. W. Hosseini, J.-M. Lehn, R. B. Sessions, *Helv. Chim. Acta.* **1985**, *68*, 289–299.

[14] a) A. Bianchi, E. García-España, *J. Chem. Educ.* **1999**, *76*, 1727–1732; b) P. Mateus, N. Bernier, R. Delgado, *Coord. Chem. Rev.* **2010**, *254*, 1726–1747.

[15] M. Duggan, N. Ray, B. Hathaway, G. Tomlinson, P. Brint, K. Pelin *J. Chem. Soc., Dalton Trans.* **1972**, 1342–1199.

[16] F. Thaler, C. D. Hubbard, F. W. Heinemann, R. van Eldik, S. Schindler, I. Fábián, A. M. Dittler-Klingemann, F. E. Hahn, C. Orvig, *Inorg. Chem.* **1998**, *37*, 4022–4029.
[17] A. Bencini, I. Bertini, D. Gatteschi, A. Scozzafava, *Inorg. Chem.* **1978**, *17*, 3194–3197.
[18] B. J. Hathaway, *J. Chem. Soc., Dalton Trans.***1972**, 1196–1199.
[19] M. Inouye, K. Hashimoto, K. J. Isagawa, *J. Am. Chem. Soc.* **1994**, *116*, 5517–5518.
[20] S. L. Wiskur, H. Ait-Haddou, J. J. Lavigne, E. V. Anslyn, *Acc. Chem. Res.* **2001**, *34*, 963–972.
[21] a) F. Wu, Z. He, Q. Luo, Y. Zeng, *Food Chem*. **1999**, *65*, 543–546; b) F. Hong, N.-O. Nilvebrant, L. J. Jönsson, *Biosens. Bioelectron.* **2003**, *18*, 1173–1181; c) A. Kazemzadeh, F. Moztarzadeh, *Sens. Actuators B* **2005**, *106*, 832–836; d) S. Milardović, I. Kereković, M. Nodilo, *Talanta* **2008**, *77*, 222–228.
[22] K. J. Wallace, R. Hanes, E. V. Anslyn, J. Morey, K. V. Kilway, J. Siegel, *Synthesis* **2005**, 2080–2083.
[23] J. P. Collman, L. Fu, P. C. Herrmann, Z. Wang, M. Rapta, M. Bröring, R. Schwenninger, B. Boitrel, *Angew. Chem. Int. Ed.* **1998**, *37*, 3397–3400.
[24] G. Schwarzenbach, W. Flaschka, *Complexometric Titrations*, Methuen & Co, London, **1969**, pages 252–258.
[25] F. J. Rossotti, H. J. Rossotti, *J. Chem. Educ.* **1965**, *42*, 375–378.
[26] P. Gans, A. Sabatini, A. Vacca, *Talanta* **1996**, *43*, 1739–1753.
[27] L. Alderighi, P. Gans, A. Ienco, D. Peters, A. Sabatini, A. Vacca, *Coord. Chem. Rev.* **1999**, *184*, 311–318.
[28] G. M. Sheldrick, *Acta Cryst.* A **2008**, *64*, 112–122.
[29] W. L. DeLano, The PyMOL Molecular Graphics System 2002 on World Wide Web http://www.pymol.org.

Chapter 6

Thermodynamics and structural aspects of dicarboxylate binding by two polyaza macrobicyclic receptors

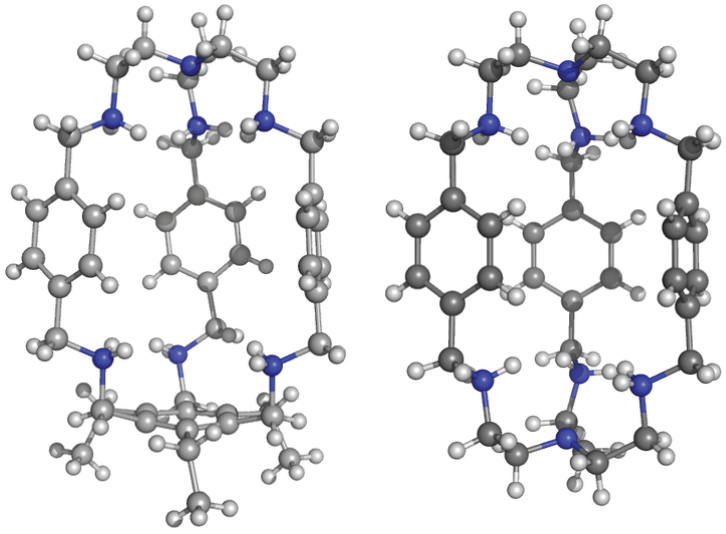

Work featured in: P. Mateus, R. Delgado, P. Brandão, V. Félix, *preliminary manuscript.*

6.1 Summary

In the present work, two ditopic polyamine macrobicyclic compounds have been studied as receptors for the recognition of dicarboxylate anions of varying chain length in aqueous solution. One of the receptors consists of two tris(2-aminoethyl)amine derived binding subunits separated by *p*-xylyl spacers while the other is a heteroditopic compound, combining two different head units, a tren derived and a 2,4,6-triethylbenzene derived one, also separated by *p*-xylyl spacers. Comparison between the binding behaviour of these two compounds showed the effect of the increased rigidity and lipophilicity of the receptor in the binding properties and the selectivity pattern. The acid-base behaviour of the compounds as well as their binding ability with oxalate (oxa^{2-}), malonate (mal^{2-}), succinate (suc^{2-}), glutarate (glu^{2-}), maleate ($male^{2-}$) and fumarate (fum^{2-}) were studied by potentiometry at 298.2 K in aqueous solution and at ionic strength 0.10 mol dm^{-3} in KTsO. NMR studies were also performed to obtain structural information in solution on the supermolecules formed by association of the cryptands with the dicarboxylate substrates. The results revealed that both compounds are able to form stable associations with the dianionic substrates in competitive aqueous solution, with unprecedent selectivity for fumarate over its *cis* isomer maleate. In addition it was found that although the selectivity pattern is unaffected by the introduction of 2,4,6-triethylbenzene head unit, the affinity towards dicarboxylates is significantly reduced.

6.2 Introduction

The design of new synthetic receptors for carboxylate anions has interested supramolecular chemists since the early days of this relatively young field of research.[1] Indeed, the carboxylate functionality is part of a wide range of biologically and environmentally active entities, in many cases accounting for their chemical and biological properties.[2] For instance, the transport of dicarboxylate anions across biological membranes is crucial in the metabolism of eukaryotic cells,[3] the sensing and signalling of amino acids is important in a number of cell functions[4] and the mechanism of action of the vancomycin

antibiotics depends on carboxylate binding.[5] On the other hand, release of carboxylates in the atmosphere from motor exhausts and wood burning has been affecting global climate by producing cloud condensation nuclei and contributing to acid rain.[6] Carboxylate binding by synthetic receptors can thus contribute to significant advances in biomedical and environmental sciences.

In order to be suitable for real-life applications, as for instance sensing and quantification of biologically active carboxylates in clinical laboratories or environmental monitoring and/or removal of pollutants, synthetic receptors need to be able to perform in water.[7] However, due to the high dielectric constant and good hydrogen bond donor and acceptor capabilities, water is the most challenging medium in anion recognition.

Among the most successful groups of receptors for the binding of carboxylate anions in aqueous medium are the polyamine compounds, as they can be protonated to provide the necessary positive charge to interact with the substrates and to impart water solubility. Thus amino groups have been incorporated in a variety of different topologies, from linear structures to mono- and polycyclic architectures and studied as receptors of carboxylates and other anions.[8]

The ability of tris(2-aminoethyl)amine (tren) derived polyammonium cryptands to strongly bind anions in aqueous media by combining electrostatic and hydrogen bonding interactions has been explored since the beginning of anion recognition as a research field.[8e,9] It was shown in Chapters 2 and 3 that 2,4,6-triethylbenzene derived polyammonium macrobicycles have also interesting anion binding properties. However, examples of carboxylate binding by polyammonium cryptands have only seldom been reported,[10] even though the ditopic nature of these compounds is expected to make them suitable for the recognition of two carboxylate groups separated by alkyl chains (Scheme 6.1).

In the present work, the binding properties of the protonated forms of two closely related polyamine cryptands (Scheme 6.2), $btpN_7$ and t_2pN_8 (cryptand **14** in Scheme 1.17, Chapter 1), towards dicarboxylate substrates were studied in aqueous solution. This study is intended to shed light on the effect of

replacement of a tren by a 2,4,6-triethylbenzene head unit of the receptor, corresponding to an increased rigidity and lipophilicity, in the binding properties and selectivity pattern of dicarboxylate anions.

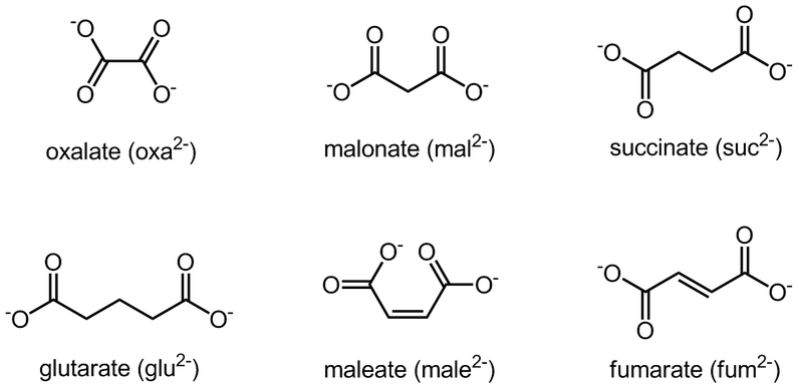

Scheme 6.1 Target dicarboxylate substrates.

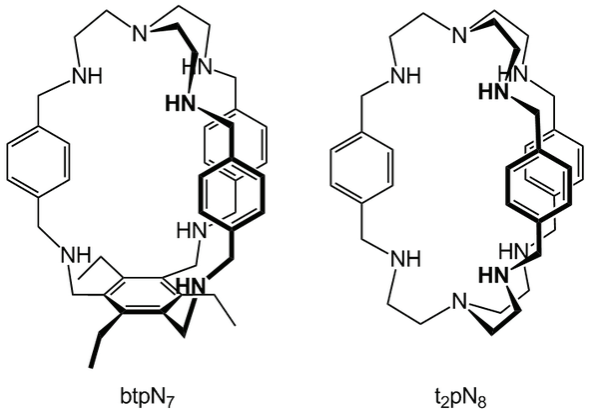

Scheme 6.2 Macrobicyclic compounds studied in this work.

6.3 Results and Discussion

6.3.1 Potentiometric studies

6.3.1.1 Acid-base behaviour of the cryptands

The protonation constants of $btpN_7$ and t_2pN_8 were determined by potentiometry in aqueous solution at 298.2 K and ionic strength 0.10 mol dm^{-3} in KTsO. The results are collected in Table 6.1 and the corresponding species distribution diagrams represented in Figure 6.1.

Table 6.1 Overall (β_i^H) and stepwise protonation (K_i^H) constants of $btpN_7$ and t_2pN_8 in H_2O.[a]

Equilibrium	log β_i^{H} [b]		Equilibrium	log K_i^H	
	$btpN_7$	t_2pN_8		$btpN_7$	t_2pN_8
$L + H^+ \rightleftharpoons HL^+$	8.99(1)	9.20(1)	$L + H^+ \rightleftharpoons HL^+$	8.99	9.20
$L + 2\,H^+ \rightleftharpoons H_2L^{2+}$	17.58(1)	18.16(1)	$HL^+ + H^+ \rightleftharpoons H_2L^{2+}$	8.59	8.96
$L + 3\,H^+ \rightleftharpoons H_3L^{3+}$	25.15(1)	25.93(1)	$H_2L^{2+} + H^+ \rightleftharpoons H_3L^{3+}$	7.57	7.77
$L + 4\,H^+ \rightleftharpoons H_4L^{4+}$	31.70(1)	33.13(1)	$H_3L^{3+} + H^+ \rightleftharpoons H_4L^{4+}$	6.55	7.20
$L + 5\,H^+ \rightleftharpoons H_5L^{5+}$	37.60(1)	38.37(1)	$H_4L^{4+} + H^+ \rightleftharpoons H_5L^{5+}$	5.90	5.24
$L + 6\,H^+ \rightleftharpoons H_6L^{6+}$	42.88(1)	43.49(1)	$H_5L^{5+} + H^+ \rightleftharpoons H_6L^{6+}$	5.27	5.12

[a] T = (298.2±0.1) K; I = (0.10±0.01) mol dm^{-3} in KTsO. [b] Values in parenthesis are standard deviations in the last significant figures.

The bulky potassium tosylate (KTsO) was chosen as supporting electrolyte based on the assumption that it does not appreciably interact with the receptors (see Chapters 2 and 3) Indeed, it was found that using KBr or KNO_3 (Table A6.1 in Appendix) as supporting electrolyte increased the protonation constants of $btpN_7$ relative to those determined in KTsO, specially the lower constants, indicative of stronger association with Br^- and NO_3^- than with TsO^-. In addition, a crystal structure of $[H_6t_2pN_8(H_2O)_3]\cdot(TsO)_6\cdot 4H_2O$ shows the tosylate counter-ion outside of the receptor cavity.[11]

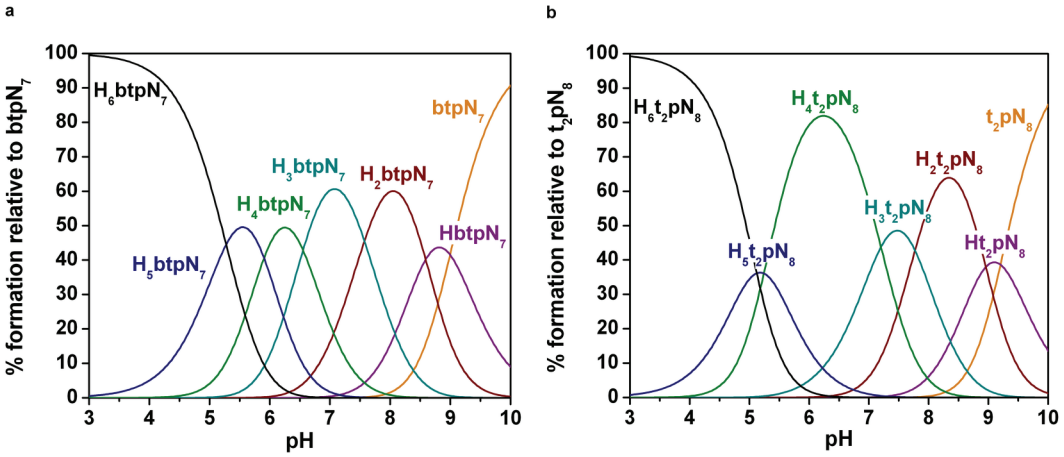

Figure 6.1 Species distribution diagram of the protonation of $btpN_7$ (a) and t_2pN_8 (b). $C_{btpN_7} = C_{t_2pN_8} = 1.0\times10^{-3}$ mol dm^{-3}. Charges were ommited.

Six protonation constants were found for both compounds in the working pH region (3.0–10.0), corresponding to the successive protonations of the secondary amines. The stepwise values decrease with increasing protonation state of the receptors due to both increasing electrostatic repulsion between positive charges and to statistical factors. The protonation constant of the tertiary amine of the tren derived head unit of $btpN_7$, as well as the protonation of both tertiary amines of t_2pN_8, are not obtained in the studied pH region, which should be very acidic due to the accumulation of positive charges within the receptors cavities. The constants have similar magnitude in pairs, as they correspond to protonation of amine centres at alternating positions in the macrobicyclic backbone, far from each other, and therefore the difference in values for each pair are mainly due to statistical factors. This behaviour is clearer in t_2pN_8 than in $btpN_7$ because the secondary amines in the 1,3,5-tris(aminomethyl)-2,4,6-triethylbenzene subunit have lower basicity than those of the tris(2-aminoethyl)amine part, due to the electron withdrawing effect of the nearby benzene ring. Nonetheless, the overall basicity of these two compounds is quite similar and, as the corresponding distribution curve diagrams show (Figure 6.1), the hexaprotonated forms of $btpN_7$ and t_2pN_8, exist as the main species at pH values lower than 5.0.

6.3.1.2 Binding affinity of the protonated forms of $btpN_7$ and t_2pN_8 towards dicarboxylates

The association constants of the protonated forms of $btpN_7$ and t_2pN_8 with several dicarboxylate anions differing in chain length were determined by potentiometry in aqueous solution at 298.2 K and 0.10 mol dm^{-3} KTsO. The values were collected in Table 6.2. The protonation constants of the dicarboxylates were also determined in the same experimental conditions and used in the calculations (Table A6.2 in Appendix).

Only species of 1:1 receptor to anion stoichiometry were found for the different protonation states of both compounds. The highest values found correspond to the association of the hexaprotonated receptors with the fully ionized dicarboxylates, with the exception of maleate. The latter anion has a

Table 6.2 Stepwise association constants (log $K_{H_hL_lA_a}$) of $H_nbtpN_7^{n+}$ and $H_nt_2pN_8^{n+}$ receptors with oxa^{2-}, mal^{2-}, suc^{2-}, glu^{2-}, $male^{2-}$ and fum^{2-} anions in H_2O.[a],[b],[c]

Equilibrium[d]	oxa^{2-}	mal^{2-}	suc^{2-}	glu^{2-}	$male^{2-}$	fum^{2-}
			$btpN_7$			
$H_6L^{6+} + HA^- \rightleftharpoons H_7LA^{5+}$	2.37(2)	2.25(2)	–	–	1.89(3)	2.60(4)
$H_6L^{6+} + A^{2-} \rightleftharpoons H_6LA^{4+}$	4.04(1)	3.66(1)	3.08(1)	2.57(1)	–	3.89(1)
$H_5L^{5+} + HA^- \rightleftharpoons H_6LA^{4+}$	–	–	–	–	2.97(2)	–
$H_5L^{5+} + A^{2-} \rightleftharpoons H_5LA^{3+}$	2.89(1)	2.64(2)	2.04(3)	2.11(2)	2.79(1)	2.85(3)
$H_4L^{4+} + A^{2-} \rightleftharpoons H_4LA^{2+}$	–	2.18(3)	1.87(3)	1.92(3)	–	2.17(6)
			t_2pN_8			
$H_6L^{6+} + HA^- \rightleftharpoons H_7LA^{5+}$	4.77(2)	3.52(2)	3.35(1)	2.99(2)	3.50(2)	–
$H_6L^{6+} + A^{2-} \rightleftharpoons H_6LA^{4+}$	6.21(1)	5.35(1)	4.63(1)	3.85(1)	–	6.06(1)
$H_5L^{5+} + HA^- \rightleftharpoons H_6LA^{4+}$	–	–	–	–	4.44(2)	–
$H_5L^{5+} + A^{2-} \rightleftharpoons H_5LA^{3+}$	3.77(6)	3.83(2)	3.45(2)	3.25(2)	–	4.02(3)
$H_4L^{4+} + HA^- \rightleftharpoons H_5LA^{3+}$	–	–	–	–	3.40(2)	–
$H_4L^{4+} + A^{2-} \rightleftharpoons H_4LA^{2+}$	2.45(3)	2.68(1)	2.68(1)	2.67(2)	2.81(1)	2.73(2)
$H_3L^{3+} + A^{2-} \rightleftharpoons H_3LA^{+}$	2.18(3)	2.39(2)	2.33(2)	2.28(3)	2.53(2)	2.44(3)
$H_2L^{2+} + A^{2-} \rightleftharpoons H_2LA$	–	1.60(5)	1.69(4)	1.65(7)	1.87(3)	1.72(6)

[a] T = (298.2±0.1) K; I = (0.10±0.01) mol dm^{-3} in KTsO. [b] Values in parenthesis are standard deviations in the last significant figures. [c] Values of the overall association constants are presented in Table A6.3 in Appendix. [d] A^{2-} denote in general the dicarboxylate anion and L the $btpN_7$ or the t_2pN_8 compounds.

higher first protonation constant and so does not exist in the fully deprotonated form in the pH region where both receptors are hexaprotonated. It was also found that the association constants decrease with decreasing protonation of the receptors and with increasing protonation of the substrates, clearly showing that electrostatic and hydrogen bonding interactions play a significant role in the binding process.

The $H_nt_2pN_8^{n+}$ receptor binds all substrates with higher association constants than $H_nbtpN_7^{n+}$. Because of differences in basicity of $btpN_7$ and t_2pN_8 direct comparison of stepwise constants of both receptors with each anion can lead to erroneous conclusions. Likewise, the differences in basicity of the studied dicarboxylates can give rise to incorrect selectivity attributions, especially when there are overlapping protonation equilibria between receptors and anions. The K_{eff} values, defined as the quotient between the total amount of supramolecular

species formed and the total amounts of the free receptor and free substrate at a given pH (K_{eff} = $\Sigma[H_{i+j}AL]/\Sigma[H_iA]\ \Sigma[H_jL]$, L is the ligand and A the anion),[12] not only allow comparisons between different supramolecular systems studied under the same experimental conditions as it takes into consideration the different basicities of receptors and substrates, but also makes it possible to distinguish the stepwise equilibria that effectively occur from all those that can be established for each case. In Figure 6.2 the plots of the effective association constant K_{eff} *versus* pH for the supramolecular associations between the protonated forms of $btpN_7$ and t_2pN_8 and the studied dicarboxylates are shown.

From these plots is clear that $H_nt_2pN_8^{n+}$ binds all the dicarboxylate anions significantly stronger than $H_nbtpN_7^{n+}$, a result which was somewhat unexpected given the structural and basicity similarities of both compounds. However at pH ≈ 4.5, where maximum interaction of both compounds with the substrates occur, the sequence of binding preference is the same (oxa^{2-} > fum^{2-} > mal^{2-} > $male^{2-}$ > suc^{2-} > glu^{2-}).

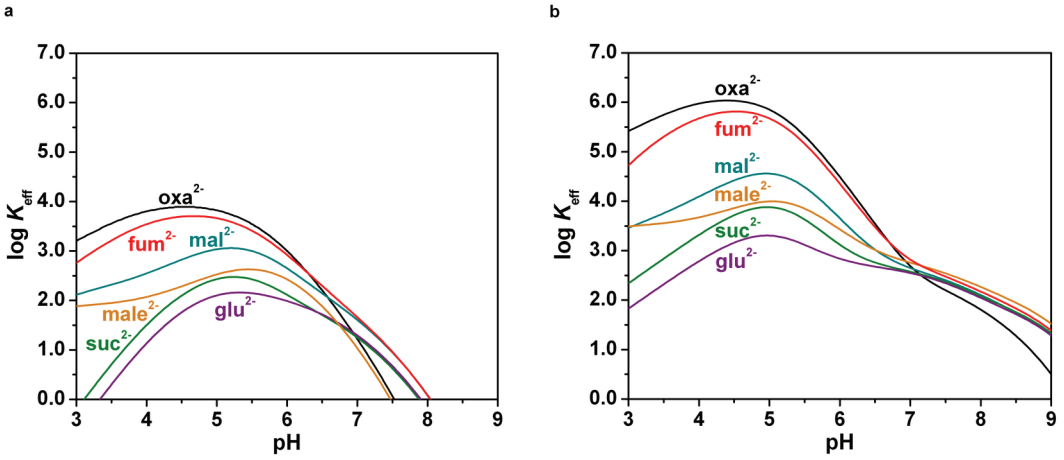

Figure 6.2 Plots of the log K_{eff} *versus* pH for the associations formed between the indicated dicarboxylate anions and $H_nbtpN_7^{n+}$ (a) or $H_nt_2pN_8^{n+}$ (b).

Indeed, the competitive binding diagrams[13] plotted for the association of each compound with the studied dicarboxylates (Figure 6.3), show that their selectivity pattern is practically identical. Thus it seems that the much higher

affinity of $H_nt_2pN_8^{n+}$ towards dicarboxylates relative to $H_nbtpN_7^{n+}$ is not translating into higher selectivity when all the studied anion are considered.

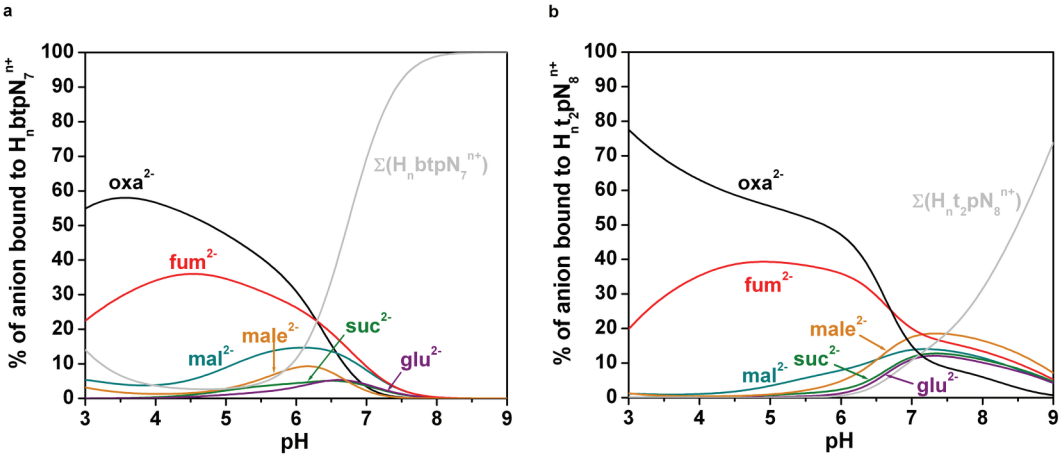

Figure 6.3 Distribution diagrams of the overall amounts of supramolecular species formed between the dicarboxylate anions and $H_nbtpN_7^{n+}$ (a) or $H_nt_2pN_8^{n+}$ (b) in equimolar ratio. $C_{btpN_7} = C_{t_2pN_8} = C_A/3 = 1.0\times10^{-3}$ mol dm^{-3}. For simplicity the amount of associated species with each anion, $[H_nLA]^{(n-2)+}$, is identified in the diagrams only by the formula of the anions, oxa^{2-}, mal^{2-}, suc^{2-}, glu^{2-}, $male^{2-}$ and fum^{2-}, respectively.

In both cases, oxa^{2-} and fum^{2-} display higher association constants than the rest of the substrates. Due to the small size of oxalate it seems unlikely that it can take advantage of the ditopic nature of the receptors, thus its higher association constant is probably due to binding of both carboxylate groups to one of the head units, in addition to its higher charge density that should also contribute to a stronger electrostatic interaction. The higher association constant of fumarate on the other hand points to a better fit into the cavities in addition to its higher rigidity when compared to the other substrates. This is especially evident comparing fumarate and succinate behaviour. Although both carboxylates have about the same size being succinate more flexible, the binding of the latter is much weaker, the K_{eff} value at pH 4.5 is 1.65 log units lower in the case of its association with $H_nbtpN_7^{n+}$ and 1.79 log units lower in the case of $H_nt_2pN_8^{n+}$. In addition, π–π interactions between the *p*-xylyl spacers of the receptors and the C=C bond of fumarate may also contribute to the enhanced affinity. Both receptors show the lowest affinity towards glutarate, most likely because this is the longest and most

flexible of the studied dicarboxylates. Interestingly, the K_{eff} value at pH 4.5 for the association of glutarate with $H_nt_2pN_8^{n+}$ is still quite significant (3.16 log units).

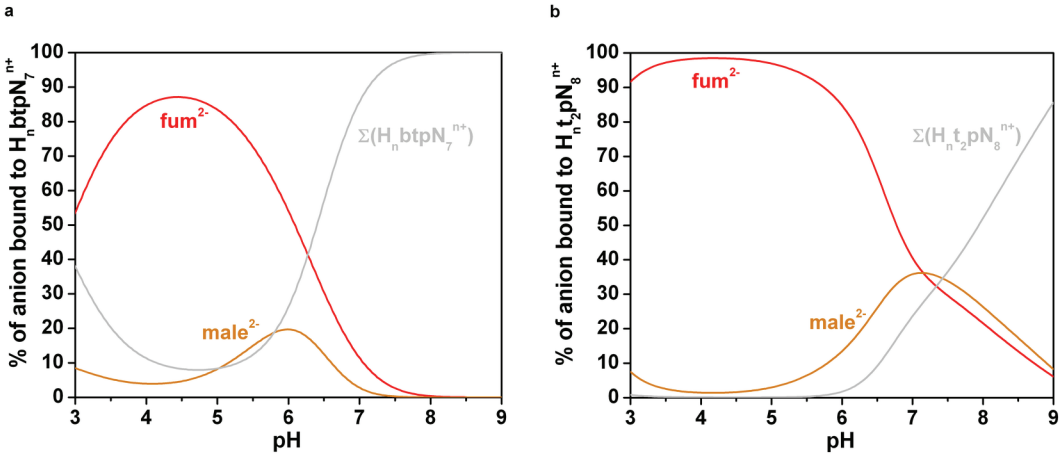

Figure 6.4 Distribution diagrams of the overall amounts of supramolecular species formed between fumarate and maleate anions and $H_nbtpN_7^{n+}$ (a) or $H_nt_2pN_8^{n+}$ (b) in equimolar ratio. $C_{btpN_7} = C_{t_2pN_8} = C_A/3 = 1.0\times10^{-3}$ mol dm^{-3}. For simplicity the amount of associated species with each anion, $[H_nLA]^{(n-2)+}$, is identified in the diagrams only by the formula of the anions, fum^{2-} and $male^{2-}$ respectively.

The most interesting feature of the two receptors is that they show selectivity for fumarate over its *cis* isomer maleate at pH ≈ 4 (Figure 6.4). This is a quite remarkable result as few receptors have been reported that can effectively discriminate these *cis*/*trans* isomers, however none of them works in water and they all show selectivity for maleate over fumarate.[14]

We expected that the increased rigidity imparted by the 2,4,6-triethylbenzene subunit of $H_nbtpN_7^{n+}$ would allow higher preorganization and thus yield higher association constants relative to $H_nt_2pN_8^{n+}$. Since the opposite occurred it is reasonable to assume that the 2,4,6-triethylbenzene subunit does not sufficiently preorganize the secondary amines and consequently a rearrangement is necessary. $H_nt_2pN_8^{n+}$ should also require a conformational rearrangement upon binding (see Scheme 6.3), however, the energetic cost of such rearrangement seems to be higher in the case of $H_nbtpN_7^{n+}$, most likely due to rigidity imparted by the 2,4,6-triethylbenzene subunit.

Another factor that may contribute to the lower binding ability towards dicarboxylates of $H_nbtpN_7^{n+}$ relative to $H_nt_2pN_8^{n+}$. It is known that removing polar

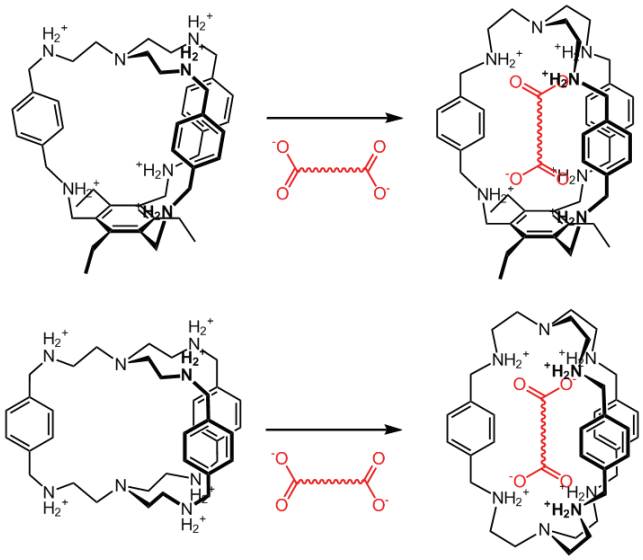

Scheme 6.3 Representation of possible conformational rearrangement of $H_6btpN_7^{6+}$ and $H_6t_2pN_8^{6+}$ upon dicarboxylate binding.

solvent from charged sites requires significant amounts of enthalpic energy such that the stability of anion/receptor associations is mostly determined by favourable entropic terms produced by the desolvation of the interacting species.[15] Thus, in this regard the binding of dicarboxylates with $H_nbtpN_7^{n+}$, which contains one more aromatic group than $H_nt_2pN_8^{n+}$, should be less entropically favoured by such desolvation processes than with $H_nt_2pN_8^{n+}$, since the former compound should be less solvated in water.[16] In addition, the electronic π cloud of the 2,4,6-triethylbenzene subunit may also be repelling the carboxylate group to some extent.

6.3.2 NMR studies

The ^{1}H-NMR spectra of solutions of equimolar amounts of the receptors and the dicarboxylate substrates in D_2O at pD= 4.50 were recorded (see Figures 6.5 and 6.6).

The number and integration of the signals observed in the ^{1}H-NMR spectra of $H_6btpN_7^{6+}$ and $H_6t_2pN_8^{6+}$ suggest highly symmetric structures in solution, consistent with averaged C_{3v} and C_{3h} symmetries, respectively. It should be noted however that the spectrum of $H_6btpN_7^{6+}$ exhibits broader peaks than that of

$H_6t_2pN_8^{6+}$ suggesting that interconversion of different conformations may be slower due to its higher rigidity.

In all cases, only one set of signals was observed for the free receptors and for the associated entities, indicating fast receptor–substrate exchanges on the NMR time scale. The signals of the protons of all substrates showed marked upfield shifts (whose magnitude correlate well with the calculated K_{eff} value at pH 4.5, see Figure 6.2), indicating that these atoms are inside the magnetically shielding region of the aromatic cavity, strongly suggesting encapsulation (Figures 6.5 and 6.6; Table 6.3).

The chemical shifts of the receptors protons are not as affected by binding as those of the substrates, a consequence of the highly symmetric nature of the

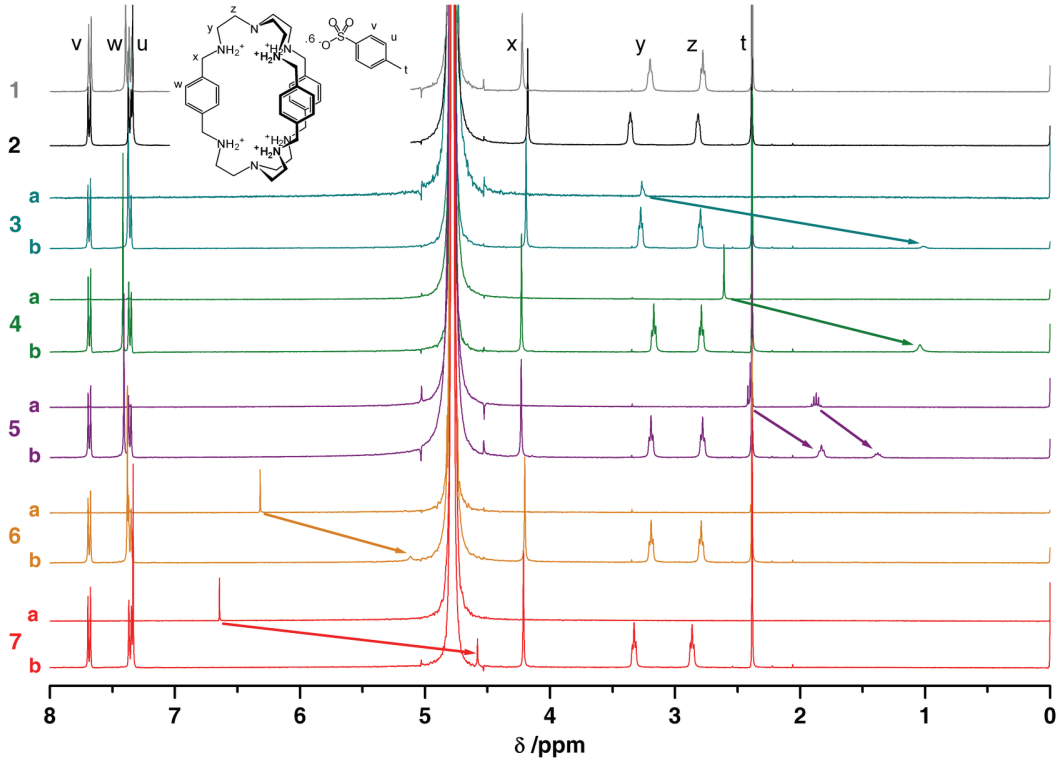

Figure 6.5 ^{1}H NMR spectra of solutions of the $H_6t_2pN_8(TsO)_6$ free receptor (1), free substrates, mal^{2-} (3a), suc^{2-} (4a), glu^{2-} (5a), $male^{2-}$ (6a) and fum^{2-} (7a) and of the association of the receptor with each dicarboxylate substrate in equimolar amounts, oxa^{2-} (2), mal^{2-} (3b), suc^{2-} (4b), glu^{2-} (5b), $male^{2-}$ (6b) and fum^{2-} (7b) , in D_2O at pD = 4.5 and 298.2 K.

compounds. In addition, interpretation of the direction of the shift of these signals is not straightforward as it depends on several factors which may operate in opposite directions, namely hydrogen bond formation, desolvation effects and association induced conformational changes in the receptors. Nonetheless, it is clear that signals of protons close to the ammonium groups (e, f, i and j in the case of $H_6btpN_7^{6+}$; e and f in $H_6t_2pN_8^{6+}$) exhibit biggest shifts and their magnitude is proportional to the calculated K_{eff} value at pH 4.5 (Figure 6.2). The spectra of the $H_6btpN_7^{6+}$ associations with the dicarboxylate anions carry more information than those of $H_6t_2pN_8^{6+}$ because it is possible to distinguish protons on the tren cap side from those of the 2,4,6-triethylbenzene head unit. With this in mind, it is possible to observe that the most shifted resonances by the association with fumarate are e, i, g, h in agreement with the fact that fumarate takes advantage

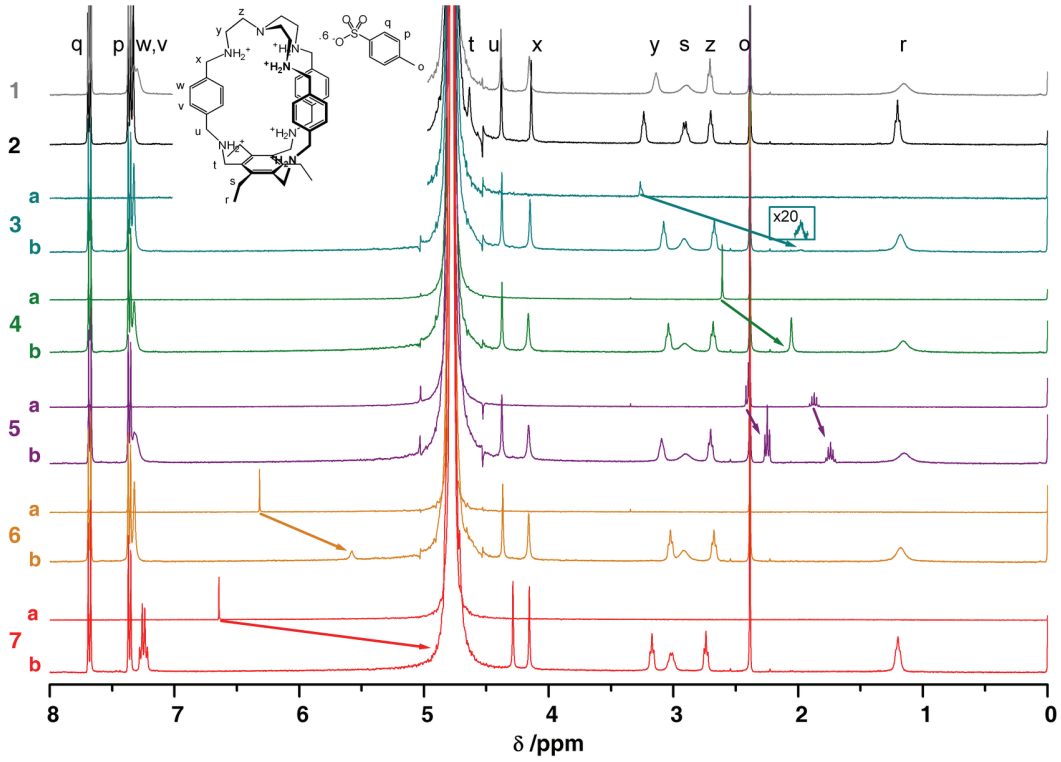

Figure 6.6 ^{1}H NMR spectra of solutions of the $H_6btpN_7(TsO)_6$ free receptor (1), free substrates, mal^{2-} (3a), suc^{2-} (4a), glu^{2-} (5a), $male^{2-}$ (6a) and fum^{2-} (7a) and of the association of the receptor with each dicarboxylate substrate in equimolar amounts, oxa^{2-} (2), mal^{2-} (3b), suc^{2-} (4b), glu^{2-} (5b), $male^{2-}$ (6b) and fum^{2-} (7b) , in D_2O at pD = 4.5 and 298.2 K.

of the ditopic nature of the receptor. In the oxalate association, peaks e and j are also the most affected indicating that oxalate is interacting with both heads of the receptor. Because oxalate is much shorter than fumarate, this one fitting well inside the receptor cavity, it is possible that oxalate moves fast inside the cavity interacting with one side of the receptor at a time or water mediated hydrogen-bonding can compensate the smaller size of this dianion. A Jobs plot confirmed 1:1 receptor:oxalate stoichiometry, ruling out the possibility of two encapsulated oxalate anions (Figure A6.1 in Appendix). Both fumarate and oxalate binding cause sharpening of the receptors proton resonances possibly by favouring a single conformation or a smaller set of conformations of the receptor.

Table 6.3 Chemical shifts ($\Delta\delta$)[a] and respective effective association constants (K_{eff}),[b] for the binding of dicarboxylate substrates by $H_nbtpN_7^{n+}$ and $H_nt_2pN_8^{n+}$.

	L = $btpN_7$		L = t_2pN_8	
	$\Delta\delta$ /ppm	log K_{eff}	$\Delta\delta$ /ppm	log K_{eff}
$H_nLoxa^{(n-2)+}$	–	3.89	–	6.03
$H_nLmal^{(n-2)+}$	1.28	2.83	2.25	4.42
$H_nLsuc^{(n-2)+}$	0.55	2.10	1.57	3.72
$H_nLglu^{(n-2)+}$	0.15	1.76	0.57	3.16
$H_nLmale^{(n-2)+}$	0.74	2.29	1.21	3.86
$H_nLfum^{(n-2)+}$	1.8±0.3 [c]	3.70	2.06	5.81

[a] Calculated upfield chemical shifts induced by binding on the α-CH_2 or vinylic protons of the substrate in D_2O and pD = 4.5. [b] Calculated for pH = 4.5 using the association constants determined in H_2O at T = 298.2±0.1 K and I = 0.10±0.01 mol dm^{-3} in KTsO. [c] In this case the vinylic protons of associated fumarate appear under the solvent peak and therefore it is not possible to determine a more precise value.

Also noteworthy was the disappearance of the malonate signal upon binding with both receptors. It is known that when malonic acid, as well as its ionized forms, is dissolved in D_2O, two isotopic-exchange reactions occur where the two methylenic hydrogen atoms are successively replaced by deuterium through an enolization mechanism.[17] As can be seen on Figure 6.7 both $H_6btpN_7(TsO)_6$ and $H_6t_2pN_8(TsO)_6$ receptors greatly enhance the rate of H/D exchange of malonate.

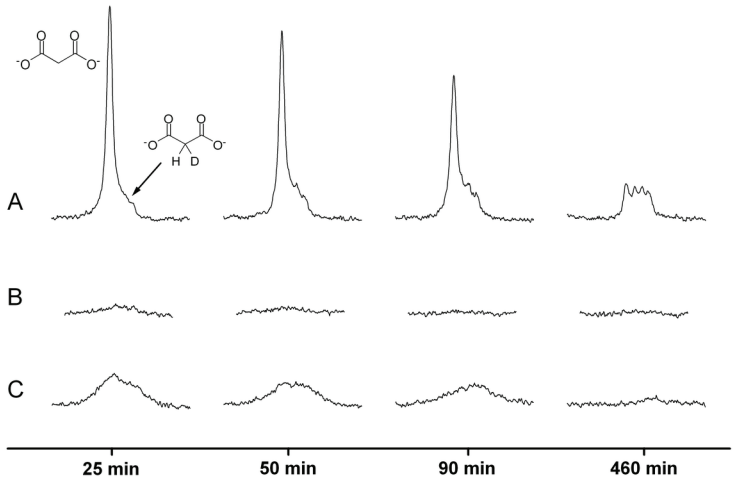

Figure 6.7 ^{1}H NMR signals of malonate recorded in the course of the H/D exchange in the absence of catalyst (A) and in the presence of $H_6btpN_7(TsO)_6$ (B) and $H_6t_2pN_8(TsO)_6$ (C). All spectra recorded were in D_2O, pD = 4.5 and $C_{mal} = C_{btpN_7} = C_{t_2pN_8} = 2.0\times10^{-3}$ mol dm^{-3}. Under these conditions, the ^{1}H NMR signals of both cryptands remain unaffected throughout the experiment.

6.4 Conclusions

Solution studies showed that $H_nbtpN_7^{n+}$ and $H_nt_2pN_8^{n+}$ are able to strongly bind dicarboxylate substrates in highly competitive aqueous medium. Although $H_nt_2pN_8^{n+}$ has much higher affinity towards dicarboxylates than structurally similar $H_nbtpN_7^{n+}$, their selectivity pattern is nearly identical. Therefore the higher affinity did not give rise to enhanced selectivity as might be expected. The identical selectivity pattern results from the fact that the two binding subunits in both compounds are separated by the same distance, defined by the *p*-xylyl spacer, yielding two cavities identical in terms of size and number of binding units, which means that the enthalpy of binding of a given substrate, which arises mainly from electrostatic attraction and hydrogen bond formation, should be very similar in both receptors.

Considering that the enthalpy of the binding process is roughly the same in both receptors, the large difference in affinity towards dicarboxylates between $H_nbtpN_7^{n+}$ and $H_nt_2pN_8^{n+}$ must have entropic origin and be related with the entropic cost of conformational rearrangement and entropic gain of desolvation. In this view the 2,4,6-triethylbenzene cap of $H_nbtpN_7^{n+}$ is probably responsible for

a more costly conformational rearrangement and lower solvation in water, and thus lower affinity.

In both receptors, oxa^{2-} and fum^{2-} display higher association constants than the rest of the substrates. Fum^{2-} appears to have the right size, shape and rigidity to fit the cavities, while oxa^{2-} high association constant is related with its higher charge density combined with possible water mediated hydrogen-bonding which may compensate the smaller size of this dianion. Mal^{2-}, suc^{2-}, glu^{2-} and $male^{2-}$ are bound less strongly, although the ^1H NMR studies showed marked upfield shifts in the proton signals of all substrates with both receptors, indicating that they are inside the magnetically shielding region of the aromatic cavity, strongly suggesting encapsulation or at least close proximity to the entrance of the cavity. The lower affinity of mal^{2-}, suc^{2-}, glu^{2-} and $male^{2-}$ may be ascribed to worse fit to the cavity arising from their own conformational preferences and flexibility, which may not allow them to take advantage of all the possible interactions that the receptors can provide. A less than perfect match will result in an amount of enthalpic gain which may not be enough to compensate the entropic cost of conformational rearrangement of both binding partners and may result in insufficient desolvation entropy, contributing to lower association constants. Comparison between the association constants of fum^{2-} and suc^{2-}, higher for fum^{2-} in both receptors, clearly shows that suc^{2-} requires additional conformational rearrangement due to its higher flexibility, resulting in a lower association constant.

In addition it was found that the two receptors show selectivity for fumarate over its *cis* isomer maleate at pH ≈ 4. This is to the best of our knowledge the first synthetic receptors that can effectively discriminate these *cis*/*trans* isomers in water, with a preference for fumarate.

In conclusion, the present study clearly shows that selectivity is not necessarily enhanced by high affinity, contrary to what might be expected, and that increased rigidity can only result in increased affinity if the receptor is sufficiently preorganized in such way that no rearrangement is necessary upon binding.

6.5 Experimental

6.5.1 General considerations

All solvents and chemicals were commercially purchased reagent grade quality and used as supplied without further purification. The compound $btpN_7$ was synthesized and described on Chapter 5 and t_2pN_8 was prepared according to a previously reported procedure.[18] The purity of both compounds was confirmed by ^{1}H-NMR (Figures A6.2 and A6.3 in Appendix) and elemental analysis. For the compound $btpN_7$: ^{1}H NMR (400 MHz, $CDCl_3$, 298 K; Me_4Si) δ = 6.81, 6.69, 3.94, 3.60, 3.37, 2.96, 2.53, 2.43, 1.69, 1.23, 1.12 ppm; elemental analysis calcd. (%) for $C_{45}H_{63}N_7$: C 77.0, H 9.0, N 14.0; found: C 76.7, H 8.9, N 13.9. For the compound t_2pN_8: ^{1}H NMR (400 MHz, $CDCl_3$, 298 K; Me_4Si) δ=7.26, 3.68, 2.83, 2.66, 1.71 ppm; elemental analysis calcd. (%) for $C_{45}H_{63}N_7$: C 72.2, H 9.1, N 18.7; found: C 72.3, H 8.7, N 18.7). Potassium *p*-toluenesulfonate (KTsO) was prepared by the neutralization of HTsO with KOH in water, followed by recrystallization from H_2O/MeOH. NMR spectra used for characterization of products were recorded on a Bruker Avance 400 instrument. TMS was used as reference for the ^{1}H NMR measurements in $CDCl_3$ and in D_2O the 3-(trimethylsilyl)propanoic acid-d_4-sodium salt. Peak assignments are based on peak integration and multiplicity for 1D ^{1}H spectra and on COSY, NOESY and HMQC experiments. Microanalyses were carried out by the ITQB/IBET Microanalytical Service.

6.5.2 Potentiometric measurements

6.5.2.1 Reagents and solutions

All the solutions were prepared using demineralised water (obtained by a Millipore/Milli-Q system). A stock solution of the receptor was prepared at *ca*. 2.0×10^{-3} mol dm^{-3}. Stock solutions of the dicarboxylic acids (analytical grade) were prepared at about 2.5×10^{-2} mol dm^{-3} and the concentrations were checked by titration with standard 0.100 mol dm^{-3} KOH solutions. Carbonate-free solutions of the KOH titrant were prepared from a Merck ampoule diluted to 1000 cm^3 with water (freshly boiled for about 2 h and allowed to cool under nitrogen). These

solutions were discarded every time carbonate concentration was about 0.5% of the total amount of base. The titrant solutions were standardized (tested by Gran's method).[19]

6.5.2.2 Equipment and working conditions

The equipment used was described in Chapter 2. The ionic strength of the experimental solutions was kept at 0.10±0.01 mol dm^{-3} with KTsO, the temperature was maintained at 298.2±0.1 K. Atmospheric CO_2 was excluded from the titration cell during experiments by passing purified nitrogen across the top of the experimental solution.

6.5.2.3 Measurements

The $[H^+]$ of the solutions was determined by the measurement of the electromotive force of the cell, $E = E^{o\prime} + Q \log [H^+] + E_j$. The term pH is defined as $-\log [H^+]$. $E^{o\prime}$, Q, E_j and K_w were determined by titration of a solution of known hydrogen-ion concentration at the same ionic strength, using the acid pH range of the titration. The liquid-junction potential, E_j, was found to be negligible under the experimental conditions used. The value of K_w was determined from data obtained in the alkaline range of the titration, considering $E^{o\prime}$ and Q valid for the entire pH range and found to be equal to $10^{-13.76}$ in our experimental conditions. Before and after each set of titrations the glass electrode was calibrated as a $[H^+]$ probe by titration of 1.0×10^{-3} mol dm^{-3} standard HCl solution with standard KOH. Potentiometric equilibrium measurements were carried out by titrating a solution consisting in 20.00 cm^3 of $\approx 2.0\times10^{-3}$ mol dm^{-3} $btpN_7$ solution diluted to a final volume of 40.00 cm^3, with standard KOH. Measurements were done with 0.10 mol dm^{-3} KTsO and 0.10 mol dm^{-3} KBr. The exact amount of $btpN_7$ was obtained by determination of the excess of acid present in a mixture of $btpN_7$ and *p*-toluenesulfonic acid 1.4×10^{-2} mol dm^{-3} by titration with standard KOH solution. The protonation constants of t_2pN_8 were determined by titration of 20.00 cm^3 of $\approx$ 2.0×10^{-3} mol dm^{-3} ligand solution (in the free base form) diluted to a final volume of 40.00 cm^3, with standard HTsO solution, because t_2pN_8 is insoluble bellow pH

4.8 in 0.10 mol dm^{-3} KTsO medium. For this reason a titration was performed in 0.05 mol dm^{-3} KTsO which allowed the determination of the exact amount of t_2pN_8 and to check if the protonation of both tertiary amines of t_2pN_8 could take place in the 2.5–4.8 pH region. Potentiometric equilibrium measurements were then carried out with both compounds in the presence of each substrate at 1:3 R:S ratios (R = receptor and S = substrate). No solubility problems where found in the titrations of t_2pN_8 in the presence of the dicarboxylate substrates throughout the whole studied pH range in 0.10 mol dm^{-3} KTsO medium. In each titration about 100 points were collected, and a minimum of two titration curves were performed.

6.5.2.4 Calculation of equilibrium constants

Overall protonation constants, β_i^H, of ligands and anions, were calculated by fitting the potentiometric data obtained for all the performed titrations in the same experimental conditions with the HYPERQUAD program.[20] All these constants were taken as fixed values to obtain the equilibrium constants of the new species from the experimental data corresponding to all the titrations at 1:3 R:A ratio, also using the HYPERQUAD program. The initial computations were obtained in the form of overall stability constants, $\beta_{H_hL_lA_a}$ values, $\beta_{H_hL_lA_a} = [H_hL_lA_a]/[H]^h[L]^l[A]^a$. The errors quoted are the standard deviations of the overall association constants given directly by the program for the input data, which include all the experimental points of all titration curves. The HYSS program[21] was used to calculate the concentration of equilibrium species from the calculated constants from which distribution diagrams were plotted. The species considered in a particular model were those that could be justified by the principles of supramolecular chemistry.

6.5.3 NMR studies

6.5.3.1 Spectra of the supermolecules

Solutions of $H_6btpN_7(TsO)_6$, $H_6t_2pN_8(TsO)_6$, free dicarboxylate substrates and respective cryptates where prepared in D_2O in 2.0×10^{-3} mol dm^{-3} concentration

and the pD was adjusted to 4.5 by addition of DTsO or KOD with an Orion 420A instrument fitted with a combined Ingold 405M3 microelectrode. The pH*, the reading of the pH meter previously calibrated with two standard aqueous buffers at pH 4 and 8, was measured directly in the NMR tube. The final pD was calculated from pD = pH* + (0.40 ± 0.02).[22]

6.5.3.2 Job's Plot

Stock solutions of 2.0×10^{-3} mol dm^{-3} $(H_6btpN_7)(TsO)_6$ and K_2oxa were prepared in D_2O. Ten NMR tubes were prepared having a total concentration of $(H_6btpN_7)(TsO)_6$ and of K_2oxa maintained at 2.0×10^{-3} mol dm^{-3}. The pD value was adjusted to 4.50 with DTsO or KOD. The chemical shift changes for each solution were measured, and the product between the increment in chemical shift and receptor concentration versus the molar fraction of the receptor was plotted. A curve is generated where the maximum point indicates the stoichiometry of the association by use of the equation, $[C] = [R]_0\times(\delta_{obs}-\delta_R)/(\delta_{max}-\delta_R)$, where $[R]_0$ is the total receptor concentration, δ_{obs} is the observed chemical shift, δ_R is the chemical shift of the free receptor, and δ_{max} is the chemical shift of the cryptate. Because $\delta_{max}-\delta_R$ is a constant, the concentration of the associated entity is proportional to $\Delta\delta\times[R]_0$ (where $\Delta\delta = \delta_{obs}-\delta_R$). Plots of $\Delta\delta X_R$ as a function of X_R (where X_R is the molar fraction of the receptor) that exhibit a maximum at $X_R = 0.5$, indicating a 1:1 association.

6.5.3.3 H/D exchange experiments

Solutions of the malonate associations with $H_6btpN_7(TsO)_6$ and $H_6t_2pN_8(TsO)_6$, were prepared in D_2O 2.0×10^{-3} mol dm^{-3} concentration (1:1 receptor to malonate ratio). The pD was adjusted to 4.5 by addition of DTsO or KOD. A malonate solution in the absence of receptors was also prepared at the same concentration and at the same pD value. ^{1}H-NMR spectra of these solutions were acquired at 25, 50, 90 and 460 minutes after each solution was prepared.

6.6 Acknowledgements

The NMR spectrometers are part of the National NMR Network and were purchased in the framework of the National Program for Scientific Re-equipment, contract REDE/1517/RMN/2005, with funds from POCI 2010 (FEDER) and Fundação para a Ciência e a Tecnologia (FCT). We also acknowledge M. C. Almeida for providing elemental analysis and ESI-MS data from the Elemental Analysis and Mass Spectrometry Service at the ITQB/IBET. Pedro Mateus thanks FCT for the grant (SFRH/BD/36159/2007).

6.7 References

[1] a) Supramolecular Chemistry of Anions, Eds.: A. Bianchi, K. Bowman-James, E. García-España, Pergamon, Oxford, Wiley-VCH, New York, **1997**; b) R. J. Fitzmaurice, G. M. Kyne, D. Douheret, J. D. Kilburn, *J. Chem. Soc., Perkin Trans.* **2002**, *1*, 841–864; c) P. A. Gale, R. Quesada, *Coord. Chem. Rev.* 2006, *250*, 3219–3244; d) P. A. Gale, S. E. García-Garrido, J. Garric, *Chem. Soc. Rev.* **2008**, *37*, 151–190; e) C. Caltagirone, P. A. Gale, *Chem. Soc. Rev.* **2009**, *38*, 520–563; f) P. A. Gale, *Chem. Soc. Rev.* **2010**, *39*, 3746–3771.

[2] J. M. Berg, J. L. Tymoczko, L. Stryer, *Biochemistry*, 5th Ed., W. H. Freeman & Co Ltd, New York, 2002, pp. 465–484.

[3] a) S. N. Yurgel, M. L. Kahn, *FEMS Microbiol. Rev.* **2004**, *28*, 489–501; b) I. G. Janausch, E. Zientz, Q. H. Tran, A. Kröger, G. Unden, *Biochim. Biophys. Acta* **2002**, *1553*, 39–56.

[4] R. Hyde, P. M. Taylor, H. S. Hundal, *Biochem. J.* **2003**, *373*, 1–18.

[5] D. H. Williams, B. Bardsley, *Angew. Chem. Int. Ed.* **1999**, *38*, 1172–1193.

[6] M. Z. H. Rozaini, P. Brimblecombe, *Water Air Soil Pollut.* **2009**, *198*, 65–75.

[7] a) S. Kubik, *Chem. Soc. Rev.* **2010**, *39*, 3648–3663; b) T. H. Rehm, C. Schmuck, *Chem. Soc. Rev.* **2010**, *39*, 3597–3611.

[8] a) A. Bianchi, M. Micheloni, P. Paoletti, *Coord. Chem. Rev.* **1991**, *110*, 17; b) B. Dietrich, *Pure Appl. Chem.* **1993**, *65* 1457–1464; c) C. A. Ilioudis, J. W. Steed, *J. Supramol. Chem.* **2001**, *1*, 165–187; d) J. M. Llinares, D. Powell, K. Bowman-James, *Coord. Chem. Rev.* **2003**, *240*, 57–75; e) V. McKee, J. Nelson, R. M. Town, *Chem. Soc. Rev.* **2003**, *32*, 309–325; f) K. Bowman-James, *Acc. Chem. Res.* **2005**, *38*, 671–678; g) S. Kubik, C. Reyheller, S. Stüwe, *J. Inclus. Phenom. Macrocycl. Chem.* **2005**, *52*, 137–187; h) E. García-España, P. Díaz, J. M. Llinares, A. Bianchi, *Coord. Chem. Rev.* **2006**, *250*, 2952–2988; i) K. Wichmann, B. Antonioli, T. Söhnel, M. Wenzel, K. Gloe, K. Gloe, J. R. Price, L. F. Lindoy, A. J. Blake, M. Schröder, *Coord. Chem. Rev.* **2006**, *250*, 2987–3003; j) E. A. Katayev, Y. A. Ustynyuk, J. L. Sessler, *Coord. Chem. Rev.* **2006**, *250*, 3004–3037; k) C. Bazzicalupi, A. Bencini, V. Lippolis, *Chem. Soc. Rev.* **2010**, *39*, 3709–3728.

[9] a) S. O. Kang, J. M. Llinares, V. W. Day, K. Bowman-James, *Chem. Soc. Rev.* **2010**, *39*, 3980–4003; b) P. Mateus, N. Bernier, R. Delgado, *Coord. Chem. Rev.* **2010**, *254*, 1726–1747; c) P. Ballester, *Chem. Soc. Rev.* **2010**, *39*, 3810–3830.

[10] a) B. Dietrich, J. Guilhem, J.-M. Lehn, C. Pascard, E. Sonveaux, *Helv. Chim. Acta* **1984**, *67*, 91–104; b) M. W. Hosseini, J.-M. Lehn, *Helv. Chim. Acta* **1988**, *71*, 749–

756; c) J.-M. Lehn, R. Meric, J.-P. Vigneron, I. Bkouche-Waksman, C. Pascard, *J. Chem. Soc., Chem. Commun.* **1991**, 62–64; d) M.-P. Teulade-Fichou, J.-P. Vigneron, J.-M. Lehn, *J. Chem. Soc. Perkin Trans. 2*, **1996**, 2169–2175; e) J. Nelson, M. Nieuwenhuyzen, I. Pál, R. M. Town, *Dalton Trans.* **2004**, 229–235; f) S. Carvalho, R. Delgado, V. Félix, *Tetrahedron* **2010**, 66, 8714–8721.

[11] Y. Li, L. Jiang, X.-L. Feng, T.-B. Lu, Cryst. Growth Des. **2008**, *8*, 3689–3694.

[12] M. T. Albelda, M. A. Bernardo, E. García-España, M. L. Godino-Salido, S. V. Luis, M. J. Melo, F. Pina, C. Soriano, *J. Chem. Soc. Perkin Trans. 2* **1999**, 2545–2549.

[13] A. Bianchi, E. García-España, *J. Chem. Educ.* **1999**, *76*, 1727–1732.

[14] a) F. Sancenón, R. Martínez-Máñez, M. A. Miranda, M.-J. Seguí, J. Soto, *Angew. Chem. Int. Ed.* **2003**, *42*, 647–650; b) Y.-P. Yen, K.-W. Ho, *Tetrahedron Lett.* **2006**, *47*, 7357–7361; c) A. M. Costero, M. Colera, P. Gavin, S. Gil, *Chem. Commun.* **2006**, 761–763; d) Y.-P. Tseng, Gu.-M. Tu, C.-H. Lin, C.-T. Chang, C.-Yung Lin, Y.-P. Yen, *Org. Biomol. Chem.* **2007**, *5*, 3592–3598; e) Y.-S. Lin, G.-M. Tu, C.-Y. Lin, Y.-T. Chang, Y.-P. Yen, *New J. Chem.* **2009**, *33*, 860–867.

[15] F. P. Schmidtchen, *Coord. Chem. Rev.* **2006***, 250*, 2918–2928.

[16] P. Arranz, A. Bencini, A. Bianchi, P. Diaz, E. García-España, C. Giorgi, S. V. Luis, M. Querol, B. Valtancoli, *J. Chem. Soc., Perkin Trans. 2*, **2001**, 1765–1770.

[17] a) J. O. Halford, L. C. Anderson, *J. Am. Chem. Soc.* **1936**, *58*, 736–740; b) E. W. Hansent, P. Ruoff, *J. Phys. Chem.* **1988**, *92*, 2641–2645.

[18] P. S. Lakshminarayanan, I. Ravikumar, E. Suresh, P. Ghosh, *Cryst. Growth Des.* **2008**, *8*, 2842–2852

[19] F. J. Rossotti, H. J. Rossotti, *J. Chem. Educ.* **1965**, *42*, 375–378.

[20] P. Gans, A. Sabatini, A. Vacca, *Talanta* **1996**, *43*, 1739–1753.

[21] L. Alderighi, P. Gans, A. Ienco, D. Peters, A. Sabatini, A. Vacca, *Coord. Chem. Rev.* **1999**, *184*, 311–318.

[22] R. Delgado, J. J. R. F. da Silva, M. T. S. Amorim, M. F. Cabral, S. Chaves, J. Costa, *Anal. Chim. Acta* **1991**, *245*, 271–282.

Chapter 7

Two new polyoxapolyaza macrobicyclic receptors for recognition of zwitterionic amino acids

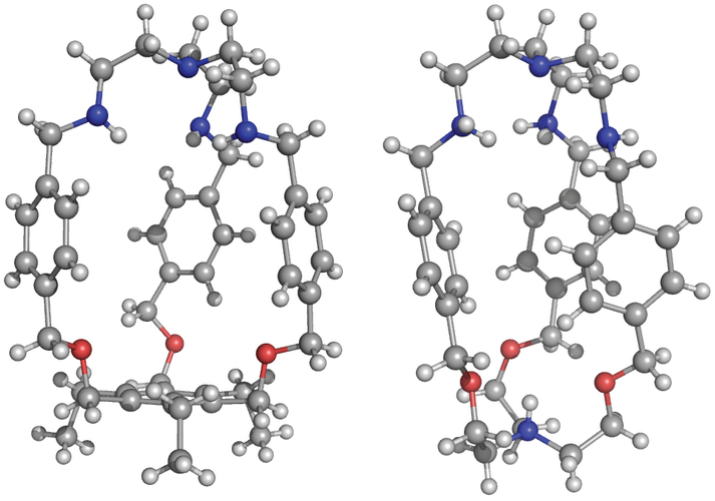

Work contained in: P. Mateus, R. Delgado, P. Brandão, V. Félix, *preliminary manuscript.*

7.1 Summary

Two polyoxapolyaza heteroditopic macrobicyclic compounds ($btpN_4O_3$ and $t_2pN_5O_3$) have been synthesized in moderate to good yields through a [1+1] "tripod-tripod coupling" strategy to be used as receptors for the recognition of amino acids. The acid-base behaviour of the compounds as well as their binding ability with glycine (Hgly), *β*-alanine (Hbala), taurine (Htau), *γ*-aminobutyric acid (Hgaba), aminomethylphosphonic acid (H_2amp) and 2-aminoethylphosphonic acid (H_2aep) were studied by potentiometry at 298.2±0.1 K in H_2O/MeOH (50:50 v/v) and at ionic strength 0.10±0.01 mol dm^{-3} in NMe_4TsO. The acid-base studies revealed that the tren subunit of $btpN_4O_3$ is fully protonated at pH ≈ 6.2 whereas $t_2pN_5O_3$ exhibits a more complicated protonation behaviour, in which the tertiary amine of the polyether compartment is protonated before the complete protonation of the tren subunit, rendering the compound inappropriate for amino acid binding. The binding studies between $H_nbtpN_4O_3^{n+}$ and the amino acid substrates in the very competing medium used led to association constant values in the range 1.85–3.33 log units, with $H_nbtpN_4O_3^{n+}$ showing a preference for amino acids containing tetrahedral anionic groups.

7.2 Introduction

Amino acids are very important anion containing substrates, not only for their use as building blocks of proteins but also for their role in the metabolism, neurotransmission and biosynthesis.[1] The design of artificial receptors for the selective recognition and sensing of amino acids in aqueous solution may have important applications. Consequently, over the last thirty years supramolecular chemists have strived to design receptors selective for amino acids.[2] However, this task has proven extremely challenging due to the intrinsic characteristics of amino acids. The zwitterionic nature of the amino acids at physiological pH requires both the existence of a cationic and an anionic binding sites in the receptor, which from a synthetic point of view is not a trivial task. In view of this, much work in the area has focused in the recognition of derivatized amino acids in which either the carboxylate or the ammonium group is protected.[3] Moreover,

strong binding of zwitterions in aqueous solutions is hampered by the high energetic cost of desolvation of the double ion. Indeed, few receptors where conceived to work in aqueous solution.[4-8]

A possible approach for binding zwitterionic species consists in developing heteroditopic macrobicyclic compounds in which both cationic (ether groups) and anionic binding sites (ammonium groups) are part of the macrobicyclic framework. Macrobicyclic compounds offer the possibility to encapsulate substrates within their well defined cavities and allow the placement of several binding units in strategical points of the molecule for multiple and cooperative binding.[9-13] It was shown that tris(2-aminoethyl)amine (tren) capped macrobicyclic polyammonium receptors strongly bind anions in aqueous media by combining electrostatic and hydrogen bonding interactions,[9-12] and they were particularly useful in the binding of carboxylates.[8] In addition, it was shown in Chapters 2, 3 and 6 that the new family of benzene capped polyammonium cryptands are also useful for the binding of anions in aqueous solutions. On the other hand, triethanolamine capped and benzene capped macrobicyclic receptors have been shown to bind ammonium,[14,15] amino alcohols and amino acids.[16] Thus it was intended to join these two types of compounds to produce “hybrid” polyoxapolyaza cryptands which were believed to be suitable for the recognition of the amino acids depicted in Scheme 7.1.

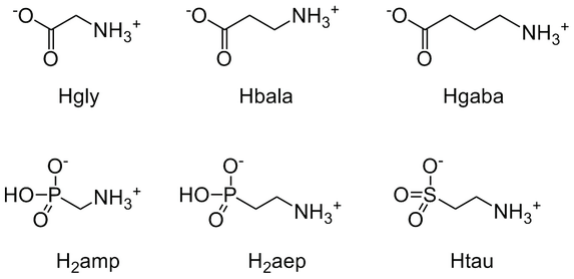

Scheme 7.1 Target amino acid substrates.

Mixed polyazapolyoxa macrobicyclic receptors have been first prepared by Bharadwaj *et al.*[17-19] and only recently their ability to bind anions have been evaluated (see cryptands **18** and **19**, Scheme 1.17, Chapter 1).[20-23] However the mixed anion/cation encapsulation has never been attempted in this class of

molecules. In fact, cryptands **18** and **19** do not seem to be appropriate for the binding of the target amino acids depicted in Scheme 7.1 as they have relatively small cavities due to the *ortho* and *meta* substitution of the benzene unit of their spacers. Furthermore the ethereal oxygens of **18** and **19** are directly attached to the benzene ring of the spacers, which should weaken their electron-donor ability and consequently render them weak hydrogen bond acceptors.

With these considerations in mind it was decided to obtain mixed polyazapolyoxa macrobicyclic compounds in which the ethereal oxygens are not directly attached to the benzene ring of the spacer in addition to using the *p*-xyly building block to construct larger cavities (Scheme 7.2) than the ones previously reported by Bharadwaj. It should be noted however that these compounds where obtained at a later stage of the work and that the results presented herein are preliminary and additional experimental work is required to complete these studies.

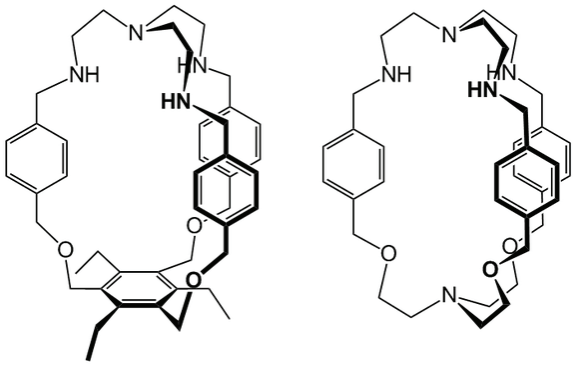

Scheme 7.2 Macrobicyclic compounds studied in this work.

7.3 Results and Discussion

7.3.1. Synthesis

As described in Chapter 5, the synthesis of heteroditopic macrobicyclic compounds requires two critical steps: formation of a tripodal intermediate and macrobicyclization through a [1+1] "tripod-tripod coupling" strategy.[24] The new polyazapolyoxa macrobicyclic compounds were prepared as outlined in Scheme 7.3.

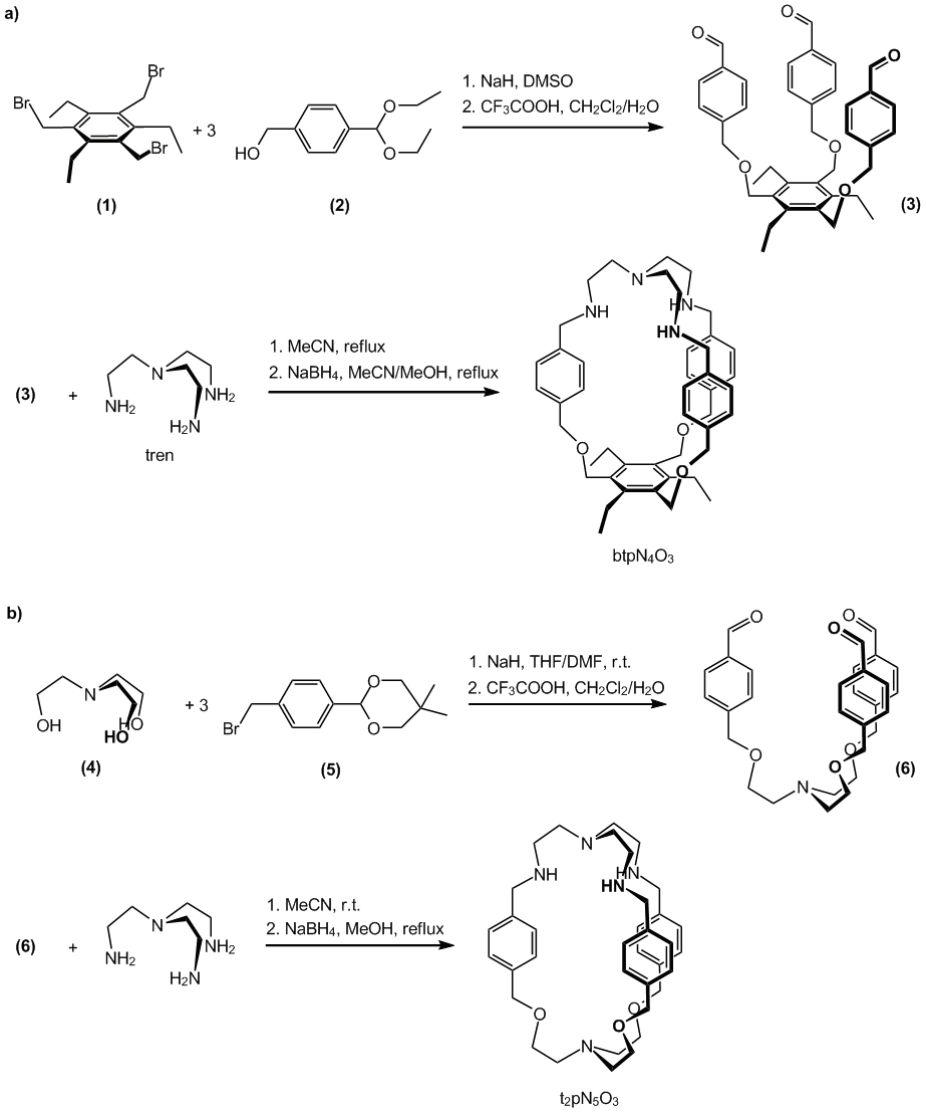

Scheme 7.3 Synthetic procedures of $btpN_4O_3$ (a) and $t_2pN_5O_3$ (b).

The synthetic strategy required a bifunctional building block in which one of the functionalities is protected while the other is available to react and produce tripodal compounds that are the precursors of the desired heteroditopic macrobicyclic receptors. In the case of the synthesis of $btpN_4O_3$ (4-diethoxymethylphenyl)methanol (**2**) was the bifuntional reagent used. This reagent has an acetal-protected aldehyde group and a OH group available to react with 1,3,5-tris(bromomethyl)-2,4,6-triethylbenzene (**1**) in a Williamson ether

synthesis procedure. Attempt to react the same bifunctional reagent with tris(2-chloroethyl)amine failed due to the poor ability of the leaving group chloride. Thus alternatively, in the synthesis of $t_2pN_5O_3$, 2-(4-bromomethyl-phenyl)-5,5-dimethyl-[1,3]dioxane (**5**) was reacted with triethanolamine (**4**) to prepare the tripodal intermediate.

After deprotection of the aldehyde groups the trialdehyde tripodal intermediates (**3** and **6**) were obtained for subsequent reaction with tren in a Schiff-base condensation cyclization step. Surprisingly, using the same reaction conditions for the cyclization step (MeCN, room temperature), $t_2pN_5O_3$ was obtained in 60% yield after imine reduction whereas only polymeric materials were obtained in the attempted synthesis of $btpN_4O_3$. It should be noted that under the same conditions $btpN_7$ was obtained in 79% yield after sodium borohydride reduction (see Chapter 5).Thus apparently the cyclization reaction requires a certain degree of flexibility of the tripodal intermediate. In order to circumvent this problem the cyclization was tried in refluxing MeCN and in more dilute conditions. Using this procedure $btpN_4O_3$ was obtained after sodium borohydride reduction in 40% yield.

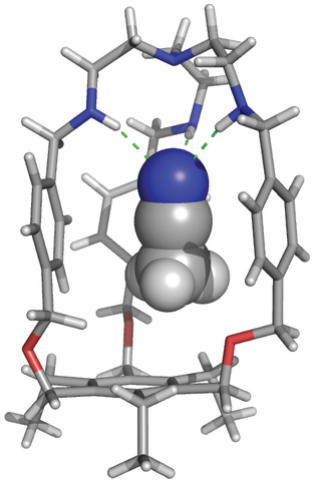

Figure 7.1 X-ray crystal structure of $btpN_4O_3$ showing an encapsulated MeCN. Molecular diagram presented was drawn with PyMOL.[26]

Crystals of $btpN_4O_3$ were grown from MeCN solution. The respective preliminary crystal structure shown in Figure 7.1[25] revealed an encapsulated

MeCN molecule held by three hydrogen bonds N–H···N between the secondary amines and the nitrogen atom of MeCN, at N···N distances of 3.27, 3.30 and 3.40 Å and N–H···N corresponding angles of 160º, 163º and 167º, respectively.

7.3.2. Potentiometric studies

7.3.2.1 Acid-base behaviour of the cryptands

The protonation constants of $btpN_4O_3$ and $t_2pN_5O_3$ were determined by potentiometry in H_2O/MeOH (50:50 v/v) solution at 298.2 K and ionic strength 0.10 mol dm^{-3} in NMe_4TsO. The results are collected in Table 7.1 and the corresponding species distribution diagrams represented in Figure 7.2.

Table 7.1 Overall (β_i^H) and stepwise protonation (K_i^H) constants of $btpN_4O_3$ and $t_2pN_5O_3$ in H_2O/MeOH (50:50 v/v).[a]

Equilibrium reaction	log β_i^H [b]		Equilibrium reaction	log K_i^H	
	$btpN_4O_3$	$t_2pN_5O_3$		$btpN_4O_3$	$t_2pN_5O_3$
$L + H^+ \rightleftharpoons HL^+$	8.76(1)	9.23(1)	$L + H^+ \rightleftharpoons HL^+$	8.65	9.23
$L + 2\,H^+ \rightleftharpoons H_2L^{2+}$	17.01 (1)	17.59(1)	$HL^+ + H^+ \rightleftharpoons H_2L^{2+}$	8.25	8.36
$L + 3\,H^+ \rightleftharpoons H_3L^{3+}$	23.27(1)	25.55(1)	$H_2L^{2+} + H^+ \rightleftharpoons H_3L^{3+}$	6.26	7.96
$L + 4\,H^+ \rightleftharpoons H_4L^{4+}$	–	29.30(1)	$H_3L^{3+} + H^+ \rightleftharpoons H_4L^{4+}$	–	3.75

[a] T = (298.2±0.1) K; I = (0.10±0.01) mol dm^{-3} in NMe_4TsO. [b] Values in parenthesis are standard deviations in the last significant figures.

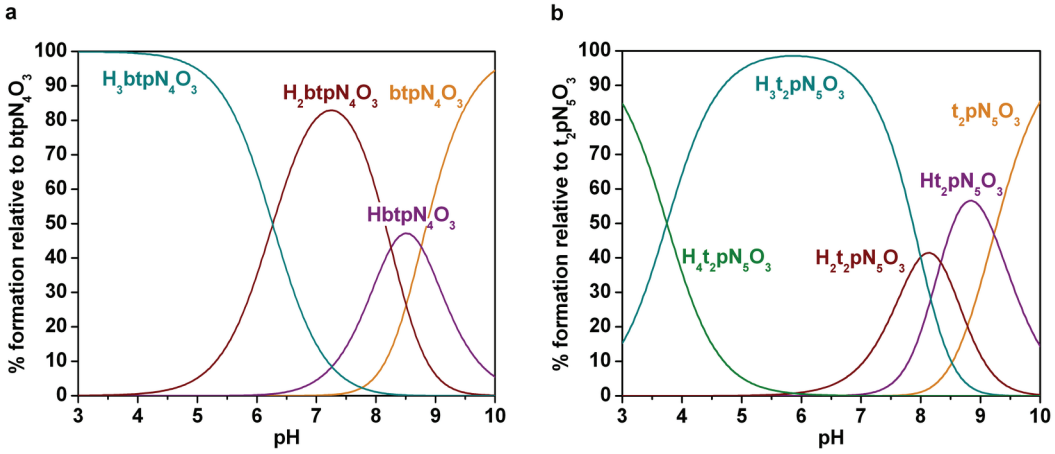

Figure 7.2 Species distribution diagram of the protonation of $btpN_4O_3$ (a) and $t_2pN_5O_3$ (b). $C_{btpN_4O_3} = C_{t_2pN_5O_3} = 1.0\times10^{-3}$ mol dm^{-3}. Charges were omitted.

The acid-base behaviour of $btpN_4O_3$ is straightforward: three protonation constants were found in the working pH region (3.0–10.0), corresponding to the successive protonations of the secondary amines. The tertiary amine is very acidic due to the nearby presence of three positive charges, hence its protonation constant cannot be obtained in the working pH region. As shown in Figure 7.2a, the fully protonated form of the receptor, $H_3btpN_4O_3^{3+}$, exists as the main species below pH ≈ 6.2. This receptor species exhibits a compartment with three protonated amines to interact with the anionic group of the amino acids through electrostatic interactions and hydrogen bonding. The other compartment has three ether oxygen atoms available to accept hydrogen bonds from the ammonium group of the substrates and an aromatic unit which may contribute to the establishment of cation-π interactions.

The acid-base behaviour of $t_2pN_5O_3$ is more complicated due to the existence of a tertiary amine in the polyether subunit. The first two protonation constants should correspond to the protonation of two secondary amines while the third protonation is likely to occur in the tertiary amine of the polyether subunit. This is in agreement with the obtained crystal structure of $H_3t_2pN_5O_3^{3+}$ (Figure 7.3).[25] In the crystal structure the two secondary amines are protonated and forming two very strong hydrogen bonds with an encapsulated water molecule with N···O distances of 2.75 and 2.77 Å and N–H···O corresponding angles of 174.3 and 171.9º, respectively. The water molecule establishes a third strong hydrogen bond with an unprotonated amine, with N···O distance of 2.60 Å and O–H···N corresponding angle of 173.7º. Thus the fourth protonation takes place at the last secondary amine. The corresponding protonation constant has an unusually low value for a secondary amine of 3.75 log units (see Table 7.1). The only explanation that was possible to advance for the moment is the effect of the enclosed water molecule. This water molecule is so tightly bound that the protonation of the last amine involved in O–H···N hydrogen bond is highly disfavoured. The protonation sequence described above still requires confirmation by a ^{1}H-NMR titration. Nonetheless this protonation behaviour makes the $H_3t_2pN_5O_3^{3+}$ inappropriate for amino acid binding. Indeed the main

receptor species in the large 3.7–8.4 pH region contains the tertiary amine of the polyether compartment protonated, which should repel the ammonium group of the substrates.

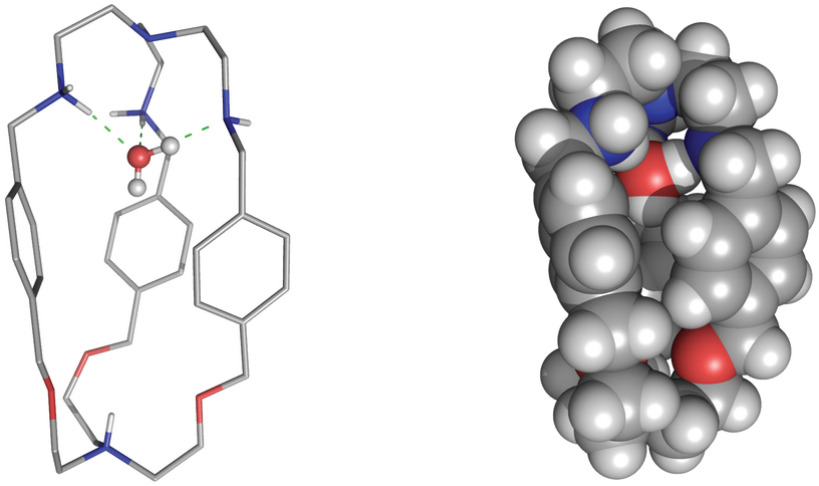

(a) (b)

Figure 7.3 Perspective views illustrating different structural features in the associated entity formed between $H_3t_2pN_5O_3^{3+}$ and a water molecule: (a) view showing the water molecule inserted into the receptor cavity, with only the amine and water molecule protons shown; (b) space-filling view emphasizing the tight encapsulation of water into the cage. Molecular diagrams presented are drawn with PyMOL.[26]

7.3.2.2 Binding affinity of the protonated forms of $btpN_4O_3$ towards amino acids

The association constants of the protonated forms of $btpN_4O_3$ with several amino acids were determined by potentiometry in H_2O/MeOH (50:50 v/v) solution at 298.2 K and 0.10 mol dm^{-3} NMe_4TsO. The values are collected in Table 7.2. The protonation constants of the amino acids were also determined in the same experimental conditions and used in the calculations (Table A7.1 in Appendix).

The protonated forms of $btpN_4O_3$ show only modest association constants for the binding of the studied amino acids. Only species of 1:1 receptor to substrate stoichiometry were found for the different protonation states of the receptor. The low affinity observed is probably a consequence of the high energetic cost of desolvation of the substrates and of the close proximity of the anionic and cationic functionalities, which mutually attenuates their respective charges, thus

lowering the effectiveness of charged receptors.[27] It is also possible that the ammonium binding sites of the receptor cause some repulsion on the ammonium group of the substrates, disfavouring the movement of the amino acids towards the receptor. In fact in the few examples of zwitterionic binding by synthetic receptors in water[5] or mixed MeOH/H_2O[4-7] the reported association constants (*K)* are in the range 17–360. These values are lower than the ones obtained in this work.

Table 7.2 Stepwise association constants ($K_{H_hL_lA_a}$) for the indicated equilibria involving $H_nbtpN_4O_3^{n+}$ and Hgly, Hbala, Htau, Hgaba, H_2amp and H_2aep in H_2O/MeOH (50:50 v/v).[a],[b],[c]

Equilibrium[d]	gly^-	$bala^-$	tau^-	$gaba^-$	amp^{2-}	aep^{2-}
$H_3L + H_2A \rightleftharpoons H_5LA$	–	–	–	–	676(1)	491(1)
$H_2L + H_2A \rightleftharpoons H_4LA$	–	–	–	–	–	748(1)
$H_3L + HA \rightleftharpoons H_4LA$	84(1)	105(1)	471(1)	43(1)	1622(1)	–
$H_2L + HA \rightleftharpoons H_3LA$	123(1)	101(1)	354(1)	54(1)	611(1)	521(1)
$HL + HA \rightleftharpoons H_2LA$	129(1)	154(1)	258(1)	67(1)	485(1)	433(1)
$L + HA \rightleftharpoons HLA$	182(1)	155(1)	–	82(1)	414(1)	275(1)
$HL + A \rightleftharpoons HLA$	–	–	492(1)	–	–	–

[a] T = (298.2±0.1) K; I = (0.10±0.01) mol dm^{-3} in NMe_4TsO. [b] Values in parenthesis are standard deviations in the last significant figures. [c] Values of the overall association constants are presented in Table A7.2 in appendix. [d] L denotes the $btpN_4O_3$ compound and A the amino acid in the completely deprotonated form. Charges where omitted for simplicity.

The plot of the K_{eff} versus pH[28] for the association of $H_nbtpN_4O_3^{n+}$ with the amino acid substrates is shown in Figure 7.4. For pH values below 6.2, where the receptor is mainly in the triprotonated form and the substrates are all in their zwitterionic form, the selectivity trend for the studied amino acids is H_2amp > H_2aep ≈ Htau > Hbala ≈ Hgly > Hgaba (Figure 7.4). Interestingly, the receptor has lower affinity for amino acids containing a carboxylate group than for amino acids with a tetrahedral anionic group. This suggests that the latter are preferred due to the 3-fold symmetry of their anionic group which should be complementary to the tren subunit of the cryptand[29] and possibly due to the formation of a higher number of hydrogen bonds.

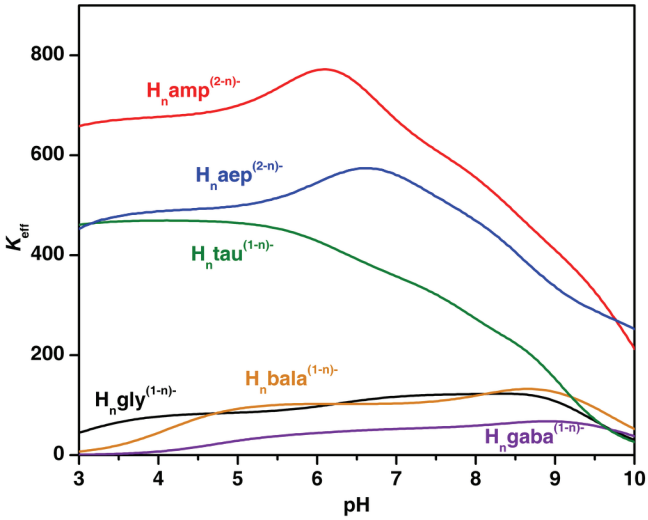

Figure 7.4 Plot of the K_{eff} *versus* pH for the associations formed between the indicated amino acids and $H_nbtpN_4O_3^{n+}$.

7.4 Conclusions

Two polyazapolyoxa heteroditopic macrobicyclic compounds, $btpN_4O_3$ and $t_2pN_5O_3$, were synthesized in moderate to good yields through a [1+1] "tripod-tripod coupling" strategy to be used as receptors for the recognition of amino acids.

The results of the acid-base properties studies revealed that below pH ≈ 6.2 $btpN_4O_3$ has a compartment with three protonated amines to interact with the anionic group of the amino acids while the other compartment has three ether oxygen atoms available to accept hydrogen bonds from the ammonium group of the substrates and an aromatic unit for the establishment of cation-π interactions. However the binding studies showed relatively modest association constants between the protonated receptor and the amino acid substrates (1.63–3.21 log units), although they are the best values in comparison with reported ones determined in identical experimental conditions. Interestingly, the receptor has a preference for amino acids containing a tetrahedral anionic group possibly due to the 3-fold symmetry of their anionic moiety, complementary to the tren subunit of the cryptand.

Due to its acid-base properties $t_2pN_5O_3$ is not appropriate for amino acid binding because its polyether compartment is susceptible to protonation and should repel the ammonium group of the substrates.

7.5 Experimental

7.5.1. General considerations

All solvents and chemicals were commercially purchased reagent grade quality and used as supplied without further purification. (4-diethoxymethylphenyl)methanol and 1,3,5-tris(bromomethyl)-2,4,6-triethylbenzene were prepared according to literature methods.[30,31] Tetramethylammonium *p*-toluenesulfonate (NMe_4TsO) was prepared by the neutralization of HTsO with NMe_4OH in water, followed by recrystallization from acetone. NMR spectra used for characterization of products were recorded on a Bruker Avance 400 instrument. TMS was used as reference for the ^{1}H-NMR measurements in $CDCl_3$. Peak assignments are based on peak integration and multiplicity for 1D ^{1}H spectra and on 2D COSY, NOESY and HMQC experiments (Figures A7.1–A7.20 in Appendix). Microanalyses were carried out by the ITQB Microanalytical Service.

7.5.2. Synthesis

7.5.2.1 4-(bromomethyl)benzaldehyde

A mixture of (4-diethoxymethylphenyl)methanol (2.447 g, 11.6 mmol) and HBr 65% (65 cm^3) was refluxed for 1 h. The solution was cooled to r.t. and extracted with CH_2Cl_2 (100 cm^3). The organic phase was washed with saturated solution of $NaHCO_3$, dried over anhydrous sodium sulfate, filtered and evaporated to dryness, yielding 4-(bromomethyl)benzaldehyde (2.190 g, 95%) which was used without purification in the next step. δ_H (400 MHz; $CDCl_3$; 298 K; Me_4Si) 4.45 (6 H, s, BrC*H*$_2$*p*-xylyl), 7.49 (6 H, d, *J* = 8.0 Hz, *H2*/*H6* of *p*-xylyl), 7.80 (6 H, d, *J* = 8.0 Hz, *H3*/*H5* of *p*-xylyl) and 9.95 (3 H, s, *H*C=O) ppm; δ_C(100 MHz; $CDCl_3$; 298 K;

Me_4Si) 32.10 (Br*C*H_2*p*-xylyl), 129.82 (C2/*C6* of *p*-xylyl), 130.31 (*C3*/*C5* of *p*-xylyl), 136.26 (*C4* of *p*-xylyl), 144.39 (*C1* of *p*-xylyl), 191.64 (*C*=O) ppm.

7.5.2.2 2-(4-bromomethyl-phenyl)-5,5-dimethyl-[1,3]dioxane

A mixture containing 4-(bromomethyl)benzaldehyde (2.190 g, 11 mmol), 2,2-dimethyl-1,3-propanediol (2.293 g, 22 mmol) and toluenesulfonic acid (7 mg) in toluene (13 cm^3) was heated to reflux for 4 h and the azeotrope of water was received in a Dean–Stark trap. The solution was allowed to cool to r.t. and the solvent was evaporated to dryness. The compound was purified by dry column vacuum chromatography using n-hexane/ethyl acetate (9:1) as eluent to yield the desired compound (2.767 g, 88%) δ_H (400 MHz; $CDCl_3$; 298 K; TMS): 0.73 (3 H, s, C*H*$_3$), 1.21 (3 H, s, C*H*$_3$), 3.58 (2 H, d, ^3J (H,H) = 12.0 Hz, C*H*$_2$), 3.70 (2 H, d, ^3J (H,H) = 12.0 Hz, C*H*$_2$), 4.41 (6 H, s, BrC*H*$_2$*p*-xylyl), 5.31 (1 H, s, C*H*), 7.32 (2 H, d, ^3J (H,H) = 8.0 Hz, *H2*/*H6* of *p*-xylyl), 7.41 (2 H, d, ^3J (H,H) = 8.0 Hz, *H3*/*H5* of *p*-xylyl) ppm; δ_C(100 MHz; $CDCl_3$; 298 K; Me_4Si) 22.02 (*C*H$_3$), 23.17 (*C*H$_3$), 30.38 (*C*(CH$_3$)$_2$), 33.27 (Br*C*H$_2$*p*-xylyl), 77.80 (O*C*H$_2$), 101.35 (*C*H), 126.77 (*C3*/*C5* of *p*-xylyl), 129.17 (*C2*/*C6* of *p*-xylyl), 138.47 (*C1* of *p*-xylyl), 138.87 (*C4* of *p*-xylyl).

7.5.2.3 Tripodal trialdehyde (3)

To a solution of (4-diethoxymethylphenyl)methanol (2.40 g, 11.4 mmol) in dry DMSO (30 cm^3) was added NaH (60% dispersion in oil) (456 mg, 11.4 mmol) under nitrogen. The temperature was raised to 90 ºC and left stirring until bubbling ceased and a clear brown solution was obtained. Then 1,3,5-tris(bromomethyl)-2,4,6-triethylbenzene (1.640 g, 3.7 mmol) was added in one portion and the solution was left stirring at 90 ºC for 3 hours. The solution was allowed to cool to r.t., poured into water (80 cm^3) and extracted with $CHCl_3$ (5×50 cm^3). The organic portions were collected in an Erlenmeyer flask, dried over anhydrous sodium sulfate, filtered and evaporated to dryness. The solid was dissolved in CH_2Cl_2 (25 cm^3) to which water (25 cm^3) and CF_3COOH 99% (25 cm^3) was added. The mixture was vigorously stirred overnight.

The mixture was transferred to a separating funnel and the aqueous phase was rejected. The organic portion was then washed with $NaHCO_3$ saturated solution (3×30 cm^3), dried over anhydrous sodium sulfate, filtered and evaporated to dryness to give the crude tripodal trialdehyde as a yellow viscous oil which solidified after drying in a vacuum line. The product was purified by dissolving a minimum amount in boiling ethyl acetate, and then n-hexane was added until the solution became turbid. After cooling the precipitate formed was filtered and dried in vacuum, yielding pure tripodal trialdehyde (**3**) (1.413 g, 61%). δ_H (400 MHz; $CDCl_3$; 298 K; TMS): 1.07 (t, ^3J (H,H) = 8.0 Hz, 9 H; bz$CH_2C\mathit{H}_3$), 2.73 (q, ^3J (H,H) = 8.0 Hz, 6 H; bz$C\mathit{H}_2CH_3$), 4.51 (s, 6 H; $C\mathit{H}_2$bz), 4.63 (6 H, s, $C\mathit{H}_2$*p*-xylyl), 7.47 (6 H, d, ^3J (H,H) = 8.0 Hz, *H2*/*H6* of *p*-xylyl), 7.79 (6 H, d, ^3J (H,H) = 8.0 Hz, *H3*/*H5* of *p*-xylyl) and 9.94 (3 H, s, *H*C=O) ppm; δ_C(100 MHz; $CDCl_3$; 298 K; Me_4Si) 16.68 ppm (bz$CH_2\mathit{C}H_3$), 23.02 (bz$\mathit{C}H_2CH_3$), 67.06 ($\mathit{C}H_2$bz), 77.49 ($\mathit{C}H_2$*p*-xylyl), 128.25 (C2/*C6* of *p*-xylyl), 129.99 (*C3*/*C5* of *p*-xylyl), 131.89 (*C2*/*C4*/*C6* of bz), 135.94 (*C4* of *p*-xylyl), 145.45 (*C1*/*C3*/*C5* of bz), 145.53 (*C1* of *p*-xylyl), 192.13 (*C*=O) ppm.

7.5.2.4 btpN_4O_3

A boiling solution of the tripodal trialdehyde (**3**) (174 mg, 0.29 mmol) in MeCN (20 cm^3) was quickly added to a refluxing solution of tren (44 mg, 0.29 mmol) in MeCN (500 cm^3) under nitrogen and left stirring for 1 hour. The solution was concentrated to a third of its volume and MeOH (350 cm^3) was added. To this solid $NaBH_4$ (320 mg, 8.46 mmol) was added in small portions to avoid excessive foaming. After the addition was completed, the mixture was left under stirring at r.t. for 1 hour, and under reflux for 2 hours. The solution was evaporated under vacuum to dryness, then water (20 cm^3) was added. The solution was made strongly basic with 6 mol dm^{-3} KOH and extracted with $CHCl_3$ (3×50 cm^3). The organic portions were collected in an Erlenmeyer flask, dried over anhydrous sodium sulfate, filtered off, evaporated to dryness to give the crude btpN_4O_3 (177 mg). The product was purified by flash column chromatography using $CHCl_3$/MeOH/NH_3(aq) (90:9:1) as eluent, followed by recrystallization from MeCN

to yield pure $btpN_4O_3$ (80 mg, 40%); δ_H (400 MHz; $CDCl_3$; 298 K; TMS): 1.11 (9 H, t, ^3J (H,H) = 8.0 Hz, $bzCH_2CH_3$), 1.19 (3H, br s, N–*H*), 2.44 (6 H, t, ^3J (H,H) = 4.0 Hz, NCH_2CH_2NH), 2.52 (6 H, t, ^3J (H,H) = 4.0 Hz, NCH_2CH_2NH), 3.09 (6 H, q, ^3J (H,H) = 8.0 Hz, $bzCH_2CH_3$), 3.34 (6 H, s, $NHCH_2$*p*-xylyl), 4.34 (6 H, s, *p*-xylylCH_2O), 4.75 (6 H, s, OCH_2bz), 6.64 (6 H, d, ^3J (H,H) = 8.0 Hz, *H3*/*H5* of *p*-xylyl), 6.78 (6 H, d, ^3J (H,H) = 8.0 Hz, *H2*/*H6* of *p*-xylyl); δ_C (100 MHz; $CDCl_3$; 298 K; Me_4Si) 16.93 ($bzCH_2CH_3$), 22.72 ($bzCH_2CH_3$), 48.22 (NCH_2CH_2NH), 55.13 (NCH_2CH_2NH), 55.54 ($NHCH_2$*p*-xylyl), 65.17 (OCH_2bz), 69.71 (*p*-xylylCH_2O), 128.31 (*C3*/*C5* of *p*-xylyl), 128.42 (*C2*/*C6* of *p*-xylyl), 131.75 (*C2*/*C4*/*C6* of bz), 137.33 (*C4* of *p*-xylyl), 139.74 (*C1* of *p*-xylyl), 145.92 (*C1*/*C3*/*C5* of bz) ppm; m/z (ESI–MS;MeOH) 705.1 $[M+H]^+$.; elemental analysis calcd (%) for $C_{45}H_{60}N_4O_3$: C 76.67, H 8.58, N 7.95; found: C 77.00, H 8.59, N 8.04.

7.5.2.5 Tripodal trialdehyde (6)

To a solution of triethanolamine (388 mg, 2.6 mmol) in dry THF (8 cm^3) was added NaH (60% dispersion in oil) (312 mg, 7.8 mmol) under nitrogen. When bubbling ceased, 2-(4-bromomethyl-phenyl)-5,5-dimethyl-[1,3]dioxane (2.280 g, 8.0 mmol) dissolved in dry THF/DMF 3:1 mixture (32 cm^3) was added during 30 min. The solution was left stirring for 24 h. The solution was poured into water (100 cm^3) and extracted with CH_2Cl_2 (3×100 cm^3). The organic portions were washed with water (3×100 cm^3) and brine (100 cm^3), collected in an Erlenmeyer flask, dried over anhydrous sodium sulfate, filtered and evaporated to dryness. The solid was dissolved in CH_2Cl_2 (100 cm^3) to which water (100 cm^3) and CF_3COOH 99% (100 cm^3) was added. The mixture was left stirring for three days at 40 ºC. The mixture was transferred to a separating funnel and the aqueous phase was rejected. The organic portion was then washed with $NaHCO_3$ saturated solution (3×100 cm^3), dried over anhydrous sodium sulfate, filtered and evaporated to dryness to give the tripodal trialdehyde (**6**) (1.178 g, 90%) which was used without purification in the next step. δ_H (400 MHz; $CDCl_3$; 298 K; TMS): 2.83 (6 H, t, ^3J (H,H) = 4.0 Hz, NCH_2CH_2NH), 3.54 (6 H, t, ^3J (H,H) = 4.0 Hz, NCH_2CH_2NH), 4.51 (6 H, s, CH_2*p*-xylyl), 7.40 (6 H, d, ^3J (H,H) = 8.0 Hz, *H2*/*H6* of

p-xylyl), 7.76 (6 H, d, ^3J (H,H) = 8.0 Hz, *H3*/*H5* of *p*-xylyl) and 9.92 (3 H, s, *H*C=O) ppm; δ_C(100 MHz; $CDCl_3$; 298 K; Me_4Si) 54.93 (N*C*H_2CH_2O), 69.64 (NCH_2*C*H_2O), 77.60 (O*C*H_2*p*-xylyl), 127.69 (C2/*C6* of *p*-xylyl), 129.98 (*C3*/*C5* of *p*-xylyl), 135.85 (*C4* of *p*-xylyl), 145.71 (*C1* of *p*-xylyl), 192.04 (*C*=O) ppm.

7.5.2.6 $t_2pN_5O_3$

A solution of tren (220 mg, 1.5 mmol) in MeCN (60 cm^3) was added dropwise over 20 minutes to a magnetically stirred solution of the tripodal trialdehyde (**6**) (758 mg, 1.5 mmol) in MeCN (200 cm^3). The mixture was left under stirring overnight. The solvent was evaporated to dryness, the product was redissolved in MeOH (80 cm^3) and solid $NaBH_4$ (1.7 g, 45 mmol) was added in small portions. After the addition was completed, the mixture was left under stirring at r.t. for two hours, and under reflux overnight. The solution was allowed to cool to r.t., filtered and evaporated under vacuum almost to dryness, then water (20 cm^3) was added and the entire methanol was evaporated. The solution was made strongly basic with 6 mol dm^{-3} KOH and extracted with $CHCl_3$ (3×50 cm^3). The organic portions were collected in an Erlenmeyer flask, dried over anhydrous sodium sulfate, filtered off and evaporated to dryness. The crude product was recristallized from n-hexane to give pure $t_2pN_5O_3$ (535 mg, 60%) as a white solid; δ_H (400 MHz; $CDCl_3$; 298 K; Me_4Si): 1.58 (3 H, br s, N–*H*), 2.56 (6 H, t, ^3J (H,H) = 4.0 Hz, NCH_2CH_2NH), 2.69 (6 H, t, ^3J (H,H) = 4.0 Hz, NCH_2CH_2NH), 2.71 (6 H, t, ^3J (H,H) = 4.0 Hz, NCH_2CH_2O), 3.53 (6 H, s, NHCH_2*p*-xylyl), 3.59 (6 H, t, ^3J (H,H) = 4.0 Hz, NCH_2CH_2O), 4.50 (6 H, s, *p*-xylylCH_2O), 6.78 (6 H, d, ^3J (H,H) = 8.0 Hz, *H3*/*H5* of *p*-xylyl), 7.02 (6 H, d, ^3J (H,H) = 8.0 Hz, *H2*/*H6* of *p*-xylyl); δ_C (100 MHz; $CDCl_3$; 298 K; Me_4Si) 48.13 (N*C*H_2CH_2O), 54.15 (N*C*H_2CH_2NH), 54.62 (NH*C*H_2*p*-xylyl), 55.67 (NCH_2*C*H_2NH), 68.66 (NCH_2*C*H_2O), 73.09 (*p*-xylyl*C*H_2O), 127.55 (*C2*/*C6* of *p*-xylyl), 127.78 (*C3*/*C5* of *p*-xylyl) 137.35 (*C4* of *p*-xylyl), 139.11 (*C1* of *p*-xylyl); ESI–MS (MeOH) m/z: 602.3 $[M+H]^+$; elemental analysis calcd. (%) for $C_{36}H_{51}N_5O_3$: C 71.85, H 8.58, N 11.64; found: C 71.80, H 8.60, N 11.73.

7.5.2.7 Crystals of $btpN_4O_3$·MeCN

The cryptand $btpN_4O_3$ (5.0 mg, 7.1 μmol) was dissolved in the minimum amount of hot MeCN then the mixture was allowed to slowly cool to r.t. Single colourless crystals suitable for X-ray crystallographic determination were obtained overnight.

7.5.2.8 Crystals of $[H_3t_2pN_5O_3(H_2O)]Cl_3$·7($H_2O$)

The cryptand $t_2pN_5O_3$ (5.0 mg, 8.3 μmol) was dissolved in acetone (0.2 cm^3) and 37% HCl (2×10^{-3} cm^3) was added. Immediately a white precipitate was formed. Water (2×10^{-2} cm^3) was added and the solution heated until it was clear, then the mixture was allowed to slowly cool to r.t. Single colourless crystals suitable for X-ray crystallographic determination were obtained overnight.

7.5.3. Potentiometric measurements

7.5.3.1 Reagents and solutions

All solutions were prepared in water/methanol (50:50 v/v) mixed solvent. A stock solution of the receptor was prepared at *ca*. 2.0×10^{-3} mol dm^{-3}. Solutions of the substrates were prepared at 0.025 mol dm^{-3} and the concentrations were checked by titration with standard 0.1 mol dm^{-3} NMe_4OH solutions. Carbonate-free solutions of the titrant NMe_4OH were obtained at *ca.* 0.1 mol dm^{-3} by treating freshly prepared silver oxide with a 500 cm^3 solution of NMe_4I, under nitrogen atmosphere and in appropriate glass apparatus according to the method of Schwarzenbach and Biederman,[32] to which 500 cm^3 of methanol was added. These solutions were discarded every time carbonate concentration was about 0.5% of the total amount of base. The titrant solutions were standardized (tested by Gran's method).[33]

7.5.3.2 Equipment and working conditions

The equipment used was described in Chapter 2. The ionic strength of the experimental solutions was kept at 0.10±0.01 M with NMe_4TsO, and the temperature was maintained at 298.2±0.1 K. Atmospheric CO_2 was excluded from the titration cell during experiments by passing purified nitrogen across the top of the experimental solution. The glass electrode was pre-treated by soaking it in the water–methanol (50:50 v/v) solution over a period of 2 days, in order to prevent erratic responses.

7.5.3.3 Measurements

The $[H^+]$ of the solutions was determined by the measurement of the electromotive force of the cell, $E = E^{o\prime} + Q \log [H^+] + E_j$. The term pH is defined as $-\log [H^+]$. $E^{o\prime}$, Q, E_j and K_w were determined by titration of a solution of known hydrogen-ion concentration at the same ionic strength, using the acid pH range of the titration. The liquid-junction potential, E_j, was found to be negligible under the experimental conditions used. The value of K_w was determined from data obtained in the alkaline range of the titration, considering $E^{o\prime}$ and Q valid for the entire pH range and found to be equal to $10^{-13.91}$ in our experimental conditions. Before and after each set of titrations the glass electrode was calibrated by titration of 1.00×10^{-3} mol dm^{-3} standard HCl solution with standard NMe_4OH. The potentiometric equilibrium measurements were carried out using 20.00 cm^3 of $\approx$ 2.00×10^{-3} mol dm^{-3} of the receptor stock solution diluted to a final volume of 40.00 cm^3, in the absence of anions, then in the presence of each amino acid at 1:3 R:A ratios (R = receptor and A = amino acid). In each titration 85 to 140 points were collected, and a minimum of two titration curves were performed. Care has been taken to maintain unaltered the methanol–water ratio in measured solution. The exact concentration of the receptors was obtained by determination of the excess of acid present in a mixture of the receptors and a known amount of standard *p*-toluenesulfonic acid by titration with standard NMe_4OH solution.

7.5.3.4 Calculation of equilibrium constants

Overall protonation constants, β_i^H, of ligands and anions, were calculated by fitting the potentiometric data obtained for all the performed titrations in the same experimental conditions with the HYPERQUAD program.[34] All these constants were taken as fixed values to obtain the equilibrium constants of the new species from the experimental data corresponding to all the titrations at 1:3 R:A ratio, also using the HYPERQUAD program. The initial computations were obtained in the form of overall stability constants, $\beta_{H_hL_lA_a}$ values, $\beta_{H_hL_lA_a} = [H_hL_lA_a]/[H]^h[L]^l[A]^a$. The errors quoted are the standard deviations of the overall association constants given directly by the program for the input data, which include all the experimental points of all titration curves. The HYSS program[35] was used to calculate the concentration of equilibrium species from the calculated constants from which distribution diagrams were plotted. The species considered in a particular model were those that could be justified by the principles of supramolecular chemistry.

7.6 Acknowledgements

The NMR spectrometers are part of the National NMR Network and were purchased in the framework of the National Program for Scientific Re-equipment, contract REDE/1517/RMN/2005, with funds from POCI 2010 (FEDER) and Fundação para a Ciência e a Tecnologia (FCT). M. C. Almeida from the Elemental Analysis and Mass Spectrometry Service at the ITQB is acknowledged for providing elemental analysis and ESI-MS data. Pedro Mateus thanks FCT for the grant (SFRH/BD/36159/2007).

7.7 References

[1] J. M. Berg, J. L. Tymoczko, L. Stryer, *Biochemistry*, 5th Ed., W. H. Freeman & Co Ltd, New York, **2002**.

[2] J. W. Steed, J. L. Atwood, *Supramolecular Chemistry*, 2nd Ed., John Wiley and Sons, Ltd, Hoboken, **2009.**

[3] J. L. Sessler, A. Andrievsky, *Chem. Eur. J.* **1998**, *4*, 159–167, and references therein.

[4] F. P. Schmidtchen, *J. Org. Chem.* **1986**, *51*, 5161–5168

[5] E. Kimura, H. Fujioka, M. Kodama, *J. Chem. Soc., Chem. Commun.* **1986**, 1158–1159.
[6] A. P. de Silva, H. Q. N. Gunaratne, C. McVeigh, G. E. M. Maguire, P. R. S. Maxwell, E. O'Hanlon, *Chem. Commun.* **1996**, 2191–2192.
[7] S.-i. Sasaki, A. Hashizume, D. Citterio, E. Fujiia, K. Suzukia, *Tetrahedron Lett.* **2002**, *43*, 7243–7245.
[8] R. J. Fitzmaurice, G. M. Kyne, D. Douheret, J. D. Kilburn, *J. Chem. Soc., Perkin Trans. 1* **2002**, 841–864.
[9] S. O. Kang, J. M. Llinares, V. W. Day, K. Bowman-James*, Chem. Soc. Rev.* **2010**, *39*, 3980–4003.
[10] P. Mateus, N. Bernier, R. Delgado, *Coord. Chem. Rev*. **2010***, 254*, 1726–1747.
[11] S. O. Kang, M. A. Hossain, K. Bowman-James, *Coord. Chem. Rev.* **2006**, *250*, 3038–3052.
[12] V. McKee, J. Nelson, R. M. Town, *Chem. Soc. Rev.* **2003**, *32*, 309–325.
[13] C. Seel, F. Vögtle, *Angew. Chem. Int. Ed.* **1992**, *31* 528–549.
[14] R. Méric, J.-P. Vigneron, J.-M. Lehn, *J. Chem. Soc., Chem. Commun.* **1993**, 129–131.
[15] B. Dietrich, J.-P. Kintzinger, J.-M. Lehn, B. Metz, A. Zahidi, *J. Phys. Chem.* **1987**, *91*, 6600–6606.
[16] H.-J. Buschmann, E. Schollmeyer, L. Mutihac, *Thermochimica Acta* **1998**, *316*, 189–192.
[17] D. K. Chand, P. K. Bharadwaj, *Inorg. Chem.* **1996**, *35*, 3380–3387.
[18] D. K. Chand, P. K. Bharadwaj, *Tetrahedron* **1997**, *53*, 10517–10522.
[19] P. Ghosh, S. S. Gupta, P. K. Bharadwaj, *J. Chem. Soc., Dalton Trans.* **1997**, 935–938.
[20] M. C. Das, P. K. Bharadwaj, *Eur. J. Inorg. Chem.* **2007**, 1229–1232.
[21] M. C. Das, S. K. Ghosh, P. K. Bharadwaj, *Dalton Trans.* **2009**, 6496–6506.
[22] M. C. Das, S. K. Ghosh, P. K. Bharadwaj, *CrystEngComm*, **2010**, *12*, 413–419.
[23] M. C. Das, S. K. Ghosh, S. Sen, P. K. Bharadwaj, *CrystEngComm*, **2010**, *12*, 2967–2974.
[24] B. Dietrich, M. W. Hosseini, J.-M. Lehn, R. B. Sessions, Helv. Chim. Acta. 1985, 68, 289–299.
[25] The structure still requires a final refinement by Prof. Vítor Félix from the University of Aveiro.
[26] W. L. DeLano, The PyMOL Molecular Graphics System DeLano Scientific, San Carlos, CA, USA, 2002. http://www.pymol.org.
[27] J. Rebek, B. Askew, D. Nemeth, K. Parris, *J. Am. Chem. Soc.* **1987**, *109*, 2432–2434.
[28] M. T. Albelda; M. A. Bernardo, E. Garcia-España, M. L. Godino-Salido, S. V. Luis, M. J. Melo, F. Pina, C. Soriano, *J. Chem. Soc., Perkin Trans. 2* **1999**, 2545–2549.
[29] C. Bazzicalupi, A. Bencini, A. Bianchi, A. Danesi, C. Giorgi, B. Valtancoli, *Inorg. Chem.* **2009**, *48*, 2391–2398.
[30] P. Sarri, F. Venturi, F. Cuda, S. Roelens, *J. Org. Chem.* **2004**, *69*, 3654–3661.
[31] K. J. Wallace, R. Hanes, E. V. Anslyn, J. Morey, K. V. Kilway, J. Siegel, *Synthesis* **2005**, 2080–2083.
[32] G. Schwarzenbach, W. Biederman, *Helv. Chim. Acta* **1948**, *31*, 311–340.
[33] F. J. Rossotti, H. J. Rossotti, *J. Chem. Educ.* **1965**, *42*, 375–378.
[34] P. Gans, A. Sabatini, A. Vacca, *Talanta* **1996**, *43*, 1739–1753.
[35] L. Alderighi, P. Gans, A. Ienco, D. Peters, A. Sabatini, A. Vacca, *Coord. Chem. Rev.* **1999**, *184*, 311–318.

Chapter 8

Final Conclusions

8.1 Final Conclusions

Macrobicyclic polyamines have been prominent compounds since the very beginning of the anion recognition field. However, although this family of compounds have proved to be particularly versatile and possess very interesting anion binding properties, the reported cases of true selectivity, are scarce. This means that there is still much work to be done to perfect the macrobicyclic architecture.

Throughout the research of this work different types of binding sites where introduced in the macrobicyclic architecture in conjunction of slight structural changes aiming to create new and improved anion receptors.

In Chapter 2 solution studies revealed that the receptor xyl is remarkably selective for dinegative anions over mononegative ones at pH values below 5. In fact, in this pH region, the protonated receptor is able to exclusively bind any of the dinegative anions in the presence of equimolar amounts of all the mononegative ones. SO_4^{2-}, SeO_4^{2-} and $S_2O_3^{2-}$ have the same charge, geometry and about the same size thus the receptor is unable to discriminate them. This was not surprising as even Nature cannot perform this task. The potentiometric studies revealed that the main interactions are of electrostatic nature although contributions of hydrogen bonding play an important role. The importance of hydrogen bonds was highlighted by the fact that when the receptor is fully protonated it lacks hydrogen bond acceptors for dihydrogen phosphate OH groups, which accounts for the low association constant found for $[(H_6xyl)(H_2PO_4)]^{5+}$, resembling the sulfate binding protein.

Since the xyl compound is a 2,4,6-triethylbenzene derived analogue of the tren derived cryptand **12** (Scheme 1.17, Chapter 1) it would be interesting to compare their binding behaviour and evaluate if the rigidification of the macrobicyclic structure indeed yield higher preorganization and enhanced affinity and selectivity. However the xyl compound was found to be too lipophilic and its solution properties could only be determined in H_2O/MeOH (50:50 v/v) solution whereas $H_n\mathbf{12}^{n+}$ was studied in pure water. Therefore direct comparison of these

two compounds cannot be performed since the media are of different polarity and this can severely affect the binding process (see Section 1.2.3, Chapter 1). In addition, and further complicating the comparison of the two compounds, the association constants of H_n**12**$^{n+}$ with anions are scarce and discrepant values are found in the literature.

Among the mononegative anions, only the interaction of F^-,[1] NO_3^- [2-4] and ClO_4^- [2] with H_n**12**$^{n+}$ have been studied. The association constant between ClO_4^- and H_6**12**$^{6+}$ was found to be 3.25 log units, while for NO_3^-, there are several reported association constants of 3.02,[4] 3.11[3] and 3.73[2] log units. These values are about 1.5 log units higher than those found for xyl even though the latter was studied in a somewhat less polar medium and consequently less competive. This suggests that $H_n$xyl^{n+} being more rigid does not adapt to the stereochemical requirements of these anions as easily as H_n**12**$^{n+}$.

Comparison of the SO_4^{2-} binding ability of $H_n$xyl^{n+} and H_n**12**$^{n+}$ is problematic as there are two different sets of association constant values with H_n**12**$^{n+}$, obtained in the same medium, reported by Nelson *et al.*[5] and Bowman-James *et al.*[3] The latter authors have determined log $K_{[H_6\mathbf{12}(SO_4)]}$ = 4.43 hence the receptor does not show any particular selectivity for SO_4^{2-} over NO_3^- and ClO_4^-.[3] On the other hand, Nelson *et al.* reported very high association constants for dinegative tetrahedral anions such as SO_4^{2-}, SeO_4^{2-} and $S_2O_3^{2-}$ of 6.57, 7.24 and 8.51 log units, respectively.[5] The log *K* value of 6.57 for the formation of $[H_6\mathbf{12}SO_4]^{4+}$ is much higher than that reported for the association with NO_3^- and ClO_4^-. Considering this value correct, one would conclude that the cryptand is highly selective for SO_4^{2-} over NO_3^- and ClO_4^-. Unfortunately, without additional experimental work, it is impossible to choose one of the values.

Nonetheless, it is odd that Bowman-James *et al.* found a heptaprotonated form of **12**, not found in any other tren derived cryptand described in Chapter 1 nor in tren itself,[6] and that it binds SO_4^{2-} by only 0.54 log units stronger than does the hexaprotonated form. It is also unexpected that Nelson *et al.* found that the H_6**12**$^{6+}$ species binds SO_4^{2-} 1.85 log units stronger than the H_5**12**$^{5+}$ form does. The first difference seems too small and the second too large as, for instance,

studies of $H_n\mathbf{5}^{n+}$ with SO_4^{2-} [7] revealed that $H_7\mathbf{5}^{7+}$ binds SO_4^{2-} 1.40 log units stronger than $H_6\mathbf{5}^{6+}$ and $H_6\mathbf{5}^{6+}$ binds the same anion 1.00 log units stronger than $H_5\mathbf{5}^{5+}$.

It is reasonable to assume that the log *K* value for the association of $H_6\mathbf{12}^{6+}$ with SO_4^{2-} is somewhere between 4.43 and 6.57. This would mean that it is of the same order of magnitude as that found for H_6xyl^{6+} and because the latter was studied in a somewhat less competitive medium its affinity towards SO_4^{2-} is probably slightly lower than that of $H_6\mathbf{12}^{6+}$. In Chapter 2 it was shown by ^{1}H-NMR studies that there is a rearrangement of the receptor upon binding, probably the rotation of the protonated amines to the inside of the cavity. Thus it seems that the receptor is not sufficiently preorganized. Its is reasonable to assume that $H_6\mathbf{12}^{6+}$ also requires such rearrangement however in this case the energetic cost should be lower due to the receptor higher flexibility. This should account for the somewhat higher association constant observed relative to H_6xyl^{6+}, however it should also lead to decreased selectivity due to a easier adaptation of the receptor to any substrate. It seems that H_nxyl^{n+} has more difficulty in rearranging its structure to adapt to NO_3^- and ClO_4^- than $H_n\mathbf{12}^{n+}$ therefore it would not be surprising if xyl is more selective. Unfortunately due to the reasons stated before it is not possible to determine exactly which receptor has the highest selectivity for SO_4^{2-} over NO_3^- and ClO_4^-.

The study described in Chapter 6 gave further insight on whether rigidification of the macrobicyclic structure indeed yields higher preorganization and enhanced selectivity. The binding properties of the protonated forms of two closely related polyamine cryptands, $btpN_7$ and t_2pN_8 (cryptand **14** in Scheme 1.17, Chapter 1), towards dicarboxylate substrates were studied in the same aqueous medium. By studying these two compounds the influence of the 2,4,6-triethylbenzene head unit in the binding properties and selectivity pattern was evaluated. Solution studies showed that $H_nbtpN_7^{n+}$ and $H_nt_2pN_8^{n+}$ are able to strongly bind dicarboxylate substrates in highly competitive aqueous medium. The $H_nt_2pN_8^{n+}$ receptor exhibited much higher affinity towards dicarboxylates than the structurally similar $H_nbtpN_7^{n+}$, however their selectivity pattern is nearly identical.

The identical selectivity pattern results from the fact that the two binding subunits in both compounds are separated by the same distance, defined by the *p*-xylyl spacer, yielding two identical cavities in terms of size, shape and number of binding units, which means that the enthalpy of binding of a given substrate, which arises mainly from electrostatic attraction and hydrogen bond formation, should be very similar in both receptors. Considering that the enthalpy of the binding process is roughly the same in both receptors, the large difference in affinity towards dicarboxylates between $H_nbtpN_7^{n+}$ and $H_nt_2pN_8^{n+}$ must have entropic origin and be related with the entropic cost of conformational rearrangement and entropic gain of desolvation. In this view the 2,4,6-triethylbenzene cap of $H_nbtpN_7^{n+}$ is probably responsible for a more costly conformational rearrangement.

From the results discussed above it appears that the 2,4,6-triethylbenzene cap does not sufficiently preorganize the receptors. There is still a necessity for rearrangement of the structure upon binding due to the fact that in the unbound form of the receptors the ammonium groups tend to move away from each other to minimize electrostatic repulsions. Thus it turns out that the rigidity of the 2,4,6-triethylbenzene cap is in fact contributing to a lowering of the association constants. Rigidity can only result in increased affinity if the receptor is sufficiently preorganized in such a way that no rearrangement is necessary upon binding.

Introducing a change in the macrobicyclic architecture as small as the replacement of a C-H fragment for a nitrogen atom in the spacers (*m*-xylyl to pyridine) yields significant changes in the selectivity pattern of a receptor and even allowed it to coordinate metal ions forming complexes that also can act as receptors for anions but with binding properties quite different from the parent compound (Chapters 3 and 4).

The presence of hydrogen bond acceptors in H_npyr^{n+} allowed it to bind dihydrogen phosphate 1.73 log units stronger than H_nxyl^{n+} at pH 4.0. In addition, at that pH the receptor has an affinity for dihydrogen phosphate of the order of that of SO_4^{2-}, in spite of the higher charge of the latter anion. At higher pH values the affinity towards SO_4^{2-} dropped concomitantly with the decrease of the charge

and hydrogen donation ability of the receptor. In the case of hydrogen phosphate binding as the pH increases the anion has a higher charge which somewhat compensated the decrease of charge of the receptor. Moreover, as deprotonation of the receptor occurs, $–N^{+}–H\cdots^{-}O–$ hydrogen bonds becomes less important while those of type $–N–H\cdots^{-}O–$, –N–H···OH– and –N:···HO– are expected to dominate. This resulted in association constants for hydrogen phosphate that did not vary much in the entire pH region studied and at pH 7 the receptor became selective for phosphate.

The present study allowed concluding that, although H_npyr^{n+} is not as efficient in discriminating hydrogen phosphate from SO_4^{2-} as the PBP protein, it is to the best of our knowledge the artificial polyamine compound with the highest reported phosphate/sulfate selectivity in aqueous solutions at pH about 7.0.

The replacement of C-H fragment for a nitrogen atom in the spacers of xyl yielded a very versatile compound that not only binds inorganic anions with very interesting binding pattern and selectivity but also coordinates three copper(II) ions in its cavity. It should be noticed that xyl cannot coordinate metal ions at all. Unexpectedly, crystals of the trinuclear copper complex grown at pH ≈ 6, revealed the presence of carbonate (formed by spontaneous CO_2 uptake from air) bridging the three copper centres. Apparently, the ability of pyr to bring into close proximity three metal ions played a crucial role in lowering the pK_a of coordinated water molecules. This allowed hydroxo complexes to be formed in slightly acid medium that in turn permited CO_2 fixation to occur without need of high pH, resembling the carbonic anhydrase enzyme. The production of $[Cu_3pyr(\mu_3\text{-}CO_3)]^{4+}$ in presence of large amount of NO_3^-, indicated that carbonate bridging is preferred to NO_3^- in spite of the same geometry of both anions and the higher concentration of NO_3^- in solution. It was also found that the architecture of pyr is responsible for the interesting magnetic properties of $[Cu_3pyr(\mu_3\text{-}CO_3)]^{4+}$ observed.

On the other hand, the cryptand $btpN_7$ was designed to have two different binding compartments, separated by relatively long rigid spacers, in which one is appropriate for the coordination of copper(II) while the other head is available for

additional hydrogen bonding and electrostatic interactions with substrates. It was expected that such a cryptate would be suitable for interaction with dicarboxylates of varying chain length, and that it might be selective for the substrate with appropriate size to take full advantage of cooperativity between the copper site and the ammonium binding sites. Indeed, oxa^{2-} was shown to have the ideal size to take full advantage of the potential binding sites of the receptor. The qualitative study provided by the indicator-displacement assay, using pyrocatechol violet as the indicator, in excellent agreement with the potentiometric studies, demonstrated that the copper cryptate receptor can be used as a selective visual sensor of oxa^{2-}.

The $H_nbtpN_7^{n+}$ cryptand, in the absence of metal ion, is also able to bind dicarboxylate substrates in aqueous medium but showed a different selectivity pattern. Fum^{2-} appeared to have the right size, shape and rigidity to fit the cavity while mal^{2-}, suc^{2-}, glu^{2-} and $male^{2-}$ were bound less strongly, although the NMR studies suggested that the latter dianions can also be encapsulated. A less than perfect fit within the cavity possibly resulted in an amount of enthalpic gain which may not be enough to compensate the entropic cost of conformational rearrangement of the binding partners and may have resulted in insufficient desolvation entropy, contributing to lower association constants. Comparison between the association constants of fum^{2-} and suc^{2-}, higher for fum^{2-}, clearly showed that suc^{2-} requires additional conformational rearrangement due to its higher flexibility, resulting in a lower association constant. In addition it was found that $H_nbtpN_7^{n+}$ and $H_nt_2pN_8^{n+}$ showed selectivity for fum^{2-} over its *cis* isomer $male^{2-}$ at pH ≈ 4. This is to the best of our knowledge the first synthetic receptors that can effectively discriminate these *cis*/*trans* isomers in water, with a preference for fum^{2-}.

The high association constant for oxa^{2-} was somewhat puzzling as this dianion does not seem to be large enough to take advantage of the ditopic nature of $H_nbtpN_7^{n+}$ and $H_nt_2pN_8^{n+}$. The high association constant for oxa^{2-} should be related with its higher charge density, but it is also possible that the occurrence of water mediated hydrogen bonding[8,9] may compensate the smaller size of this

dianion. In fact there are several examples shown in this work where water mediated hydrogen bonding compensates the smaller size of the anion relative to the size of the receptor cavity. In Chapter 1, Figure 1.5b shows that mal^{2-} is too small to take advantage of the ditopic nature of the binding pocket of DctB, having only one of the carboxylate groups directly interacting with a positively charged arginine, while the other carboxylate is bound to two water molecules that mediate the hydrogen bonding networks between mal^{2-} and the protein. In Figure 1.15 (b and c) is shown that Cl^- and Br^- are too small to occupy the whole $H_nt_2pN_8^{n+}$ cavity and take advantage of both tren subunits, nevertheless they are encapsulated and held in place by water mediated hydrogen bonding. In Chapter 2, the crystal structure of the association of H_6xyl^{6+} with SO_4^{2-} (Figure 2.9) showed that four water molecules mediate hydrogen bonding between H_6xyl^{6+} and SO_4^{2-} suggesting that the molecular recognition of SO_4^{2-} involves multiple and cooperative hydrogen bonding interactions. Finally, in Chapter 3 the crystal structure of the association of H_6pyr^{6+} with NO_3^- (Figure 3.7) showed that the anion is too small to fit the cavity and is 1.25 Å deviated from the N_6 center of the cage establishing only three straight N–H···O hydrogen bonds while three water mediated hydrogen bonds help to keep NO_3^- held inside the cavity.

All these examples show that the solvent water has indeed a very important role in the binding process, on one hand it is a highly competitive entity and, on the other hand it can help in the stabilization of receptor-substrate interactions.

Amino acids are very important anion containing substrates for their role in many biochemical processes, and their recognition by synthetic receptors is one of the current challenges of Supramolecular Chemistry. In order to contribute to this subject, two polyoxapolyaza heteroditopic macrobicyclic compounds, $btpN_4O_3$ and $t_2pN_5O_3$, were designed to have cationic (ether groups) and anionic binding sites (ammonium groups) as parts of the macrobicyclic framework, separated by *p*-xylyl spacers. This was considered as a possible approach for binding α,ω- amino acid zwitterions in aqueous solution. Hence $btpN_4O_3$ and $t_2pN_5O_3$ were synthesized in moderate to good yields through a [1+1] “tripod-tripod coupling” strategy. Below pH 6.2, $btpN_4O_3$ has a compartment with three

protonated amines to interact with the anionic group of the amino acids while the other compartment has three ether oxygen atoms available to accept hydrogen bonds from the ammonium group of the substrates and an aromatic unit for the establishment of cation-π interactions. However, the binding studies showed relatively modest association constants between the protonated receptor and the amino acid substrates (1.63–3.21 log units), although they are the highest values for the binding on zwitterionic substrates in aqueous solution to date. Interestingly, the receptor has a preference for amino acids containing a tetrahedral anionic group possibly due to the 3-fold symmetry of their anionic moiety, complementary to the tren subunit of the cryptand. On the other hand, the second cryptand, $t_2pN_5O_3$, was found not appropriate for amino acid binding because its polyether compartment is susceptible to protonation and should repel the ammonium group of the substrates.

These results allowed to conclude that the polyether compartment of the cryptands cannot be derived from triethanolamine, the 2,4,6-triethylbenzene scaffold being a more appropriate building block. It could also be concluded that a triprotonated receptor does not have enough charge to be effective for the uptake of amino acids in highly competitive polar medium. Nonetheless this study is the starting point from which new and improved compounds can now be designed. For instance, as charged receptors seem to have low effectiveness in binding zwitterionic amino acids due to the mutual attenuation of charge cause by proximity of the anionic and cationic functionalities, the incorporation of metal ions in the receptor framework should help in this regard. The copper(II) cryptate of $btpN_4O_3$ may have enhanced affinity for the amino acids, in the same way that the copper(II) cryptate of $btpN_7$ has enhanced affinity for dicarboxylates in comparison with the protonated forms of $btpN_7$.

Throughout this research, macrobicyclic architectures were designed with different types of binding sites as well as different building blocks and used as receptors for anionic substrates allowing selectivity to be tuned. In this way it was not only possible to achieve selectivity between inorganic substrates of similar size and shape but also build new compounds appropriate for the binding of more

complicated substrates such as the dicarboxylates and amino acids, and provide starting points for further investigation. This work also gave interesting insights on the binding mechanisms of synthetic receptors, on how they can be perfected and on how they compare with their natural counterparts. Therefore, it is hoped that the present work has given a relevant contribution to the anion recognition field.

8.2 References

[1] J. A. Aguilar, T. Clifford, A. Danby, J. M. Llinares, S. Mason, E. García-España, K. Bowman-James, *Supramol. Chem.* **2001**, *13*, 405–417.

[2] M. J. Hynes, B. Maubert, V. McKee, R. M. Town, J. Nelson, J. Chem. Soc., *Dalton Trans.* **2000**, 2853–2859.

[3] T. Clifford, A. Danby, J. M. Llinares, S. Mason, N. W. Alcock, D. Powell, J. A. Aguilar, E. García-España, K. Bowman-James, *Inorg. Chem.* **2001**, *40*, 4710–4720.

[4] S. Mason, T. Clifford, L. Seib, K. Kuczera, K. Bowman-James, *J. Am. Chem. Soc.* **1998**, *120*, 8899–8900.

[5] J. Nelson, M. Nieuwenhuyzen, I. Pál, R. M. Town, *Dalton Trans.* **2004**, 2303–2308.

[6] C. Bazzicalupi, A. Bencini, A. Bianchi, A. Danesi, C. Giorgi, B. Valtancoli, *Inorg. Chem.* **2009**, *48*, 2391–2398.

[7] M. W. Hosseini, J.-M. Lehn, *Helv. Chim. Acta* **1988**, *71*, 749–756.

[8] C.S. Poornima, P.M. Dean, *J. Comput.-Aided Mol. Des.* **1995**, *9*, 500–512.

[9] R. Sabarinathan, K. Aishwarya, R. Sarani, M. K. Vaishnavi, K. Sekar, *J. Biosci*. **2011**, *36*, 253–263.

Appendix

A1 Determination of protonation, association and stability constants by the potentiometric method

A1.1 The potentiometric method

In this work the determination of protonation, stability and association constants was performed using the potentiometric method (with a glass electrode as indicator electrode). The method was first developed by Jannik Bjerrum for the determination of stability constants of metal-amine complexes.[1] Bjerrum showed that when the ligand is a conjugate base of a weak acid the formation constants of its metal complexes can be determined through pH measurements of a series of solutions containing known amounts of metal ion and ligand. This process has been largely used, being the most exact and precise method.[2]

In the determination of equilibrium constants by potentiometric methods an indicator electrode and a reference electrode are used. When the indicator electrode is a glass electrode and the reference electrode is the Ag/AgCl one, the electrochemical cell used may be represented as:

$$Ag|AgCl_{(sat)}|Cl^-||\text{test solution}|\text{glass membrane}|H^+, Cl^-, AgCl_{(sat)}|Ag$$

The glass electrode is an ion-selective electrode possessing bulb made of a doped glass membrane sensitive to H^+ ion.

In the potentiometric titration the difference in potential established between the indicator electrode (glass electrode) and the reference electrode is measured. The potential of the electrochemical cel (E_{cel}) ia given by:

$$E_{cel} = E_{ind} - E_{ref} + E_j \qquad (A.1)$$

The E_{ind} term can be expressed by the Nernst equation which relates the measured potential with the composition of the test solution:

$$E_{ind} = E_{ind}^{o} + E_{asy} + Q \log a_{H^+} \qquad (A.2)$$

By inserting the previous expression in Equation A.1 the following is obtained:

$$E_{cel} = E_{ind}^{o} - E_{ref} + E_j + E_{asy} + Q \log a_{H^+} \quad (A.3)$$

where E_{cel} is the electrochemical cell potential; E_{ind}^{o} "normal potential" of the indicator electrode; E_{ref} is the reference electrode potential; E_j the liquid junction potential formed at the contact surface between the test solution and the filling solution of the reference electrode; E_{asy} is the asymmetry potential of the glass electrode; Q = (RT ln 10)/F, R being the universal gas constant, T the absolute temperature and F the Faraday constant; a_{H^+} the hydrogen ion activity. If the electrode presents a theoretical behaviour Q = 59.162 mV at 298.2 K.

In practice it is more convenient to use concentrations instead of activities, hence stoichiometric constants instead of thermodynamic constants, which are determined in a medium of ionic strength that is constant throughout the experiment and much higher than the concentration of the other species in solution. Values determined in such way are valid only for that specific ionic strength and for that particular ionic medium composition, however it is generally accepted to compare values obtained for different systems provided that the ionic strength is approximately the same and the supporting electrolyte ions do not form complexes or associations with the ligands or receptors.

Since the activity of a given species in solution (a_i) relates to its concentration at a certain ionic strength by $a_i = \nu_i c_i$, where ν_i is the activity coeficient of species i, the following equation can be obtained:

$$E_{cel} = \underbrace{E_{ind}^{o} - E_{ref} + E_j + E_{asy} + Q \log \nu_i}_{E^{o\prime}} + Q \log [H^+] + E_j' \quad (A.4)$$

where $E_j + Q \log \nu_I$ are the terms relative to the junction potential and the activity coefficient which are independent of hydrogen ion concentration and E_j' corresponds to the term relative to the junction potential and the activity coefficient that are dependent of hydrogen ion concentration given by the expression:

$$E_j' = j_{H^+} [H^+] + j_{OH^-} [OH^-] \quad (A.5)$$

where j_{H+} and j_{OH-} are characteristic of the ionic medium. Using a salt bridge filled with a supporting electrolyte minimizes the potential difference and keeps it constant. If the ions of the supporting electrolyte have identical mobilities the liquid junction potential will be even lower. However, although the titrations are performed in a constant ionic strength, when the concentration of H^+ or OH^- in solution is sufficiently high, the E_j' varies due to the different mobility of these ions relative to the other species in solution, hence the E_j' cannot be disregarded. The j_{H+} and j_{OH-} values are characteristic of the ionic medium and can be determined by titration of a strong acid with a strong base. The liquid junction potential is only relevant in titrations performed below pH 2 or above pH 12. The E_j' may also be disregarded when the titre is a weak acid at an ionic strength ≥ 0.1 mol dm^{-3}.

With this in mind it is possible to simplify Equation A.4 writing it in a form similar to the Nernst equation:

$$E_{cel} = E^{o\prime} + Q \log [H^+] \qquad (A.6)$$

From the values obtained experimentally it is possible to calculate the hydrogen ion concentration using Equation A.6 if the values of $E^{o\prime}$ and Q are determined by an appropriate calibration method.

Theoretically the glass electrode response to the hydrogen ion obeys to the Nernst equation in a wide pH range of values of 0-14 or 0-11 for most commercial electrodes. However some precautions are needed. A common source of error in measurements with the glass electrode comes from variation during measurement of the asymmetry potential and, consequently, of the formal potential of the electrode. In alkaline aqueous medium these variations are mainly due to attack of the membrane surface by the OH^- ion. Glass electrodes have high selectivity for the H^+ cation, however when the $[H^+]$ is too low the alkaline metal cations interfere with its functioning, especially the Na^+. The interferences increase with the exposure time of the electrode to solutions of high pH due to the possible ion exchange between the proton in the surface of the

membrane and the alkali metal cation in solution, originating errors by excess in the response of glass electrodes.

A1.2 Determination of protonation, association and stability constants.

A1.2.1 Protonation constants

The polyammonium macrobicyclic compounds described in this work are polybasic acids of general formula H_nL^{n+} and can therefore successively dissociate according to the following equilibria:

$$H_nL^{n+} \rightleftharpoons H_{(n-1)}L^{(n-1)+} + H^+ \qquad K_{a_1} = [H^+][H_{(n-1)}L^{(n-1)+}]/[H_nL^{n+}] \quad (A.6)$$

$$H_{(n-1)}L^{(n-1)+} \rightleftharpoons H_{(n-2)}L^{(n-2)+} + H^+ \qquad K_{a_2} = [H^+][H_{(n-2)}L^{(n-2)+}]/[H_{(n-1)}L^{(n-1)+}] \quad (A.7)$$

$$\vdots \qquad\qquad \vdots$$

$$H_{(n-m)}L^{(n-m)+} \rightleftharpoons L + H^+ \qquad K_{a_m} = [H^+][L]/[H_{(n-m)}L^{(n-m)+}] \quad (A.8)$$

K_{a_1}, K_{a_2}, …, K_{a_m} are stepwise dissociation constants relate to the stepwise association constants according to:

$$K_1 = 1/K_{a_m},\ K_2 = 1/K_{a_{m-1}},\ \ldots,\ K_n = 1/K_{a_1} \quad (A.8)$$

Notice that the first acid dissociation constant is equal to the last stepwise association constant and the numerical ordering of the stepwise dissociation constant is the reversed one of the stepwise association constants. In addition, in the equilibria shown above and in the ones that will follow, water molecules are omitted and the H_3O^+ is represented as H^+.

In computer fitting programs such as Hyperquad[3] all equilibrium constants are defined as overall association constants. This means that for a polybasic acid the equilibrium constants are defined as follows:

$$L + H^+ \rightleftharpoons HL^+ \qquad \beta_1 = [HL^+]/[L]\,[H^+] \quad (A.10)$$

$$L + 2\,H^+ \rightleftharpoons H_2L^{2+} \qquad \beta_2 = [H_2L^{2+}]/[L]\,[H^+]^2 \quad (A.11)$$

$$\vdots \qquad\qquad \vdots$$

$$L + n\,H^+ \rightleftharpoons H_nL^{n+} \qquad \beta_n = [H_nL^{n+}]/[L]\,[H^+]^n \quad (A.12)$$

The relationship between the overall association constants and the stepwise association constants is the following:

$$\beta_1 = K_1;\ \beta_2 = K_1 \times K_2;\ \beta_n = K_1 \times K_2 \times \ldots \times K_n = \beta_{n-1} \times K_n \quad \text{(A.13)}$$

Hence, the first log overall association constant is equal to the first pK_a and the last log overall association constant is equal to the sum of the pK_a's.

Curves obtained by titration of a polybasic acid compound with a standard solution of a strong base using the potentiometric method allows the determination of the molar concentration of the compound, the neutralized portion in each point as well as the corresponding hydrogenionic concentration.

The total concentration of acid in solution is given by the mass balance of all species:

$$C_L = [HL^+] + [H_2L^{2+}] + \ldots + [H_nL^{n+}] \quad \text{(A.14)}$$

Considering the charge balance equation and supposing that the titrant is a KOH solution one can write:

$$[K^+] + [H^+] + [HL^+] + 2\,[H_2L^{2+}] + \ldots + n\,[H_nL^{n+}] = [OH^-] + [C^-] \quad \text{(A.15)}$$

where C^- is the counterion of the polyammonium compound. Applying Equations A.9 and A.13 in the mass and charge balance Equations A.9 and A.15 it is possible to determine the values of the formation constants of protonated species of L from the corresponding definitions. In the present work the Hyperquad program[3] was used for the calculations.

A1.2.2 Binding (or association) constants

When a receptor is a polybasic acid of general formula H_nL^{n+} and is in the presence of an anionic substrate, several protonated species are formed depending on the protonated state of the receptor and the substrate. The formation of such protonated associated species can be generically represented by:

$$h\,H + l\,L + a\,A \rightleftharpoons H_hL_lA_a \quad \text{(A.16)}$$

where H represents the proton and A the substrate and charges where omitted for simplicity. The respective overall association constants are given by:

$$\beta_{H_hL_lA_a} = [H_hL_lA_a]/[H]^h[L]^l[A]^a \quad (A.17)$$

From the supramolecular chemist point of view the stepwise association constants are more informative as they specify the location of the protons in the receptor and substrate:

$$H_{h'}L_l + H_{h''}A_a \rightleftharpoons H_hL_lA_a \qquad K_{H_hL_lA_a} = [H_hL_lA_a]/[H_{h'}L_l][\,H_{h''}A_a] \quad (A.18)$$

being h = h'+ h'' and charges were omitted for simplicity. Stepwise association constants are calculated from overall association constants using the following equation:

$$K_{H_hL_lA_a} = \beta_{H_hL_lA_a}/(\beta_{H_{h'}L_{l'}} \times \beta_{H_{h''}A_a}) \quad (A.19)$$

If the receptor and substrate can participate in several overlapping protonation equilibria it is not straightforward to decide which stepwise equilibria are involved in the association process. For instance, the supramolecular entity H_6LA can be formed by association of H_6L with A or by association of H_5L with HA of even by association of H_4L with H_2A. Wrongly attributed equilibria for the stepwise constants will give rise to misinterpretations of the constants hence to wrongful conclusions. To overcome these problems, García-España *et al.* proposed the use of the effective association constants (K_{eff}). [4] The K_{eff} value is defined as the quotient between the total amount of supramolecular species formed and the total amounts of the free receptor and free substrate:

$$K_{eff} = \Sigma[H_hL_lA_a]/\Sigma[H_{h'}L_l]\times\Sigma[H_{h''}A_a] \quad (A.20)$$

The expressing equibilibria that will afford association constant values too different from the corresponding K_{eff} value at the pH where the supramolecular entity in question is prevalent should be discarded.

A1.2.3 Stability constants of metal complexes

In the formation of a metal complex with a ligand (which is the base of a poliprotic acid) there is competition between the metal ion (M) and the hydrogen ion (H) for the ligand (L). Hence, by following the hydrogen ion concentration during the titration of a mixture of M and H_nL^{n+} with a strong base, and knowing the protonation constants of H_nL^{n+}, the stability constant for the formation of ML can be determined. The equilibria involved and respective overall stability constants are given by:

$$m\,M + l\,L + h\,H \rightleftharpoons M_mH_hL_l \qquad \beta_{M_mH_hL_l} = [M_mH_hL_l]/[M]^m[H]^h[L]^l \qquad (A.21)$$

where charges were omitted for simplicity. Many types of equilibria can be established between the metal ion and the ligand, such as the formation of mono and polinuclear complexes, protonated metal complexes and hydroxocomplexes:

$$M + L \rightleftharpoons ML \qquad K_{ML} = [ML]/[M][L] \qquad (A.22)$$

$$\vdots \qquad\qquad \vdots$$

$$M_{m-1}L + M \rightleftharpoons M_mL \qquad K_{M_nL} = [M_mL]/[M_{m-1}L][M] \qquad (A.23)$$

$$ML + H^+ \rightleftharpoons MHL \qquad K_{MHL} = [MHL]/[ML][H] \qquad (A.24)$$

$$\vdots \qquad\qquad \vdots$$

$$MH_{h-1}L + H^+ \rightleftharpoons MH_hL \qquad K_{MH_hL} = [MH_hL]/[MH_{h-1}L][H] \qquad (A.25)$$

$$ML \rightleftharpoons ML(OH) + H^+ \qquad K_{ML(OH)} = [ML(OH)][H]/[ML] \qquad (A.26)$$

$$\vdots \qquad\qquad \vdots$$

$$ML(OH)_{h-1} \rightleftharpoons ML(OH)_h + H^+ \qquad K_{ML(OH)_h} = [ML(OH)_h][H]/[ML(OH)_{h-1}] \qquad (A.27)$$

Stepwise stability constants are calculated from overall stability constants using the following relationships:

$K_{ML} = \beta_{ML}$; $K_{M_nL} = \beta_{M_nL}/\beta_{M_{m-1}L}$; $K_{MH_{h-1}L} = \beta_{MH_hL}/\beta_{MH_{h-1}L}$; $K_{ML(OH)_h} = \beta_{ML(OH)_h}/\beta_{ML(OH)_{h-1}}$.

A1.2.4 Stability constants of cascade complexes

Metal complexes can also be used as anion receptors by a so called cascade mechanism in which ternary complexes are formed.[5] The cascade mechanism

involves two successive processes: complexation of the metal ion by the ligand and binding of the anionic substrate to form the cascade complex. As in the cases presented before, several equilibria can be established and generically represented by:

$$m\,M + l\,L + a\,A + h\,H \rightleftharpoons M_mH_hL_lA_a \qquad \beta_{M_mH_hL_lA_a} = [M_mH_hL_lA_a]/[M]^m[H]^h[L]^l[A]^a \tag{A.28}$$

where the charges were omitted for simplicity. The stepwise stability constant of the cascade complexes can be defined in a manner similar to the binding constant:

$$M_mH_{h'}L_l + H_{h''}A_a \rightleftharpoons M_mH_hL_lA_a \qquad K_{M_mH_hL_lA_a} = [M_mH_hL_lA_a]/[M_mH_{h'}L_l][H_{h''}A_a] \tag{A.29}$$

where h = h'+ h'' and charges were omitted for simplicity. Stepwise stability constants are calculated from overall stability constants using the following equation:

$$K_{M_mH_hL_lA_a} = \beta_{M_mH_hL_lA_a}/(\beta_{M_mH_{h'}L_l} \times \beta_{H_{h''}A_a}) \tag{A.30}$$

A1.3 References

[1] M. T. Beck, I. Nagypál, *Chemistry of Complex Equilibria*, Ellis Horwood ltd, Chichester, **1990**.

[2] H. M. Irving, M. G. Miles, L. D. Petit, *Anal. Chim. Acta* **1967**, *38*, 475–488.

[3] P. Gans, A. Sabatini, A. Vacca, *Talanta* **1996**, *43*, 1739–1753.

[4] M. T. Albelda; M. A. Bernardo, E. Garcia-España, M. L. Godino-Salido, S. V. Luis, M. J. Melo, F. Pina, C. Soriano, *J. Chem. Soc., Perkin Trans. 2* **1999**, 2545–2549.

[5] J.-M. Lehn, *Pure Appl. Chem.* **1980**, *52*, 2441–2459.

A.2 Supplementary Information of Chapter 2

Table A2.1 Stepwise protonation (log K_i^H) constants of the anions in H_2O/MeOH (50:50 v/v).[a]

Equilibrium quotient[b]	SO_4^{2-}	SeO_4^{2-}	$S_2O_3^{2-}$	AcO^-	PO_4^{3-}
[HA]/[A][H]	2.51(1)	2.36(1)	2.04(1)	5.28(1)	n.d.[b]
$[H_2A]/[HA][H]$	–	–	–	–	7.46(1)
$[H_3A]/[H_2A][H]$	–	–	–	–	2.82(1)

[a] T = (298.2 ± 0.1) K; I = (0.10 ± 0.01) mol dm^{-3} in KTsO. [b] A is the anion. [c] Too high to be accurately determined by potentiometry.

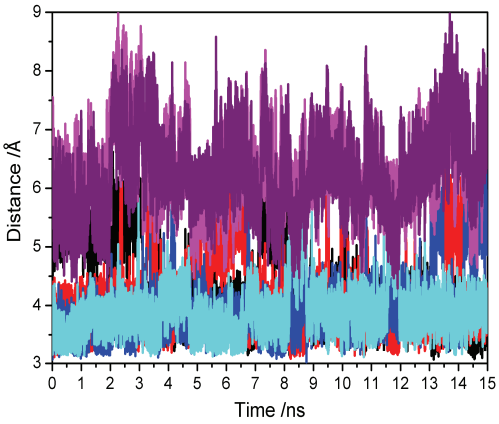

Figure A2.1 Evolution of the six S···N distances over 15 ns long simulation

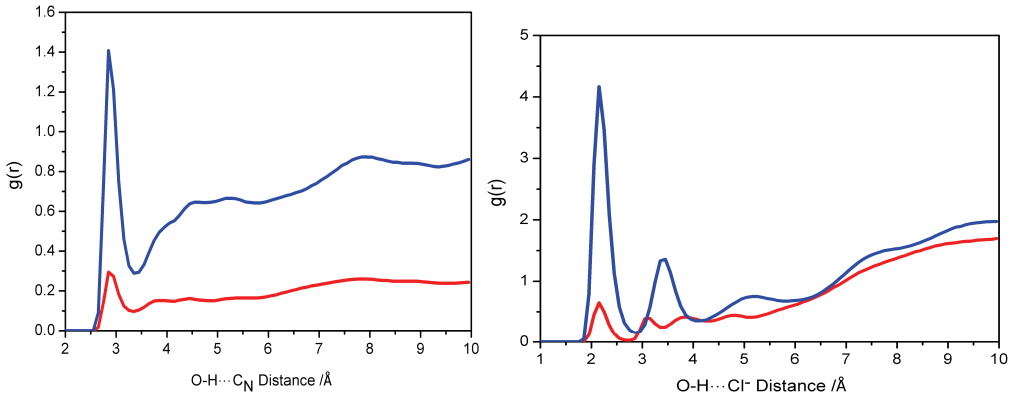

Figure A2.2 Rdfs for O–H···C_N and O–H···Cl distances between the water (blue) and methanol (in red) molecules and the centre of mass of the receptor (left) and the anion (right). The Rdfs were calculated over the 15 ns of simulation.

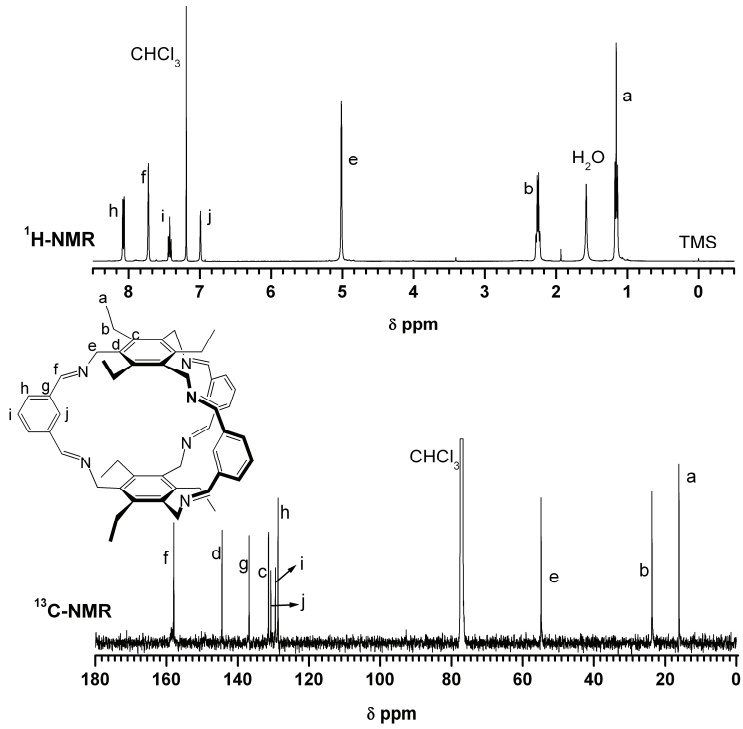

Figure A2.3 ^{1}H and ^{13}C NMR spectra of the hexaimine in $CDCl_3$.

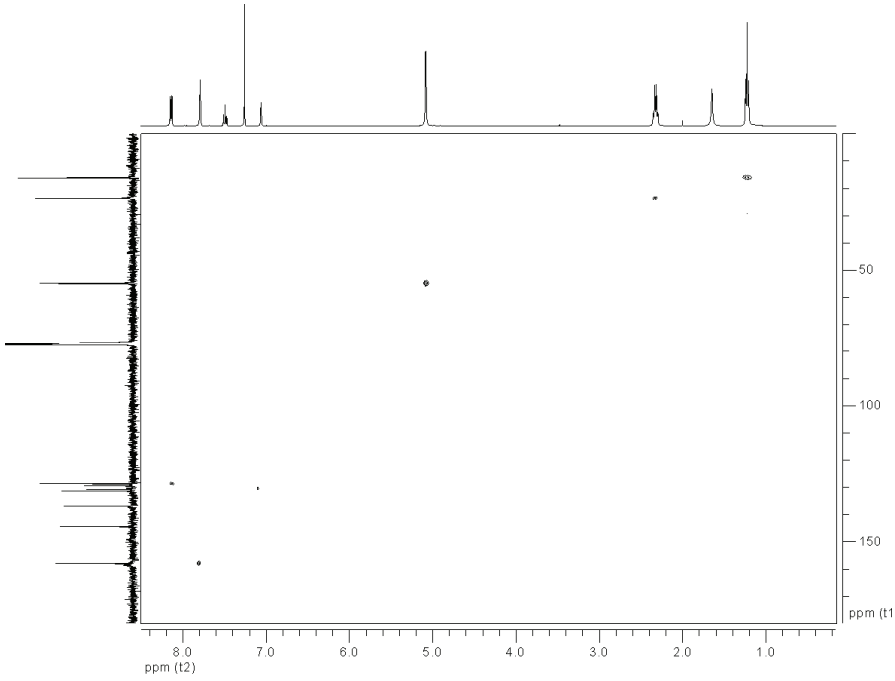

Figure A2.4 HMQC spectra of the hexaimine in $CDCl_3$.

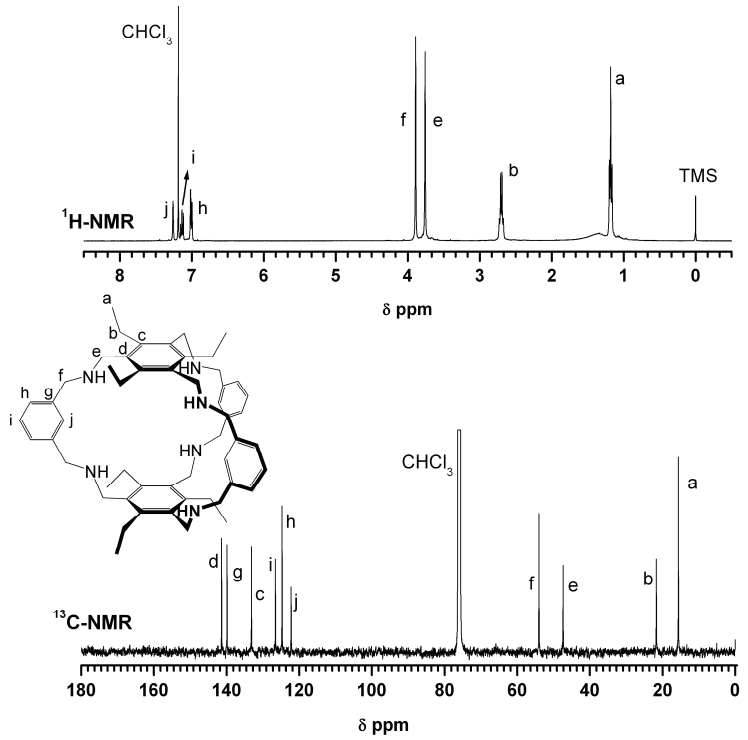

Figure A2.5 ^{1}H and ^{13}C NMR spectra of xyl in $CDCl_3$.

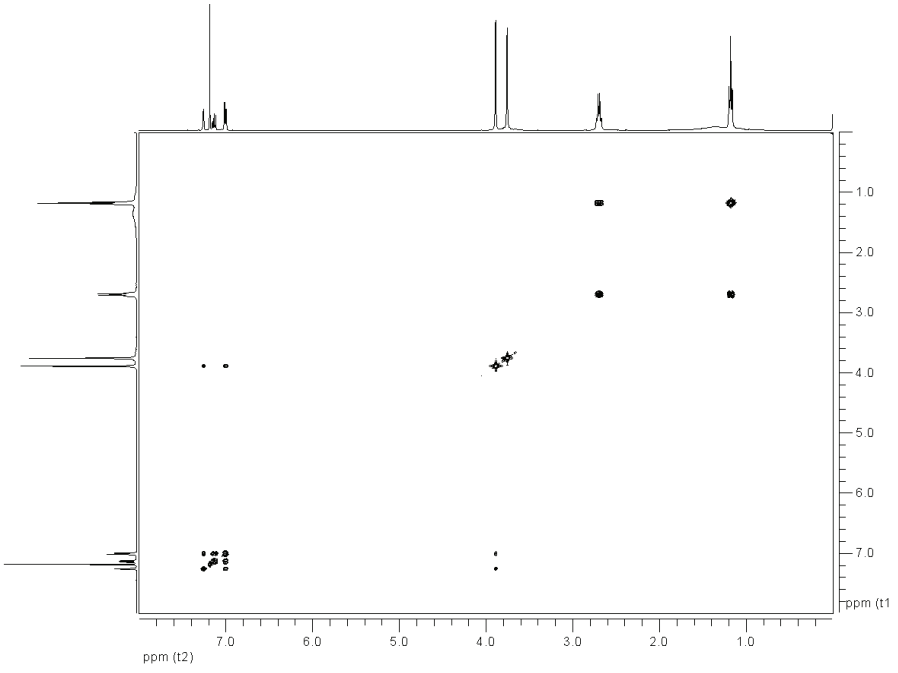

Figure A2.6 COSY spectra of xyl in $CDCl_3$.

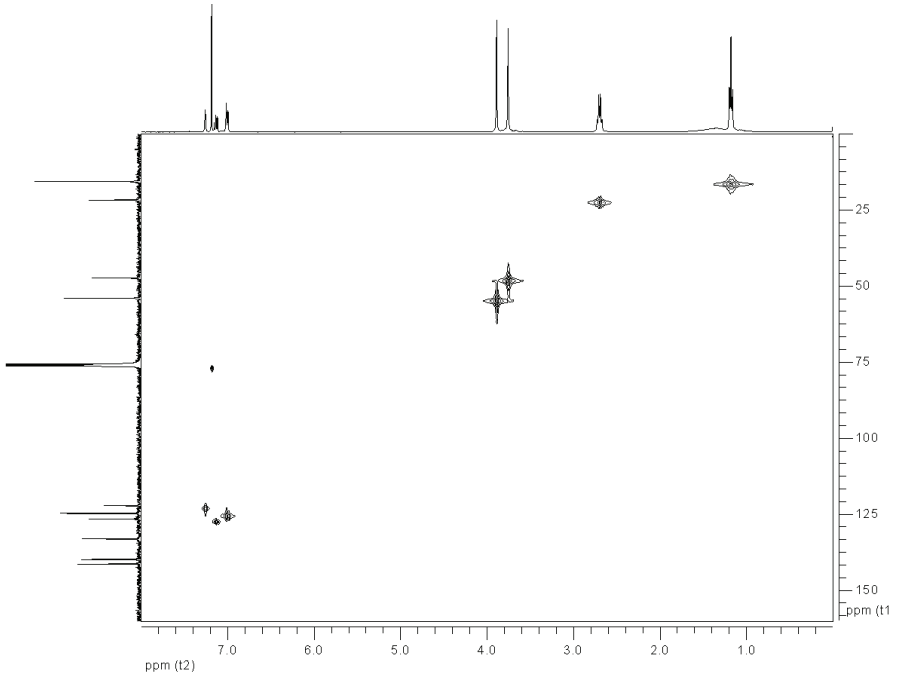

Figure A2.7 HMQC spectra of xyl in $CDCl_3$.

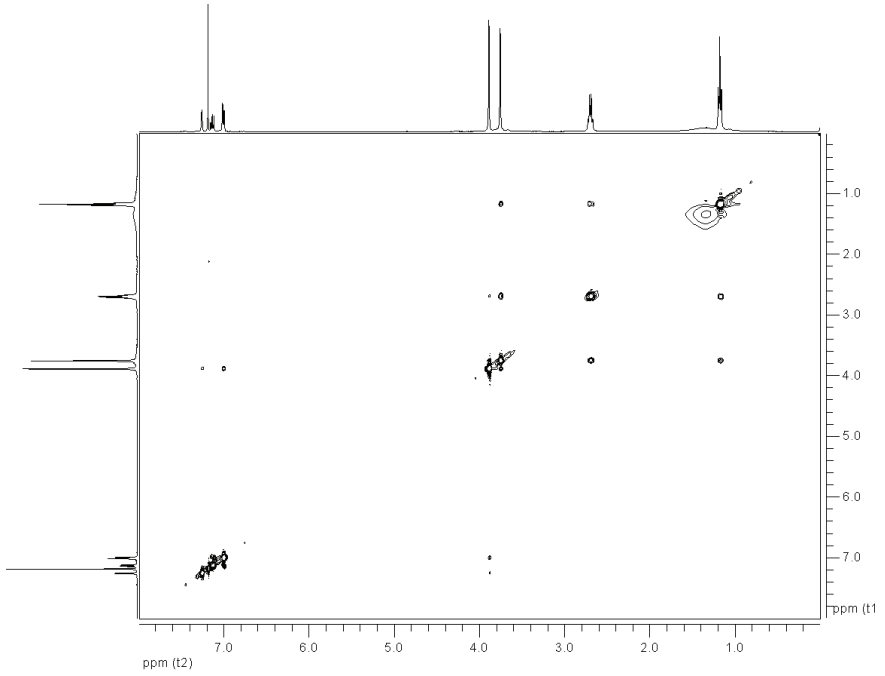

Figure A2.8 NOESY spectra of xyl in $CDCl_3$.

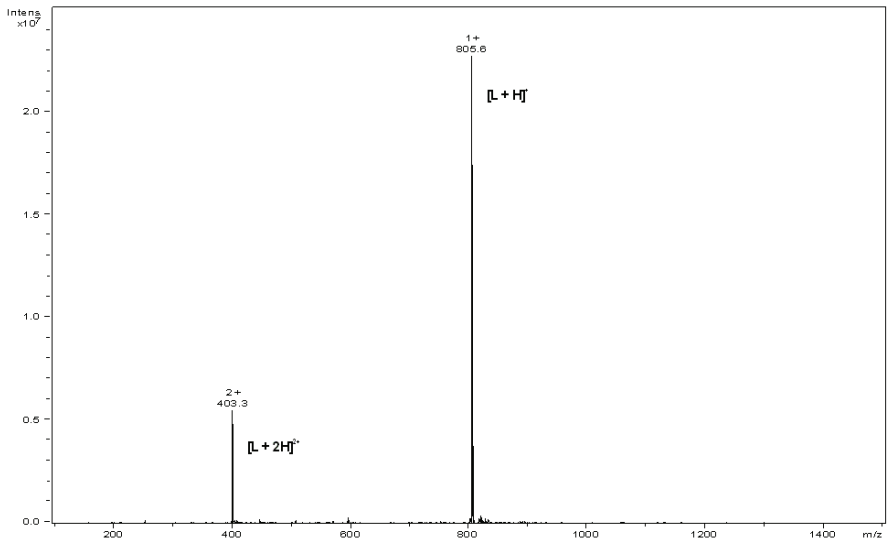

Figure A2.9 ESI mass spectra of xyl in MeOH.

A3. Supplementary Information of Chapter 3

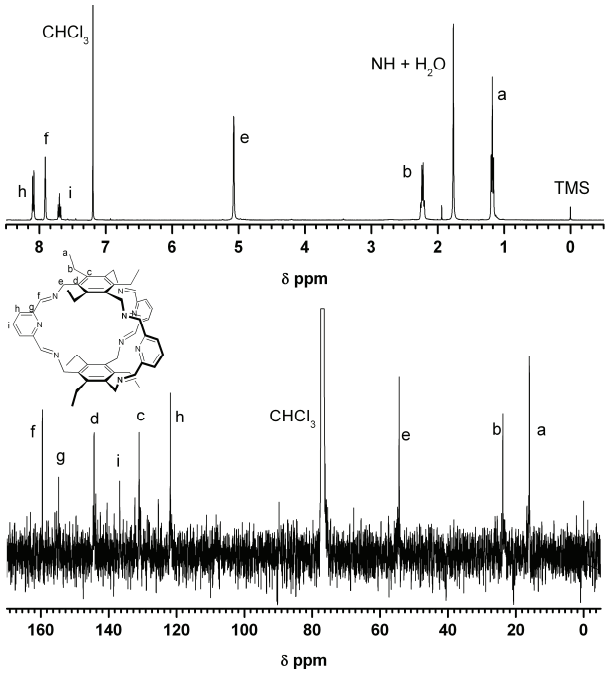

Figure A3.1 ^{1}H and ^{13}C NMR spectra of the hexaimine in $CDCl_3$.

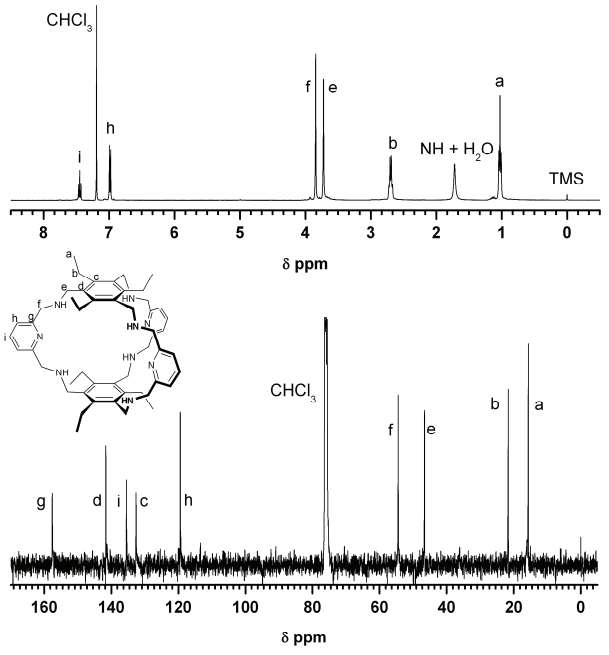

Figure A3.2 ^{1}H and ^{13}C NMR spectra of pyr in $CDCl_3$.

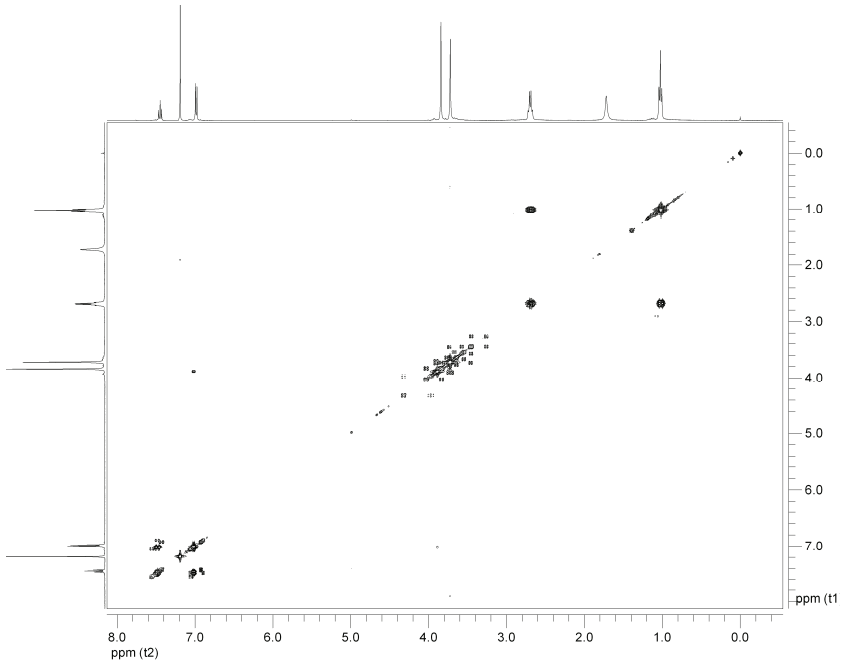

Figure A3.3 COSY spectrum of pyr in $CDCl_3$.

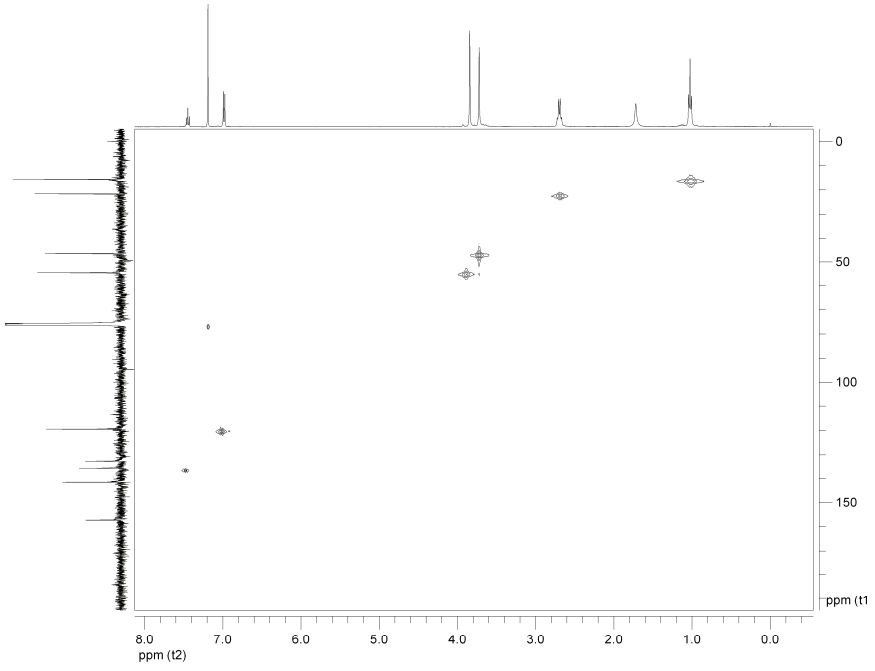

Figure A3.4 HMQC spectrum of pyr in $CDCl_3$.

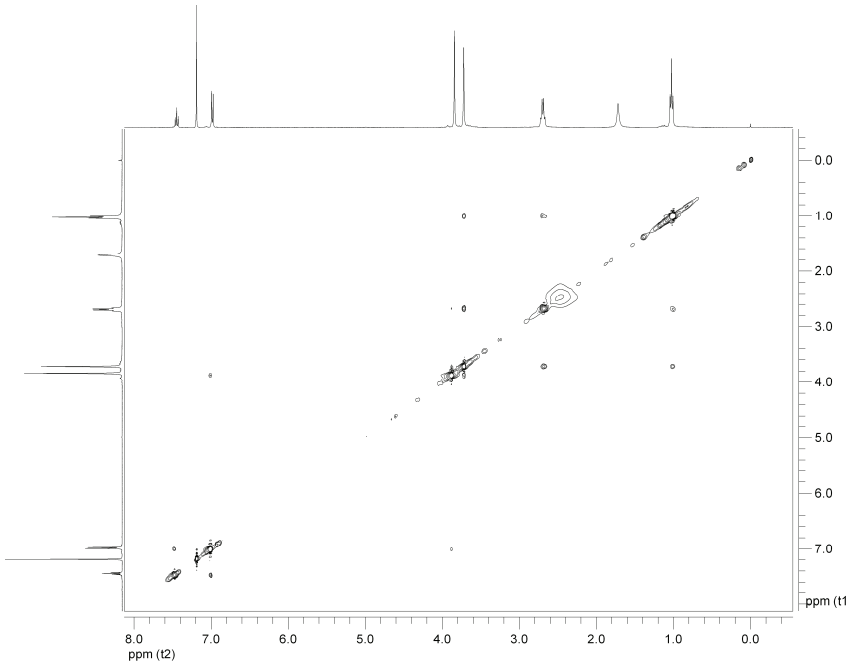

Figure A3.5 NOESY spectrum of pyr in $CDCl_3$.

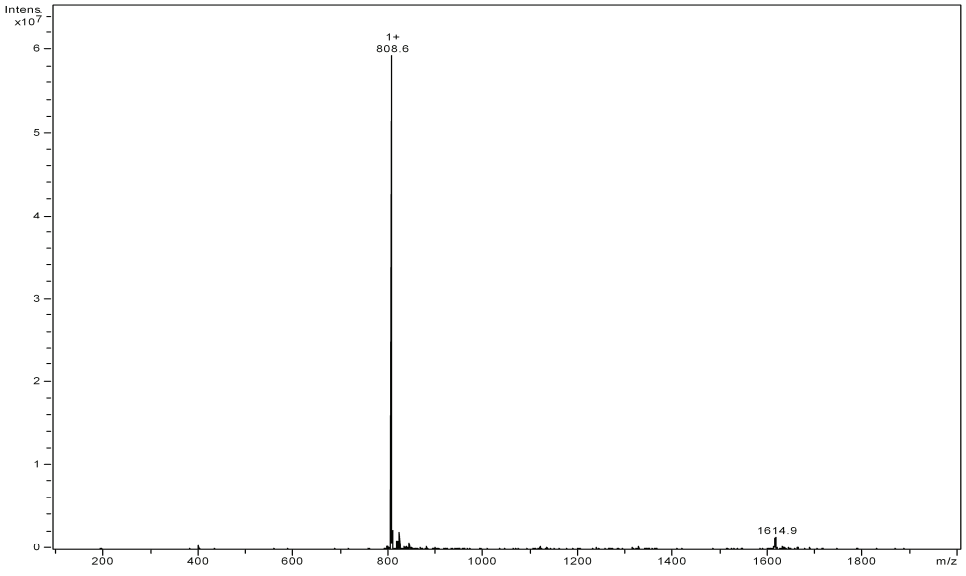

Figure A3.6 ESI mass spectrum of pyr in MeOH.

Table A3.1 Overall (log $\beta_{H_hL_lA_a}$) association constants for the indicated equilibria in H_2O/MeOH (50:50 v/v).[a],[b]

Equilibrium[c]	Cl^-	NO_3^-	ClO_4^-	AcO^-	SO_4^{2-}	HPO_4^{2-}	$HAsO_4^{2-}$
$7\ H^+ + pyr + A \rightleftharpoons H_7pyrA$	–	–	–	–	–	51.90(1)	51.26(1)
$6\ H^+ + pyr + A \rightleftharpoons H_6pyrA$	42.76(4)	42.93(1)	n.d.[c]	42.91(3)	44.73(1)	47.30(1)	46.77(1)
$5\ H^+ + pyr + A \rightleftharpoons H_5pyrA$	–	–	–	37.89(2)	39.08(1)	41.63(1)	41.11(1)
$4\ H^+ + pyr + A \rightleftharpoons H_4pyrA$	–	–	–	32.22(2)	32.36(3)	35.22(1)	34.74(1)
$3\ H^+ + pyr + A \rightleftharpoons H_3pyrA$	–	–	–	25.50(2)	–	28.07(1)	27.64(1)
$2\ H^+ + pyr + A \rightleftharpoons H_2pyrA$	–	–	–	18.03(6)	–	20.29(1)	19.98(1)
$H^+ + pyr + A \rightleftharpoons HpyrA$	–	–	–	–	–	11.89(1)	11.61(1)

[a] T = (298.2±0.1) K; I = (0.10±0.01) mol dm^{-3} in KTsO. [b] Values in parentheses are standard deviations for the last significant figure. [c] L = pyr, A = Cl^-, NO_3^-, ClO_4^-, AcO^-, SO_4^{2-}, HPO_4^{2-} and $HAsO_4^{2-}$ (because only $H_2PO_4^-$, HPO_4^{2-}, $H_2AsO_4^-$, $HAsO_4^{2-}$ are important in the pH range studied these anions were considered diprotic). Charges were omitted in species involving A for simplicity. [c] n.d. = too small to be determined.

Table A3.2 N–H···O hydrogen bond dimensions of $[(H_6pyr)(NO_3)_3(H_2O)_3](NO_3)_3{\cdot}4H_2O$

N–H···O	H···O/Å	N···O/Å	N–H···O/^{o}
N(16)–H(16B)···O(102)	2.51	3.041(7)	117
N(10)–H(10B)···O(201) [-*x*+1, *y*-1/2, -z+3/2]	2.24	2.851(7)	124
N(35)–H(35A)···O(202)	2.28	3.035(8)	140
N(44)–H(44A)···O(203)	2.27	3.041(8)	141
N(44)–H(44B)···O(301) [x+1/2, -*y*+1/2, -z+2]	2.17	2.937(7)	141
N(25)–H(25A)···O(401)	2.48	3.181(7)	134
N(16)–H(16A)···O(403)	2.08	2.971(7)	161
N(25)–H(25A)···O(403)	2.09	2.973(7)	161
N(44)–H(44B)···O(501)	2.38	3.090(7)	134
N(35)–H(35A)···O(502)	2.22	2.961(7)	137
N(44)–H(44A)···O(502)	2.30	2.962(7)	128
N(35)–H(35B)···O(W1) [*x*+1/2, -*y*+1/2, -z+2]	1.88	2.707(7)	148
N(16)–H(16B)···O(W2)	2.08	2.945(7)	156
N(25)–H(25B)···O(W2)	1.94	2.816(7)	160
N(10)–H(10B)···O(W3)	2.17	2.896(7)	135
N(1)–H(1A)···O(W3)	2.33	2.984(7)	128
N(1)–H(1B)···O(W4) [-*x*+1, *y*-1/2, -*z*+3/2]	2.04	2.940(7)	166
N(10)–H(10A)···O(W4) [-*x*+1, *y*-1/2, -z+3/2]	2.14	3.002 (7)	157
N(1)–H(1A)···O(W5) [-*x*+1, *y*-1/2, -*z*+3/2]	2.00	2.787(7)	142

Table A3.3 Hydrogen bond dimensions of $[(H_6pyr)(SO_4)_2(H_2O)_4](HSO_4)_2 \cdot 6H_2O$

D–H···A*	H···A/Å	D···A/Å	D–H···A/°
N(16)–H(16B)···O(102)	1.98	2.872(2)	163
N(16)–H(16B)···O(103)	2.57	3.266(2)	132
N(25)–H(25A)···O(101)	1.86	2.752(2)	162
N(35)–H(35B)···O(104)	1.79	2.691(2)	165
N(10)–H(10A)···O(201)	1.98	2.872(2)	164
N(44)–H(44B)···O(202)	1.89	2.773(2)	160
N(1)–H(1B)···O(203)	2.56	3.215(2)	129
O(W1)–H(1D)···O(102)	2.012(18)	2.829(2)	171.5(18)
O(W8)–H(8C)···O(104) [-*x*+1, -*y*+1, -z]	2.33(3)	3.062(3)	145(3)
O(W4)–H(4C)···O(103) [-*x*+1, -*y*+1, -z]	1.873(18)	2.680(2)	161(2)
O(W8)–H(8C)···O(103) [-*x*+1, -*y*+1, -z]	2.18(3)	2.946(3)	151(3)
O(W2)–H(2C)···O(201) [3/2-*x*, *y*+1/2, -z+1/2]	2.00(2)	2.808(2)	166(2)
O(W5)–H(5C)···O(202) [3/2-*x*, *y*+1/2,-z+1/2]	2.071(18)	2.907(2)	176.9(19)
O(W7)–H(7D)···O(202) [*x*, *y*+1, z]	2.10(2)	2.866(3)	149(2)
O(W3)–H(3D)···O(203) [3/2-*x*, *y*+1/2, -z+1/2]	1.98(2)	2.813(2)	173(3)
O(W6)–H(6D)···O(302)	2.20(2)	2.971(3)	158(2)
O(W6)–H(6C)···O(304) [-*x*+1, -*y*+1,-z]	2.17(3)	2.967(3)	164(3)
O(W2)–H(2D)···O(401) [*x*+1, *y*, z]	1.95(2)	2.763(3)	164(2)
O(W4)–H(4D)···O(404)	2.071(18)	2.841(3)	153(2)
O(W9)–H(9D)···O(304) [*x*-1, *y*+1, z]	2.12(2)	2.946(3)	166(3)
O(W1)–H(1C)···O(204)	2.034(12)	2.822(19)	161(2)
N(44)–H(44A)···O(W1)	1.99	2.849(2)	154
N(25)–H(25B)···O(W2)	2.30	3.012(3)	134
N(16)–H(16A)···O(W3)	1.94	2.831(2)	162
N(1)–H(1A)···O(W5)	2.31	3.072(2)	140
N(10)–H(10B)···O(W5)	1.96	2.865(2)	167

Continues in the next page

Continuation of previous page			
N(1)–H(1A)···O(W7) [-*x*+3/2, *y*-1/2, -*z*+1/2]	2.36	2.942(3)	121
O(W3)–H(3C)···O(W2)	2.00(2)	2.777(2)	155(3)
O(W5)–H(5D)···O(W3)	2.173(19)	2.966(2)	159(2)
O(W7)–H(7C)···O(W10) [*x*-1, *y*+1,*z*]	1.97(3)	2.797(3)	162(3)
O(W9)–H(9C)···O(W8) [*x*+1, *y*-1, *z*]	2.09(3)	2.919(3)	174(3)
O(W10)–H(10C)···O(W9)	1.903(12)	2.751(3)	178(3)
O(W10)–H(10D)···O(W7) [*x*+1, *y*-1,*z*]	1.99(2)	2.797(3)	159(3)

* D = O or N; A = O

Table A3.4 N–H···O hydrogen dimensions of $[(H_6pyr)(HPO_4)_2(H_2PO_4)(H_2O)_2](H_2PO_4)\cdot 16H_2O$

N–H···O	H···O/Å	N···O/Å	N–H···O/ °
N(25)–H(25B)···O(101)	1.82	2.720(4)	164
N(16)–H(16A)···O(102)	1.99	2.878(4)	163
N(10)–H(10B)···O(104)	1.79	2.660(5)	157
N(44)–H(44A)···O(202)	1.74	2.636(4)	164
N(1)–H(1A)···O(202)	1.75	2.643(5)	162
N(25)–H(25A)···O(302)	1.90	2.775(5)	158
N(16)–H(16B)···O(303)	1.77	2.682(4)	173
N(35)–H(35A)···O(W1) [*x*-1, *y*, *z*]	2.25	2.999(4)	138
N(44)–H(44B)···O(W1) [*x*-1, *y*, *z*]	1.98	2.866(4)	160
N(1)–H(1B)···O(W3)	2.01	2.873(5)	156

TABLE A3.5 Crystal data and selected refinement parameters for anion binding complexes

Compound	$[(H_6pyr)(NO_3)_3(H_2O)_3](NO_3)_3{\cdot}4H_2O$	$[(H_6pyr)(SO_4)_2(H_2O)_4](HSO_4)_2{\cdot}6H_2O$	$[(H_6pyr)(HPO_4)_2(H_2PO_4)(H_2O)_2](H_2PO_4){\cdot}16H_2O$
Empirical Formula	$C_{51}H_{89}N_{15}O_{25}$	$C_{51}H_{95}N_9O_{26}S_4$	$C_{51}H_{93}N_9O_{34}P_4$
M_w	1312.37	1378.60	1500.22
Crystal System	Orthorhombic	Monoclinic	Triclinic
Space group	$P2_12_12_1$	$P2_1/n$	$P\bar{1}$
a / [Å]	12.17(2)	12.8516(17)	13.1972(4)
b / [Å]	17.79(3)	15.2203(19)	15.0825(5)
c / [Å]	29.23(5)	33.144(4)	19.0406(5)
α / [º]	(90)	(90)	84.423(2)
β / [º]	(90)	91.517(6)	79.896(2)
γ / [º]	(90)	(90)	79.271(2)
V [$Å^3$]	6328(18)	6480.9(14)	3657.80(19)
Detector Distance [mm]	45	50	35
Time couting [s]	80	60	120
Z	4	4	2
D_c [Mg m^{-3}]	1.377	1.413	1.362
μ / [mm^{-1}]	0.111	0.234	0.195
Reflections collected	30722	55877	32361
Unique reflections, [R_{int}]	13412 [0.0602]	17270 [0.0382]	14378 [0.0371]
Final *R* indices			
R_1, wR_2 [$I>2\sigma I$]	0.0729, 0.1847 [8624]	0.0494, 0.1360 [12853]	0.0745, 0.1895 [9403]
R_1, wR_2 (all data)	0.1240, 0.2109	0.0741, 0.1553	0.1185, 0.2211

A4 Supplementary Information of Chapter 4

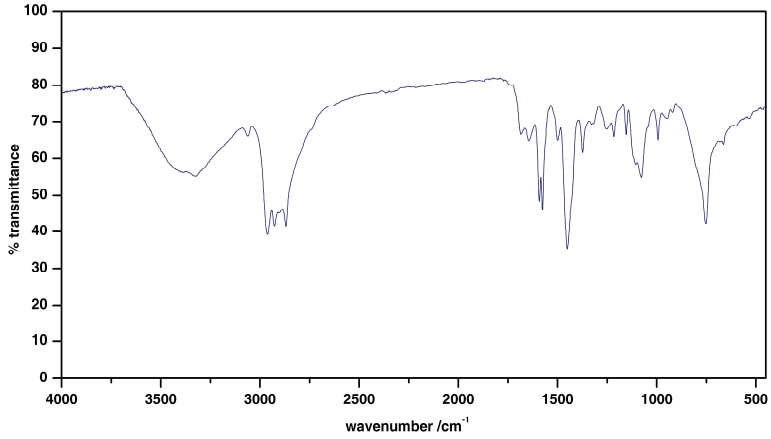

Figure A4.1 FTIR spectrum of the free ligand pyr (KBr pellet).

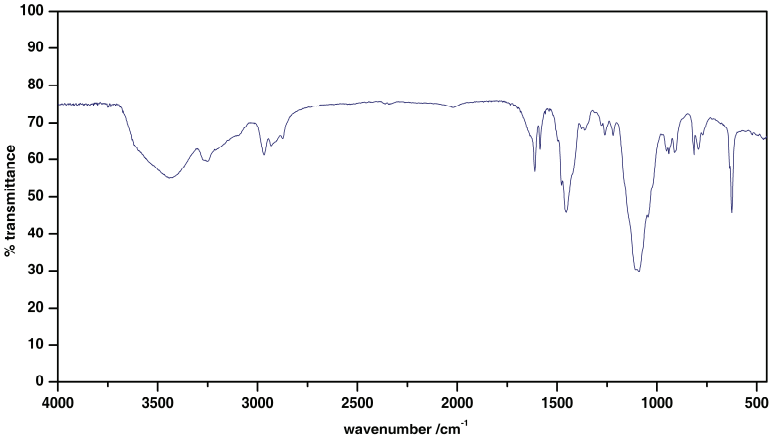

Figure A4.2 FTIR spectrum of $[Cu_3pyr(\mu_3\text{-}CO_3)]\cdot(ClO_4)_4\cdot H_2O$ (KBr pellet).

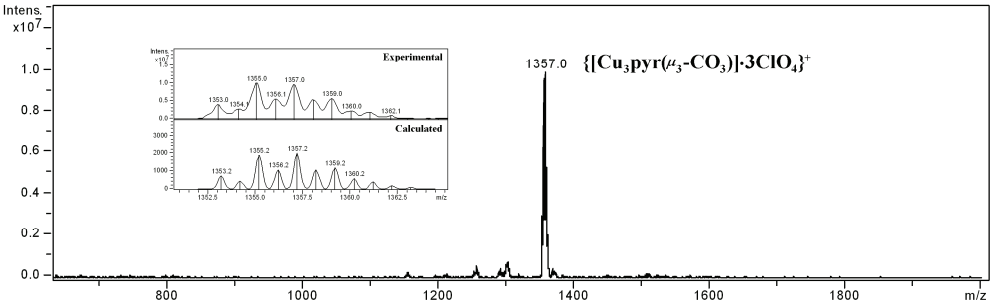

Figure A4.3 ESI mass spectrum of $[Cu_3pyr(\mu_3\text{-}CO_3)]\cdot(ClO_4)_4$, H_2O/MeOH (50:50 v/v), pH = 6.0.

Table A4.1 Crystal data and refinement details of $[Cu_3pyr(\mu_3\text{-}CO_3)](ClO_4)_4\cdot(MeOH)\cdot 2H_2O$ **1** and $[Cu_3pyr(\mu_3\text{-}CO_3)](NO_3)_4\cdot 9H_2O$ **2**.

Compound	**1**	**2**
Empirical Formula	$C_{53}H_{77}N_9O_{22}Cl_4Cu_3$	$C_{52}H_{87}N_9O_{26}S_4$
M_w	1524.66	1468.97
Crystal System	Monoclinic	Monoclinic
Space group	*P21/n*	*C2/c*
a / [Å]	12.8226(5)	17.553(10)
b / [Å]	20.9859(8)	18.823(9)
c / [Å]	23.7684(7)	19.150(11)
β / [º]	96.0050(10)	90.27(3)
V [$Å^3$]	6360.8(4)	6327(6)
Z	4	4
D_c [Mg m^{-3}]	1.592	1.542
μ / [mm^{-1}]	1.245	1.089
Reflections collected	39659	25581
Unique reflections, [R_{int}]	12699, [0.0620]	5577, [0.0345]
Final *R* indices		
R_1, wR_2 ,[I>2σI]	0.0561, 0.1210, [8204]	0.0474, 0.1149, [4602]
R_1, wR_2 (all data)	0.1071, 0.1403	0.0599, 0.1206

A.5 Supplementary Information of Chapter 5

Table A5.1 Hydrogen bond dimensions of $[H_7btpN_7(H_2O)(MeOH)Cl_2]Cl_6\cdot(H_3O)\cdot3(H_2O)\cdot3MeOH$

D–H···A[a]	H···A (Å)	D···A (Å)	D–H···A (°)
N(1)–H(1A) ···Cl(4)	2.37(2)	3.189(3)	157(3)
N(1)–H(1B) ···Cl(3)	2.49(3)	3.330(3)	162(3)
N(10)–H(10A) ···Cl(1)	2.26(3)	3.113(4)	165(4)
N(10)–H(10B) ···Cl(2) [-*x*, *y*-1/2, -z+1/2]	2.19(4)	3.074(4)	170(4)
N(16)–H(16A) ··· Cl(2)	2.34(4)	3.062(4)	141(3)
N(16)–H(16B) ··· Cl(6) [*x*, -*y*+3/2, z+1/2]	2.22(3)	3.065(4)	162(4)
N(25)–H(25A) ··· Cl(3)	2.44(3)	3.294(3)	167(3)
N(41)–H(41A) ··· Cl(4)	2.48(4)	3.282(4)	154(4)
N(50)–H(50A) ··· Cl(5)	2.27(3)	3.100(3)	159(4)
N(50)–H(50B) ··· Cl(7)	2.14(4)	2.988(4)	164(4)
N(13)–H(13A) ··· O(500)	1.86(4)	2.726(5)	170(4)
N(25)–H(25B) ··· O(302)	2.15(2)	2.978(4)	159(4)
N(41)–H(41B) ··· O(302)	2.12(4)	2.970(6)	165(4)
O(500)–H(50C) ··· Cl(4)	2.42(4)	3.206(4)	157(4)
O(500)–H(50D) ··· Cl(3)	2.39(3)	3.189(3)	163(3)
O(400)–H(400) ···Cl(6) [*x*, -*y*+3/2, z+1/2]	2.35(?)	3.14(4)	158(?)

[a] A and D mean a hydrogen bond acceptor and donor, respectively.

Table A5.2 Overall (β_i^H) and stepwise protonation (K_i^H) constants of the studied dicarboxylates in aqueous solution.[a]

Equilibrium reaction[b]	oxa^{2-}	mal^{2-}	suc^{2-}	fum^{2-}	$male^{2-}$
			$\log \beta_i^H$ [c]		
$A^{2-} + H^+ \rightleftharpoons HA^-$	3.83(1)	5.28(1)	5.26(1)	4.10(1)	5.84(1)
$A^{2-} + 2\ H^+ \rightleftharpoons H_2A$	5.33(1)	7.96(1)	9.28(1)	6.97(1)	7.70(1)
			$\log K_i^H$		
$A^{2-} + H^+ \rightleftharpoons HA^-$	3.83	5.28	5.26	4.10	5.84
$HA^- + H^+ \rightleftharpoons H_2A$	1.50	2.68	4.02	2.87	1.86

[a] T = (298.2±0.1) K; I = (0.10±0.01) mol dm^{-3} in KNO_3. [b] A denotes the dicarboxylate anions in general. [c] Values in parenthesis are standard deviations in the last significant figures.

Table A5.3 Overall (log $\beta_{M_mH_hA_a}$) and stepwise (log $K_{M_mH_hA_a}$) stability constants of the copper(II) complexes of the studied dicarboxylates in aqueous solution.[a]

Equilibrium reaction[b]	oxa^{2-}	mal^{2-}	suc^{2-}	fum^{2-}	$male^{2-}$
			log $\beta_{M_mH_hA_a}$ [c]		
$Cu^{2+} + H^+ + A^{2-} \rightleftharpoons CuHA^+$	–	–	7.07(1)	5.69(1)	7.41(4)
$Cu^{2+} + A^{2-} \rightleftharpoons CuA$	5.35(1)	4.98(1)	2.83(1)	2.26(1)	3.53(1)
$Cu^{2+} + 2\ A^{2-} \rightleftharpoons CuA_2^{2-}$	9.23(1)	7.86(2)	–	–	5.38(5)
			log $K_{M_mH_hA_a}$		
$Cu^{2+} + HA^- \rightleftharpoons CuHA^+$	–	–	4.24	3.43	3.88
$Cu^{2+} + A^{2-} \rightleftharpoons CuA$	5.35	4.98	2.83	2.26	3.53
$CuA + A^{2-} \rightleftharpoons CuA_2^{2-}$	3.88	2.88	–	–	1.85

[a] T = (298.2±0.1) K; I = (0.10±0.01) mol dm^{-3} in KNO_3. [b] A denotes the dicarboxylate anions in general. [c] Values in parenthesis are standard deviations in the last significant figures.

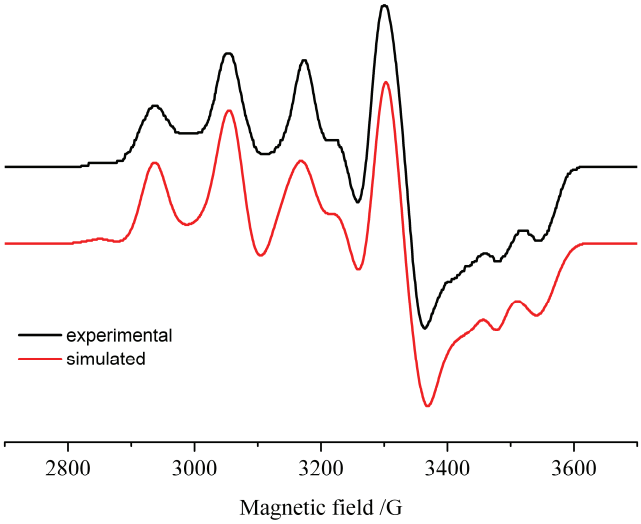

Figure A5.1 Experimental and simulated X-band EPR spectrum of $[CuH_hbtpN_7]^{(2+h)+}$ at pH = 6.3. The complex was prepared at 5.0×10^{-4} mol dm^{-3} in H_2O/ethylene glycol (1:1) and the spectrum was recorded at a microwave power of 2.0 mW, frequency (v) 9.67 GHz, T = 89 K.

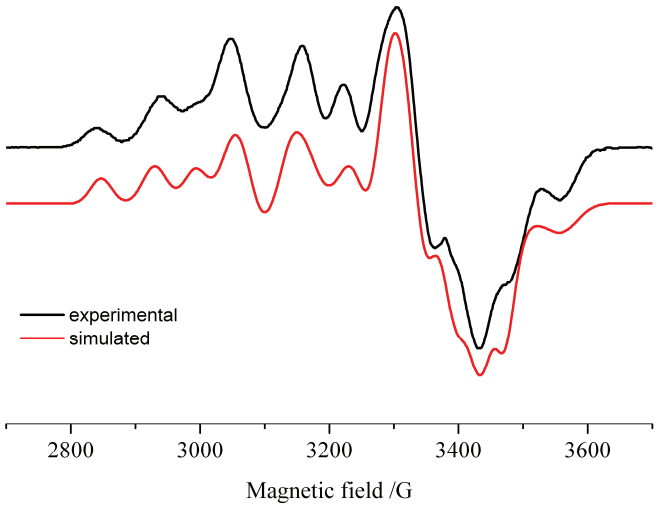

Figure A5.2 Experimental and simulated X-band EPR spectrum of $[CuH_hbtpN_7]^{(2+h)+}$ at pH = 11.4. The complex was prepared at 5.0×10^{-4} mol dm^{-3} in H_2O/ethylene glycol (1:1) and the spectrum was recorded at a microwave power of 2.0 mW, frequency (v) 9.67 GHz, *T* = 89 K.

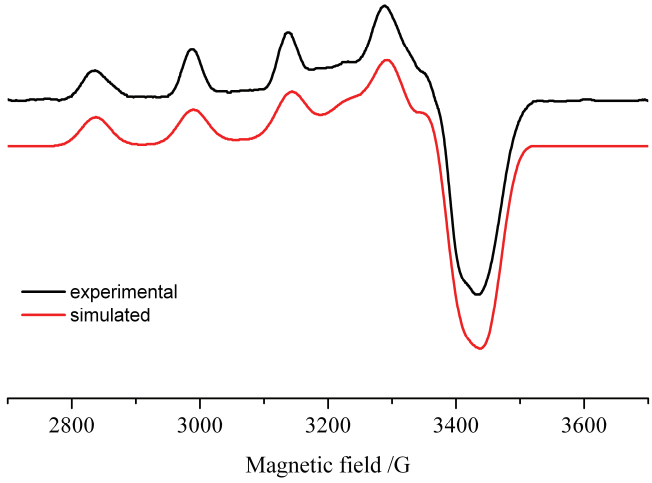

Figure A5.3 Experimental and simulated X-band EPR spectrum of $[CuH_hbtpN_7(oxa)]^{h+}$ at pH = 7.0. The complex was prepared at 5.0×10^{-4} mol dm^{-3} in H_2O/ethylene glycol (1:1) and the spectrum was recorded at a microwave power of 2.0 mW, frequency (v) 9.67 GHz, *T* = 89 K.

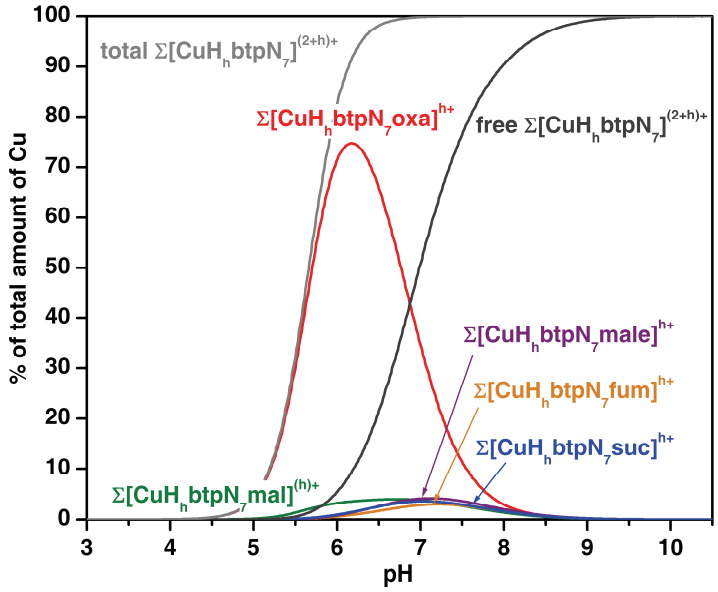

Figure A5.4 Distribution diagram of the overall amounts of supramolecular species formed between $[CuH_hbtpN_7]^{(2+h)+}$ and each dicarboxylate. $C_{btpN_7}/2 = C_{Cu} = C_A/3 = 5.0\times10^{-5}$ mol dm^{-3}.

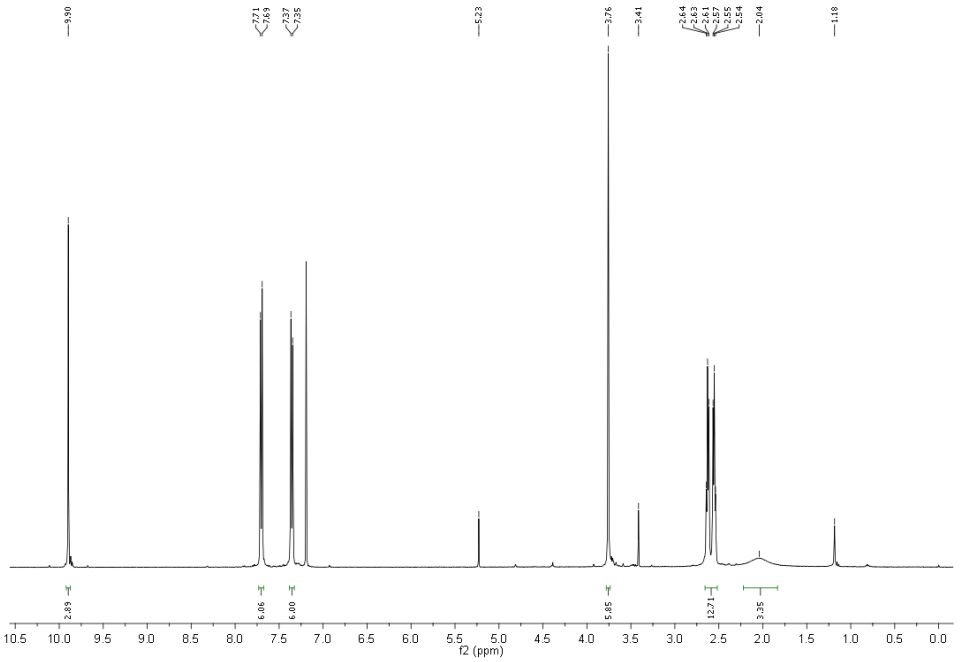

Figure A5.5 ^{1}H NMR spectrum of the tripodal trialdehyde in $CDCl_3$.

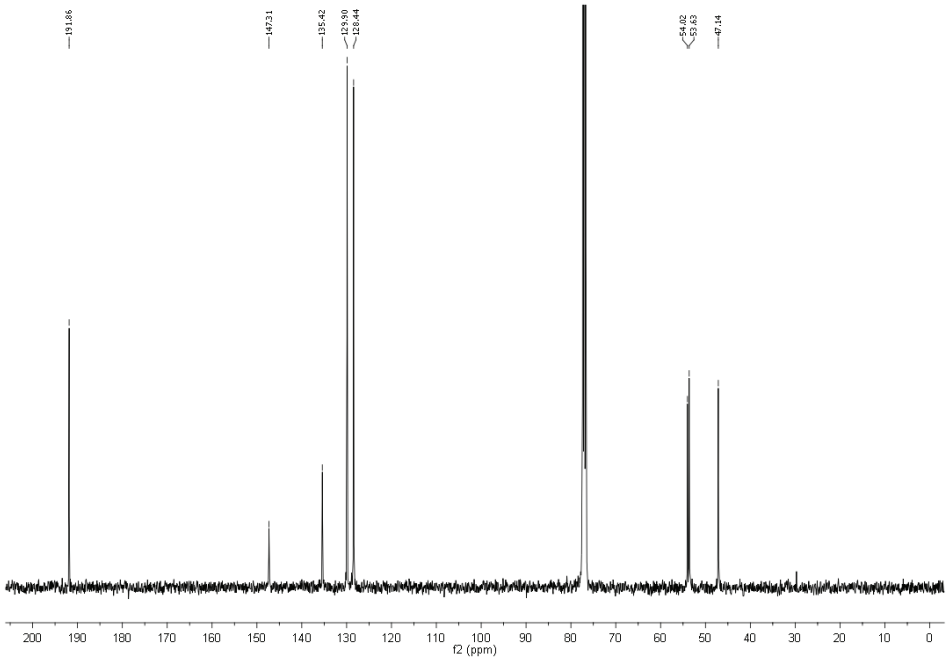

Figure A5.6 ^{13}C NMR spectrum of the tripodal trialdehyde in $CDCl_3$.

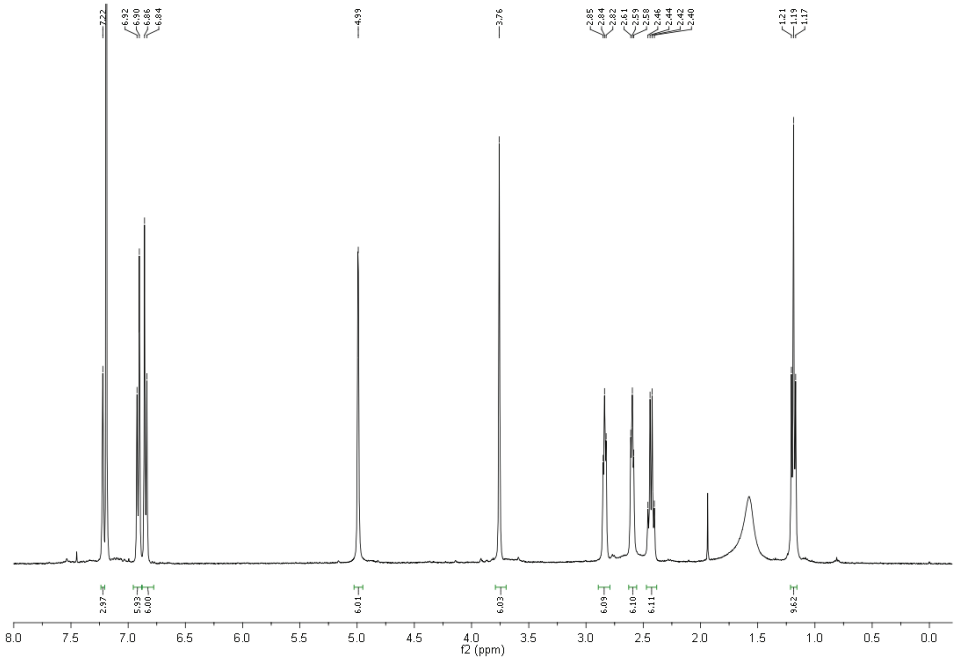

Figure A5.7 ^{1}H NMR spectrum of the triimine in $CDCl_3$.

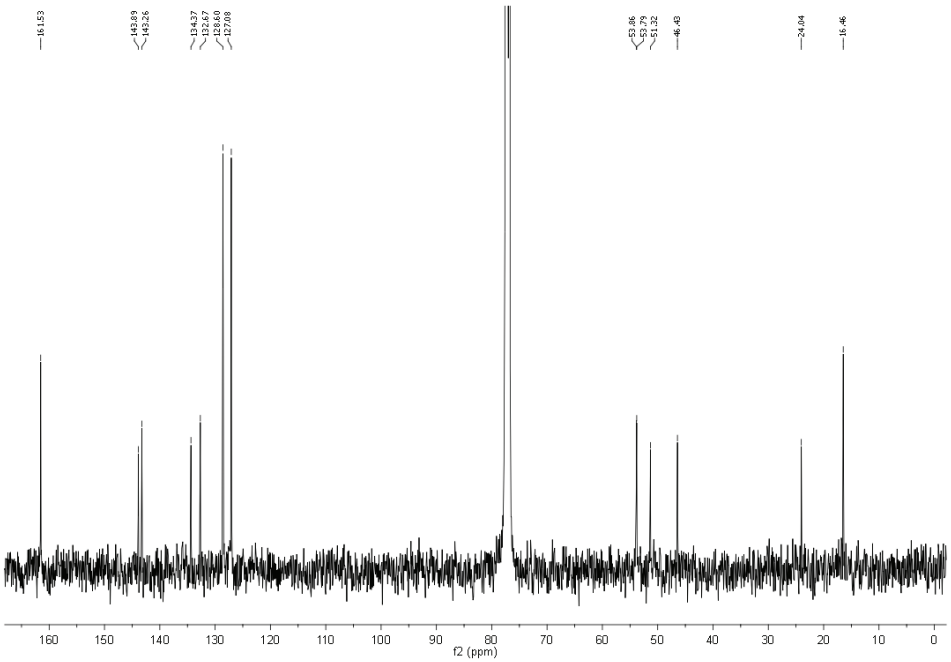

Figure A5.8 ^{13}C NMR spectrum of the triimine in $CDCl_3$.

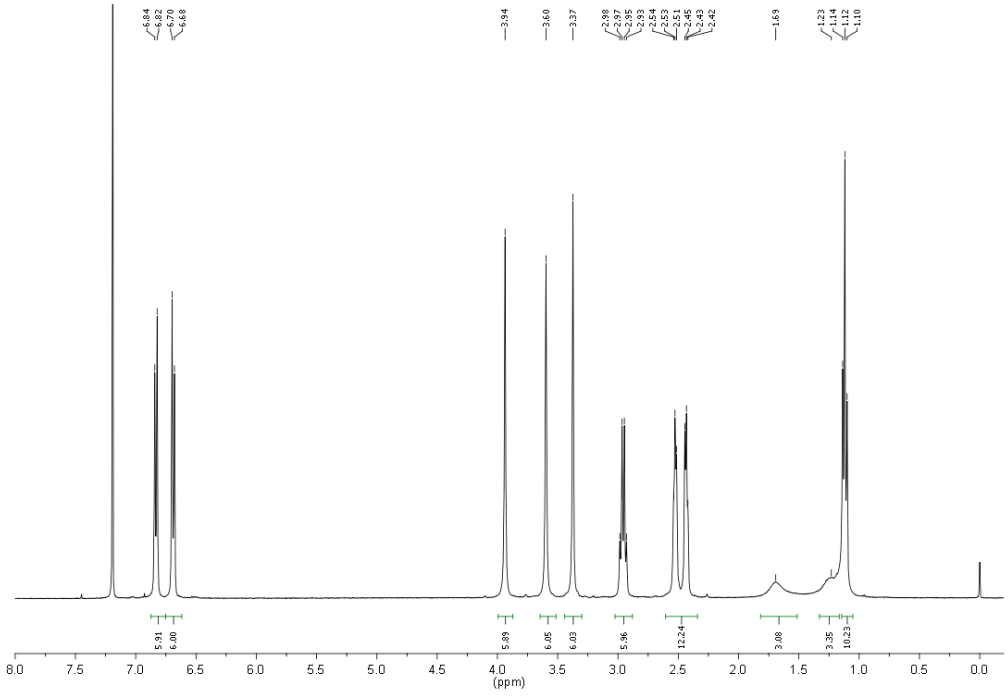

Figure A5.9 ^{1}H NMR spectrum of $btpN_7$ in $CDCl_3$.

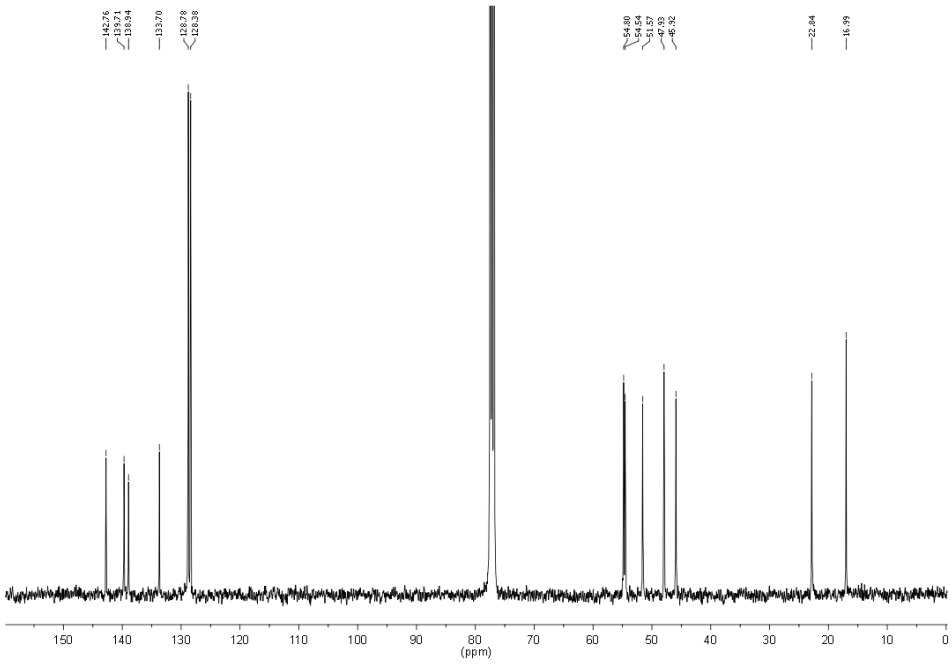

Figure A5.10 ^{13}C NMR spectrum of $btpN_7$ in $CDCl_3$.

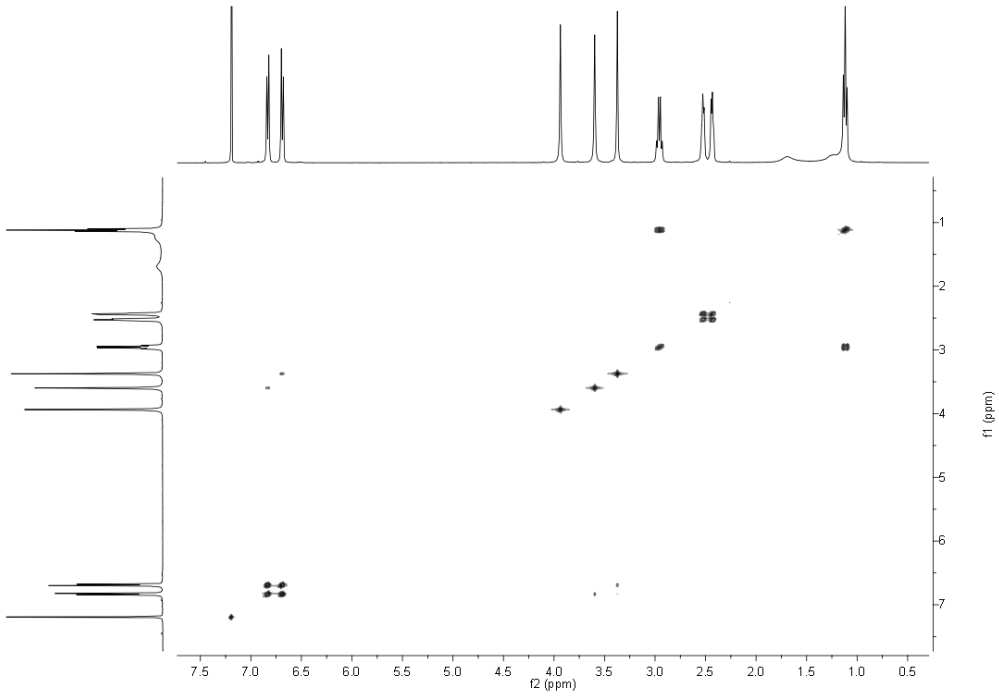

Figure A5.11 COSY spectrum of $btpN_7$ in $CDCl_3$.

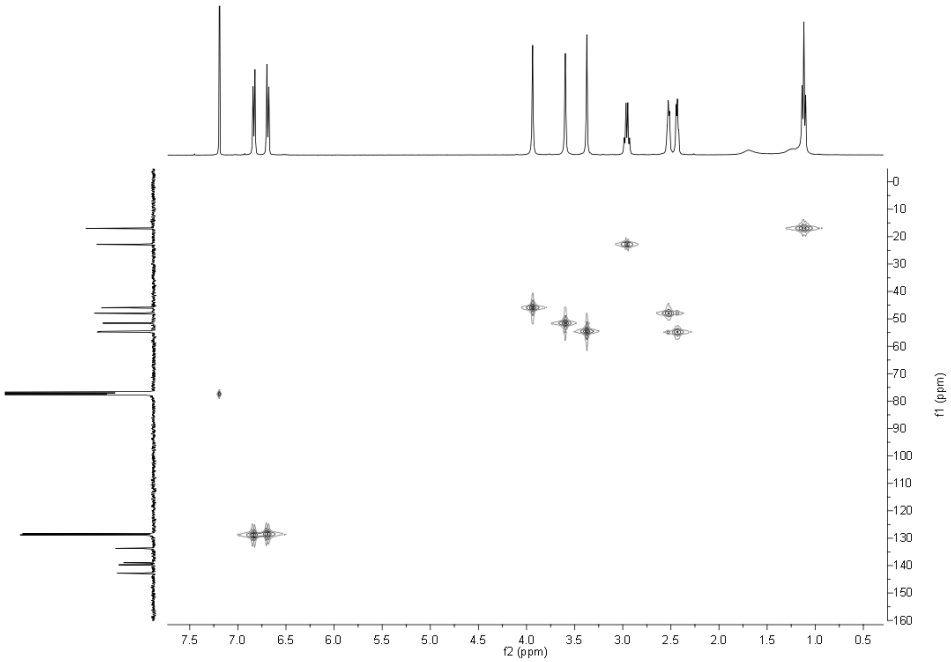

Figure A5.12 HMQC spectrum of $btpN_7$ in $CDCl_3$.

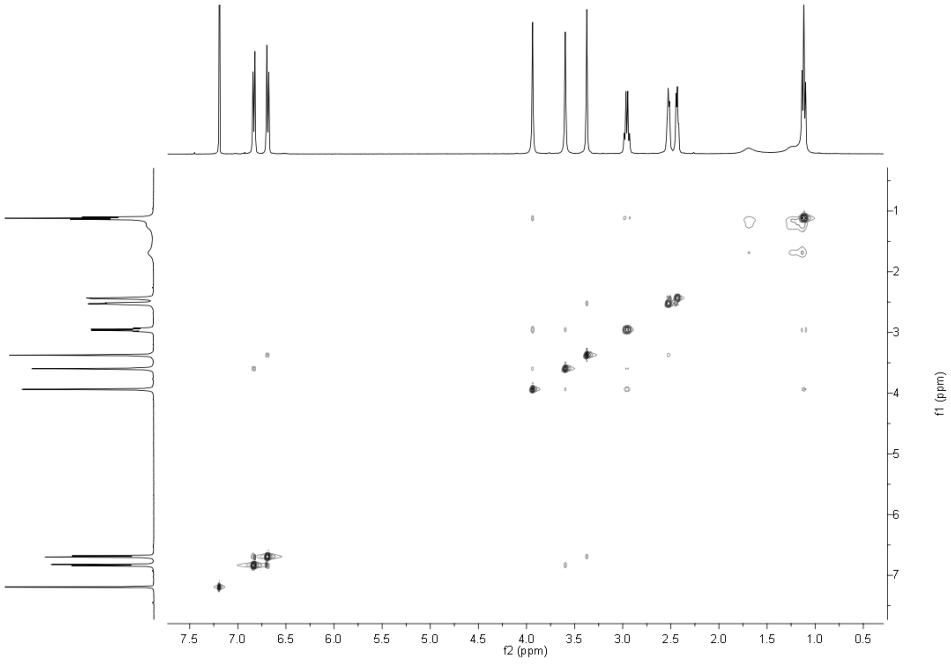

Figure A5.13 NOESY spectrum of $btpN_7$ in $CDCl_3$.

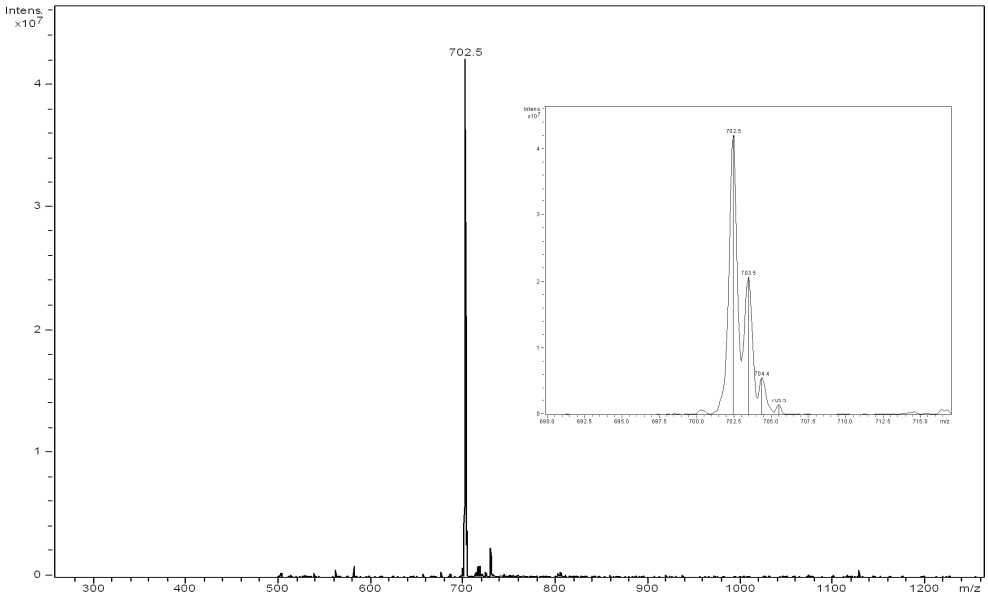

Figure A5.14 ESI mass spectrum of $btpN_7$ in MeOH.

A6. Supplementary Information of Chapter 6

Table A6.1 Stepwise protonation (K_i^H) constants of $btpN_7$ in H_2O.

Equilibrium reaction	log K_i^{H} [a]		
$btpN_7 + H^+ \rightleftharpoons HbtpN_7^+$	8.99(1)[b]	8.79(1)[c]	9.05(1)[d]
$HbtpN_7^+ + H^+ \rightleftharpoons H_2btpN_7^{2+}$	8.59(1)[b]	8.42(1)[c]	8.52(1)[d]
$H_2btpN_7^{2+} + H^+ \rightleftharpoons H_3btpN_7^{3+}$	7.57(1)[b]	7.43(1)[c]	7.65(1)[d]
$H_3btpN_7^{3+} + H^+ \rightleftharpoons H_4btpN_7^{4+}$	6.55(1)[b]	6.65(1)[c]	6.86(1)[d]
$H_4btpN_7^{4+} + H^+ \rightleftharpoons H_5btpN_7^{5+}$	5.90(1)[b]	6.59(1)[c]	6.67(1)[d]
$H_5btpN_7^{5+} + H^+ \rightleftharpoons H_6btpN_7^{6+}$	5.27(1)[b]	5.84(1)[c]	5.93(1)[d]

[a] Values in parenthesis are standard deviations in the last significant figures. [b] This work; T = 298.2±0.1 K; I = 0.10±0.01 mol dm^{-3} in KTsO. [c] This work; T = 298.2±0.1 K; I = 0.10±0.01 mol dm^{-3} in KBr. [d] See Chapter 5; T = 298.2±0.1 K; I = 0.10±0.01 mol dm^{-3} in KNO_3.

Table A6.2 Overall (β_i^H) and stepwise protonation (K_i^H) constants of the studied dicarboxylate anions in aqueous solution.[a]

Equilibrium[b]	oxa^{2-}	mal^{2-}	suc^{2-}	glu^{2-}	$male^{2-}$	fum^{2-}
			log β_i^{H} [c]			
$A^{2-} + H^+ \rightleftharpoons HA^-$	3.82(1)	5.29(1)	5.24(1)	5.02(1)	5.85(1)	4.07(1)
$A^{2-} + 2\,H^+ \rightleftharpoons H_2A$	5.14(1)	8.00(1)	9.25(1)	9.18(1)	7.66(1)	6.95(1)
			log K_i^{H}			
$A^{2-} + H^+ \rightleftharpoons HA^-$	3.82	5.29	5.24	5.02	5.85	4.07
$HA^- + H^+ \rightleftharpoons H_2A$	1.32	2.71	4.01	4.16	1.82	2.88

[a] T = 298.2±0.1 K; I = 0.10±0.01 mol dm^{-3} in KTsO. [b] A^{2-} denote in general the dicarboxylate anion. [c] Values in parenthesis are standard deviations in the last significant figures.

Table A6.3 Overall association constants (log $\beta_{H_hL_lA_a}$) for the indicated equilibria between the $H_nbtpN_7^{n+}$ and $H_nt_2pN_8^{n+}$ receptors and oxa^{2-}, mal^{2-}, suc^{2-}, glu^{2-}, $male^{2-}$ and fum^{2-} anions in H_2O.[a],[b],[c]

Reaction equilibrium	oxa^{2-}	mal^{2-}	suc^{2-}	glu^{2-}	$male^{2-}$	fum^{2-}
			$btpN_7$			
$7\,H^+ + L + A^{2-} \rightleftharpoons H_7LA^{5+}$	49.07(2)	50.41(2)	–	–	50.61(3)	49.55(4)
$6\,H^+ + L + A^{2-} \rightleftharpoons H_6LA^{4+}$	46.91(1)	46.54(1)	45.96(1)	45.45(1)	46.42(1)	46.77(1)
$5\,H^+ + L + A^{2-} \rightleftharpoons H_5LA^{3+}$	40.49(1)	40.25(2)	39.64(3)	39.71(2)	40.39(1)	40.46(3)
$4\,H^+ + L + A^{2-} \rightleftharpoons H_4LA^{2+}$	–	33.88(3)	33.57(3)	33.62(3)	–	33.87(6)
			t_2pN_8			
$7\,H^+ + L + A^{2-} \rightleftharpoons H_7LA^{5+}$	52.08(2)	52.29(1)	52.07(1)	51.49(2)	52.83(1)	–
$6\,H^+ + L + A^{2-} \rightleftharpoons H_6LA^{4+}$	49.71(1)	48.84(1)	48.11(1)	47.34(1)	48.65(1)	49.55(1)
$5\,H^+ + L + A^{2-} \rightleftharpoons H_5LA^{3+}$	42.14(6)	42.20(2)	41.82(2)	41.62(2)	42.37(1)	42.38(3)
$4\,H^+ + L + A^{2-} \rightleftharpoons H_4LA^{2+}$	35.57(3)	35.80(1)	35.80(1)	35.80(2)	35.94(1)	35.86(2)
$3\,H^+ + L + A^{2-} \rightleftharpoons H_3LA^{+}$	28.10(3)	28.31(2)	28.25(2)	28.21(3)	28.45(2)	28.37(3)
$2\,H^+ + L + A^{2-} \rightleftharpoons H_2LA$	–	19.76(5)	19.84(4)	19.80(7)	20.03(3)	19.88(6)

[a] T = 298.2±0.1 K; I = 0.10±0.01 mol dm^{-3} in KTsO. [b] A^{2-} denote in general the dicarboxylate anion and L the $btpN_7$ or the t_2pN_8 compounds. [c] Values in parenthesis are standard deviations in the last significant figures.

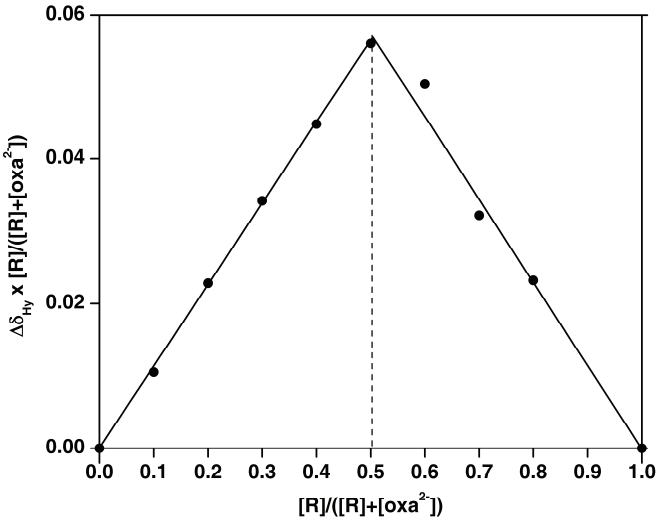

Figure A6.1 Job's plot between $H_nbtpN_7^{n+}$ (R) and oxalate (oxa^{2-}) in D_2O at pD = 4.50 and 298.2 *K*. In all the recorded spectra [R] + [oxa^{2-}] = 2×10^{-3} mol dm^{-3}. Changes of chemical shift of the H_y resonance in the receptor were monitored.

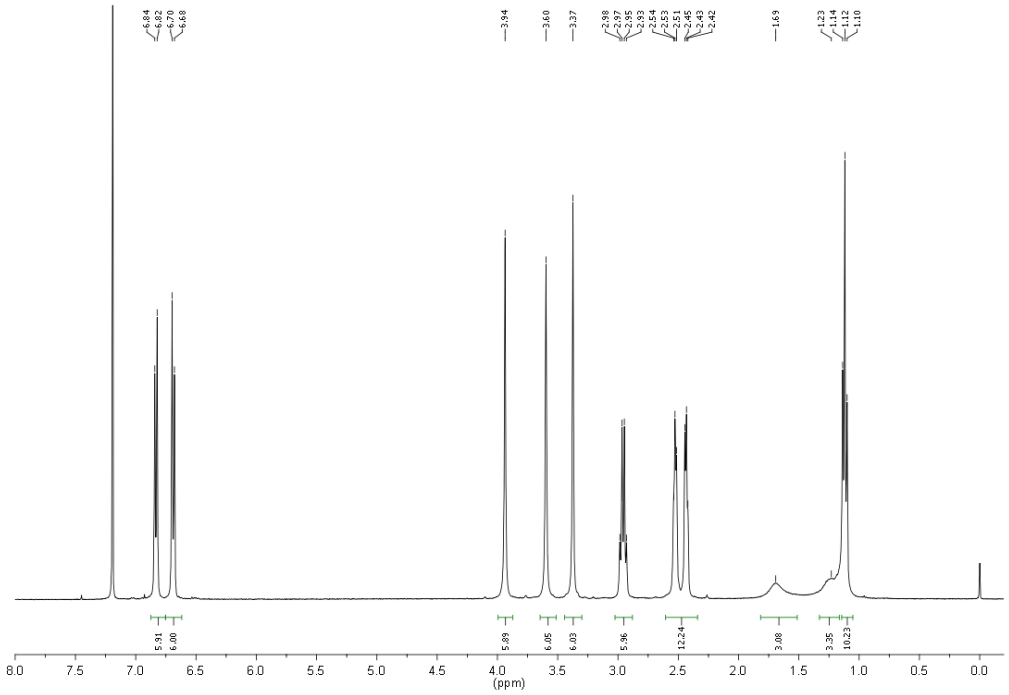

Figure A6.2 ^1H NMR spectrum of $btpN_7$ in $CDCl_3$.

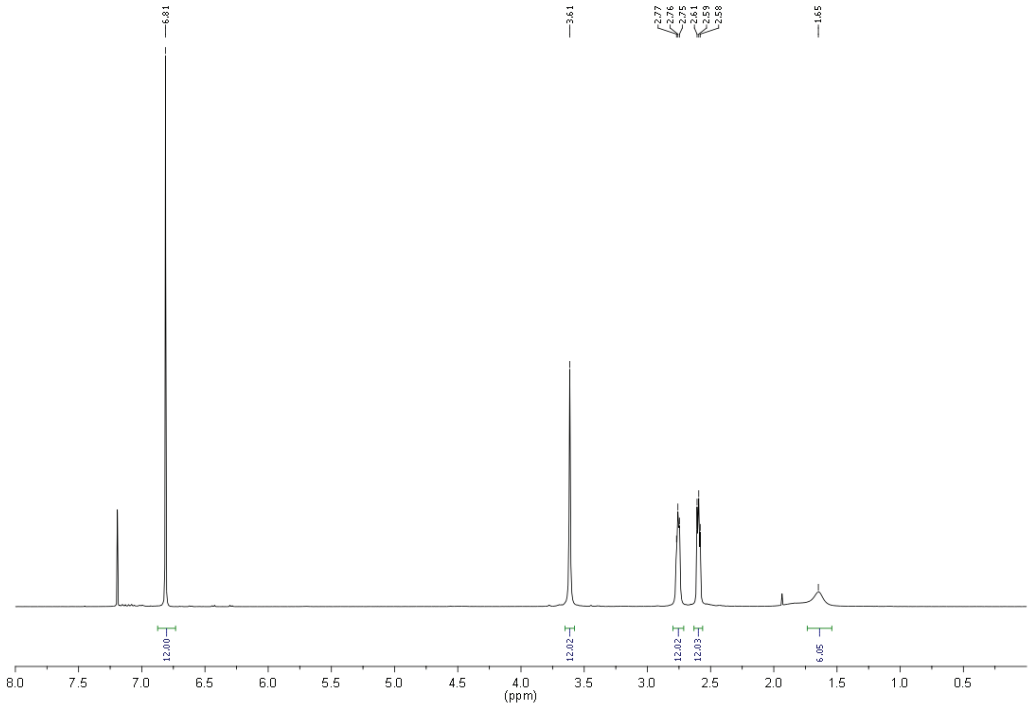

Figure A6.3 ^{1}H NMR spectrum of t_2pN_8 in $CDCl_3$.

A7. Supplementary Information of Chapter 7

Table A7.1 Overall (β_i^H) and stepwise protonation (K_i^H) constants of the studied amino acids in aqueous solution.[a]

Equilibrium[b]	gly$^-$	bala$^-$	tau$^-$	gaba$^-$	amp^{2-}	aep^{2-}
			log β_i^{H} [c]			
A + H ⇌ HA	9.32(1)	9.68(1)	8.57(1)	9.95(1)	10.05(1)	10.90(1)
A + 2 H ⇌ H_2A	12.23(1)	13.81(1)	9.94(1)	14.67(1)	16.24(1)	17.92(1)
A + 3 H ⇌ H_3A	–	–	–	–	17.65(1)	19.84(1)
			log K_i^H			
A + H ⇌ HA	9.32	9.68	8.57	9.95	10.05	10.90
HA + H ⇌ H_2A	2.91	4.13	1.37	4.72	6.18	7.02
H_2A + H ⇌ H_3A	–	–	–	–	1.42	1.92

[a] T = (298.2±0.1) K; I = (0.10±0.01) mol dm^{-3} in NMe_4TsO. [b] A denote in general the aminoacids in their deprotonated form, charges where omitted for simplicity. [c] Values in parenthesis are standard deviations in the last significant figures.

Table A7.2 Overall association constants (log $\beta_{H_nL_lA_a}$) for the indicated equilibria between the $H_nbtpN_4O_3^{n+}$ receptor and Hgly, Hbala, Htau, Hgaba, H_2amp and H_2aep substrates in MeOH/H_2O.[a],[b]

Equilibrium[c]	gly$^-$	bala$^-$	tau$^-$	gaba$^-$	amp^{2-}	aep^{2-}
5 H + L + A ⇌ H_5LA	–	–	–	–	42.29(5)	43.89(3)
4 H + L + A ⇌ H_4LA	34.51(2)	35.00(3)	34.51(3)	34.85(1)	36.50 (5)	37.81(3)
3 H + L + A ⇌ H_3LA	28.41(3)	28.72(3)	28.12(3)	28.68(1)	29.81(5)	30.62(6)
2 H + L + A ⇌ H_2LA	20.18(3)	20.65(3)	19.73(4)	20.53(1)	21.46(5)	22.29(3)
H + L + A ⇌ HLA	11.57(3)	11.89(2)	11.45(3)	11.86(1)	12.63(7)	13.34 (3)

[a] T = (298.2±0.1) K; I = (0.10±0.01) mol dm^{-3} in NMe_4TsO. [b] Values in parenthesis are standard deviations in the last significant figures. [c] A denote in general the amino acids in their deprotonated form and L the $btpN_4O_3$ compound, charges where omitted for simplicity.

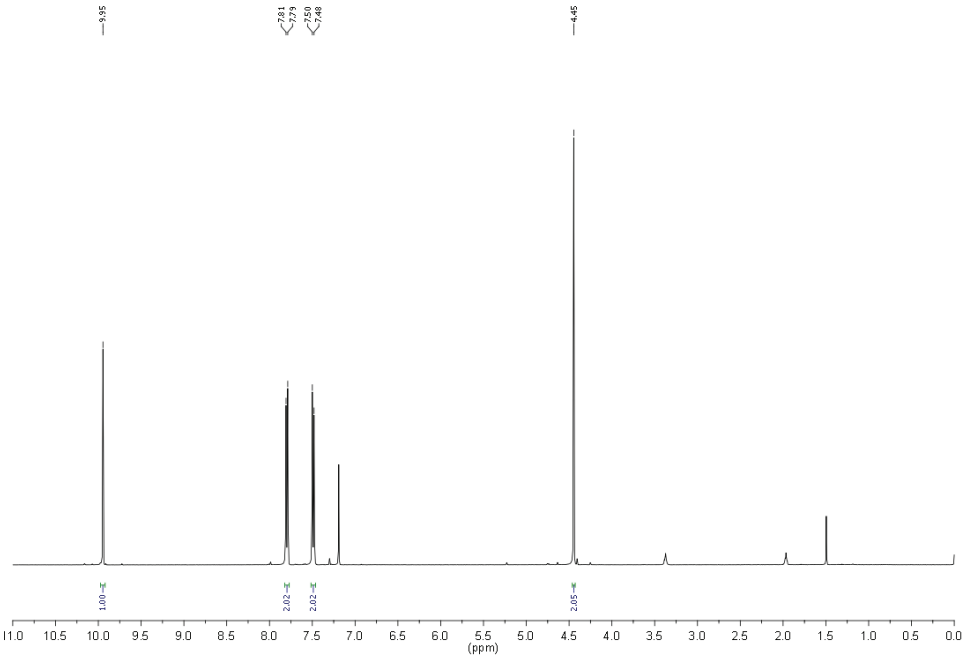

Figure A7.1 ^{1}H NMR spectrum of 4-(bromomethyl)benzaldehyde in $CDCl_3$.

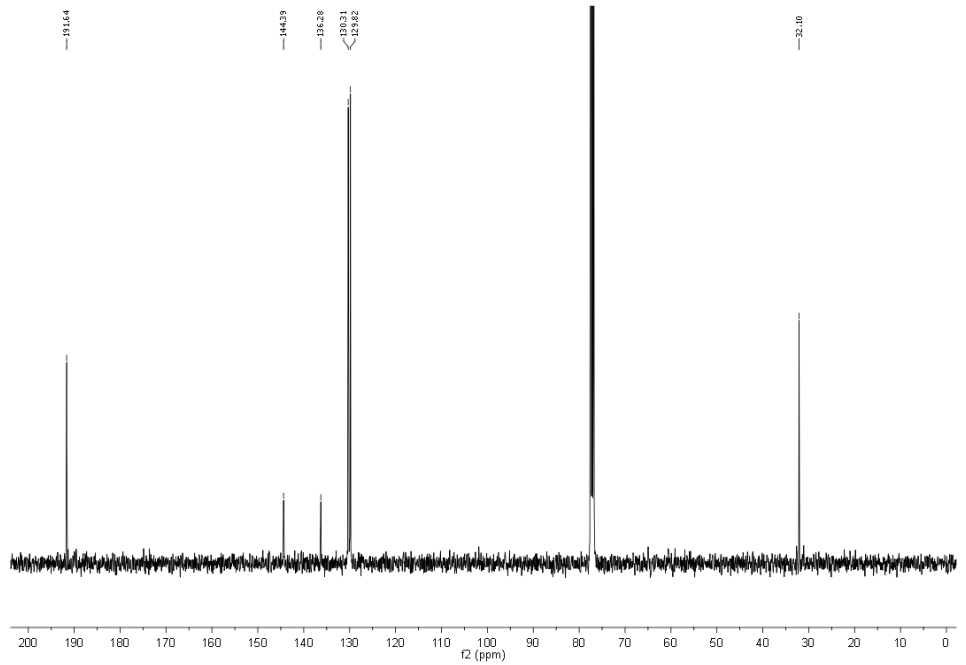

Figure A7.2 ^{13}C NMR spectrum of 4-(bromomethyl)benzaldehyde in $CDCl_3$.

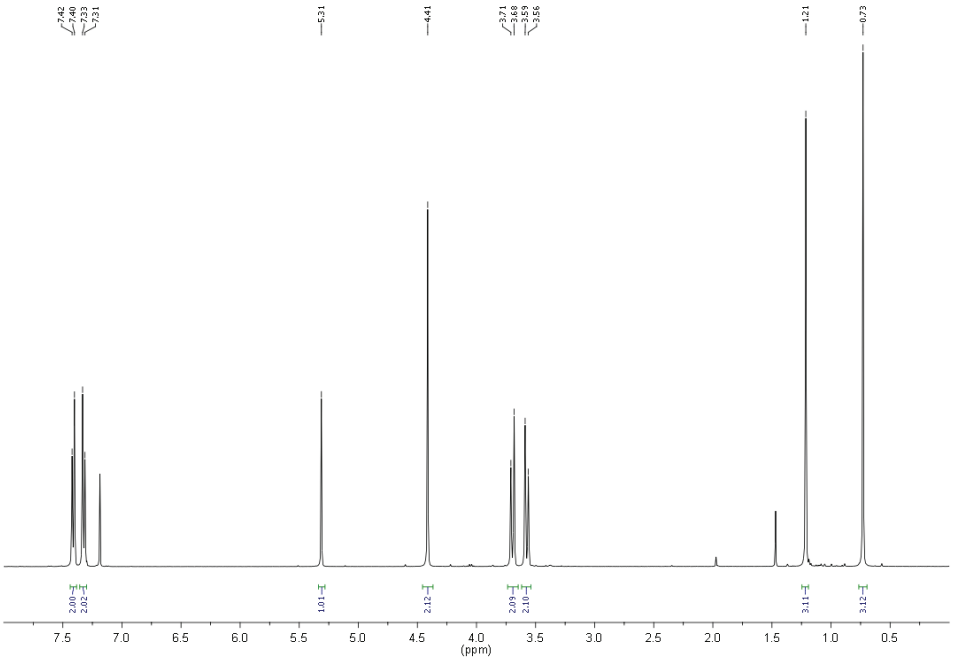

Figure A7.3 ^{1}H NMR spectrum of 2-(4-bromomethyl-phenyl)-5,5-dimethyl-[1,3]dioxane in $CDCl_3$.

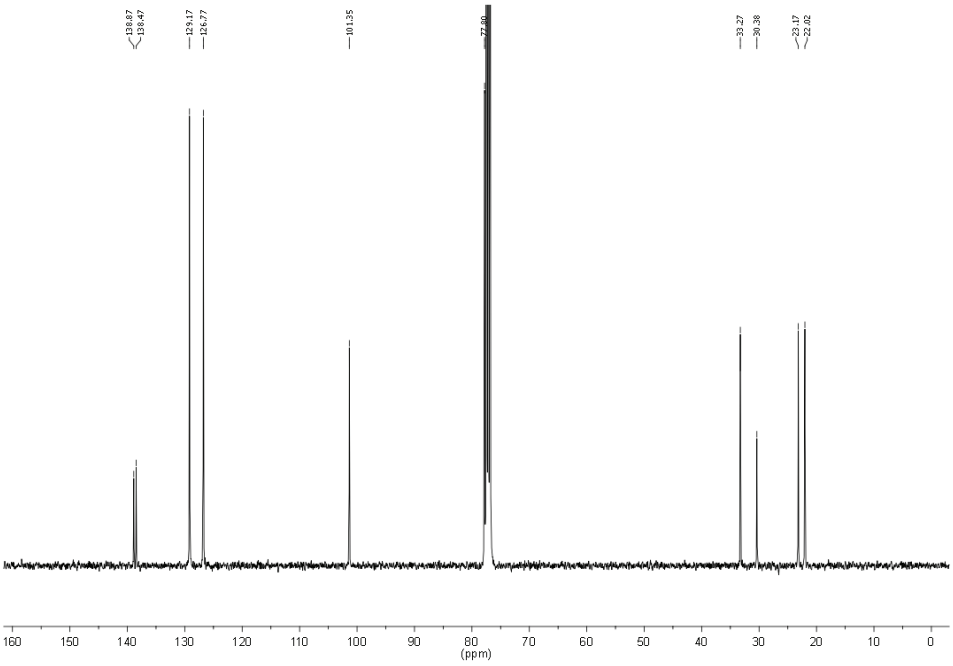

Figure A7.4 ^{13}C NMR spectrum of 2-(4-bromomethyl-phenyl)-5,5-dimethyl-[1,3]dioxane in $CDCl_3$.

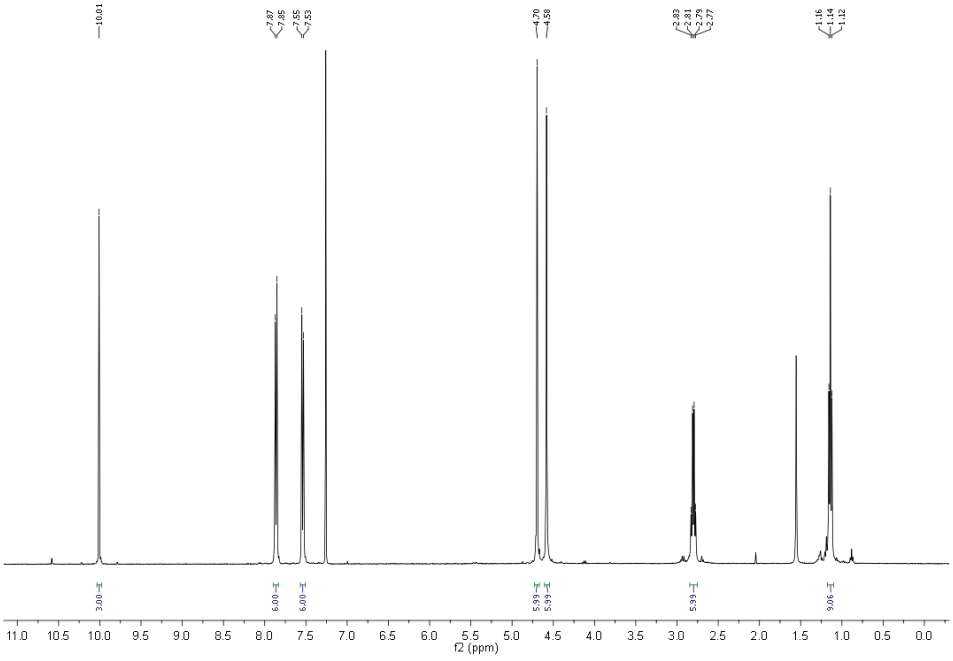

Figure A7.5 ^{1}H NMR spectrum of the tripodal trialdehyde (**3**) in $CDCl_3$.

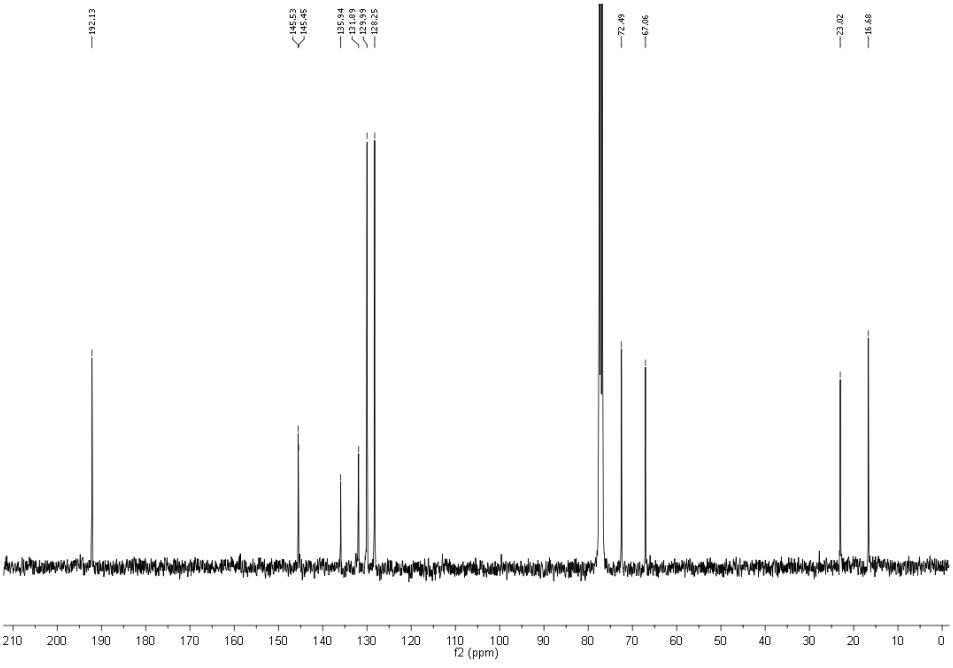

Figure A7.6 ^{13}C NMR spectrum of the tripodal trialdehyde (**3**) in $CDCl_3$.

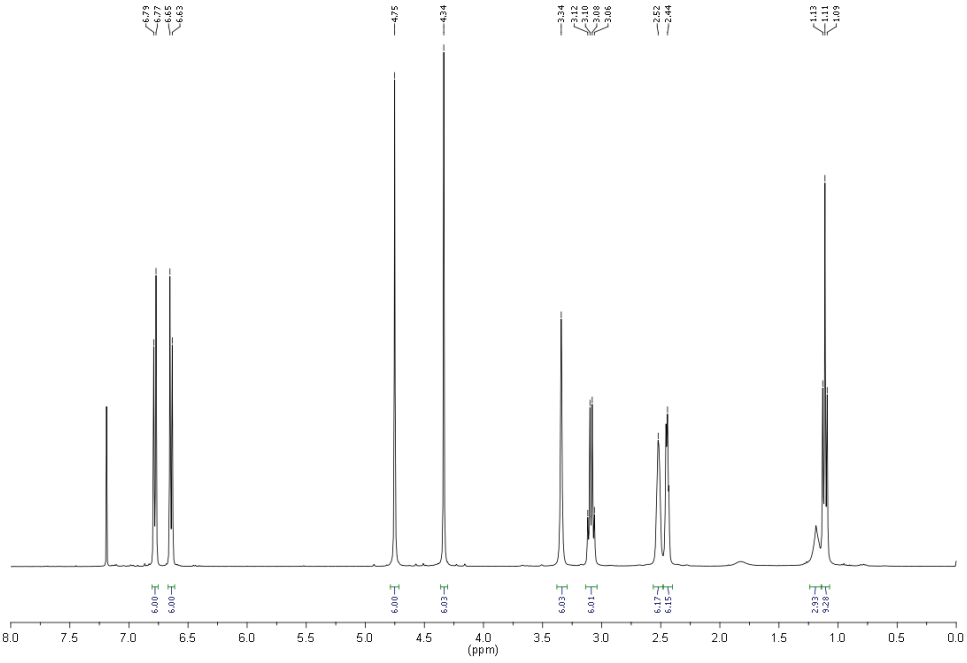

Figure A7.7 ^{1}H NMR spectrum $btpN_4O_3$ in $CDCl_3$.

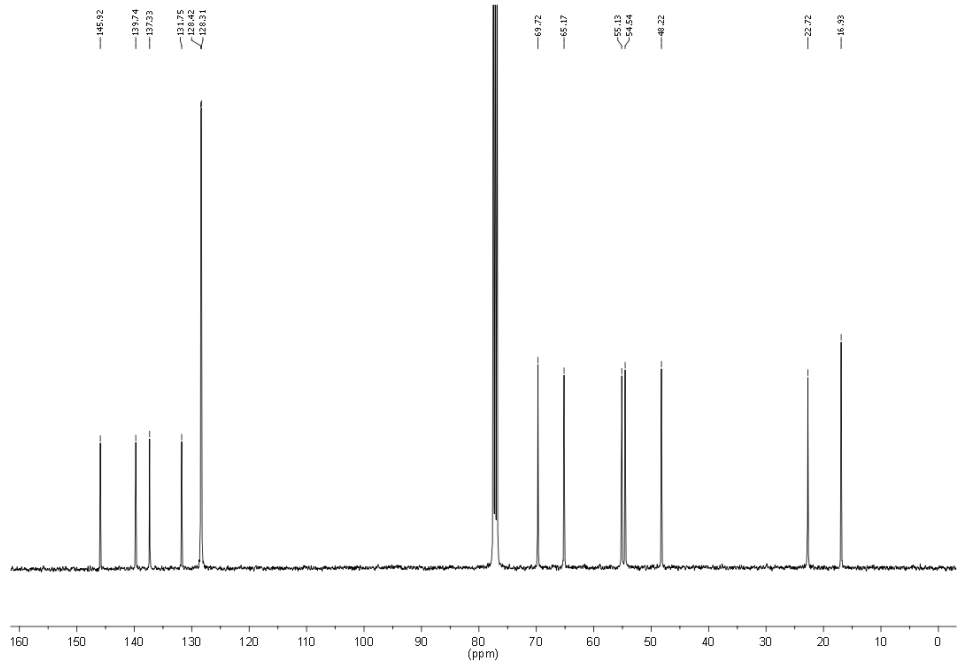

Figure A7.8 ^{13}C NMR spectrum of $btpN_4O_3$ in $CDCl_3$.

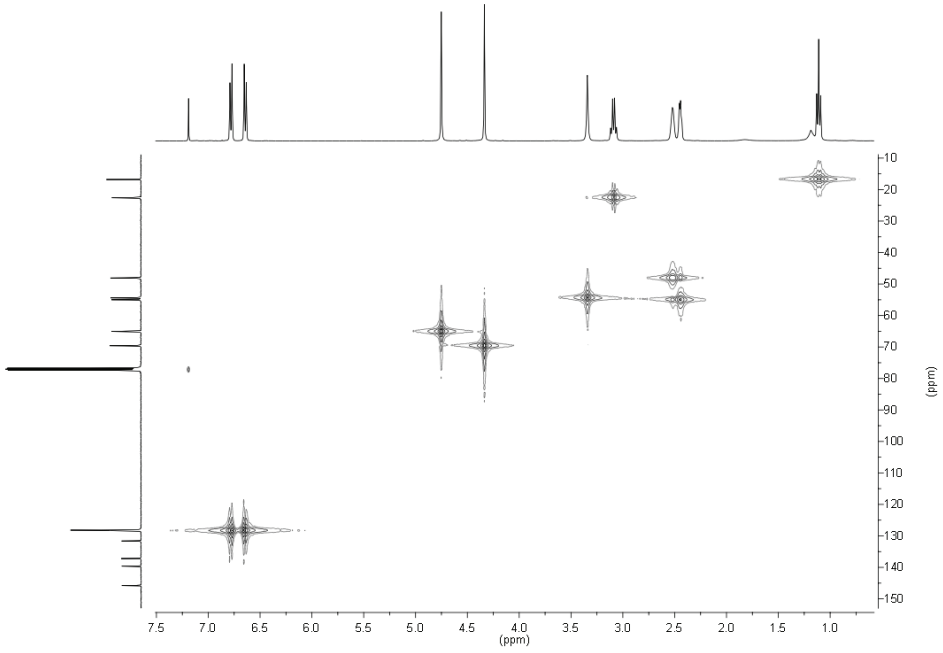

Figure A7.9 HMQC spectrum of $btpN_4O_3$ in $CDCl_3$.

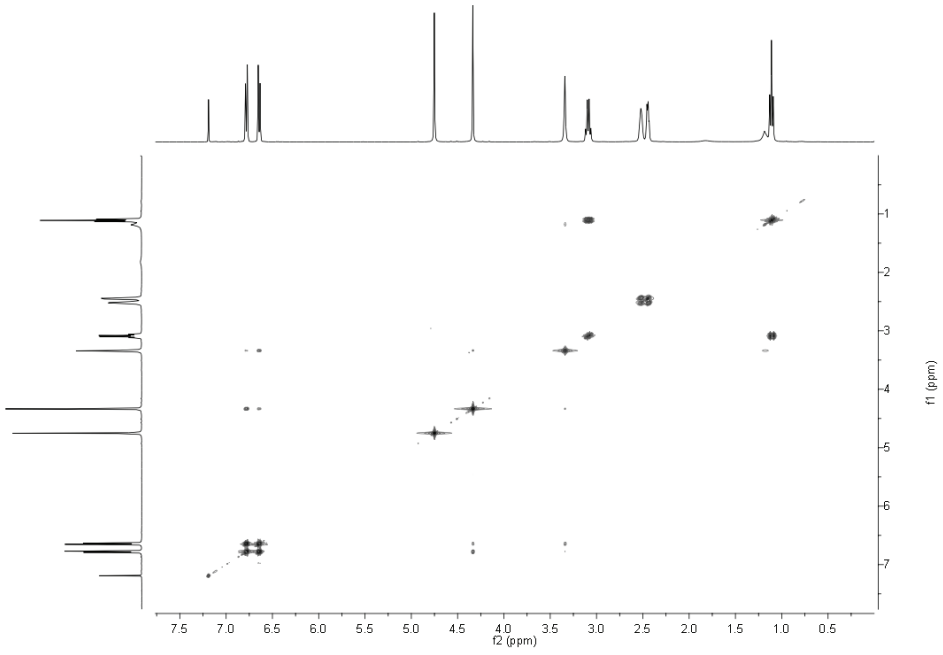

Figure A7.10 COSY spectrum of $btpN_4O_3$ in $CDCl_3$.

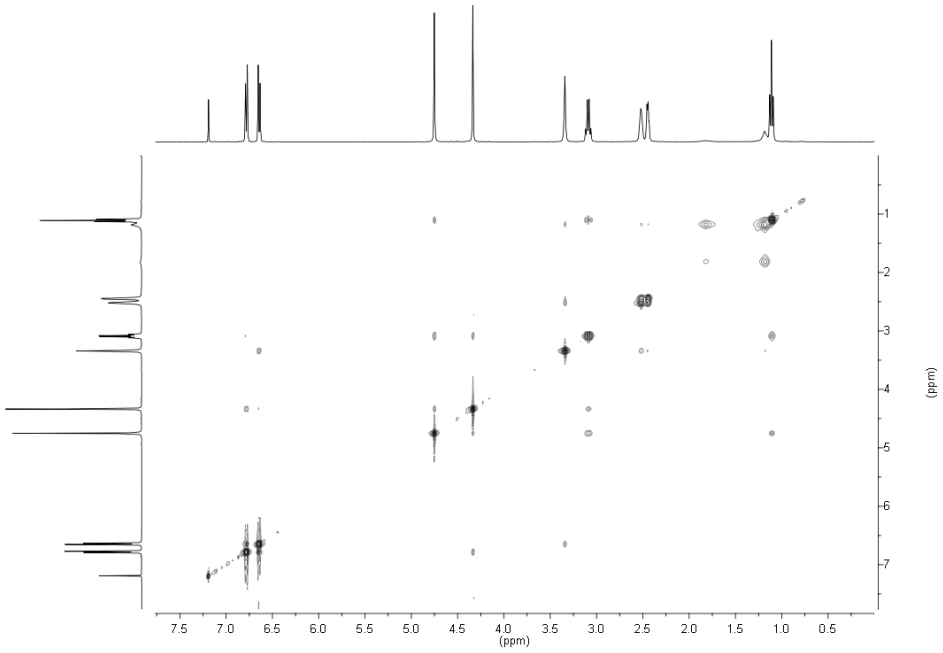

Figure A7.11 NOESY spectrum of $btpN_4O_3$ in $CDCl_3$.

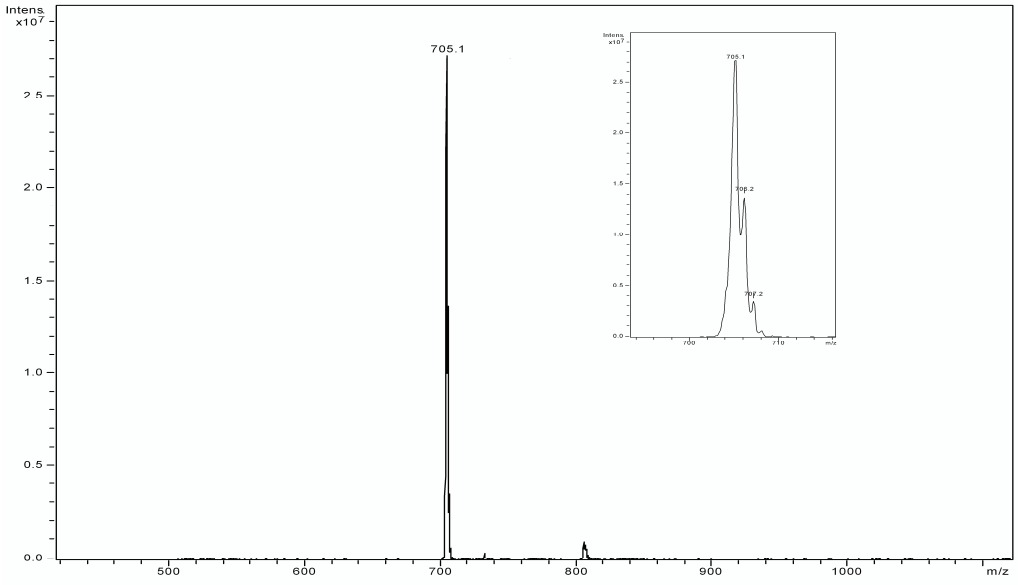

Figure A7.12 ESI mass spectrum of $btpN_4O_3$ in MeOH.

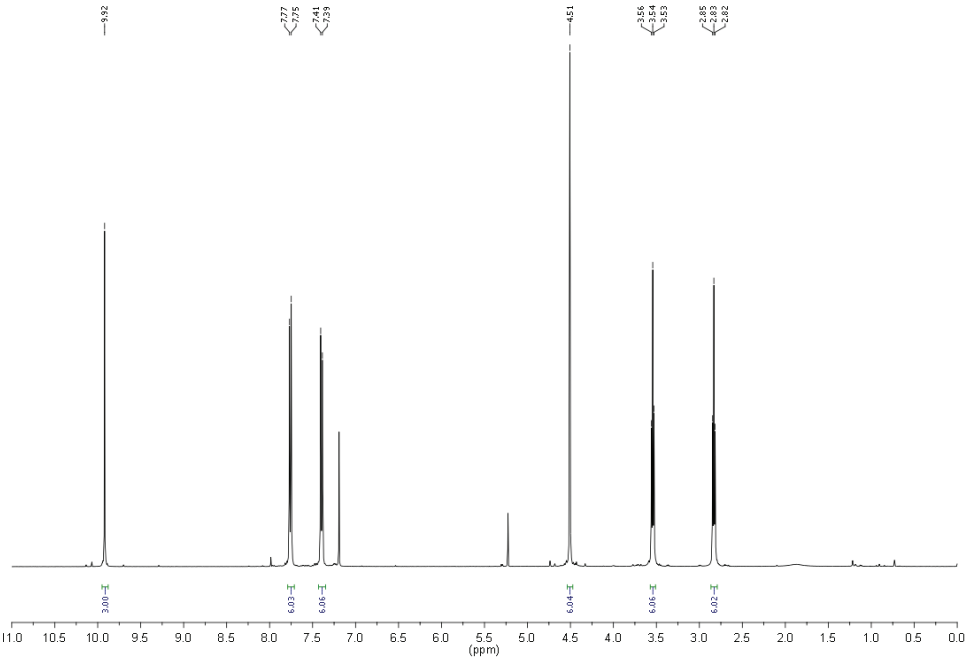

Figure A7.13 ^{1}H NMR spectrum the tripodal trialdehyde (**6**) in $CDCl_3$.

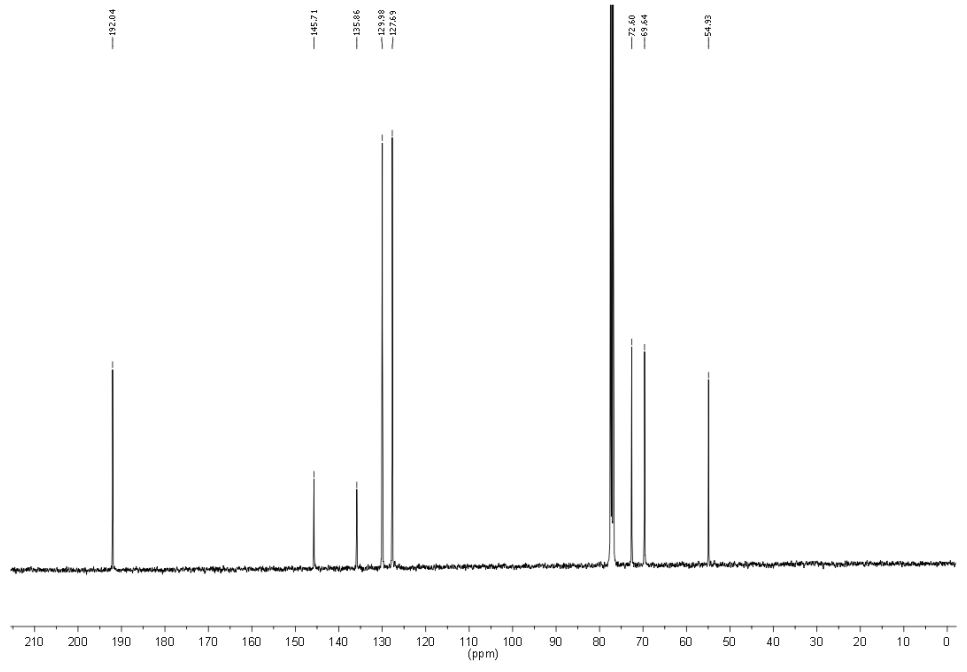

Figure A7.14 ^{13}C NMR spectrum of the tripodal trialdehyde (**6**) in $CDCl_3$.

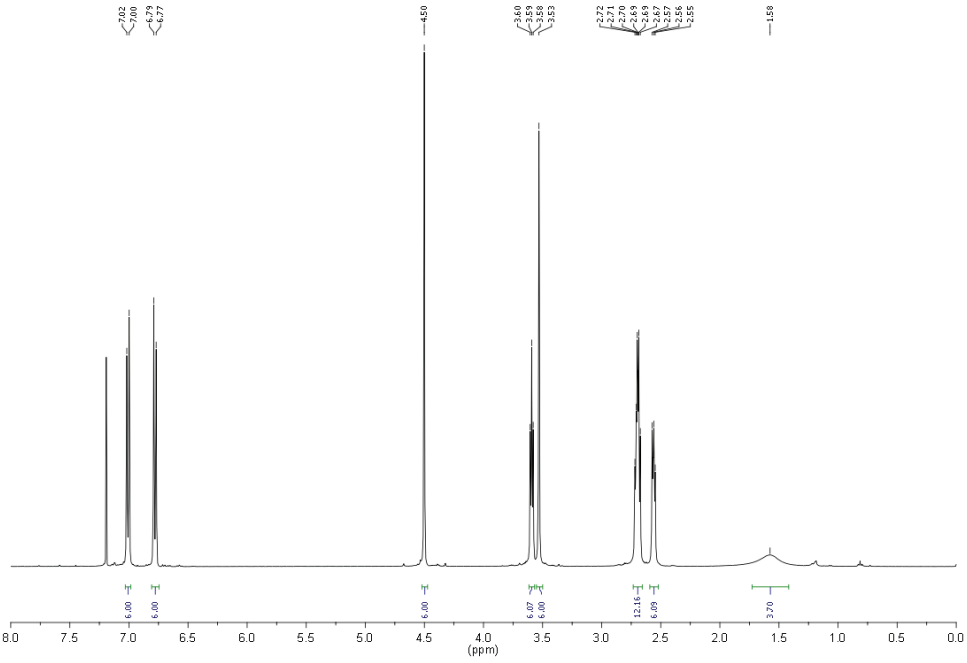

Figure A7.15 ^{1}H NMR spectrum $t_2pN_5O_3$ in $CDCl_3$.

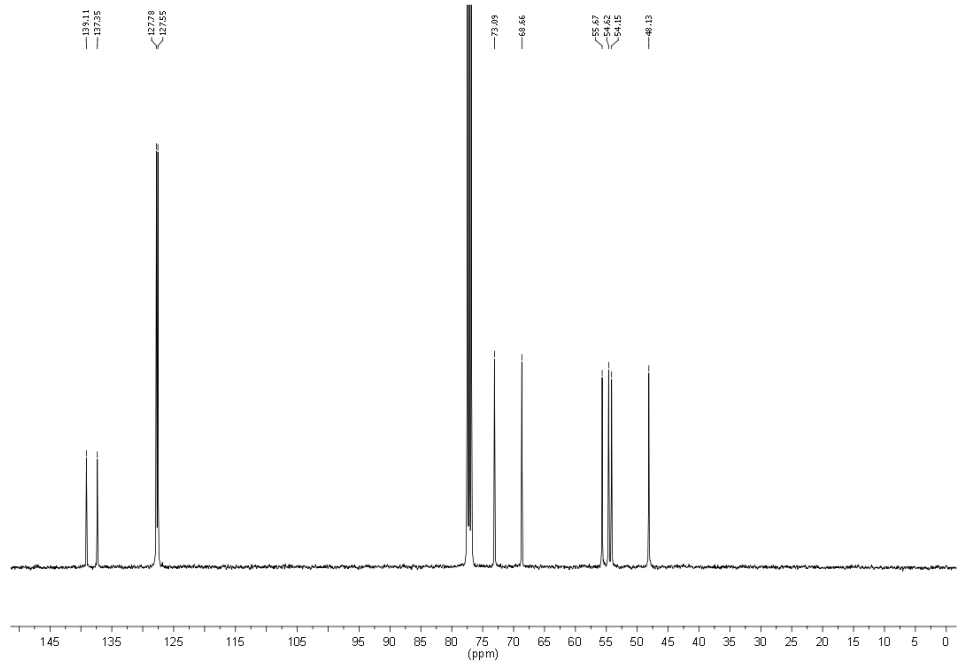

Figure A7.16 ^{13}C NMR spectrum $t_2pN_5O_3$ in $CDCl_3$.

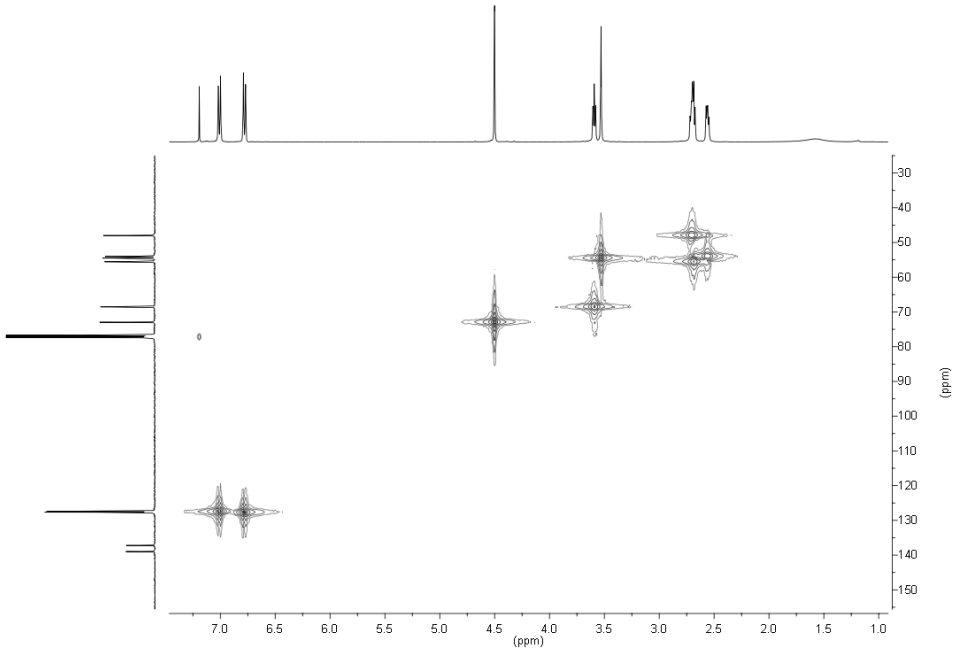

Figure A7.17 HMQC spectrum of $t_2pN_5O_3$ in $CDCl_3$.

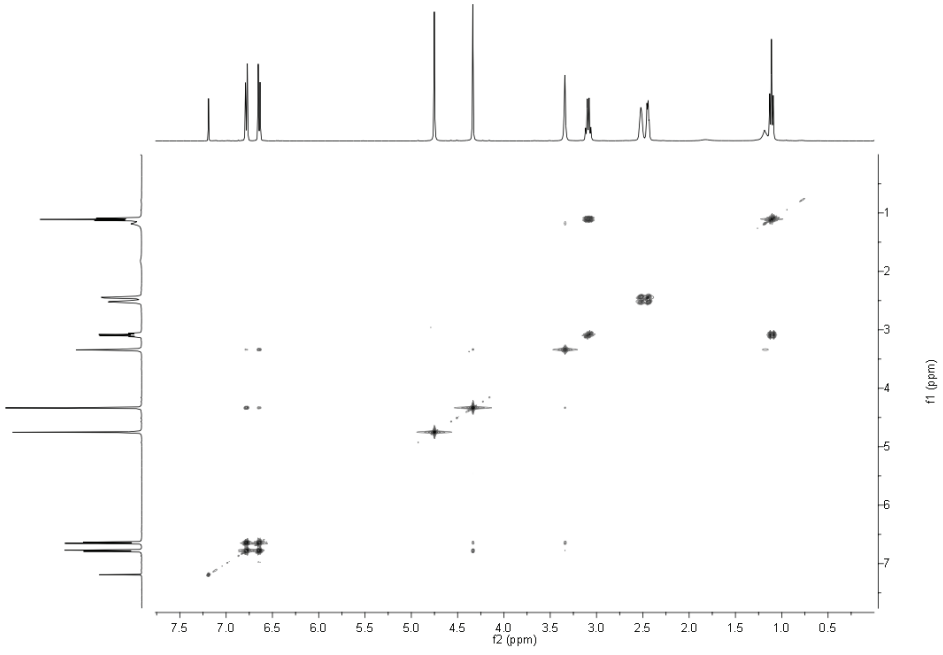

Figure A7.18 COSY spectrum of $t_2pN_5O_3$ in $CDCl_3$.

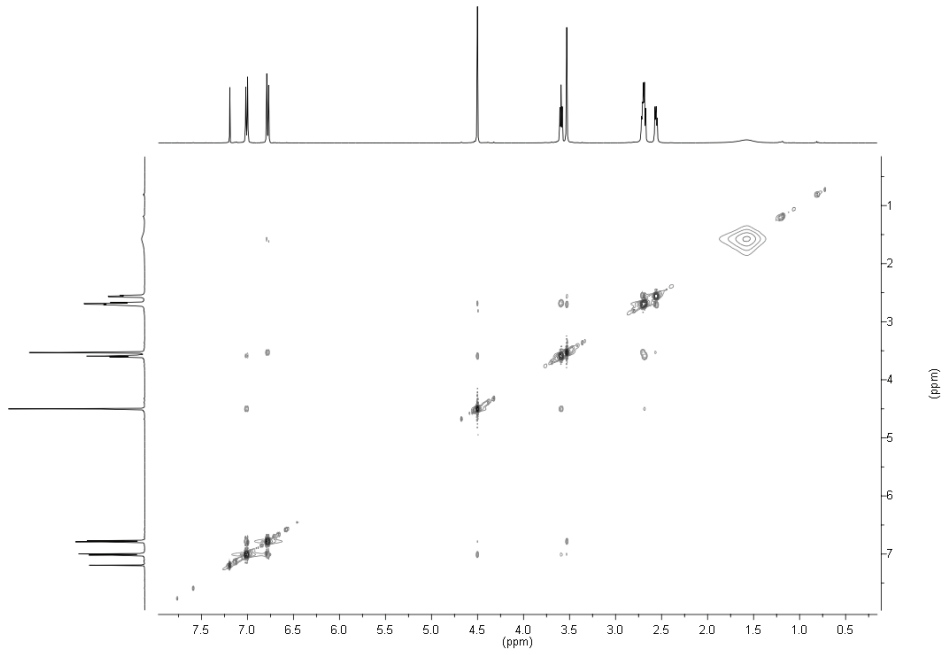

Figure A7.19 NOESY spectrum of $t_2pN_5O_3$ in $CDCl_3$.

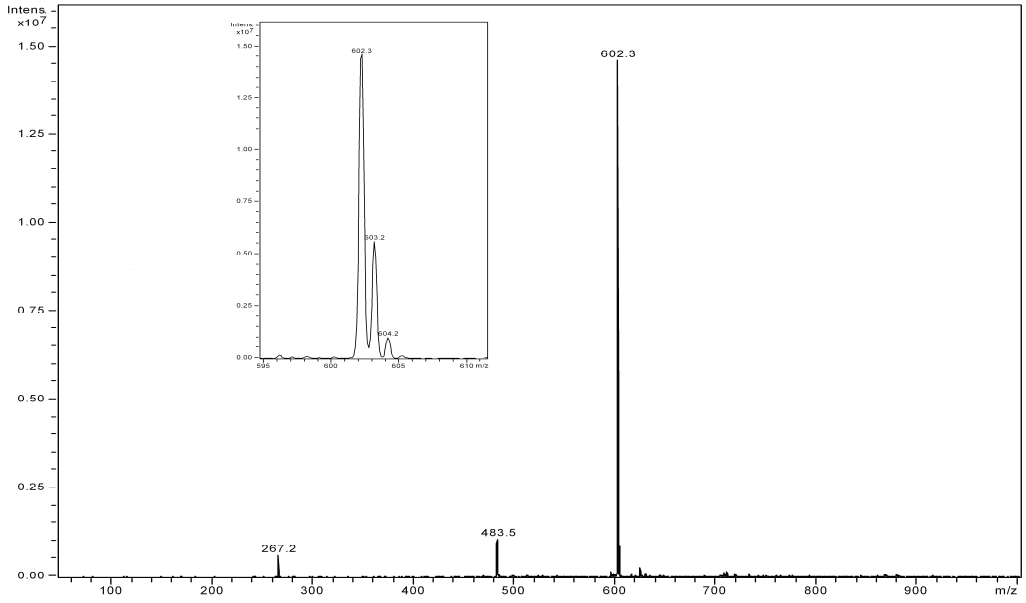

Figure A7.20 ESI mass spectrum of $t_2pN_5O_3$ in MeOH.

ITQB-UNL | Av. da República, 2780-157 Oeiras, Portugal
Tel (+351) 214 469 100 | Fax (+351) 214 411 277

www.itqb.unl.pt